

*Estimating Soil Pressure against Unyielding Surfaces*

**Final Report**

**FDOT Contract No. BDV31-977-89**

**Submitted to:**

Project Manager: Rodrigo Herrera, P.E.  
Co-Project Manager: Jose Hernando, P.E.  
Florida Department of Transportation

**Submitted By:**

UF Principal Investigator: Michael Rodgers, Ph.D., P.E.  
UF Co-Principal Investigator: Michael McVay, Ph.D.  
UF Graduate Researcher: Wyatt Kelch, M.E.

**August 2022**

University of Florida  
Engineering School of Sustainable Infrastructure & Environment

## **Disclaimer**

*The opinions, findings, and conclusions expressed in this publication are those of the authors and not necessarily those of the State of Florida Department of Transportation.*

## SI (Modern Metric) Conversion Factors (from FHWA) Approximate Conversions to SI Units

SYMBOL	WHEN YOU KNOW	MULTIPLY BY	TO FIND	SYMBOL
LENGTH				
in	inches	25.4	millimeters	mm
ft	feet	0.305	meters	m
yd	yards	0.914	meters	m
mi	miles	1.61	kilometers	km
SYMBOL	WHEN YOU KNOW	MULTIPLY BY	TO FIND	SYMBOL
AREA				
in <sup>2</sup>	square inches	645.2	square millimeters	mm <sup>2</sup>
ft <sup>2</sup>	square feet	0.093	square meters	m <sup>2</sup>
yd <sup>2</sup>	square yard	0.836	square meters	m <sup>2</sup>
ac	acres	0.405	hectares	ha
mi <sup>2</sup>	square miles	2.59	square kilometers	km <sup>2</sup>
SYMBOL	WHEN YOU KNOW	MULTIPLY BY	TO FIND	SYMBOL
VOLUME				
fl oz	fluid ounces	29.57	milliliters	mL
gal	gallons	3.785	liters	L
ft <sup>3</sup>	cubic feet	0.028	cubic meters	m <sup>3</sup>
yd <sup>3</sup>	cubic yards	0.765	cubic meters	m <sup>3</sup>
NOTE: volumes greater than 1000 L shall be shown in m <sup>3</sup>				
SYMBOL	WHEN YOU KNOW	MULTIPLY BY	TO FIND	SYMBOL
MASS				
oz	ounces	28.35	grams	g
lb	pounds	0.454	kilograms	kg
T	short tons (2000 lb)	0.907	megagrams (or "metric ton")	Mg (or "t")
SYMBOL	WHEN YOU KNOW	MULTIPLY BY	TO FIND	SYMBOL
TEMPERATURE (exact degrees)				
°F	Fahrenheit	5 (F-32)/9 or (F-32)/1.8	Celsius	°C
SYMBOL	WHEN YOU KNOW	MULTIPLY BY	TO FIND	SYMBOL
ILLUMINATION				
fc	foot-candles	10.76	lux	lx
fl	foot-Lamberts	3.426	candela/m <sup>2</sup>	cd/m <sup>2</sup>
SYMBOL	WHEN YOU KNOW	MULTIPLY BY	TO FIND	SYMBOL
FORCE and PRESSURE or STRESS				
lbf	pound force	4.45	newtons	N
lbf/in <sup>2</sup>	pound force per square inch	6.89	kilopascals	kPa

## Approximate Conversions to English Units

SYMBOL	WHEN YOU KNOW	MULTIPLY BY	TO FIND	SYMBOL
LENGTH				
mm	millimeters	0.039	inches	in
m	meters	3.28	feet	ft
m	meters	1.09	yards	yd
km	kilometers	0.621	miles	mi
SYMBOL	WHEN YOU KNOW	MULTIPLY BY	TO FIND	SYMBOL
AREA				
mm <sup>2</sup>	square millimeters	0.0016	square inches	in <sup>2</sup>
m <sup>2</sup>	square meters	10.764	square feet	ft <sup>2</sup>
m <sup>2</sup>	square meters	1.195	square yards	yd <sup>2</sup>
ha	hectares	2.47	acres	ac
km <sup>2</sup>	square kilometers	0.386	square miles	mi <sup>2</sup>
SYMBOL	WHEN YOU KNOW	MULTIPLY BY	TO FIND	SYMBOL
VOLUME				
mL	milliliters	0.034	fluid ounces	fl oz
L	liters	0.264	gallons	gal
m <sup>3</sup>	cubic meters	35.314	cubic feet	ft <sup>3</sup>
m <sup>3</sup>	cubic meters	1.307	cubic yards	yd <sup>3</sup>
SYMBOL	WHEN YOU KNOW	MULTIPLY BY	TO FIND	SYMBOL
MASS				
g	grams	0.035	ounces	oz
kg	kilograms	2.202	pounds	lb
Mg (or "t")	megagrams (or "metric ton")	1.103	short tons (2000 lb)	T
SYMBOL	WHEN YOU KNOW	MULTIPLY BY	TO FIND	SYMBOL
TEMPERATURE (exact degrees)				
°C	Celsius	1.8C+32	Fahrenheit	°F
SYMBOL	WHEN YOU KNOW	MULTIPLY BY	TO FIND	SYMBOL
ILLUMINATION				
lx	lux	0.0929	foot-candles	fc
cd/m <sup>2</sup>	candela/m <sup>2</sup>	0.2919	foot-Lamberts	fl
SYMBOL	WHEN YOU KNOW	MULTIPLY BY	TO FIND	SYMBOL
FORCE and PRESSURE or STRESS				
N	newtons	0.225	pound force	lbf
kPa	kilopascals	0.145	pound force per square inch	lbf/in <sup>2</sup>

## Technical Report Documentation Page

1. Report No.	2. Government Accession No.	3. Recipient's Catalog No.	
4. Title and Subtitle Estimating Soil Pressure against Unyielding Surfaces		5. Report Date August 2022	
		6. Performing Organization University of Florida - ESSIE	
7. Author(s) Michael Rodgers, Ph.D., P.E., Michael McVay, Ph.D., Wyatt Kelch, M.E.		8. Performing Organization Report No.	
9. Performing Organization Name and Address University of Florida –Engineering School of Sustainable Infrastructure and Environment 365 Weil Hall – P.O. Box 116580 Gainesville, FL 32511-6580		10. Work Unit No. (TRAIS)	
		11. Contract or Grant No. BDV31-977-89	
12. Sponsoring Agency Name and Address Florida Department of Transportation 605 Suwannee Street, MS 30 Tallahassee, FL 32399		13. Type of Report and Period Covered Final Report 02/01/2018 – 10/31/2022	
		14. Sponsoring Agency Code	
15. Supplementary Notes			
<p>16. Abstract:</p> <p>This report focuses on the earth pressures that develop when two MSE walls are tied together, creating an unyielding condition. During the research an extensive literature review was completed that included current design practices and standards, and construction and quality control procedures. This ensured the constructed wall configurations adhered to the FDOT’s standard specifications for road and bridge construction and complied with the AASHTO Design code. This also ensured proper construction and sequencing took place to provide structures that were representative of the practice. For the research, two relative compaction efforts were investigated, 95% and 103% of the backfill soil’s optimum dry density. During construction, earth pressure coefficients were derived for each compacted soil lift for each state of soil density. Once construction was complete, a reaction frame loading system was utilized to induce controlled incremental surcharge loads, and earth pressure coefficients were derived for each incremental surcharge load applied. The final surcharge loads provided the necessary B/H = 0.3 for both compaction efforts to ensure the results were representative of the practice. From the derived earth pressure coefficients, it was observed that in an unyielding condition, the earth pressures move from a passive condition to either an active or at-rest condition as the soil height increases above the reinforcement level, which is different from conventional MSE wall design and construction. Consequently, a new equation was developed from the research that incorporates a variable friction angle (<math>\phi</math>) based on the compaction effort for an unyielding condition, and FDOT design and construction requirements. When compared to the measured results, the new equation followed the trends of the data well.</p>			
17. Key Words Mechanically Stabilized Earth, Earth Pressure Coefficient, Inextensible Reinforcement, Unyielding Condition, Soil Arching, Vertical Stress, Horizontal Stress, Strip Tension		18. Distribution Statement No restrictions.	
19. Security Classif. (of this report): Unclassified	20. Security Classif. (of this page): Unclassified	21. No. of Pages 256	22. Price

## **Acknowledgements**

The UF research team would like to thank the Florida Department of Transportation (FDOT) for supporting this research effort. A special thanks is extended to the FDOT State Materials Office Field Operations Specialists, FDOT Central Office Geotechnical Engineers, and the Reinforced Earth Company for their continuous support, guidance, and assistance. Without their efforts, this research would not have been possible.

## Executive Summary

Mechanically Stabilized Earth (MSE) walls are a type of soil retaining structure that consist of facing panels, usually made of concrete, mechanically attached to geosynthetic or metallic reinforcing strips or grids that are layered between lifts of granular backfill. In standard MSE wall construction, frictional resistance developed along the surface of the reinforcement opposes the lateral earth pressure exerted on the facing panels by the granular backfill. The lateral earth pressure imposed on an MSE wall reinforced fill is approximately equal to the active lateral pressure developed in conventional earth pressure theory, which applies to most cases where the back end of the reinforcement is not attached to any structure and is free to move. However, in certain cases, such as acute corners or when the base to wall height (B/H) ratio is 0.3, the reinforcement actually ties two walls together, creating an unyielding condition. The earth pressure that develops from material placed and compacted behind an unyielding structure is not well defined. The focus of this research was to construct a full-scale MSE wall with an unyielding condition and investigate the resulting earth pressures that develop for such a case with a B/H = 0.3.

The research began by conducting a thorough literature review of current design practices and standards, and construction and quality control procedures. This ensured the constructed wall configurations adhered to the FDOT's standard specifications for road and bridge construction and complied with the AASHTO design code. This also ensured proper construction and sequencing took place to provide structures that were representative of the practice. From the literature review, AASHTO LRFD approved wall designs were developed for two wall configurations. Each wall configuration considered a different relative compaction effort. One wall implemented an under-compacted scenario with a relative compaction effort of 95% of the optimum dry density obtained from modified proctor (T-180) tests and the other wall configuration implemented an over-compacted scenario with a relative compaction effort of 103% of T-180. As a result, a wide range of compaction efforts commonly experienced in practice were investigated in a controlled manner for MSE walls that utilize inextensible reinforcement in an unyielding condition. Due to the necessary B/H ratio of 0.3 and limited overhead clearance in the University of Florida laboratory, a reaction frame loading system was also designed to simulate 23 feet of overburden that allowed the research to achieve the required B/H = 0.3.

Throughout the construction of the MSE walls, a significant amount of instrumentation was added within the investigated area to properly quantify the earth pressures that develop when typical MSE wall panels are mechanically fastened to an unyielding structure. During the research effort, 32 soil embedded EPCs were placed to measure the vertical earth pressure within the reinforced zone, 16 wall mounted EPCs were placed on the front MSE wall to measure the horizontal earth pressure that develops within the reinforced zone, 80 full bridge strain gauge locations were added to the reinforcement strips to measure the strip tension within the reinforced zone, 4 EPCs were placed underneath the leveling pads to quantify the down drag stresses that develop on the MSE wall panels from the confined loading, 2 draw wire sensors were attached to the exterior of the front MSE wall panels to monitor wall movement, and strain gauges were added to each of the six reaction frame threaded rods and set up in full bridge to monitor the reaction frame loads during surcharge loading. In total, 140 instrumented/monitored

locations were present within the investigated area. Each of these instruments were continuously logged after being added to the system.

During construction, earth pressure coefficients were derived for each compacted soil lift completed. Once the wall construction was complete, the reaction frame loading system was utilized to induce controlled incremental surcharge loads, and earth pressure coefficients were derived for each incremental surcharge load applied. The final surcharge loads provided the necessary  $B/H = 0.3$  for both compaction efforts to ensure the results were representative of the practice. After the surcharge load phase was complete, a force equilibrium analysis was performed for both compaction efforts that ensured all stresses and forces were accounted for with minimal error. The analyses and derived earth pressure coefficients were then determined valid for design recommendations.

From the derived earth pressure coefficients, it was observed that in an unyielding condition, the earth pressure moves from a passive condition to either an active or at-rest condition as the soil height increases above the reinforcement level. This is different from conventional MSE wall design and construction, where the earth pressure coefficients generally move from an at-rest condition to an active condition, and it was found that conventional design methods were inadequate to quantify the increased lateral stress that developed from the compaction effort in an unyielding condition. Consequently, a new equation was developed from the research that incorporates a variable friction angle ( $\phi$ ) based on the compaction effort for an unyielding condition, and FDOT design and construction requirements. When compared to the measured results, the new equation followed the trends of the data well.



# Table of Contents

Disclaimer .....	ii
SI (Modern Metric) Conversion Factors (from FHWA) Approximate Conversions to SI Units ..	iii
Technical Report Documentation Page .....	v
Acknowledgements.....	vi
Executive Summary .....	vii
List of Figures .....	xiv
List of Tables .....	xxi
1 Introduction and Background .....	1
1.1 Introduction.....	1
1.2 Background.....	1
2 Literature Review.....	4
2.1 Current Design Practices and Standards.....	4
2.1.1 External Stability .....	4
2.1.2 Internal Stability.....	4
2.1.3 Reinforcement – Inextensible and Extensible.....	4
2.2 Design Methods .....	6
2.2.1 National Concrete Masonry Association Procedure (NCMA) .....	6
2.2.2 Geosynthetic Reinforced Soil (GRS) Analysis Model .....	7
2.2.3 Tieback Wedge Method.....	7
2.2.4 Tieback FHWA Structure Stiffness Method.....	7
2.2.5 K-Stiffness Method.....	8
2.2.6 Coherent Gravity Method .....	11
2.2.7 The Simplified Method.....	13
3 Soil Testing and Design.....	15
3.1 Design Objectives, Requirements, and Site Preparation .....	15
3.1.1 List and Quantities of Instrumentation .....	20
3.1.2 Geometry.....	21
3.1.3 Loading Conditions.....	21
3.1.4 Performance Criteria.....	21
3.1.5 Maximum Tolerable Vertical Displacement.....	21
3.1.6 Maximum Tolerable Horizontal Displacement .....	22
3.1.7 Design Life.....	22
3.1.8 Construction and Quality Control Procedures .....	23

3.1.9	Construction Constraints.....	23
3.2	Project Parameters .....	23
3.2.1	Subsurface Conditions across the Site .....	23
3.2.2	Reinforced Wall Fill .....	23
3.2.3	Retained Backfill .....	24
3.3	Soil Properties.....	24
3.3.1	Sieve Analysis of Fine and Coarse Aggregates, AASHTO T-27 and FM 1-T011:..	24
3.3.2	Determining the Liquid Limit of Soils, AASHTO T-89, and Determining the Plastic Limit and Plasticity Index of Soils, AASHTO T-90: .....	24
3.3.3	Standard Method of Test for Specific Gravity of Soils, AASHTO T-100: .....	24
3.3.4	Determination of Organic Content by Loss of Ignition, AASHTO T-267: .....	25
3.3.5	Electrochemical Properties as Determined by FDOT FM 5-550 (pH in Soil and Water), FM 5-551 (Resistivity in Soil and Water), FM 5-552 (Chloride in Soil and Water), and FM 5-553 (Sulfate in Soil and Water): .....	25
3.3.6	Moisture-Density Relations of Soils, AASHTO T-180:.....	25
3.3.7	Direct Shear of Soils, AASHTO T-236: .....	25
3.3.8	Comments .....	25
3.4	Wall Embedment Depth, Design Height, and Reinforcement Length.....	26
3.5	Nominal Loads.....	26
3.6	Load Combinations, Load Factors, and Resistance Factors .....	28
3.7	External Stability Design .....	29
3.7.1	Sliding .....	30
3.7.2	Eccentricity .....	31
3.7.3	Bearing on Foundation Soil .....	32
3.7.4	Settlement Analysis .....	33
3.8	Internal Stability Design .....	34
3.8.1	Soil Reinforcement .....	34
3.8.2	Critical Failure Surface.....	36
3.8.3	Unfactored Loads.....	37
3.8.4	Vertical Layout of Soil Reinforcement.....	40
3.8.5	Factored Horizontal Stress and Maximum Tension (at each reinforcement level) ..	41
3.8.6	Nominal and Factored Long-term Tensile Resistance of Soil Reinforcements.....	42
3.8.7	Grade of Soil Reinforcement and Number of Soil Reinforcement Elements.....	44
3.8.8	Connection Resistance at MSE Wall Facing .....	45
3.8.9	Estimated Lateral Wall Movement (at service limit state) .....	50

3.8.10	Vertical Movement and Bearing Pads .....	50
3.9	Facing Elements.....	50
3.10	Internal Overall/Global Stabilityd.....	55
3.11	Compound Stability .....	55
3.12	Wall Drainage System .....	56
3.13	Simulated Surcharge Reaction Frame Design and Calculations.....	57
3.13.1	Method 1 .....	64
3.13.2	Force from Soil Box I-beams to Perpendicular Girders (103% compaction).....	64
3.13.3	Force from Soil Box I-beams to Perpendicular Girders (95% compaction).....	65
3.13.4	Method 2 .....	69
3.13.5	Tributary Area for Soilbox I-Beams (Method 2).....	69
3.13.6	Force from Soil Box I-beams to Perpendicular Girders (103% compaction).....	70
3.13.7	Force from Soil Box I-beams to Perpendicular Girders (95% compaction).....	70
3.13.8	Maximum Moments and Deflections.....	74
3.13.9	Steel Selection and Connection Details .....	74
3.13.10	Reaction Frame Connection Details .....	76
3.13.11	Strong Floor Connection Details .....	77
3.13.12	Bolts Connecting Floor Plates .....	77
3.13.13	Dwyidag Threaded Rod Selection .....	78
4	MSE Wall Construction.....	79
4.1	Design Construction Sequencing.....	79
4.2	Instrumentation .....	108
5	Construction Analysis.....	120
5.1	Nuclear Density Results.....	120
5.2	Construction Analysis.....	127
5.3	Row 1 Construction Analysis .....	127
5.3.1	Row 1 Vertical Earth Pressure.....	128
5.3.2	Row 1 Horizontal Earth Pressure.....	131
5.3.3	Row 1 Reinforcement Strip Tension.....	132
5.3.4	Row 1 Average Earth Pressures and Strip Tension .....	136
5.3.5	Row 1 Construction Earth Pressure Coefficient Analysis – 95% of T-180.....	137
5.3.6	Row 1 Construction Earth Pressure Coefficient Analysis – 103% of T-180.....	140
5.4	Row 2 Construction Analysis .....	143
5.4.1	Row 2 Vertical Earth Pressure.....	143

5.4.2	Row 2 Horizontal Earth Pressure.....	146
5.4.3	Row 2 Reinforcement Strip Tension.....	147
5.4.4	Row 2 Average Earth Pressures and Strip Tension .....	150
5.4.5	Row 2 Construction Earth Pressure Coefficient Analysis – 95% of T-180.....	151
5.4.6	Row 2 Construction Earth Pressure Coefficient Analysis – 103% of T-180.....	153
5.5	Row 3 Construction Analysis .....	156
5.5.1	Row 3 Vertical Earth Pressure.....	156
5.5.2	Row 3 Horizontal Earth Pressure.....	159
5.5.3	Row 3 Reinforcement Strip Tension.....	161
5.5.4	Row 3 Average Earth Pressures and Strip Tension .....	165
5.5.5	Row 3 Construction Earth Pressure Coefficient Analysis – 95% of T-180.....	166
5.5.6	Row 3 Construction Earth Pressure Coefficient Analysis – 103% of T-180.....	168
5.6	Row 4 Construction Analysis .....	170
5.6.1	Row 4 Vertical Earth Pressure.....	170
5.6.2	Row 4 Horizontal Earth Pressure.....	173
5.6.3	Row 4 Reinforcement Strip Tension.....	175
5.6.4	Row 4 Average Earth Pressures and Strip Tension .....	179
5.6.5	Row 4 Construction Earth Pressure Coefficient Analysis – 95% of T-180.....	180
5.6.6	Row 4 Construction Earth Pressure Coefficient Analysis – 103% of T-180.....	182
5.7	Leveling Pad EPC Construction Analysis .....	184
5.8	Earth Pressure Coefficient Construction Analysis.....	187
6	Simulated Earth Surcharge and Deriving Earth Pressure Coefficients.....	194
6.1	Simulated Earth Surcharge .....	194
6.2	Simulated Earth Surcharge Observations – 95% of T-180.....	198
6.2.1	Row 1 Analysis.....	198
6.2.2	Row 2 Analysis.....	200
6.2.3	Row 3 Analysis.....	202
6.2.4	Row 4 Analysis.....	204
6.3	Simulated Earth Surcharge Observations – 103% of T-180.....	206
6.3.1	Row 1 Analysis.....	206
6.3.2	Row 2 Analysis.....	208
6.3.3	Row 3 Analysis.....	210
6.3.4	Row 4 Analysis.....	212
6.4	Force Equilibrium Analysis .....	214

6.5	Derived Earth Pressure Coefficients and Design Recommendations .....	219
6.5.1	Derived Earth Pressure Coefficients.....	219
6.5.2	Design Recommendations for Soil Pressure Against Unyielding Surfaces.....	221
7	Conclusions.....	229
8	Recommendations.....	231
9	References.....	232

## List of Figures

Figure 1-1. Lateral stress ratio $k_r/k_a$ for internal stability of MSE walls (AASHTO LRFD Bridge Design Specifications, Seventh Edition).....	2
Figure 1-2. MSE wall embankment widening scenario.....	2
Figure 2-1. Inextensible reinforcement, bilinear failure plane (Anderson et al., 2010). ....	5
Figure 2-2. Extensible reinforcement, Rankine failure plane (Anderson et al, 2010). ....	6
Figure 2-3. $D_{t_{max}}$ as a function of normalized depth below wall top plus average surcharge depth. ....	11
Figure 2-4. Coherent Gravity Method. ....	12
Figure 2-5. Forces for calculating the vertical stress distribution in MSE walls.....	13
Figure 2-6. Determination of $k_r/k_a$ for the Simplified Method (AASHTO, 1999). ....	14
Figure 3-1. MSE wall configuration (Note: Right side Strong Wall and reinforced fill are not depicted for visualization of the reinforcements and instrumentation). ....	16
Figure 3-2. Back-to-back wall construction displaying embedded and clip angle connections that will both be mechanically fastened to the respective reinforcement. ....	17
Figure 3-3. MSE wall configuration in profile view, indicating the tributary wall areas.....	18
Figure 3-4. MSE wall configuration in plan view. ....	20
Figure 3-5. Nominal MSE wall earth pressures for horizontal back slopes. ....	27
Figure 3-6. MSE-Strong Wall configuration with surcharge loading (Note: Right side Strong Wall is not depicted). ....	28
Figure 3-7. External failure mechanisms for an MSE wall. ....	30
Figure 3-8. Determination of $k_r/k_a$ for the Simplified Method (AASHTO, 1999). ....	34
Figure 3-9. Coherent Gravity Method. ....	35
Figure 3-10. Narrow MSE wall in front of a stabilized face (Kniss et al. 2007).....	35
Figure 3-11. Bilinear critical slip surface. ....	36
Figure 3-12. Depth vs. unfactored lateral earth pressure for $k$ coefficients @ 95% of T-180.....	38
Figure 3-13. Depth vs. unfactored lateral earth pressure for $k$ coefficients @ 104% of T-180....	39
Figure 3-14. Vertical reinforcement layout. ....	41
Figure 3-15. RECo panel strip connection detail.....	46
Figure 3-16. Square panel – Type A. ....	51
Figure 3-17. Reinforcing strip and connection to tie strip. ....	52
Figure 3-18. Clip angle details.....	53
Figure 3-19. High adherence ribbed reinforcing strip. ....	54
Figure 3-20. Global and compound stability (Figure 6.3.3; RECo, 2011). ....	55
Figure 3-21. Matjack-airbag system, overburden detail 1. ....	58
Figure 3-22. Soil areas attributed to Matjacks 95% compaction effort.....	59
Figure 3-23. Soil areas attributed to Matjacks 103% compaction effort. ....	59
Figure 3-24. Calculated pressures for each Matjack to induce the required surcharge. ....	60
Figure 3-25. Reaction frame tied into Strong Floor.....	61
Figure 3-26. Method 1 – I-beam tributary areas. ....	64
Figure 3-27. Calculated forces for right-side compaction of 103% (Method 1). ....	67
Figure 3-28. Calculated forces for left-side compaction of 95% (Method 1).....	67
Figure 3-29. Visual Analysis with Matjack forces applied (Method 1). ....	68
Figure 3-30. Visual Analysis reaction forces derived for Dwyidag tie-ins (Method 1). ....	68
Figure 3-31. Calculated forces for right-side compaction of 103% (Method 2). ....	72

Figure 3-32. Calculated forces for right-side compaction of 95% (Method 2). .....	72
Figure 3-33. Visual Analysis with Matjack forces applied (Method 2). .....	73
Figure 3-34. Visual Analysis reaction forces derived for Dwyidag tie-ins (Method 2). .....	73
Figure 3-35. Moments and deflections for right-side compaction of 103%. .....	74
Figure 3-36. Moments and deflections for right-side compaction of 95%. .....	74
Figure 3-37. Side connections (non-moment connection). .....	76
Figure 3-38. Center connections (non-moment connection). .....	76
Figure 3-39. Steel plates and hardware for Strong Floor connections. ....	77
Figure 3-40. Dywidag Threadbar Properties with #14 and #18 indicated. ....	78
Figure 4-1. Constructing forms to cast base layer retaining concrete blocks. ....	79
Figure 4-2. Retaining blocks mechanically fastened to strong floor. ....	80
Figure 4-3. EPDM rubber placed throughout the research area to protect metal tie-ins. ....	80
Figure 4-4. Structural geotextile placed and threaded rods mechanically fastened to strong floor. ....	81
Figure 4-5. Crane lifting soil bags with gravel into the wall area and compacting the gravel layer. ....	81
Figure 4-6. Base layer soil placement. ....	82
Figure 4-7. Base layer soil compaction and nuclear density testing. ....	83
Figure 4-8. Placing EPCs under leveling pad locations and testing using handheld readout. ....	84
Figure 4-9. Building steel reinforced leveling pad forms and casting concrete. ....	85
Figure 4-10. Smoothing out imperfections on the leveling pads with a grinder. ....	85
Figure 4-11. Cutting trenches in the base layer for leveling pads and placing the leveling pads. ....	86
Figure 4-12. Placing first course of MSE wall panels, temporary bracing, and checking plumbness. ....	86
Figure 4-13. First course of MSE wall panels completed. ....	87
Figure 4-14. Checking the level of the backside MSE panels between the two compaction sides. ....	88
Figure 4-15. Checking the level of frontside MSE panels between the two compaction sides. ....	88
Figure 4-16. Checking the level of the front and back MSE panels. ....	89
Figure 4-17. Constructing the frame for the compaction effort divider. ....	90
Figure 4-18. Compaction effort divider first level complete. ....	90
Figure 4-19. Back MSE wall prior to the first lift above the base layer. ....	91
Figure 4-20. Front MSE wall prior to the first lift above the base layer. ....	91
Figure 4-21. Soil compaction prior to installing the first row of reinforcement strips. ....	92
Figure 4-22. Soil compacted and leveled prior to installing the first row of reinforcement strips. ....	93
Figure 4-23. Frist row of reinforcement strips with filter cloth placed in the joints of wall panels. ....	94
Figure 4-24. Front MSE wall with fatback EPCs mounted to measure horizontal earth pressure. ....	95
Figure 4-25. Running instrumentation cables through the divider wall. ....	95
Figure 4-26. Labeled instrumentation cables running through the divider wall to the multiplexer. ....	96
Figure 4-27. Additional temporary bracing added to control front MSE wall movement. ....	96
Figure 4-28. Temporary wall bracing, spacers, wedges, and clamps in place. ....	97
Figure 4-29. Adding the second course of MSE wall panels. ....	98

Figure 4-30. Adding the third course of MSE wall panels. ....	99
Figure 4-31. Adding the final course of MSE wall panels. ....	100
Figure 4-32. Temporary wall bracing removed after completing wall construction. ....	101
Figure 4-33. Overview of MSE wall area. ....	102
Figure 4-34. Matjack airbag system in place on the 95% compaction effort side. ....	103
Figure 4-35. Matjack airbag system in place on the 103% compaction effort side. ....	104
Figure 4-36. Crane lifting the first soil box wall in place. ....	105
Figure 4-37. First soil box wall in place, resting on matjack system. ....	106
Figure 4-38. C-channels added and secured in place to complete the matjack reaction frame. .	107
Figure 4-39. MSE wall with reaction frame in place. ....	108
Figure 4-40. Geokon splice kit. ....	109
Figure 4-41. EPC test box for calibration after splicing was completed. ....	110
Figure 4-42. Load testing a soil embedded EPC for calibration. ....	110
Figure 4-43. Installing strain gauges, moisture coating, and rugged coating on reinforcement strips. ....	111
Figure 4-44. Load testing reinforcement strips to develop individual calibration curves. ....	112
Figure 4-45. Calibration curves prior to adding moisture and protective coating. ....	112
Figure 4-46. Calibration curves after adding moisture and protective coating. ....	113
Figure 4-47. Strip tension vs. time using direct multiplexer system prior to loading. ....	114
Figure 4-48. Voltage vs. settling time indicating stabilization was never achieved. ....	115
Figure 4-49. CR6 tiered multiplexer wiring diagram to resolve voltage settling issues. ....	116
Figure 4-50. Voltage vs. settling time indicating stabilization was achieved using tiered system. ....	117
Figure 4-51. Strip tension vs. time using tiered multiplexer system prior to loading. ....	117
Figure 4-52. CR10x wiring diagram. ....	118
Figure 4-53. Draw wire sensor attached to base MSE wall panel to measure wall movement. .	119
Figure 4-54. Draw wire sensor protective enclosure. ....	119
Figure 5-1. MSE wall area plan view of quadrants for nuclear density testing. ....	120
Figure 5-2. Nuclear density vertical earth pressure vs. soil height for 95% compaction effort side. ....	126
Figure 5-3. Nuclear density vertical earth pressure vs. soil height for 103% compaction effort side. ....	126
Figure 5-4. Row 1 – 95% compaction EPC vertical earth pressure vs. depth. ....	128
Figure 5-5. Row 1 – 103% compaction EPC vertical earth pressure vs. depth. ....	129
Figure 5-6. Row 1 – 95% compaction EPC earth pressure compared to nuclear density. ....	130
Figure 5-7. Row 1 – 103% compaction EPC earth pressure compared to nuclear density. ....	130
Figure 5-8. Row 1 – 95% compaction EPC horizontal earth pressure vs. depth. ....	131
Figure 5-9. Row 1 – 103% compaction EPC horizontal earth pressure vs. depth. ....	132
Figure 5-10. Row 1 – Column 1 - 95% compaction reinforcement strip tension vs. depth. ....	133
Figure 5-11. Row 1 – Column 2 - 95% compaction reinforcement strip tension vs. depth. ....	133
Figure 5-12. Row 1 – 95% compaction average reinforcement strip tension vs. depth. ....	134
Figure 5-13. Row 1 – Column 3 - 103% compaction reinforcement strip tension vs. depth. ....	134
Figure 5-14. Row 1 – Column 4 - 103% compaction reinforcement strip tension vs. depth. ....	135
Figure 5-15. Row 1 – 103% compaction average reinforcement strip tension vs. depth. ....	135
Figure 5-16. Row 1 – 95% compaction vertical and horizontal stress and strip tension vs. depth. ....	136



Figure 5-17. Row 1 – 103% compaction vertical and horizontal stress and strip tension vs. depth.	137
Figure 5-18. Row 1 – 95% compaction earth pressure coefficients from EPCs.....	138
Figure 5-19. Row 1 – 95% compaction earth pressure coefficients from reinforcement strips.	138
Figure 5-20. Comparing Row 1 – 95% compaction $k_h$ using vertical stress from EPCs.....	139
Figure 5-21. Comparing Row 1 – 95% compaction $k_h$ using vertical stress from nuclear density.	139
Figure 5-22. Row 1 – 103% compaction earth pressure coefficients from EPCs.....	140
Figure 5-23. Row 1 – 103% compaction earth pressure coefficients from reinforcement strips.	141
Figure 5-24. Comparing Row 1 – 103% compaction $k_h$ using vertical stress from EPCs.....	141
Figure 5-25. Comparing Row 1 – 103% compaction $k_h$ using vertical stress from nuclear density.	142
Figure 5-26. Row 2 – 95% compaction EPC vertical earth pressure vs. depth. ....	143
Figure 5-27. Row 2 – 103% compaction EPC vertical earth pressure vs. depth. ....	144
Figure 5-28. Row 2 – 95% compaction EPC earth pressure compared to nuclear density. ....	144
Figure 5-29. Row 2 – 103% compaction EPC earth pressure compared to nuclear density. ....	145
Figure 5-30. Row 2 – 95% compaction EPC horizontal earth pressure vs. depth. ....	146
Figure 5-31. Row 2 – 103% compaction EPC horizontal earth pressure vs. depth. ....	146
Figure 5-32. Row 2 – Column 1 - 95% compaction reinforcement strip tension vs. depth. ....	147
Figure 5-33. Row 2 – Column 2 - 95% compaction reinforcement strip tension vs. depth. ....	147
Figure 5-34. Row 2 – 95% compaction average reinforcement strip tension vs. depth. ....	148
Figure 5-35. Row 2 – Column 3 - 103% compaction reinforcement strip tension vs. depth. ....	148
Figure 5-36. Row 2 – Column 4 - 103% compaction reinforcement strip tension vs. depth. ....	149
Figure 5-37. Row 2 – 103% compaction average reinforcement strip tension vs. depth. ....	149
Figure 5-38. Row 2 – 95% compaction vertical and horizontal stress and strip tension vs. depth.	150
Figure 5-39. Row 2 – 103% compaction vertical and horizontal stress and strip tension vs. depth.	150
Figure 5-40. Row 2 – 95% compaction earth pressure coefficients from EPCs.....	151
Figure 5-41. Row 2 – 95% compaction earth pressure coefficients from reinforcement strips. .	151
Figure 5-42. Comparing Row 2 – 95% compaction $k_h$ using vertical stress from EPCs.....	152
Figure 5-43. Comparing Row 2 – 95% compaction $k_h$ using vertical stress from nuclear density.	152
Figure 5-44. Row 2 – 103% compaction earth pressure coefficients from EPCs.....	153
Figure 5-45. Row 2 – 103% compaction earth pressure coefficients from reinforcement strips.	154
Figure 5-46. Comparing Row 2 – 103% compaction $k_h$ using vertical stress from EPCs.....	154
Figure 5-47. Comparing Row 2 – 103% compaction $k_h$ using vertical stress from nuclear density.	155
Figure 5-48. Row 3 – 95% compaction EPC vertical earth pressure vs. depth. ....	156
Figure 5-49. Row 3 – 103% compaction EPC vertical earth pressure vs. depth. ....	157
Figure 5-50. Row 3 – 95% compaction EPC earth pressure compared to nuclear density. ....	157
Figure 5-51. Row 3 – 103% compaction EPC earth pressure compared to nuclear density. ....	158
Figure 5-52. Row 3 – 95% compaction EPC horizontal earth pressure vs. depth. ....	159
Figure 5-53. Row 3 – 103% compaction EPC horizontal earth pressure vs. depth. ....	160

Figure 5-54. Row 3 – Column 1 - 95% compaction reinforcement strip tension vs. depth. ....	161
Figure 5-55. Row 3 – Column 2 - 95% compaction reinforcement strip tension vs. depth. ....	162
Figure 5-56. Row 3 – 95% compaction average reinforcement strip tension vs. depth. ....	162
Figure 5-57. Row 3 – Column 3 - 103% compaction reinforcement strip tension vs. depth. ....	163
Figure 5-58. Row 3 – Column 4 - 103% compaction reinforcement strip tension vs. depth. ....	163
Figure 5-59. Row 3 – 103% compaction average reinforcement strip tension vs. depth. ....	164
Figure 5-60. Row 3 – 95% compaction vertical and horizontal stress and strip tension vs. depth. .....	165
Figure 5-61. Row 3 – 103% compaction vertical and horizontal stress and strip tension vs. depth. .....	165
Figure 5-62. Row 3 – 95% compaction earth pressure coefficients from EPCs.....	166
Figure 5-63. Row 3 – 95% compaction earth pressure coefficients from reinforcement strips.	166
Figure 5-64. Comparing Row 3 – 95% compaction $k_h$ using vertical stress from EPCs.....	167
Figure 5-65. Comparing Row 3 – 95% compaction $k_h$ using vertical stress from nuclear density. .....	167
Figure 5-66. Row 3 – 103% compaction earth pressure coefficients from EPCs.....	168
Figure 5-67. Row 3 – 103% compaction earth pressure coefficients from reinforcement strips. .....	168
Figure 5-68. Comparing Row 3 – 103% compaction $k_h$ using vertical stress from EPCs.....	169
Figure 5-69. Comparing Row 3 – 103% compaction $k_h$ using vertical stress from nuclear density. .....	169
Figure 5-70. Row 4 – 95% compaction EPC vertical earth pressure vs. depth. ....	170
Figure 5-71. Row 4 – 103% compaction EPC vertical earth pressure vs. depth. ....	171
Figure 5-72. Row 4 – 95% compaction EPC earth pressure compared to nuclear density. ....	171
Figure 5-73. Row 4 – 103% compaction EPC earth pressure compared to nuclear density. ....	172
Figure 5-74. Row 4 – 95% compaction EPC horizontal earth pressure vs. depth. ....	173
Figure 5-75. Row 4 – 103% compaction EPC horizontal earth pressure vs. depth. ....	174
Figure 5-76. Row 4 – Column 1 - 95% compaction reinforcement strip tension vs. depth. ....	175
Figure 5-77. Row 4 – Column 2 - 95% compaction reinforcement strip tension vs. depth. ....	176
Figure 5-78. Row 4 – 95% compaction average reinforcement strip tension vs. depth. ....	176
Figure 5-79. Row 4 – Column 3 - 103% compaction reinforcement strip tension vs. depth. ....	177
Figure 5-80. Row 4 – Column 4 - 103% compaction reinforcement strip tension vs. depth. ....	177
Figure 5-81. Row 4 – 103% compaction average reinforcement strip tension vs. depth. ....	178
Figure 5-82. Row 4 – 95% compaction vertical and horizontal stress and strip tension vs. depth. .....	179
Figure 5-83. Row 4 – 103% compaction vertical and horizontal stress and strip tension vs. depth. .....	179
Figure 5-84. Row 4 – 95% compaction earth pressure coefficients from EPCs.....	180
Figure 5-85. Row 4 – 95% compaction earth pressure coefficients from reinforcement strips.	180
Figure 5-86. Comparing Row 4 – 95% compaction $k_h$ using vertical stress from EPCs.....	181
Figure 5-87. Comparing Row 4 – 95% compaction $k_h$ using vertical stress from nuclear density. .....	181
Figure 5-88. Row 4 – 103% compaction earth pressure coefficients from EPCs.....	182
Figure 5-89. Row 4 – 103% compaction earth pressure coefficients from reinforcement strips. .....	182
Figure 5-90. Comparing Row 4 – 103% compaction $k_h$ using vertical stress from EPCs.....	183

Figure 5-91. Comparing Row 4 – 103% compaction $k_h$ using vertical stress from EPCs.....	183
Figure 5-92. EPC vertical earth pressures under the leveling pads vs. depth. ....	185
Figure 5-93. 95% compaction leveling pad pressures compared to the soil and wall weight. ..	185
Figure 5-94. 103% compaction leveling pad pressures compared to the soil and wall weight. .	186
Figure 5-95. Wall displacement on the 95% of T-180 side. ....	186
Figure 5-96. Wall displacement on the 103% of T-180 side. ....	187
Figure 5-97. Comparing 95% of T-180 earth pressure coefficients from EPCs and strips vs. depth.....	188
Figure 5-98. Comparing 103% of T-180 earth pressure coefficients from EPCs and strips vs. depth.....	188
Figure 5-99. All earth pressure coefficients from EPCs and strips vs. depth. ....	189
Figure 5-100. Average earth pressure coefficients as a function of depth including EPCs and strips.....	189
Figure 5-101. 95% compaction earth pressure coefficients from EPCs vs. depth.....	191
Figure 5-102. 95% of T-180 EPC average earth pressure coefficients as a function of depth. ..	191
Figure 5-103. 103% compaction earth pressure coefficients from EPCs vs. depth.....	192
Figure 5-104. 103% of T-180 EPC average earth pressure coefficients as a function of depth. 192	192
Figure 5-105. Comparing Row 1 earth pressure coefficients vs. depth.....	193
Figure 5-106.. Row 1 average earth pressure coefficients as a function of depth. ....	193
Figure 6-1. Matjack system manifold with six bays. ....	194
Figure 6-2. Matjack failures on the 103% side during simulated surcharge Phases 1, 2, and 3. 195	195
Figure 6-3. Depth profiles of applied and measured vertical earth pressure on the 95% side....	197
Figure 6-4. Depth profiles of applied and measured vertical earth pressure on the 103% side..	197
Figure 6-5. Depth profiles of earth pressure and strip tension at Row 1 on the 95% side.....	198
Figure 6-6. Depth profiles of earth pressure and wall displacement at Row 1 on the 95% side. 199	199
Figure 6-7. Depth profiles of earth pressure and pressure coefficients at Row 1 on the 95% side. ....	199
Figure 6-8. Depth profiles of earth pressure and strip tension at Row 2 on the 95% side.....	200
Figure 6-9. Depth profiles of earth pressure and wall displacement at Row 2 on the 95% side. 201	201
Figure 6-10. Depth profiles of earth pressure and pressure coefficients at Row 2 on the 95% side. ....	201
Figure 6-11. Depth profiles of earth pressure and strip tension at Row 3 on the 95% side.....	202
Figure 6-12. Depth profiles of earth pressure and wall displacement at Row 3 on the 95% side. ....	203
Figure 6-13. Depth profiles of earth pressure and pressure coefficients at Row 3 on the 95% side. ....	203
Figure 6-14. Depth profiles of earth pressure and strip tension at Row 4 on the 95% side.....	204
Figure 6-15. Depth profiles of earth pressure and wall displacement at Row 4 on the 95% side. ....	205
Figure 6-16. Depth profiles of earth pressure and pressure coefficients at Row 4 on the 95% side. ....	205
Figure 6-17. Depth profiles of earth pressure and strip tension at Row 1 on the 103% side.....	207
Figure 6-18. Depth profiles of earth pressure and wall displacement at Row 1 on the 103% side. ....	207
Figure 6-19. Depth profiles of earth pressure and pressure coefficients at Row 1 on the 103% side. ....	208

Figure 6-20. Depth profiles of earth pressure and strip tension at Row 2 on the 103% side.....	209
Figure 6-21. Depth profiles of earth pressure and wall displacement at Row 2 on the 103% side. .....	209
Figure 6-22. Depth profiles of earth pressure and pressure coefficients at Row 2 on the 103% side. ....	210
Figure 6-23. Depth profiles of earth pressure and strip tension at Row 3 on the 103% side.....	211
Figure 6-24. Depth profiles of earth pressure and wall displacement at Row 3 on the 103% side. .....	211
Figure 6-25. Depth profiles of earth pressure and pressure coefficients at Row 3 on the 103% side. ....	212
Figure 6-26. Depth profiles of earth pressure and strip tension at Row 4 on the 103% side.....	213
Figure 6-27. Depth profiles of earth pressure and wall displacement at Row 4 on the 103% side. .....	213
Figure 6-28. Depth profiles of earth pressure and pressure coefficients at Row 4 on the 103% side. ....	214
Figure 6-29. Force equilibrium diagram. ....	215
Figure 6-30. Depth profiles of leveling pad pressure and wall displacement on the 95% side..	216
Figure 6-31. Depth profiles of leveling pad pressure and wall displacement on the 103% side.	216
Figure 6-32. Depth profiles of earth pressure coefficients for 95% of T-180. ....	220
Figure 6-33. Depth profiles of earth pressure coefficients for 103% of T-180. ....	220
Figure 6-34. Depth profiles of earth pressure coefficients compared to the Coherent Gravity Method. ....	221
Figure 6-35. Depth profiles of earth pressure coefficients compared to the Simplified Method. .....	222
Figure 6-36. Depth profiles of earth pressure coefficients compared to Spangler & Handy's Method. ....	222
Figure 6-37. Depth profiles of earth pressure coefficients compared to the UF $k_p$ - $k_a$ equation with a $k_a$ cutoff applied. ....	225
Figure 6-38. Depth profiles of earth pressure coefficients compared to the UF $k_p$ - $k_0$ equation with a $k_0$ cutoff applied. ....	226
Figure 6-39. $k_p$ - $k_0$ equation with $z = 20$ feet compared to strip tension derived earth pressure coefficients. ....	227
Figure 6-40. $k_p$ - $k_0$ equation with $z = 9.84$ feet compared to strip tension derived earth pressure coefficients. ....	228

## List of Tables

Table 3-1. Relationship between joint width and limiting differential settlements for MSE precast panels (AASHTO, 2007; C11.10.4.1).....	22
Table 3-2. Sieve analysis and AASHTO requirements. ....	24
Table 3-3. LRFD load factors. ....	29
Table 3-4. LRFD load factors. ....	29
Table 3-5. External stability resistance factors for MSE walls.....	30
Table 3-6. Bearing resistance factors (Table 10.6.3.1.2a-1; AASHTO, 2007).....	33
Table 3-7. Unfactored vertical and horizontal earth pressures @ 95% of T-180. ....	38
Table 3-8. Unfactored vertical and horizontal earth pressures at 104% of T-180.....	39
Table 3-9. O’steen Soil Electrochemical Properties with Acceptance Criteria. ....	43
Table 3-10. Resistance factors, $\phi$ , for tensile and pullout resistance for MSE walls. ....	44
Table 3-11. Connection detail mechanical properties.....	47
Table 3-12. Resistance components summary.....	48
Table 3-13. Connection strength stability check for 95% of T-180 (Simplified Method). ....	48
Table 3-14. Connection strength stability check for 95% of T-180 (Coherent Gravity Method). ....	48
Table 3-15. Connection strength stability check for 95% of T-180 (At-rest condition).....	48
Table 3-16. Connection strength stability check for 95% of T-180 (Active state).....	48
Table 3-17. Connection strength stability check for 95% of T-180 (Spangler and Handy Method). .....	49
Table 3-18. Connection strength stability check for 104% of T-180 (Simplified Method). ....	49
Table 3-19. Connection strength stability check for 104% of T-180 (Coherent Gravity Method). .....	49
Table 3-20. Connection strength stability check for 104% of T-180 (At-rest condition).....	49
Table 3-21. Connection strength stability check for 104% of T-180 (Active state).....	49
Table 3-22. Connection strength stability check for 104% of T-180 (Spangler and Handy Method).....	49
Table 3-23. No. 89 Gradation summary comparing FDOT specifications with select aggregate. ....	56
Table 3-24. Geotextile test methods and requirements.....	57
Table 3-25. W-Shapes – Available Moment vs. Unbraced Length of 8’-6”. ....	75
Table 5-1. Nuclear density results for soil lift 1 located in the base layer.....	120
Table 5-2. Nuclear density results for soil lift 2 located in the base layer.....	120
Table 5-3. Nuclear density results for soil lift 3 located in the base layer.....	121
Table 5-4. Nuclear density results for soil lift 4 located in the reinforced zone of the soil.....	121
Table 5-5. Nuclear density results for soil lift 5 located in the reinforced zone of the soil.....	121
Table 5-6. Nuclear density results for soil lift 6 located in the reinforced zone of the soil.....	121
Table 5-7. Nuclear density results for soil lift 7 located in the reinforced zone of the soil.....	122
Table 5-8. Nuclear density results for soil lift 8 located in the reinforced zone of the soil.....	122
Table 5-9. Nuclear density results for soil lift 9 located in the reinforced zone of the soil.....	122
Table 5-10. Nuclear density results for soil lift 10 located in the reinforced zone of the soil....	122
Table 5-11. Nuclear density results for soil lift 11 located in the reinforced zone of the soil....	123
Table 5-12. Nuclear density results for soil lift 12 located in the reinforced zone of the soil....	123
Table 5-13. Nuclear density results for soil lift 13 located in the reinforced zone of the soil....	123
Table 5-14. Nuclear density results for soil lift 14 located in the reinforced zone of the soil....	123
Table 5-15. Nuclear density results for soil lift 15 located in the reinforced zone of the soil....	124

Table 5-16. Nuclear density results for soil lift 16 located in the reinforced zone of the soil....	124
Table 5-17. Nuclear density results for soil lift 17 located in the reinforced zone of the soil....	124
Table 5-18. Nuclear density results for soil lift 18 located in the reinforced zone of the soil....	124
Table 5-19. Nuclear density results for soil lift 19 located in the reinforced zone of the soil....	125
Table 5-20. Nuclear density results for soil lift 20 located in the reinforced zone of the soil....	125
Table 5-21. Nuclear density results for soil lift 21 located in the reinforced zone of the soil....	125
Table 5-22. Nuclear density results for soil lift 22 located in the reinforced zone of the soil....	125
Table 5-23. Summary of average soil compaction between MSE wall reinforcement levels. ....	127
Table 6-1. Simulated surcharge loading results for 95% of T-180.....	195
Table 6-2. Simulated surcharge loading results for 103% of T-180.....	196

# 1 Introduction and Background

## 1.1 Introduction

Reinforced earth retaining walls, or mechanically stabilized earth (MSE) walls, are generally a cost-effective option to meet the demands of earth retention systems for bridge abutments, highway separations, and when construction space is limited. The use of reinforced earth for retaining structures involves reinforcing strips or grids of either metallic or geosynthetic material, placed between layers of compacted soil and mechanically attached to the wall facing. The wall facing itself is typically precast concrete with a positive connection mechanism that attaches to the reinforcement. The lateral earth pressures exerted on the facing wall by the granular backfill are opposed by the frictional resistance developed along the surface of the reinforcement.

## 1.2 Background

In general design, the lateral earth pressure imposed on an MSE wall reinforced fill is approximately equal to the active lateral pressure developed in conventional earth pressure theory, which applies to most cases where the back end of the reinforcement is not attached to any structure and is free to move. For internal stability analysis, a lateral earth pressure coefficient “ $k_r$ ” is utilized, as per Figure 1-1 below. In some instances, such as acute corners and road widening conditions when the base (distance from new wall panels to existing wall panels or a structure) to wall height (B/H) ratio is equal to or less than 0.3, MSE wall reinforcements are directly tied to an existing MSE wall or structure, generating an unyielding condition. The actual soil pressure that results from material placed and compacted behind an unyielding surface is not well defined. For example, the current design recommendations for MSE walls in FHWA Geotechnical Engineering Circular, GEC, number 11 (FHWA-NHI-10-024), acknowledges that “much higher” soil reinforcement tension develops when back-to-back walls are tied to each other. These added stresses occur because stress relief through minor deformation of the retaining structure that typically occurs in conventional construction, is prevented by connecting the walls, e.g., construction of roadway embankment widening where the new wall is tied to the existing structure as shown in Figure 1-2.

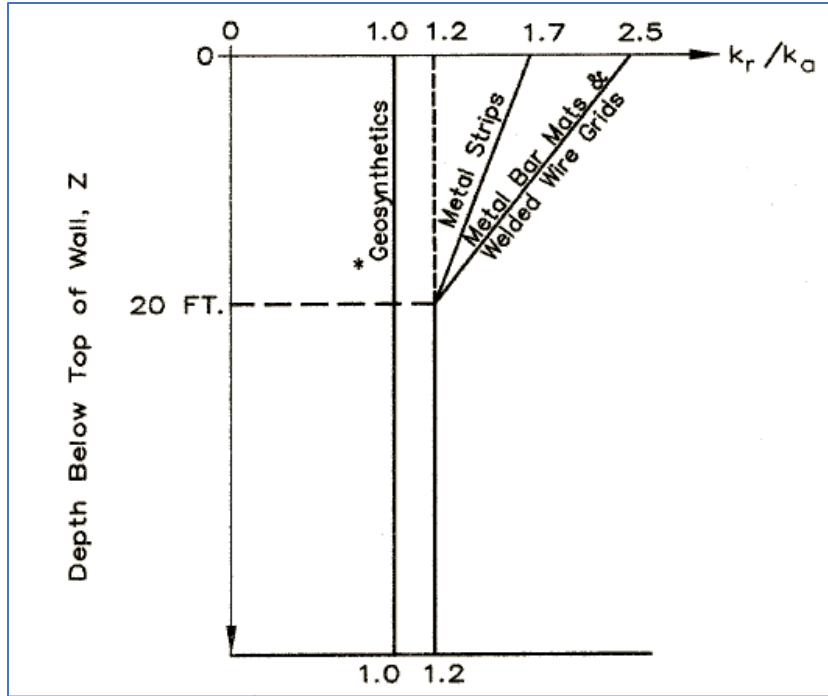


Figure 1-1. Lateral stress ratio  $k_r/k_a$  for internal stability of MSE walls (AASHTO LRFD Bridge Design Specifications, Seventh Edition)



Figure 1-2. MSE wall embankment widening scenario.

While GEC # 11 recognizes the problem, it does not provide a clear recommendation for the estimation of soil pressure of compacted soils, and simply states that higher stresses are to be expected at the connection. The common notion that at-rest stresses apply seemed to be valid



only for cases where the soil is not well compacted, and the assumption of passive conditions for compacted soils appeared to be likely over-conservative. Therefore, the MSE wall scenario presented needed to be constructed in a controlled environment and the resulting earth pressure coefficients needed to be investigated. The empirical results and numerical methods developed would then provide increased accuracy in geotechnical design and could be applied to MSE walls with acute corners, widening conditions where a new wall is tied to the existing wall, and other scenarios where fill is placed and compacted against any unyielding structure. The objective of this research was to investigate the resulting earth pressure coefficients derived from an approved MSE wall configuration for a wide range of soil density with a B/H ratio of 0.3 or less, which is when inextensible MSE wall reinforcement would be tied to an unyielding structure in practice.

## 2 Literature Review

### 2.1 Current Design Practices and Standards

The design of MSE Walls requires sizing the reinforced mass (reinforced fill) to resist external loads from the retained soil (retained backfill) and surcharges, then verifying internal stability by checking the reinforcement for pullout and tensile failure. The reinforced fill is the fill material in which the reinforcements are placed and the retained backfill is the fill material located behind the mechanically stabilized soil zone.

#### 2.1.1 External Stability

External stability considers three modes of failure: sliding, overturning, and bearing capacity. During external stability analyses, the reinforced mass is assumed to behave as a rigid body and the same procedures employed for conventional gravity-type walls systems are instituted (Chalermyanont and Benson, 2005). External forces imposed on the rigid reinforced mass by the retained soil and/or surcharge loading are considered during the analyses. However, external forces from surcharge loading cannot be used improve the reliability of the structure, as these forces may be temporary. External factors of safety for Allowable Stress Design (ASD) are generally as follows:

Sliding  $\geq 1.5$

Limiting Eccentricity (Overturning)  $\geq 2.0$

Bearing Resistance  $\geq 2.5$

Overall/global stability  $\geq 1.5$

#### 2.1.2 Internal Stability

The internal stability of MSE walls considers two modes of failure, pullout and structural failure of the reinforcement (AASHTO 11.10.6.1). For internal stability analyses, the effective lateral earth pressure is calculated at each reinforcement level within the reinforced soil mass and considers all forces at the specified elevation. The lateral earth pressure is derived by multiplying the effective vertical stress (at depth) within the reinforced soil mass by a designated earth pressure coefficient. Internal factors of safety for Allowable Stress Design (ASD) are generally as follows:

Pullout resistance  $\geq 1.5$

Tensile failure and connection to the face units  $\geq 1.5$

#### 2.1.3 Reinforcement – Inextensible and Extensible

In MSE design there are two main types of reinforcement, inextensible and extensible. Reinforcement such as metal strips, metal bar mats, and welded wire grids are inextensible, whereas reinforcement consisting of geotextiles, geogrids, composite plastic strips, or woven wire mesh are extensible. MSE structures that utilize inextensible reinforcement generally behave as a rigid body, where the reinforcement prevents internal deformation and is under tension over the full length (Anderson et al., 2010). Consequently, the soil is restricted from

reaching full active pressure. This ultimately affects the shape of the active zone, producing a bilinear failure surface as displayed in (Figure 2-1).

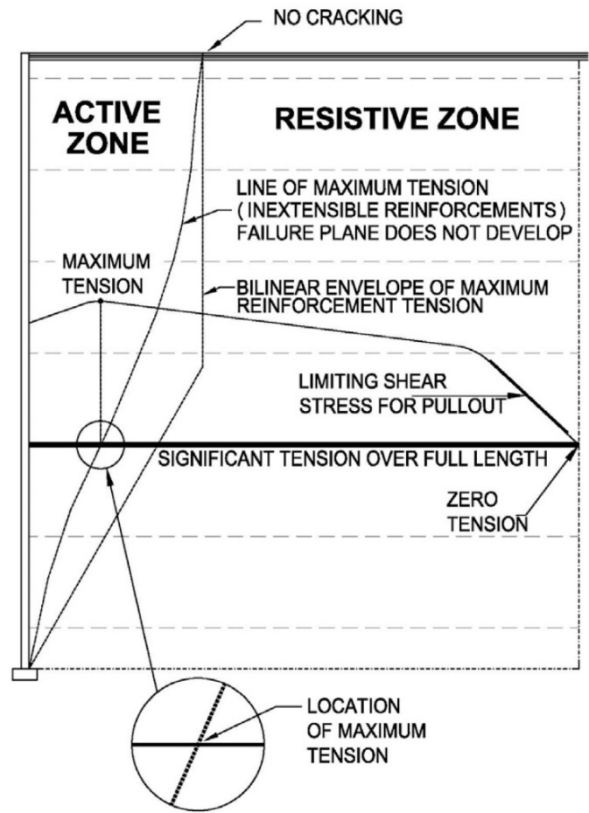


Figure 2-1. Inextensible reinforcement, bilinear failure plane (Anderson et al., 2010).

For extensible reinforcement, the reinforcement is not under tension over its full length (Anderson et al., 2010) and sufficient deformation develops to engage full active pressure within the reinforced mass. Therefore, the active zone is linear and defined by the Rankine failure plane, Figure 2-2.

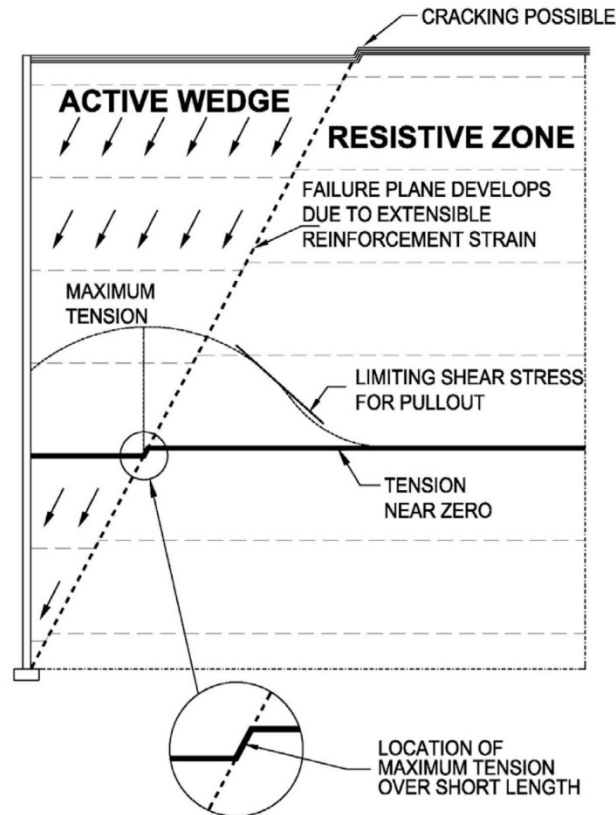


Figure 2-2. Extensible reinforcement, Rankine failure plane (Anderson et al, 2010).

For the purposes of this research, only inextensible reinforcement was used. Therefore, the remainder of the discussion and design process will focus mostly on the behavior of MSE walls supported by inextensible reinforcement.

## 2.2 Design Methods

### 2.2.1 National Concrete Masonry Association Procedure (NCMA)

The NCMA method was developed in 1993 (Simac et al.) for modular block, geosynthetic reinforced soil walls using allowable strength design (ASD) methodology. For internal stability, the lateral pressure is set equal to the Coulomb active earth pressure and the assumed failure plane is the Coulomb active pressure wedge (FHWA, 2009). The minimum reinforcement length to wall height ( $L/H$ ), is 0.6 and the connection strength requirements are based on short term testing which is not compliant with AASHTO's long term testing requirements. Since the method is specifically developed for geosynthetic reinforcement, does not allow a  $B/H = 0.3$ , uses ASD design methodology, and does not fully comply with AASHTO requirements; it was not considered further.

### 2.2.2 Geosynthetic Reinforced Soil (GRS) Analysis Model

The GRS method is another analysis model used with ASD procedures and was specifically developed for geosynthetic reinforcement. Therefore, this method was not considered for design.

### 2.2.3 Tieback Wedge Method

The Tieback Wedge Method assumes the wall is flexible for internal design. This leads to a case where the developed lateral soil stresses in the retained backfill have no influence on the vertical stresses within the reinforced soil mass. The method is typically used only for extensible geosynthetic reinforcement which assumes enough deformation takes place to engage an active state of stress within the reinforced zone. Consequently, the active zone is defined by a Rankine failure plane and the active earth pressure coefficient ( $k_a$ ) is used to calculate the lateral earth pressure and peak reinforcement load at each reinforcement level. In the early stages of developing the method, the at-rest earth pressure coefficient ( $k_0$ ) was recommended but was later determined to be too conservative. As stated, the method is typically used only for extensible reinforcement, likely due to the reinforcement coverage ratio resulting in an underestimate of the peak reinforcement load for inextensible reinforcement strips with large horizontal spacing. Therefore, the method was not considered for design.

$$T_{max} = S_v R_c k_a (\gamma z + S + q) \quad (2-1)$$

where,

- $T_{max}$  = peak reinforcement load at each reinforcement level
- $S_v$  = vertical spacing of the reinforcement
- $R_c$  = reinforcement coverage ratio (reinforcement unit width/horizontal spacing of reinforcement)
- $k_a$  = active earth pressure coefficient
- $\gamma$  = unit weight of the reinforced soil
- $z$  = depth of the reinforcement level below the top of the wall
- $S$  = average soil surcharge above the top of the wall
- $q$  = vertical stress due to traffic surcharge

### 2.2.4 Tieback FHWA Structure Stiffness Method

The FHWA Structure Stiffness Method is similar to the Tieback Wedge Method, except the lateral earth pressure coefficient is determined as a function of depth below the top of the wall, reinforcement type, and global wall stiffness, rather than using  $k_a$  directly (Allen et al., 2001). The method also assumes a bilinear failure plane for inextensible reinforcement, Figure 1-1. The approach was developed from numerous full-scale MSE walls that were constructed and monitored through an FHWA research project. Observations indicated a strong relationship exists between reinforcement stiffness and reinforcement stress levels which was theoretically verified through model tests and numerical modeling (FHWA, 2009).

$$T_{max} = S_v R_c k_r (\gamma z + S + q) \quad (2-2)$$

where,

$$k_r = k_a \left[ \Omega_1 \left( 1 + \left( \frac{0.4S_R}{1,000 \text{ ksf}} \right) \right) \left( 1 - \frac{z}{20} \right) + \frac{\Omega_2 z}{20} \right] \quad (2-3)$$

if  $z \leq 20$  ft and,

$$k_r = k_a \Omega_2 \quad (2-4)$$

if  $z \geq 20$  ft and,

$$S_R = \frac{EA}{H/n} \text{ (ksf)} \quad (2-5)$$

where,

- $T_{\max}$  = peak reinforcement load at each reinforcement level
- $S_v$  = vertical spacing of the reinforcement
- $R_c$  = reinforcement coverage ratio (reinforcement unit width/horizontal spacing of reinforcement)
- $k_a$  = active earth pressure coefficient
- $\gamma$  = unit weight of the reinforced soil
- $z$  = depth of the reinforcement level below the top of the wall
- $S$  = average soil surcharge above the top of the wall
- $q$  = vertical stress due to traffic surcharge
- $EA$  = reinforcement modulus times the reinforcement area in units of force per unit width of wall (lb/ft)
- $H/n$  = the average vertical spacing of the reinforcement, and  $n$  is the total number of reinforcement layers (ft)
- $\Omega_1$  = dimensionless coefficient equal to 1.0 for strip and sheet reinforcement or equal to 1.5 for grids and welded wire mats
- $\Omega_2$  = dimensionless coefficient equal to 1.0 if  $S_R \leq 1,000$  ksf, or equal to  $\Omega_1$  if  $S_R \geq 1,000$  ksf

### 2.2.5 K-Stiffness Method

The K-Stiffness Method calculates the maximum gravity force resulting from the gravity forces within the reinforced soil backfill to determine the maximum reinforcement load within the entire wall reinforced backfill ( $T_{\max}$ ) and then adjusts the maximum reinforcement load with depth for each of the layers using a load distribution factor ( $D_{\max}$ ) to determine  $T_{\max}$ . The method was researched, developed, and calibrated against measurements of loads and strains from a large database of full-scale geosynthetic and full-scale steel reinforced walls; and is intended to accurately predict working loads in the soil reinforcement (FHWA, 2009). Wall behavior near failure due to excessive deformation and/or rupture was considered in the development of the method (Allen et al., 2003) – Note, defining a soil failure limit state for design is not considered

by any other method. The method limits the strain in the soil to prevent it from going past peak to a residual value (i.e., failure by excessive deformation and/or rupture is prevented, and equilibrium is maintained). Analysis indicates the method is more accurate for estimating loads in the soil reinforcement than any other current design model and has the potential to reduce reinforcement requirements and improve the economy of MSE walls (Allen et al., 2003 and 2004). For example, geosynthetic reinforcement in a full-scale wall was reduced by a third to one-half of the reinforcement required by the AASHTO design code (FHWA, 2009).

WSDOT (2010), states that the K-Stiffness Method, as described by Allen and Bathurst (2003), may be used as an alternative to the AASHTO recommended Simplified Method for MSE wall internal stability design and provides detailed LRFD guidelines for using the method. Design requirements state that the MSE walls must be less than or equal to 25 feet in height, does not support any other structures, and is not used in high settlement areas.

For the K-Stiffness Method, the load in the reinforcements is obtained by multiplying the factored vertical earth pressure by a series of empirical factors which take into account the reinforcement global stiffness for the wall, the facing stiffness, the facing batter, the local stiffness of the reinforcement, the soil strength and stiffness, and how the load is distributed to the reinforcement layers. The maximum factored load in each reinforcement layer shall be determined as follows:

$$T_{max} = 0.5S_v K \sigma_v D_{tmax} \Phi_{fs} \Phi_{local} \Phi_{fb} + \gamma_p \Delta \sigma_H S_v \quad (2-6)$$

where,

- $T_{max}$  = peak reinforcement load at each reinforcement level
- $S_v$  = tributary area which is equivalent to the average vertical spacing of the reinforcement at each layer location when analyses are carried out per unit length of wall (ft)
- $K$  = is an index lateral earth pressure coefficient for the reinforced backfill and shall be set equal to  $k_0$  as calculated per Article 3.11.5.2 of the AASHTO LRFD Specifications.  $K$  shall be no less than 0.3 for steel reinforced systems.
- $\sigma_v$  = the factored pressure due to resultant of gravity forces from soil self-weight within and immediately above the reinforced wall backfill, and any surcharge loads present, as calculated in Equation 7 (ksf)
- $D_{tmax}$  = distribution factor to estimate  $T_{max}$  for each layer as a function of its depth below the wall top relative to  $T_{max}$  (the maximum value of  $T_{max}$  within the wall), see Figure 3.
- $S_{global}$  = global reinforcement stiffness (ksf)
- $\Phi_g$  = global stiffness factor
- $\Phi_{local}$  = local stiffness factor
- $\Phi_{fb}$  = facing batter factor (there will be no batter on the wall for the research) = 1
- $\Phi_{fs}$  = facing stiffness factor = 1 for all steel reinforcement (WSDOT, 2010)
- $\gamma_p$  = the load factor for vertical earth pressure (EV) from Table 4
- $\Delta \sigma_H$  = horizontal stress increase at reinforcement level resulting from a concentrated horizontal surcharge per Article 11.10.10.1 of the AASHTO LRFD specifications (ksf)

and,

$$\sigma_v = \gamma_p \gamma_r H + \gamma_p \gamma_f S + \gamma_{LL} q + \gamma_p \Delta \sigma_v \quad (2-7)$$

$$S_{global} = \frac{J_{ave}}{H/n} \quad (2-8)$$

$$\Phi_g = 0.25 \left( \frac{S_{global}}{P_a} \right)^{0.25} \quad (2-9)$$

$$S_{local} \frac{J}{S_v} \quad (2-10)$$

$$\Phi_{local} = 0.25 \left( \frac{S_{local}}{S_{global}} \right)^a \quad (2-11)$$

$$F_f = \frac{1.5H^5}{ELb_w^3 h_{eff}} P_a \quad (2-12)$$

$$\Phi_{fs} = \eta (F_f)^k \quad (2-13)$$

where,

- $\gamma_p$  = the load factor for vertical earth pressure (EV) from Table 4
- $\gamma_{LL}$  = the load factor for live load surcharge per the AASHTO LRFD specifications
- $q$  = live load surcharge (ksf)
- $H$  = the total vertical wall height at the wall face (ft)
- $S$  = average soil surcharge depth above the wall top (ft)
- $\Delta \sigma_v$  = vertical stress increase from concentrated surcharge load above the wall (ksf)
- $J_{ave}$  = the average stiffness of all the reinforcement layers within the entire wall section on a per foot of wall width basis (kips/ft)
- $n$  = the number of reinforcement layers within the entire wall section
- $P_a$  = atmospheric pressure (2.11 ksf)
- $J$  = the stiffness of an individual reinforcement layer (kips/ft)
- $a$  = a coefficient which is also a function of stiffness. Based on observations from available data, set  $a = 1.0$  for geosynthetic walls and  $a = 0.0$  for steel reinforced walls
- $F_f$  = a non-dimensional facing column stiffness parameter
- $E$  = the modulus of the facing material (ksf)
- $L$  = unit length of wall (ft)
- $b_w$  = thickness of the facing column (ft)
- $h_{eff}$  = the equivalent height of an un-jointed facing column that is 100% efficient in transmitting moment throughout the facing column (ft)
- $\eta$  = dimensionless coefficient determined from an empirical regression of full-scale wall data = 0.5
- $k$  = dimensionless coefficient determined from an empirical regression of full-scale wall data = 0.14



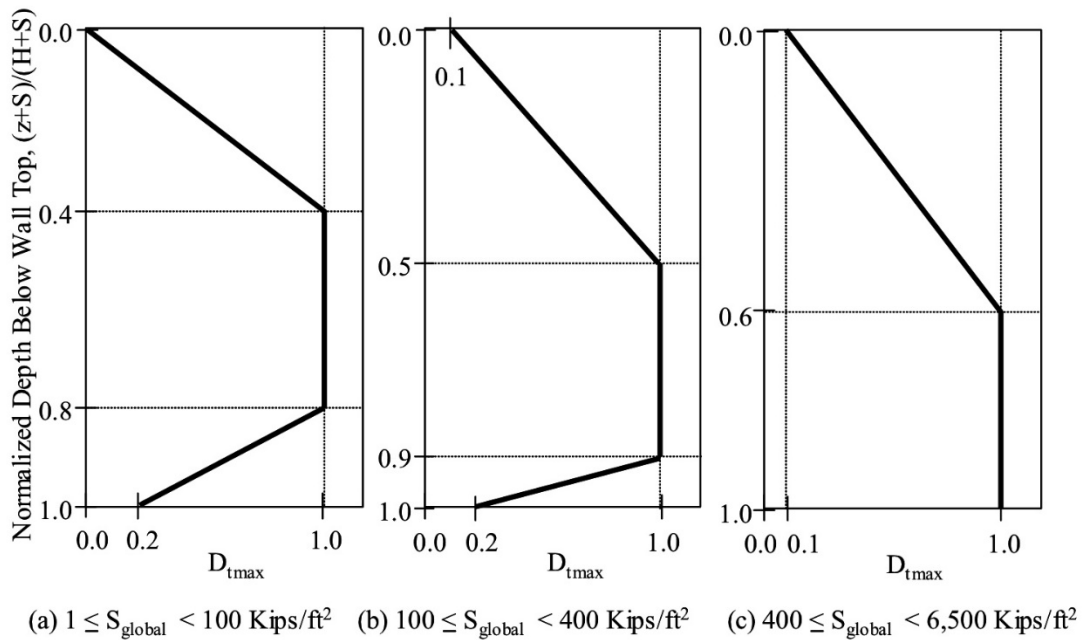


Figure 2-3.  $D_{t\max}$  as a function of normalized depth below wall top plus average surcharge depth.

Although prior analysis indicated the K-stiffness method was more accurate for estimating reinforcement loads, the design requirements of the method would only allow a reinforcement length of 7.5 feet due to the  $B/H = 0.3$  requirement for when two walls would be tied together in practice, which is an unlikely scenario. Furthermore, a simulated surcharge will also be applied to achieve a  $B/H = 0.3$ , which requires the wall to support a structure (load frame assembly) to induce the surcharge, which also goes against the method design requirements. Therefore, the K-Stiffness Method was not considered for the research.

### 2.2.6 Coherent Gravity Method

The Coherent Gravity Method was developed to estimate steel strip reinforcement stresses for precast panel-faced MSE Walls (Allen et al., 2001). The reinforced soil mass is assumed to behave as a rigid body and the lateral load developed from the retained soil acts upon the rigid body similar to lateral forces acting upon a conventional gravity-type wall system. The lateral stress is derived by applying a lateral earth pressure coefficient to the vertical stress which is calculated using the soil friction angle. The stress carried by each level of reinforcement is assumed to be equivalent to the lateral soil stress acting on a defined tributary wall area. Essentially, the method assumes that the wall is fully supported by the reinforcement and acts as a tieback (FHWA, 2009).

The lateral earth pressure coefficient is assumed to be  $K_0$  at the top of the wall and decreases to  $K_a$  at a depth ( $z$ ) of 20 feet below the top of the wall; producing Equation 1 when  $z < 20$  ft.

$$k_r = k_a + (k_0 - k_a) \left( \frac{20-z(ft)}{20} \right) \quad (2-14)$$

The  $K_0$  condition is assumed at the top of the wall because of possible locked-in-compaction stresses and the stiff reinforcement prevents the active stress condition from developing. As the depth increases the overburden stress overcomes the locked-in-compaction and deformations become great enough to mobilize an active stress condition (Allen et al., 2001). This produces a bilinear failure plane as depicted in Figure 2-4.

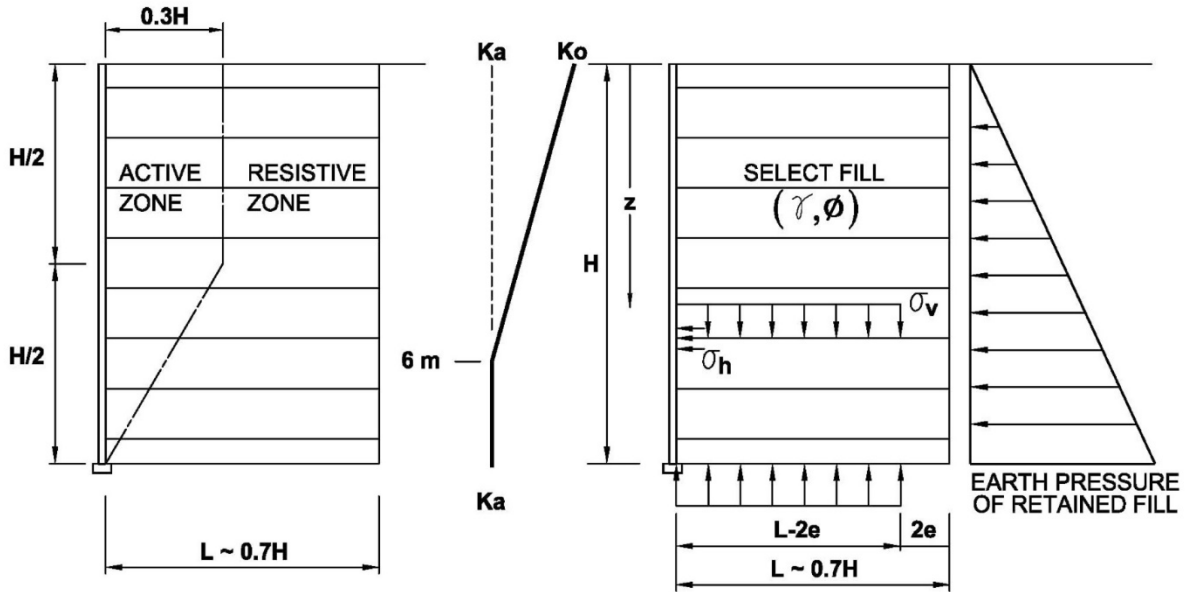


Figure 2-4. Coherent Gravity Method.

$$T_{max} = S_v R_c (\sigma_v k_r) \quad (2-15)$$

where,

- $T_{max}$  = peak reinforcement load at each reinforcement level
- $S_v$  = vertical spacing of the reinforcement
- $R_c$  = reinforcement coverage ratio (reinforcement unit width/horizontal spacing of reinforcement)
- $\sigma_v$  = vertical stress at each reinforcement level (defined by Equation 15 and Figure 5)
- $k_r$  = earth pressure coefficient within the reinforced soil mass

$$\sigma_v = \frac{V_1 + V_2 + F_T \sin \beta}{L - 2e} \quad (2-16)$$

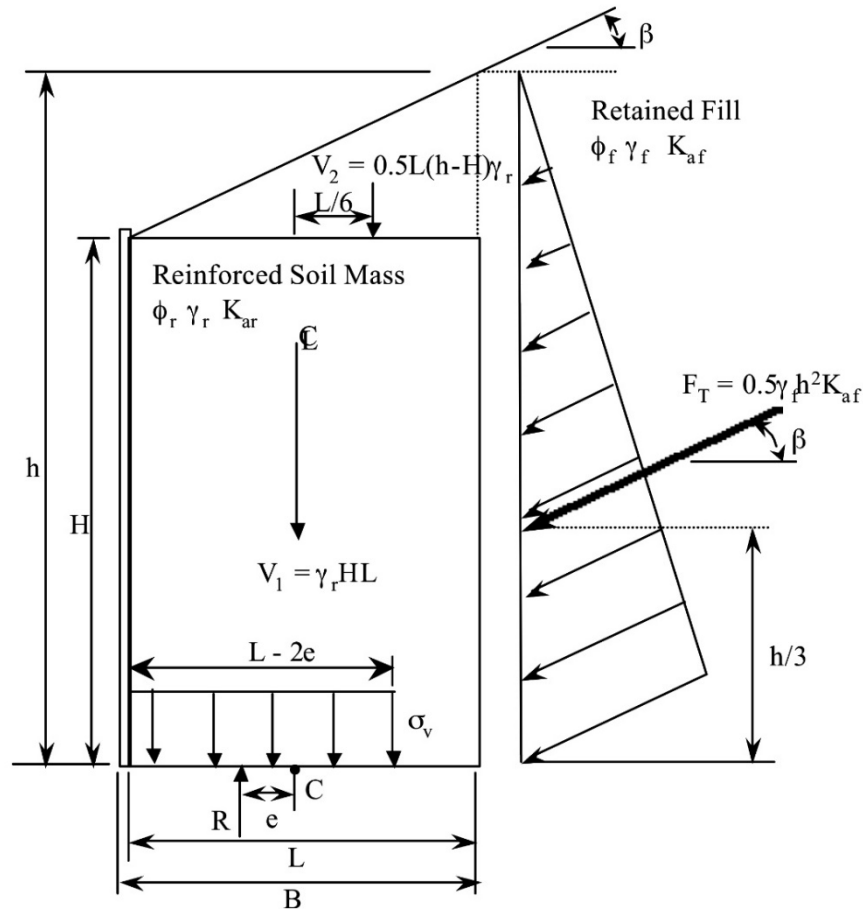


Figure 2-5. Forces for calculating the vertical stress distribution in MSE walls.

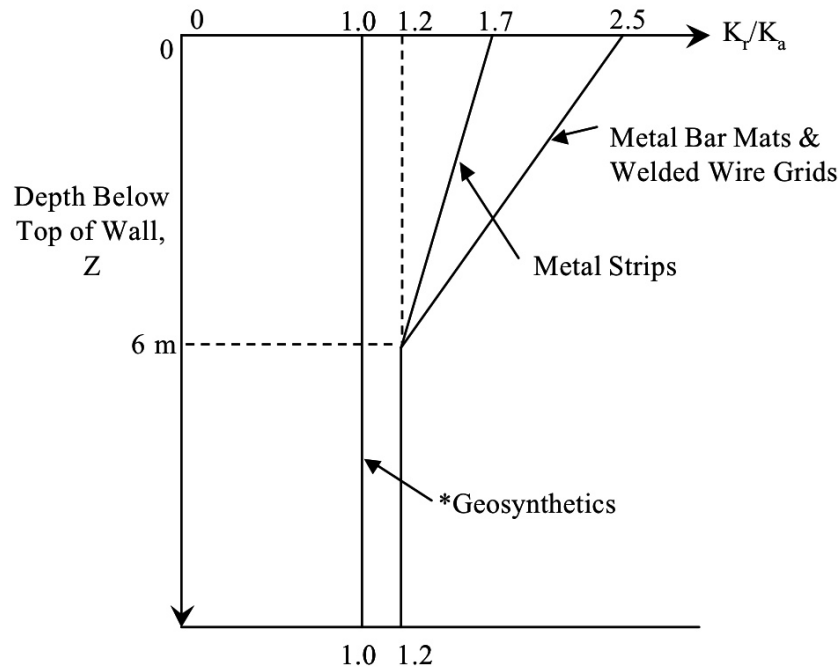
Note: The equation typically used to calculate  $K_0$  was derived for normally consolidated soils, and compaction tends to make the soil behave as if it were over-consolidated (Allen et al., 2001).

### 2.2.7 The Simplified Method

The Simplified Method, also known as the Simplified Coherent Gravity Method, was developed as an attempt to combine the best and simplest features of the various design methods allowed by the AASHTO Standard Specifications into a single method (Allen et al., 2001). One of the key elements of the Simplified Method is that it accounts for the differences in global stiffness of the various reinforcement types. The method also simplifies calculations by avoiding the need to reiterate each time the reinforcement density is adjusted to match the reinforcement stress to the available reinforcement capacity. This is different from the Coherent Gravity Method that does not provide a means to differentiate between reinforcement types where  $k_a$  and  $k_0$  are used directly, regardless of reinforcement type. Consequently, a goal of the Simplified method was to develop a single  $k_r/k_a$  curve for each reinforcement type simply based on the type of reinforcement utilized. Another issue addressed by the simplified method was whether or not the wall should be treated internally as a rigid body. When treated as a rigid body, the overturning

moment is transmitted throughout the reinforced soil mass which increases the vertical stress in the wall. This typically adds a significant complication to internal stress computations; and the validity of the approach was considered questionable by the FHWA, as well as a Technical Working Group (TWG) that was assigned by AASHTO to reevaluate the design specifications for MSE walls (Allen et al., 2001). Consequently, the approach of not considering the overturning moment for internal vertical stress computations was incorporated into the Simplified Method; however, the overturning moment is still used for external bearing stress computations as a conservative measure.

The design methodology for the Simplified Method is similar to that of the FHWA Structure Stiffness and Tieback Wedge Methods and Equation 2-2 can be used for  $T_{max}$  calculations. However,  $k_r/k_a$  is determined from Figure 2-6 and/or Equation 2-17, and not the FHWA Structure Stiffness equations.



\*Does not apply to polymer strip reinforcement.

Figure 2-6. Determination of  $k_r/k_a$  for the Simplified Method (AASHTO, 1999).

$$k_r = k_a \left( 1.2 + (1.7 - 1.2) \left( \frac{20 - z(ft)}{20} \right) \right) \quad (2-17)$$

### 3 Soil Testing and Design

#### 3.1 *Design Objectives, Requirements, and Site Preparation*

The objective of this research was to investigate the resulting earth pressure coefficients derived from an MSE wall configuration where the reinforcements are tied to an unyielding structure, for two states of soil density representative of field conditions. Tying one side of the reinforcements to an unyielding structure will prevent minor wall deformations in the yielding MSE wall. As a result, the lateral earth pressure was expected to increase which would inherently increase the tension that develops in the reinforcements. The actual earth pressure and reinforcement tension that develops for a case such as this is not well understood. Therefore, the outcome of the research was intended to adequately address design methodology and earth pressure coefficients for earthen fill compacted behind unyielding structures. The two states of soil density were intended to provide a high and low internal friction angle,  $\phi$ , which also directly affects the developing lateral earth pressure and reinforcement tension. The research MSE wall design presented in Figure 3-1 simulates two walls tied together, with one side unyielding (MSE wall near Strong Wall) and the other yielding (front MSE wall). This is representative of widening conditions where a new wall is tied to an existing wall, Figure 3-2, and acute corner construction.

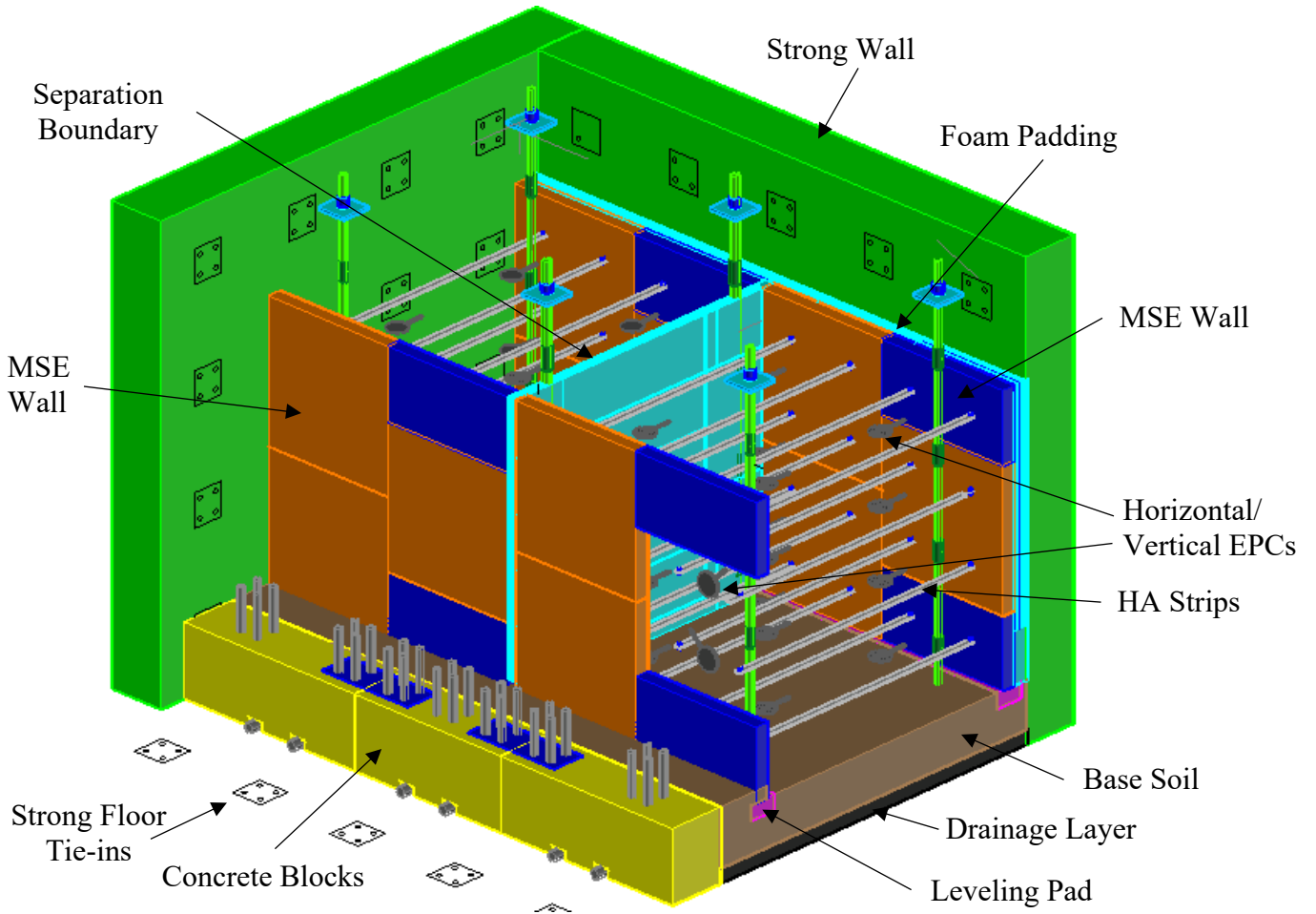


Figure 3-1. MSE wall configuration (Note: Right side Strong Wall and reinforced fill are not depicted for visualization of the reinforcements and instrumentation).



Figure 3-2. Back-to-back wall construction displaying embedded and clip angle connections that will both be mechanically fastened to the respective reinforcement.

Figure 3-3 illustrates a "tributary wall area" used for checking the internal stability of the structure under Coherent Gravity or Simplified methods (AASHTO 11.10.6.2.1). This provides four layers to investigate for each state of soil density using square wall panels. Square panels ( $\approx 5' \times 5'$ ) are considered standard in Florida per the approved FDOT vendors, which will be discussed in Section 3.8.4. The tributary wall area is a  $1/2$  panel tall and 2 panels wide, or approximately 2.5 feet tall and 10 feet wide. Note, the tributary wall areas in the horizontal direction are separated by a high strength Styrofoam "divider". A different relative compaction effort (soil density) was implemented on each side of the divider. On one side the relative compaction effort target was 95% of T-180 and the other side was 103% of T-180. From discussions between UF researchers and FDOT officials, it was determined that the designated compaction efforts were representative of the range commonly experienced in the field.

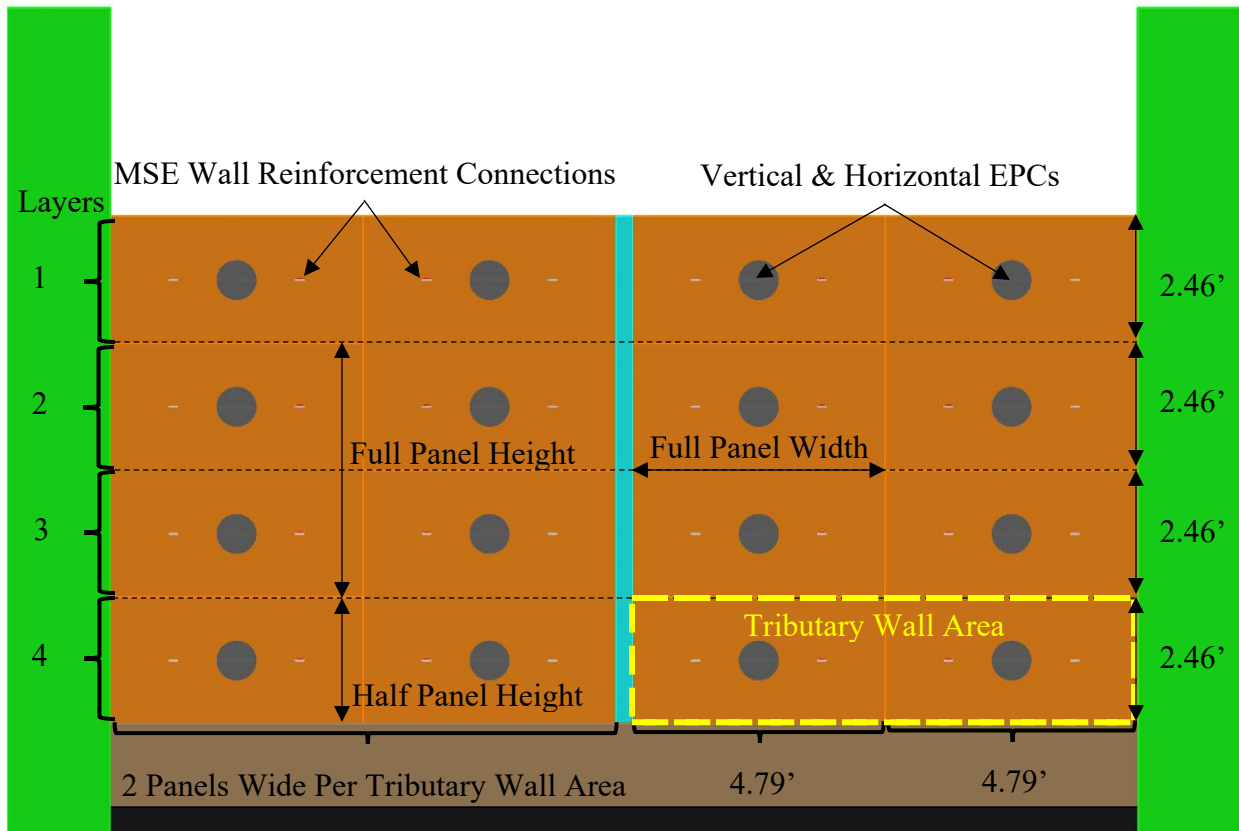


Figure 3-3. MSE wall configuration in profile view, indicating the tributary wall areas.

Prior to wall construction, concrete blocks were cast and used to construct a base soil layer (previously determined to be two feet in height). Geotextile non-woven fabric was placed at the base of the soil overlaying an approved gravel layer to collect and route free draining water. The side strong walls were lined with plastic sheeting to reduce friction at the sidewall-soil interface. Leveling pads were also cast and placed in the soil prior to MSE wall construction.

Prior to any soil being placed, steel plates with threaded rod couplers were mechanically attached to the Strong Floor in six locations. Throughout construction threaded rod was added in sections and used to attach a reaction frame to provide incremental surcharge loading. Once the MSE walls were constructed and backfilled, UF's Matjack-airbag system was placed atop the soil. Two of UF's Soil Box walls were then placed atop the airbag system and tied into the threaded rods to complete the reaction system. Incremental surcharge loading was then implemented. The simulated surcharge heights and length of sustained incremental loading were determined by the Project Managers and the Principal Investigators based on data collected on-site. Horizontal earth pressure cells, EPCs, were embedded in the soil in quadrants as indicated in Figure 3-4 and at the midpoint of each tributary wall area layer as indicated in Figure 3-3. Vertical EPCs were placed on the MSE walls at the same vertical location as the horizontal EPCs as indicated in Figure 3-3. This provided direct measurement of the vertical and horizontal stresses in 16 different zones. Using this approach, earth pressure coefficients were derived from multiple stress states, based on depth of embedment and soil density, simultaneously. In addition, strain



gauges placed in multiple locations along the reinforcements, as indicated in Figure 3-4, were converted to axial force and lateral stress (force/tributary area) for comparison to soil stresses measured by the EPCs within the soil mass. The strain gauges were located in strategic locations to “map” the active zone within the reinforced fill, if it developed. Two draw-wire sensors were placed on the exterior of each wall configuration (different relative compaction efforts) to measure the horizontal movement of the walls. This allowed researchers to investigate the effects of restricted wall movement from tying two walls together in two states of soil density that are representative of field conditions.

For convenience the reinforcement strip lengths were established as 10 feet from the bolt holes of each MSE wall. Due to building constraints, the as-built lengths of the reinforcement strips were 9.75 feet in length. Locations of the soil embedded EPCs and strain gages were measured from the bolted locations. To map the possible active wedge, strain gages were placed at 0.5', 2', and 3.5' from the front MSE wall reinforcement bolted connection. The active wedge was assumed to be approximately three feet from the facing of the MSE wall panels in the top five feet and then decrease linearly to the wall facing in the bottom five feet of the wall. Placing the strain gages in the designated locations ensured that at least one gage was inside and outside of the theoretical failure plane at all monitored depths. Strain gages were also placed near the back MSE wall and equally spaced around the soil embedded EPCs in the long direction of the strips. These gages were used for comparative purposes with the EPCs and to measure the tensile stress that was anticipated to develop over the full reinforcement length. At each strain gauge location, two gauges were placed on the top and bottom of each strip and setup in full bridge to compensate for bending and thermal effects. Moisture protection coating was applied to each gauge to ensure water did not affect the results. Finally, it was not feasible to instrument every reinforcement strip as this would have required 640 strain gauges based on the layout of Figure 3-4 and the number of reinforcement strips. Therefore, the two innermost strip locations (horizontally) for each compaction effort were selected for instrumentation to reduce potential disturbance from the sidewall-soil interface and the soil-divider interface between the two compaction efforts.

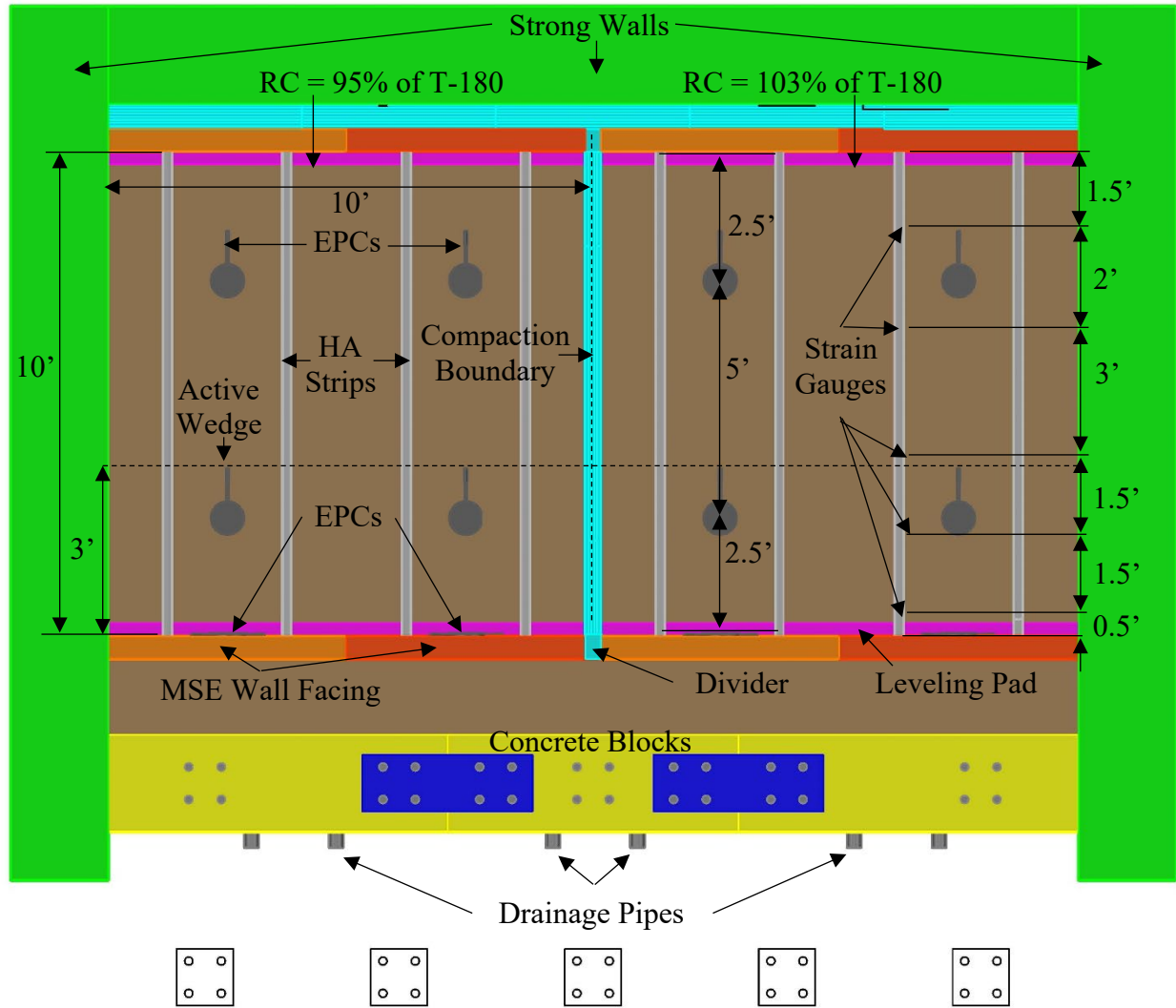


Figure 3-4. MSE wall configuration in plan view.

### 3.1.1 List and Quantities of Instrumentation

Soil embedded earth pressure cells → 36 – Geokon 4800 VW series

Wall mounted earth pressure cells → 16 – Geokon 4810 VW “Fatback” series

Strain gauges → On reinforcements strips: 320 – VPG (Vishay) C2A-06-062LW-350, On

Reaction frame: 320 – VPG (Vishay) CEA-06-125UWA-350/P2

Displacement transducers → 2 – Micro-Epsilon WDS-750-P60-CR-P

Data acquisition modules → 2 – Campbell Scientific CR6 w/ 9 – AM16/32b Multiplexers,  
Campbell Scientific CR10X w/2 – AM416 Multiplexers

### 3.1.2 Geometry

- Wall height  $\approx$  10 feet
- Wall batter = No wall batter
- Back slope = No back slope
- Toe slope = No toe slope

### 3.1.3 Loading Conditions

Incremental simulated soil surcharge loads were applied after the wall was constructed using two of UF's Soil Box walls (8' x 11') and the Matjack-airbag system. The simulated soil surcharge loads were estimated to range from 450 to 2,500 psf. This is representative of 4 to 23 feet of overburden placed atop the wall at 103% of T-180.

A Live load was anticipated during construction and was estimated to be 2,100 lbs which included the weight of a vibratory compactor ( $\approx$  1,600 lbs) and two researchers ( $\approx$  500 lbs). Live load is accounted for in conventional MSE wall design with the use of the Coherent Gravity Method (where  $k$  varies from  $k_o$  at ground surface to  $k_a$  at 20 ft of depth) or the Simplified method (where  $K$  varies from  $1.7k$  to  $1.2k_a$ ). The higher  $k$  values near the top of wall are due to "locked in" compaction loads.

No seismic loading was induced. There were no traffic barrier impacts.

### 3.1.4 Performance Criteria

AASHTO LRFD design code was used in compliance with FDOT's standard specifications for road and bridge construction.

### 3.1.5 Maximum Tolerable Vertical Displacement

MSE structures have significant deformation tolerance both longitudinally along the wall and perpendicular to the front face. Square panels generally adapt to larger longitudinal differential settlements better than long rectangular panels of the same surface area. A joint width of  $\frac{3}{4}$  inch is generally recommended and guidance on differential settlements that can be tolerated are provided in Table 3-1 (FHWA, 2009). Square panels purchased from the Reinforced Earth Company (RECo) were used for the research. The RECo square panels are approximately 25 ft<sup>2</sup> and therefore the maximum tolerable differential settlement should be limited to 1/100. FDOT (2017) Section 548-8.4.1.1 states that for reinforced concrete MSE wall systems, the vertical tolerance (plumbness) must not exceed  $\frac{3}{4}$  inch when measured with a 10 foot straightedge; the maximum allowable offset in the joint between precast components is  $\frac{3}{4}$  inch; the final overall vertical tolerance of the completed wall (plumbness from top to bottom) must not exceed  $\frac{1}{2}$  inch per 10 feet of wall height; and the vertical joints between precast components must not be less than  $\frac{1}{2}$  inch or more than 1-1/4 inches. Based on the wall height, backfill compaction

requirements and foundation conditions, the vertical displacement of the wall was negligible, likely less than ¼” (per RECo).

Table 3-1. Relationship between joint width and limiting differential settlements for MSE precast panels (AASHTO, 2007; C11.10.4.1).

Joint Width	Limiting Differential Settlement	
	Area ≤ 30 ft <sup>2</sup>	30 ft <sup>2</sup> ≤ Area ≤ 75 ft <sup>2</sup>
¾ - inch (20 mm)	1/100	1/200

### 3.1.6 Maximum Tolerable Horizontal Displacement

For the maximum tolerable horizontal displacement, there is no current method available to definitively predict lateral displacements, most of which occur during construction. The horizontal movements depend on compaction efforts, reinforcement extensibility, reinforcement length, reinforcement-to-panel connection details, and details of the facing system. Since the walls were tied across, and the expected strain in the soil reinforcements was low, the horizontal displacement was a function of the slip at each bolt hole (approximately 1/16” x 2 per strip) = 1/8” +/-, plus any slack in the connections. Total horizontal displacement should be less than 3/8” (per RECo).

FDOT (2017) Section 548-8.4.1.1 states that for reinforced concrete MSE wall systems, the vertical alignment tolerance must not exceed ¾ inch when measured with a 10 foot straightedge; the maximum allowable offset in the joint between precast components is ¾ inch; and the horizontal joints between precast components must not be less than ½ inch or more than 1-1/4 inches.

### 3.1.7 Design Life

The design life was planned to be 6 months and not extend beyond one year from the end of construction. FHWA (2009) states that retaining walls for temporary applications are typically designed for a service life of 36 months or less. The design life was discussed between FDOT officials and UF researchers to determine the appropriate corrosion loss in the cross-section of the reinforcements to be used in the final design. It was determined that a four-year design life would be used to determine the cross-section to be used in design.

For the research, the reinforcement was measured prior to use to determine the cross-sectional area available four years after construction to provide a CDR > 1.0 based on the corrosion rates provided in the FDOT Structures Design Guidelines (SDG) Section 3.13.2, Article J. The reinforced fill was tested to ensure it meets the “electro-chemical” requirements of the Specification (Section 548-2.6.2), otherwise the SDG corrosion rates would not apply. For the final design, the full cross-section of the reinforcements was assumed (details provided in Section 3.8.6).

### *3.1.8 Construction and Quality Control Procedures*

A field construction manual describing construction requirements and sequencing for the Reinforced Earth Company's (RECo) wall system was submitted prior to construction per FDOT (2017) Section 548-3 Item 10. The manual is to be submitted in an 8-1/2-inch x 11 inch format in either pdf or MS Word format. The following link provides the RECo construction manual for square panel wall systems:

<https://reinforcedearth.com/content/uploads/2020/09/RE-Square-Panel-Construction-Manual-v2020.1.pdf>

### *3.1.9 Construction Constraints*

Construction constraints included low overhead clearance of the UF Weil Hall laboratory in which the Strong Wall is located, a confined MSE wall structure similar to a Bin Wall, limited space to use larger compaction equipment, two different compaction efforts implemented during construction, and limited space to store the select backfill. The limited overhead clearance prevented construction of a full scale MSE wall capable of achieving the necessary base to wall height ratio of 0.3. To overcome this, the UF team designed a reaction frame utilizing equipment from the FDOT Soil box capable of simulating the additional wall height required. Overhead limitations also inhibited use of traditional backfilling methods. Two overhead cranes (5-ton capacity) mounted in the laboratory were used to place soil and panels and lift compaction and reaction frame equipment into the construction area. OSHA approved safety harnesses were needed to be worn by construction personnel, when necessary, based on OSHA guidelines. Vibratory patterns within the reinforced fill area were developed for the compaction equipment during base soil placement to ensure each respective compaction effort was achieved. The soil needed to be obtained in stages to accommodate the limited soil storage area. Soil had to be loaded into ½ yard soil sacks at the offsite storage location and brought to the lab.

## **3.2 Project Parameters**

### *3.2.1 Subsurface Conditions across the Site*

The engineering properties of the foundation soils were the same as the reinforced wall fill. Soil properties are provided in Section 3.3. The foundation soil is an approximate 1.5-foot layer of select fill underlain by a six-inch layer of select gravel for drainage and the concrete laboratory floor. Since the MSE wall was constructed in a controlled laboratory environment, groundwater conditions were not a factor in design.

### *3.2.2 Reinforced Wall Fill*

The reinforced wall fill was select fill obtained from the O'steen Bros. Pit located west of Gainesville in Archer, Florida. Soil properties obtained from tests performed at the FDOT's State Materials Office are provided in Section 3.3.

### 3.2.3 Retained Backfill

The MSE wall was tied into an unyielding structure (MSE Wall near UF Strong Wall). Therefore, there was no retained backfill.

### 3.3 Soil Properties

The following soil properties were obtained from tests conducted on the O'steen soil by the FDOT at the State Materials Office.

#### 3.3.1 Sieve Analysis of Fine and Coarse Aggregates, AASHTO T-27 and FM 1-T011:

Table 3-2. Sieve analysis and AASHTO requirements.

Sieve Size	Required Percent Passing (AASHTO T-27)	Reported Percent Passing (AASHTO T-88)
3-1/2 inches	100	N/A
¾ inch	70 to 100	100
No. 4	30 to 100	100
No. 40	15 to 100	99.4
No. 60	N/A	77.9
No. 100	0 to 65	23.8
No. 200	0 to 12	2.3

- $D_{10} \approx 0.105$  mm
- $D_{60} \approx 0.210$  mm
- $D_{85} \approx 0.270$  mm
- Coefficient of Uniformity ( $C_u$ ) = 2
- AASHTO Classification = A-3
- USCS Classification = SP – Poorly Graded Sand

#### 3.3.2 Determining the Liquid Limit of Soils, AASHTO T-89, and Determining the Plastic Limit and Plasticity Index of Soils, AASHTO T-90:

- Liquid Limit = Non-plastic (NP)
- Plastic Limit = NP
- Plasticity Index = NP

#### 3.3.3 Standard Method of Test for Specific Gravity of Soils, AASHTO T-100:

- Specific Gravity ( $G_s$ ) = 2.65

3.3.4 *Determination of Organic Content by Loss of Ignition, AASHTO T-267:*

- Organic Content (%) = 0.3

3.3.5 *Electrochemical Properties as Determined by FDOT FM 5-550 (pH in Soil and Water), FM 5-551 (Resistivity in Soil and Water), FM 5-552 (Chloride in Soil and Water), and FM 5-553 (Sulfate in Soil and Water):*

- pH = 5.32 (Pass)
- Resistivity = 58,900  $\Omega$ -cm (Pass)
- Chloride = 54 ppm (Pass)
- Sulfate = 6.5 ppm (Pass)

Note: “Pass” indicates compliance with FDOT specifications, presented in Table 7-3.

3.3.6 *Moisture-Density Relations of Soils, AASHTO T-180:*

- Maximum Dry Density ( $\gamma_{d-max}$ ) = 105.7 pcf
- Optimum Moisture Content ( $w_{opt}$ ) = 12.7 %

3.3.7 *Direct Shear of Soils, AASHTO T-236:*

Compaction Effort 1

- Compaction (%) = 95.7 %
- Dry Density ( $\gamma_d$ ) = 101.2 pcf
- Moisture Content ( $w$ ) = 12.8 %
- Internal Friction Angle ( $\Phi$ ) = 31.0°

Compaction Effort 2

- Compaction (%) = 103.5 %
- Dry Density ( $\gamma_d$ ) = 109.4 pcf
- Moisture Content ( $w$ ) = 12.8 %
- Internal Friction Angle ( $\Phi$ ) = 40.5°

3.3.8 *Comments*

The soil identified from the O’steen pit is classified as A-3 from AASHTO T-88. Note: there is optional acceptance criteria for A-3 and A-2-4 materials which states that a minimum density of 95% of the maximum dry density as determined by AASHTO T99 must be obtained within three feet behind the wall face and a minimum density of 100% of the maximum dry density as determined by AASHTO T99 must be obtained beyond three feet behind the wall face (FDOT, 2017). However, due to the research criteria, the same soil density was maintained within three feet of the wall and beyond three feet from the wall. Two compaction efforts were implemented:

95% of T-180 and 103% of T-180. Each state of soil density was utilized for half of the wall in the horizontal direction parallel to the wall facing.

The density of the soil was periodically checked in accordance with FDOT specifications via nuclear density testing (Section 5.1). These tests were performed at a frequency of two sets of tests per LOT for each compaction effort due to potential variability and the importance of moisture on compaction. A LOT was defined as a single lift of compacted soil. A single lift of loose soil was approximately eight to nine inches in height compacted into a final height of six inches.

### ***3.4 Wall Embedment Depth, Design Height, and Reinforcement Length***

The minimum wall embedment depth is typically based on bearing, settlement, and slope stability considerations (FHWA, 2009). The recommended minimum embedment depth to the top of the leveling pad is  $H/20$  for horizontal walls. Since the design wall height was approximately 10 feet with 23 feet of simulated height, this would have required 1.65 ft embedment. However, a minimum 2 ft embedment depth is required for all wall geometries and therefore controls the design. Based on the unique circumstances of the MSE wall being tied to an unyielding structure and bearing on a reinforced concrete slab, external loading was virtually nonexistent, and the required embedment depth was reevaluated. The minimum embedment depth agreed upon between UF researchers and FDOT officials was 0.5 ft.

### ***3.5 Nominal Loads***

The primary sources of external loading on an MSE wall are the earth pressure from the retained backfill behind the reinforced zone and any surcharge loading above the reinforced zone and/or retained backfill. Thus, the loads for MSE walls may include loads due to horizontal earth pressure, vertical earth pressure, live load surcharge, and earth surcharge (FHWA, 2009) as depicted in Figure 3-5.



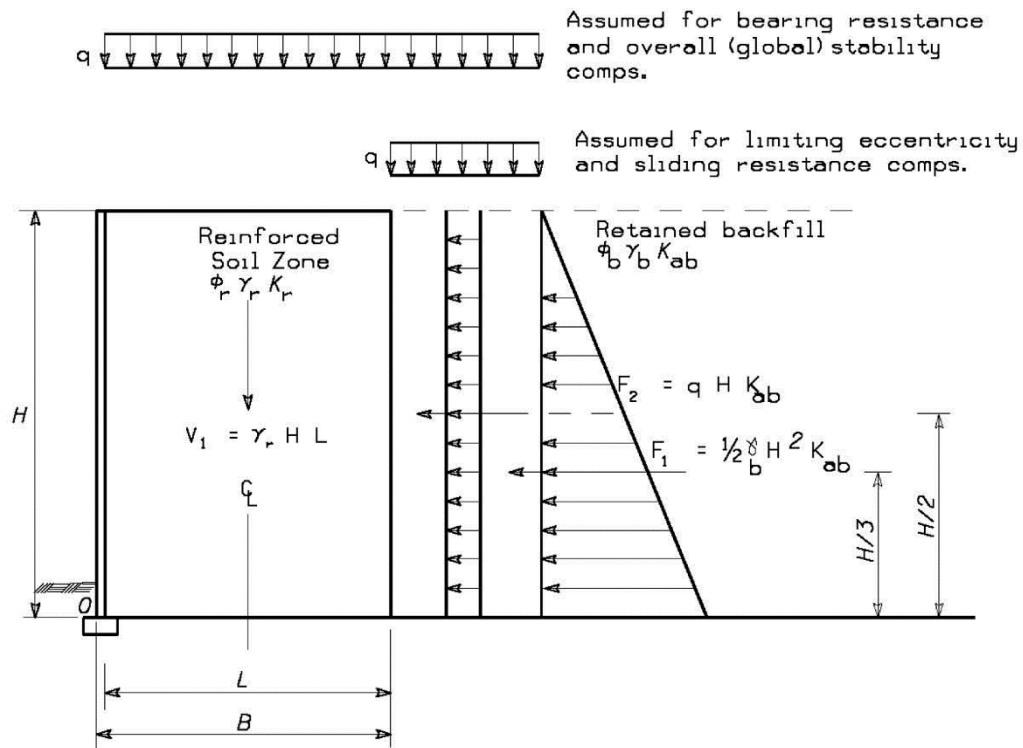


Figure 3-5. Nominal MSE wall earth pressures for horizontal back slopes.

The MSE wall configuration with surcharge loading (Matjack Reaction System) is displayed in Figure 3-6 and the nominal loads are calculated for both densities of the soil (i.e., 95.7% and 103.5% of T-180):

$$V_{1-95\%} = \gamma_r H L = 114.2 \text{ pcf} \times 10 \text{ ft} \times 10 \text{ ft} = 11,420 \text{ lbf per linear foot of wall} \quad (3-1)$$

$$V_{1-103\%} = \gamma_r H L = 123.4 \text{ pcf} \times 10 \text{ ft} \times 10 \text{ ft} = 12,340 \text{ lbf per linear foot of wall}$$

$$q_{\text{smax}95\%} = 2,600 \text{ psf (incremental simulated earth surcharge applied above the reinforced zone)}$$

$$q_{\text{smax}103\%} = 2,850 \text{ psf (incremental simulated earth surcharge applied above the reinforced zone)}$$

$$F_1 = F_2 = 0 \text{ (MSE wall is adjacent and connected to an unyielding structure)}$$

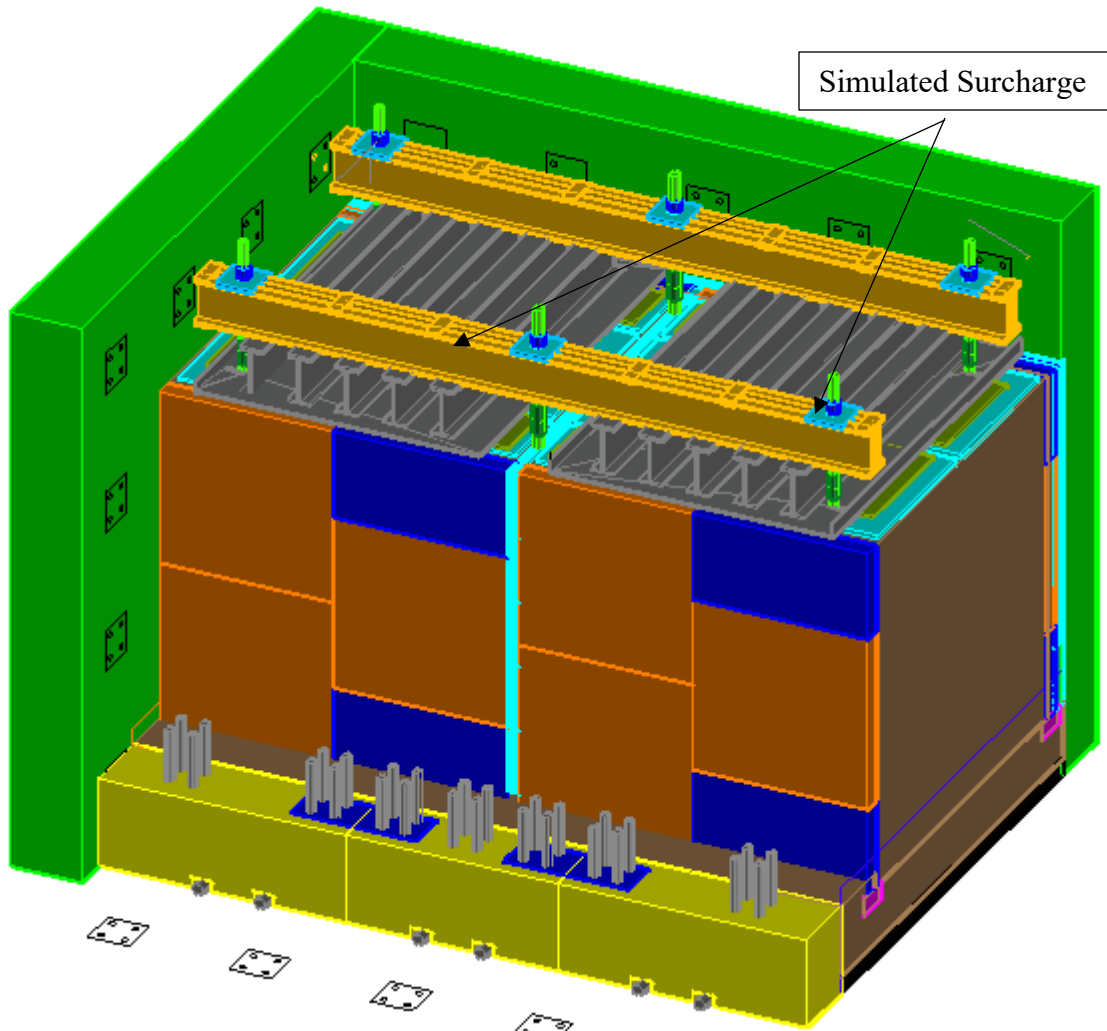


Figure 3-6. MSE-Strong Wall configuration with surcharge loading (Note: Right side Strong Wall is not depicted).

### 3.6 Load Combinations, Load Factors, and Resistance Factors

With respect to MSE wall structures, only a few of the loads and load combinations presented in AASHTO (2007) are applicable on a routine basis (FHWA, 2009). The applicable loads for most MSE wall applications are summarized below followed by a summary of applicable load factor combinations in Table 3-3 and Table 3-4.

Applicable Loads:

#### *Permanent Loads*

- Vertical pressure from dead load of earth fill (EV)
- Horizontal earth loads (EH)
- Earth surcharge load (ES)

### Transient Loads

- Live load surcharge (LS)
- Vehicular collision force (CT)
- Earthquake load (EQ)
- Vehicular live load (LL)

Table 3-3. LRFD load factors.

Load Combination Limit State	EH ES EV	LL LS	Use One of These at a Time	
			EQ	CT
STRENGTH I	$\gamma_p$	1.75	–	–
EXTREME EVENT I	$\gamma_p$	$\gamma_{EQ}$	1.00	–
EXTREME EVENT II	$\gamma_p$	0.50	–	1.00
SERVICE I	1.00	1.00	–	–

Notes:  
 $\gamma_p$  = load factor for permanent loading. May subscript as  $\gamma_{p-EV}$ ,  $\gamma_{p-EH}$ , etc.  
 $\gamma_{EQ}$  = load factor for live load applied simultaneously with seismic loads

Table 3-4. LRFD load factors.

Type of Load	Load Factor	
	Maximum	Minimum
DC: Component and Attachments	1.25	0.90
EH: Horizontal Earth Pressure <ul style="list-style-type: none"> <li>• Active</li> </ul>	1.50	0.90
EV: Vertical Earth Pressure <ul style="list-style-type: none"> <li>• Overall Stability</li> <li>• Retaining Walls and Abutments</li> </ul>	1.00 1.35	N/A 1.00
ES: Earth Surcharge	1.50	0.75

Note: May subscript as  $\gamma_{EV-MIN}$ ,  $\gamma_{EV-MAX}$ ,  $\gamma_{EH-MIN}$ ,  $\gamma_{EH-MAX}$ , etc.

### 3.7 External Stability Design

Like classical gravity retaining structures, four potential external failure mechanisms are usually considered in sizing MSE walls (FHWA, 2009) which include:

- Sliding of the base
- Limiting eccentricity (formerly overturning)

- Bearing resistance
- Overall/global stability (Section 3.10 and 3.11)

Figure 3-7 provides visualization of the first three failure mechanisms and Table 3-5 provides the resistance factors for external stability analyses for MSE walls.

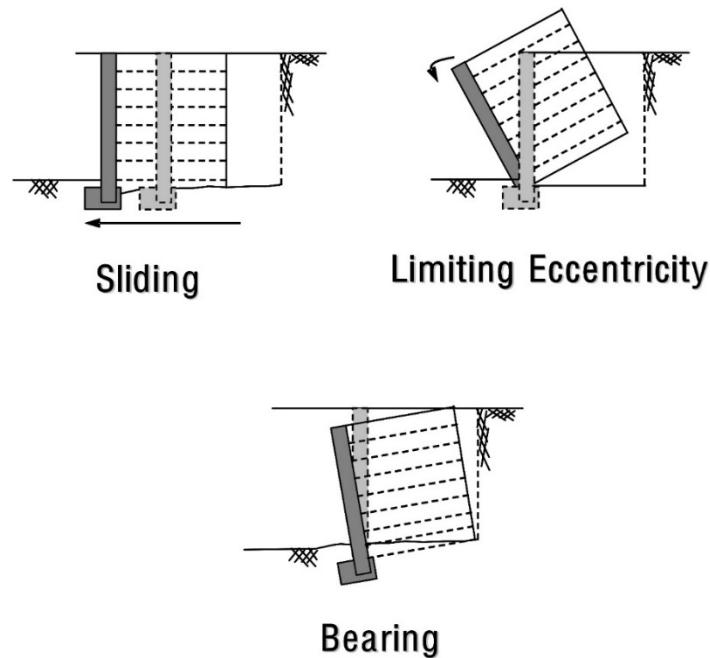


Figure 3-7. External failure mechanisms for an MSE wall.

Table 3-5. External stability resistance factors for MSE walls.

Stability Mode	Condition	Resistance Factor
Bearing Resistance		0.65
Sliding		1.0
Overall (global) Stability	Where geotechnical parameters are well defined, and the slope does not support or contain a structural element	0.75
	Where geotechnical parameters are based on limited information, or the slope contains or supports a structural element	0.65

### 3.7.1 Sliding

Sliding resistance along the base of the wall is evaluated using the same procedures as for spread footings on soil per Article 10.6.3.4 (AASHTO, 2007). The resisting force is the shear resistance along the base of the MSE wall or a weak layer near the base of the wall, whichever provides less resistance. The horizontal thrust component is the external force generated by the retained

backfill and surcharge loading above the retained backfill. In the case of the research MSE wall, the external forces are nonexistent and therefore the factored horizontal driving force is zero.

$$P_d = \gamma_{EH-MAX}F_1 + \gamma_{ES-MAX}F_2 = 1.5(0 \text{ lbf}) + 1.5(0 \text{ lbf}) = 0 \text{ lbf} \quad (3-2)$$

Where,

- $P_d$  = factored driving force
- $F_1$  = retained backfill resultant
- $F_2$  = uniform surcharge resultant
- $\gamma_{EH-MAX}$  = horizontal earth pressure maximum load factor
- $\gamma_{ES-MAX}$  = earth surcharge maximum load factor

The factored resisting force per unit length of wall is calculated as follows:

$$R_r = \Phi_\tau R_\tau = \Phi \gamma_{EV-MIN} V_{1-95\%} \times \mu = 1.0 \times 1.0 \times 11,420 \frac{\text{lbf}}{\text{LF}} \times \tan(31) = 6,862 \frac{\text{lbf}}{\text{LF}} \quad (3-3)$$

Where,

- $R_r$  = factored resistance against failure by sliding
- $R_\tau$  = nominal resistance against failure by sliding
- $\Phi_\tau$  = resistance factor for shear resistance between the soil and the foundation = 1.0
- $V_{1-95\%}$  = reinforced fill resultant (based on soil density at 95% of T-180)
- $\mu$  = minimum soil friction angle (based on direct shear test results at 95% of T-180)
- $\gamma_{EV-MIN}$  = vertical earth pressure minimum load factor = 1.0

Therefore,

$$R_r \gg P_d \therefore \text{ok.}$$

Note: Sliding would not typically be checked in the case of two walls tied together.

### 3.7.2 Eccentricity

Eccentricity (e) is the distance between foundation load resultant “ $V_1$ ” and the center of the reinforced fill zone. Limiting eccentricity is a required strength limit state check formerly referred to as overturning. For vertical walls with a horizontal back slope and uniform surcharge load above the retained backfill, eccentricity is calculated as follows:

$$e = \frac{\gamma_{EH-MAX}F_1(H/3) + \gamma_{ES-MAX}F_2(H/2)}{\gamma_{EV-MIN}V_{1-95\%}} = \frac{1.5(0 \text{ lbf})(10/3 \text{ ft}) + 1.5(0 \text{ lbf})(10/2 \text{ ft})}{1.0 \times 11,420 \frac{\text{lbf}}{\text{LF}}} = 0 \text{ ft} \quad (3-4)$$

Therefore, the resultant foundation load was not eccentric, and overturning was not a concern.

### 3.7.3 Bearing on Foundation Soil

Bearing calculations for the LRFD strength limit ensure that the factored bearing pressure is less than the factored bearing resistance. Service limit calculations are used to compute the nominal bearing pressure for use in settlement analysis to be discussed in Section 3.7.4 (FHWA, 2009). For general shear, the factored vertical pressure at the base of the wall, calculated with a uniform Meyerhof distribution, must not exceed the factored bearing resistance to prevent bearing failure on a uniform foundation soil (FHWA, 2009):

$$q_R \geq q_{V-F} \quad (3-5)$$

Where,

- $q_R$  = factored bearing resistance (psf)
- $q_{V-F}$  = factored vertical pressure at the base of the wall (psf)

For bearing calculations, a different calculation for eccentricity is required, where maximum load factors are used with the vertical forces from the reinforced fill zone.

$$e_B = \frac{\gamma_{EH-MAX}F_1(H/3) + \gamma_{ES-MAX}F_2(H/2)}{\gamma_{EV-MAX}V_{1-103\%} + \gamma_{ES-MAX}q_sL} = \frac{1.5(0 \text{ lbf})(10/3 \text{ ft}) + 1.5(0 \text{ lbf})(10/2 \text{ ft})}{1.35(12,340 \frac{\text{lbf}}{\text{LF}}) + [1.5(250 \text{ psf}) \times 10 \text{ ft}]} = 0 \text{ ft} \quad (3-6)$$

The factored vertical pressure at the base of the wall is calculated using 104% of T-180,

$$q_{V-F} = \frac{\gamma_{EV-MAX}V_{1-103\%} + \gamma_{ES-MAX}q_sL}{L - 2e_B} = \frac{1.35(12,340 \frac{\text{lbf}}{\text{LF}}) + [1.5(2,850 \text{ psf}) \times 10 \text{ ft}]}{10 \text{ ft} - 0 \text{ ft}} = 5,941 \text{ psf}. \quad (3-7)$$

The nominal bearing resistance of the base soil layer is calculated using 95% of T-180 (See Table 3-6 for bearing resistance factors),

$$q_n = \frac{1}{2}L'\gamma_f N_\gamma = \frac{1}{2}(10 \text{ ft})(114.2 \text{ pcf})(25.9) = 14,789 \text{ psf}, \quad (3-8)$$

the resistance factor is applied,

$$q_R = \Phi q_n = 0.65 \times 14,789 \text{ psf} = 9,613 \text{ psf}, \quad (3-9)$$

and a stability check is conducted,

$$q_R = 9,613 \text{ psf} > q_{V-F} = 5,941 \text{ psf} \rightarrow CDR = 1.62 \therefore \text{ok}.$$

Table 3-6. Bearing resistance factors (Table 10.6.3.1.2a-1; AASHTO, 2007)

$\phi$	$N_c$	$N_q$	$N_\gamma$	$\phi$	$N_c$	$N_q$	$N_\gamma$
0	5.14	1.0	0.0	23	18.1	8.7	8.2
1	5.4	1.1	0.1	24	19.3	9.6	9.4
2	5.6	1.2	0.2	25	20.7	10.7	10.9
3	5.9	1.3	0.2	26	22.3	11.9	12.5
4	6.2	1.4	0.3	27	23.9	13.2	14.5
5	6.5	1.6	0.5	28	25.8	14.7	16.7
6	6.8	1.7	0.6	29	27.9	16.4	19.3
7	7.2	1.9	0.7	30	30.1	18.4	22.4
8	7.5	2.1	0.9	31	32.7	20.6	25.9
9	7.9	2.3	1.0	32	35.5	23.2	30.2
10	8.4	2.5	1.2	33	38.6	26.1	35.2
11	8.8	2.7	1.4	34	42.2	29.4	41.1
12	9.3	3.0	1.7	35	46.1	33.3	48.0
13	9.8	3.3	2.0	36	50.6	37.8	56.3
14	10.4	3.6	2.3	37	55.6	42.9	66.2
15	11.0	3.9	2.7	38	61.4	48.9	78.0
16	11.6	4.3	3.1	39	37.9	56.0	92.3
17	12.3	4.8	3.5	40	75.3	64.2	109.4
18	13.1	5.3	4.1	41	83.9	73.9	130.2
19	13.9	5.8	4.7	42	93.7	85.4	155.6
20	14.8	6.4	5.4	43	105.1	99.0	186.5
21	15.8	7.1	6.2	44	118.4	115.3	224.6
22	16.9	7.8	7.1	45	133.9	134.9	271.8
Note: $N_c$ (Prandtl, 1921), $N_q$ (Reisner, 1924), and $N_\gamma$ (Vesic, 1975). $N_q$ is embedment term, which is typically not used in MSE wall design.							

### 3.7.4 Settlement Analysis

The total settlement of a reinforced earth structure is the sum of the settlement of the foundation soil due to overburden pressure (reinforced zone is the overburden), and the internal compression of the reinforced fill due to the compaction effort used and the vertical forces applied to the structure (RECo, 2011). The internal settlement of the reinforced mass is limited to negligible compression of the select backfill due to the “block” behavior of the reinforced zone (RECo, 2011). The settlement of the foundation soil caused by construction of the reinforced mass can be estimated using classical soil mechanics (e.g., Schmertmann method). However, the foundation

soil used in the research was only an approximate 1.5 ft layer of compacted sand, underlain by a six-inch compacted gravel layer, underlain by a concrete floor. Therefore, settlement was deemed negligible (RECo confirmed the assumption valid).

Note: Due to the concrete walls on three sides of the soil mass and the stiff reinforcement, the scenario could be treated as 1-D similar to an oedometer test and the constrained modulus could be used to better estimate the settlement.

### 3.8 Internal Stability Design

#### 3.8.1 Soil Reinforcement

For the research, flat steel strips were used as the reinforcement. Based on the type of reinforcement (steel strips), a bilinear failure surface was assumed that separates the reinforced soil mass into an active zone and resistant zone in which an equilibrium state must be achieved for a successful design. Internal stability design following the Simplified Method incorporates lateral pressure varying from a multiple of  $k_a$  at the top of the wall to a near active earth pressure state,  $k_a$ , 20 feet below the top of the wall, Figure 3-8. The Coherent Gravity method suggests an at-rest condition,  $k_0$ , at the top of the wall and an active state at 20 feet below the top of the wall, Figure 3-9.

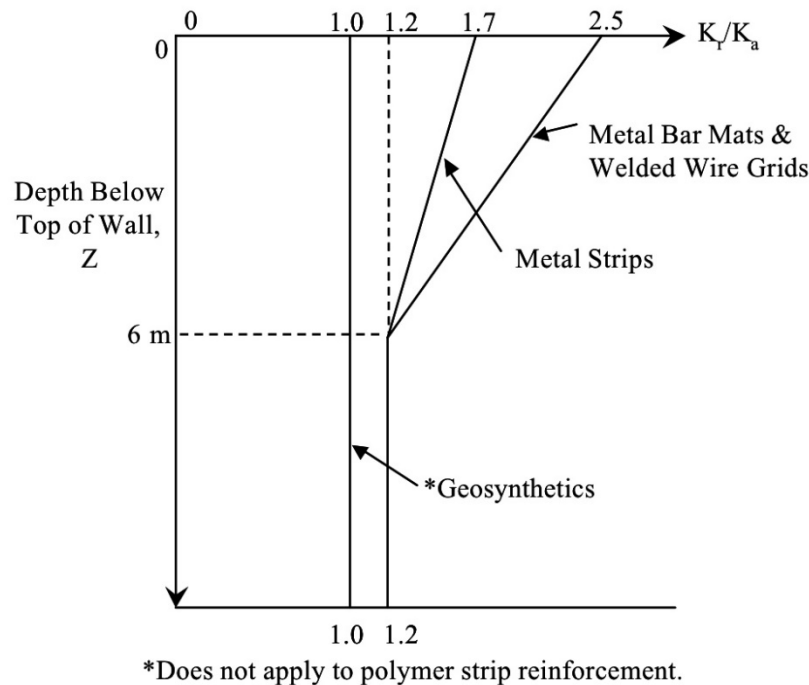


Figure 3-8. Determination of  $k_r/k_a$  for the Simplified Method (AASHTO, 1999).



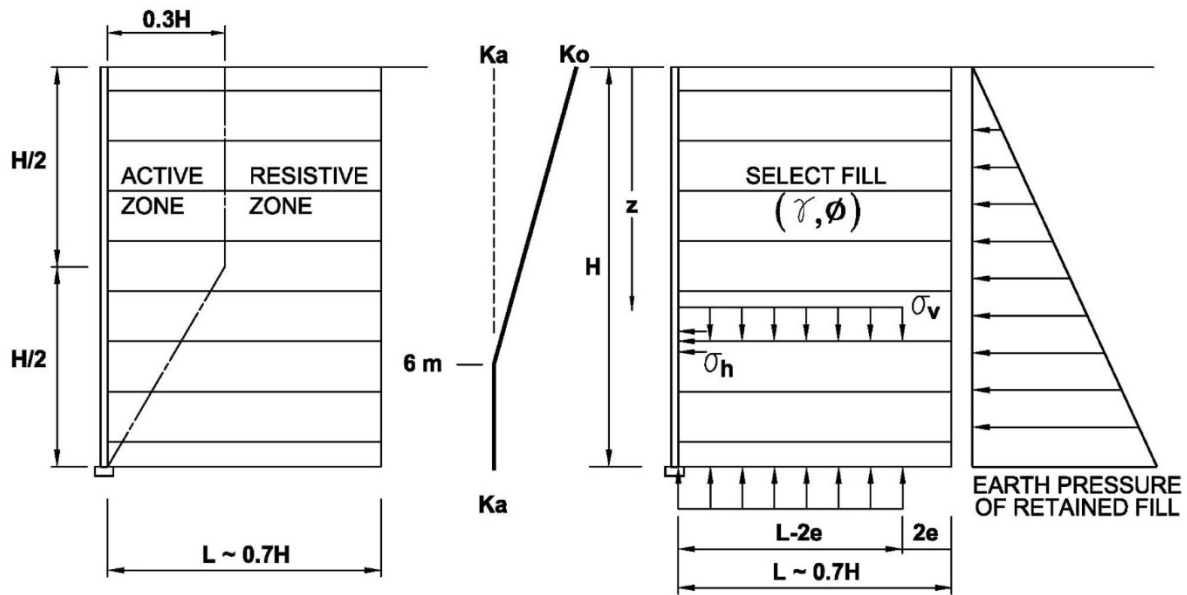


Figure 3-9. Coherent Gravity Method.

The method developed by Spangler and Handy (1984) considers the silo effect (soil arching) for narrow MSE walls in front of a stabilized face (i.e., unyielding surfaces) as shown in Figure 3-10. The method proposes that as soil is placed in layers it settles due to its self-weight and the load applied by additional overburden. Simultaneously, the wall provides a vertical shear load due to friction that resists the settlement of the soil. The vertical shear load reduces the soil overburden pressure and inherently reduces the lateral earth pressure. Kniss et al. (2017) states that earth pressure theories that do not consider the arching effects may be overly conservative when applied to narrow walls.

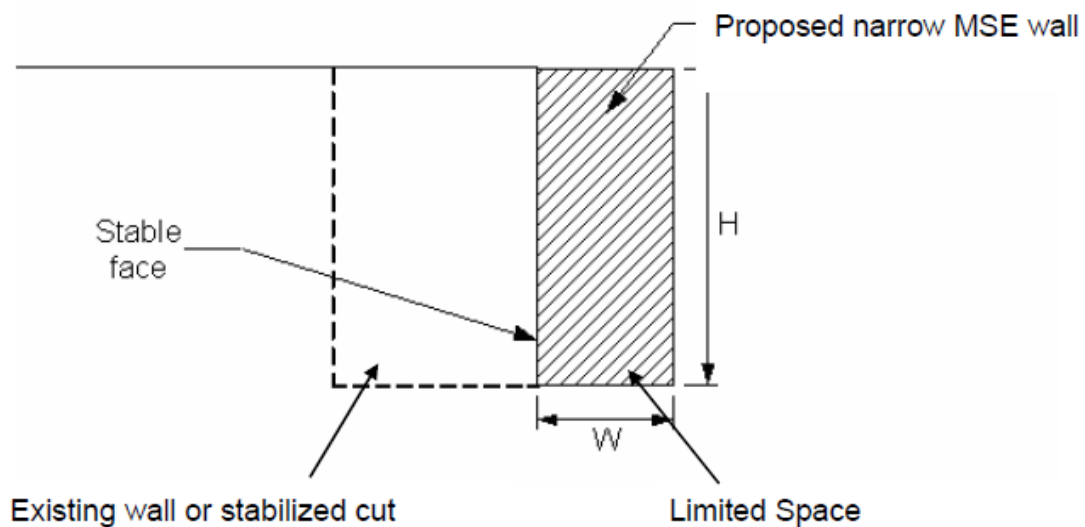


Figure 3-10. Narrow MSE wall in front of a stabilized face (Kniss et al. 2007).

The Spangler and Handy equation is provided:

$$k' = \frac{1}{2 \tan \delta} * \left(\frac{B}{z}\right) * \left[1 - \exp\left(-2k_0 * \left(\frac{z}{B}\right) \tan \delta\right)\right] \quad (3-10)$$

Where,

- B is reinforcement length (ft)
- z is depth below top of wall (ft)
- $\delta$  is the interface friction angle between the soil and wall (estimated at 30 degrees)
- $k_0$  is the at-rest earth pressure coefficient

### 3.8.2 Critical Failure Surface

The critical slip surface in an MSE wall is assumed to coincide with the locus of the maximum tensile force ( $T_{\max}$ ) in each reinforcement layer (FHWA, 2009). For inextensible reinforcement, the approximate critical failure surface is assumed to be bilinear and falls within the active wedge, Figure 3-11. For typical MSE wall design with a wall height of ten feet, the critical slip surface would be approximately three feet behind the wall facing at depths zero to five feet, and decrease linearly from three feet to zero feet behind the wall facing as the depth increases from five feet to ten feet below the top of the wall as depicted in Figure 3-11. However, this critical slip surface generally only applies to conventional MSE walls with independent reinforcements and not the tied across scenario investigated.

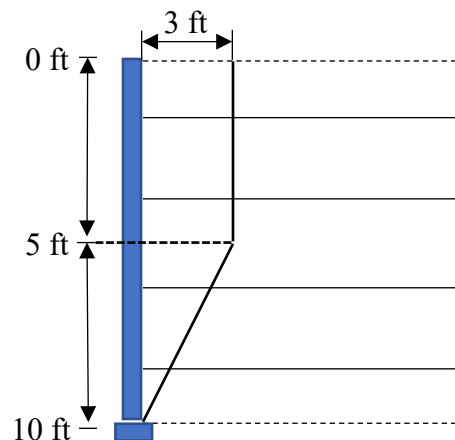


Figure 3-11. Bilinear critical slip surface.

Note: If failure develops in the tied across scenario, the reinforcement may elongate and be deformed at its intersection with the failure surface. This results in rotation and an increase in the tensile force within the reinforcement. However, elongation and rotation may be negligible for stiff inextensible reinforcements such as steel strips. Reinforcement rotation is ignored for

internal stability calculations using the AASHTO recommended Simplified Method but may be considered in compound slope stability analysis (FHWA, 2009).

### 3.8.3 Unfactored Loads

The unfactored loads of an MSE wall are the reinforced fill and any surcharge loading on top of the reinforced zone (FHWA, 2009). The unfactored loads of an MSE wall may include loading due to,

- Vertical earth pressure (EV),
- Live load surcharge (LS),
- Earth surcharge (ES).

Water, seismic, and vehicle impact loads are typically evaluated but were unnecessary for the research. Live loads (weight of compaction equipment and researchers) were present during construction; however, they were not present at the time the simulated earth surcharge was applied. Based on the data provided in Section 3.3,

$$\gamma_{d-max} = 105.7 \text{ pcf and } w = 12.7\% = 0.127,$$

$$\gamma = (1 + w)\gamma_d = (1 + 0.127)105.7 = 119.1 \text{ pcf.} \quad (3-11)$$

For a relative compaction effort of 95% of T-180:

$$\gamma_{d-field} = RC * \gamma_{d-max} = 0.95 * 105.7 \text{ pcf} = 100.4 \text{ pcf}, \quad (3-12)$$

$$\gamma = (1 + w)\gamma_{d-field} = (1 + 0.127)100.4 = 113.2 \text{ pcf}.$$

The following vertical and lateral earth pressures, Table 3-7 and Figure 3-12, are derived at each respective depth increment using the at-rest ( $k_0$ ) and active ( $k_a$ ) earth pressure coefficients as well as the earth pressure coefficients derived for the Coherent Gravity ( $k_{rCG}$ ), Simplified ( $k_{rS}$ ), and Spangler and Handy ( $k_{rS\&H}$ ) Methods.

Table 3-7. Unfactored vertical and horizontal earth pressures @ 95% of T-180.

Known Parameters		Earth Pressures for Various k-Values				
Depth (ft)	$\sigma_v$ (psf)	$k_0$	$k_a$	$k_{rCG}$	$k_{rS}$	$k_{rS\&H}$
1	113	55	36	54	61	53
2	226	110	72	106	120	104
3	340	165	109	156	177	152
4	453	220	145	205	232	197
5	566	274	181	251	285	239
6	679	329	217	296	337	280
7	792	384	254	338	387	318
8	905	439	290	379	435	354
9	1,019	494	326	418	481	388
10	1,132	549	362	456	525	420

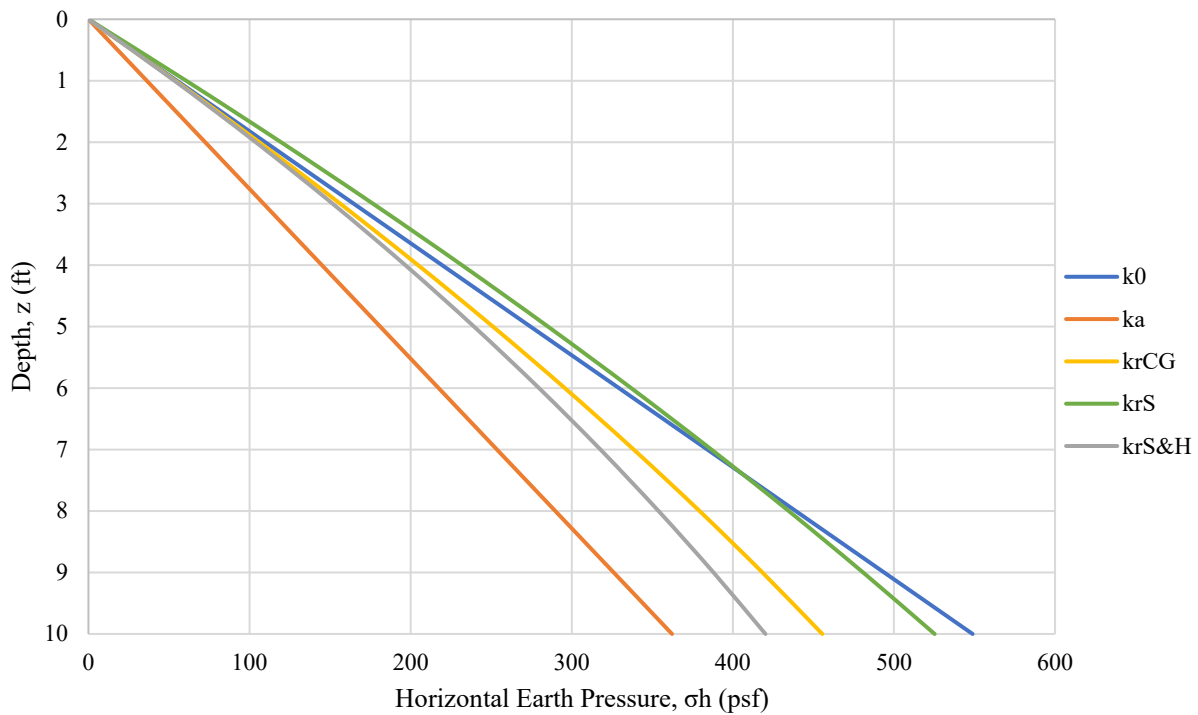


Figure 3-12. Depth vs. unfactored lateral earth pressure for k coefficients @ 95% of T-180.

For a relative compaction of 104% of T-180 (Note: 104% was used as a conservative approach because this degree of compaction was achieved in one of the modified proctor tests):

$$\gamma_{d-field} = RC * \gamma_{d-max} = 1.04 * 105.7 \text{ pcf} = 109.9 \text{ pcf},$$

$$\gamma = (1 + w)\gamma_{a-field} = (1 + 0.127)109.9 = 123.9 \text{ pcf.}$$

The following lateral earth pressures, Table 3-8 and Figure 3-13, are derived at each depth using the At-rest and Active earth pressure coefficients as wells as the earth pressure coefficients derived for the Coherent Gravity, Simplified, and Spangler and Handy Methods.

Table 3-8. Unfactored vertical and horizontal earth pressures at 104% of T-180.

Known Parameters		Earth Pressures for Various k-Values				
Depth (ft)	$\sigma_v$ (psf)	$k_0$	$k_a$	$k_{rCG}$	$k_{rS}$	$k_{rS\&H}$
		$\sigma_h$ (psf)	$\sigma_h$ (psf)	$\sigma_h$ (psf)	$\sigma_h$ (psf)	$\sigma_h$ (psf)
1	124	43	26	42	43	42
2	248	85	51	82	85	82
3	372	128	77	120	125	121
4	496	170	103	157	165	158
5	619	213	129	192	203	193
6	743	256	154	225	239	227
7	867	298	180	257	275	260
8	991	341	206	287	309	292
9	1,115	383	232	315	342	322
10	1,239	426	257	342	373	352

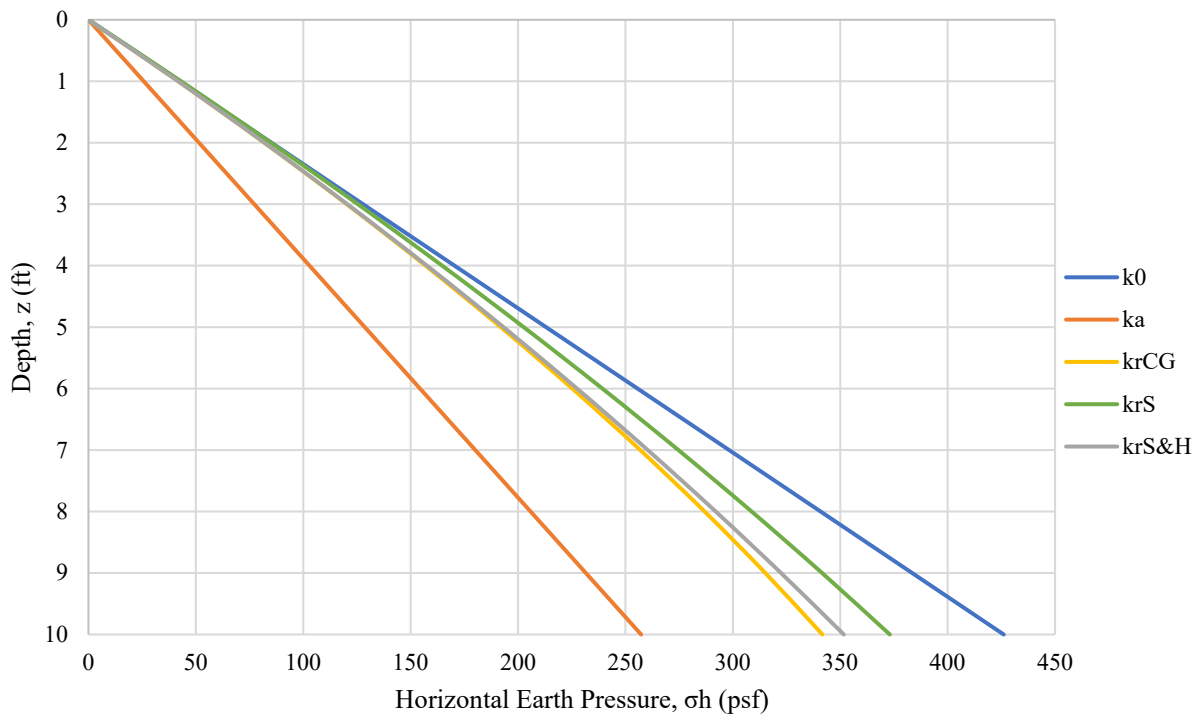


Figure 3-13. Depth vs. unfactored lateral earth pressure for k coefficients @ 104% of T-180.

The live load surcharge included the weight of researchers constructing the wall and the equipment used during construction. The equipment included the weight of the vibratory compaction device used during backfilling.

A simulated earth surcharge was incrementally applied to the reinforced fill. The intent of the incremental surcharge was to investigate the resulting earth pressures at various reinforcement-to-wall height ratios (B/H). In practice, walls are only tied together when B/H = 0.3. This required a simulated surcharge to be applied that was the equivalent of approximately 23 feet of overburden soil at each state of soil density. Due to the limited overhead clearance in the laboratory, a reaction frame was constructed using UF's Soil Box walls and the Matjack-airbag system (Figure 3-6).

#### *3.8.4 Vertical Layout of Soil Reinforcement*

In order to determine a standard/generic wall panel size for the State of Florida, multiple vendors from the FDOT's approved vendors list were surveyed. The following provides the results:

- SSL - 5' x 5' square panel
- The Neel Company - 5' x 7' rectangular
- Tensar Int. Corp. - 5' x 5' square panel (5' x 10' rectangular is also used but less common in Florida)
- Tri-Con Precast - 5' x 5' square panel
- Sine Wall, LLC - 5' x 5' square panel (5' x 10' rectangular is also used but less common in Florida)
- Sanders Pre-cast - 5' x 5' square panel (5' x 10' rectangular is also used)
- Earth Wall Products - 4' x 8' rectangular
- Visit-A-Wall Systems - 5' x 5' square panel (5' x 10' rectangular is also used but less common in Florida)
- RECo - 5' x 5' square panel (5' x 10' rectangular is also used but less common in Florida)

From the results it was determined that 5' x 5' square panels would be considered "standard" or "generic". The select panels were purchased from the Reinforced Earth Company (RECo). The actual dimensions of RECo's nominal 5' x 5' square panel are 4.79' x 4.92'. This provided 2.46' spacing between the reinforcement levels as depicted in Figure 3-14 for the vertical reinforcement layout.

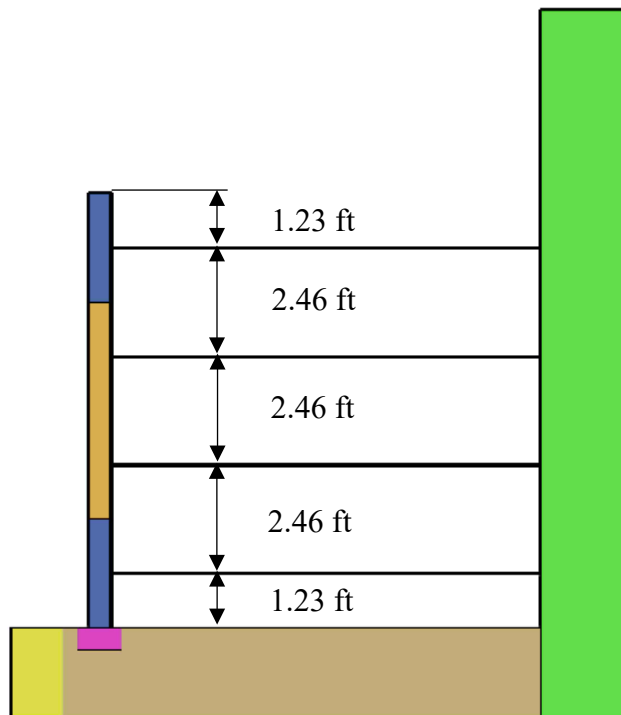


Figure 3-14. Vertical reinforcement layout.

### 3.8.5 Factored Horizontal Stress and Maximum Tension (at each reinforcement level)

The maximum tensile force is primarily based on the type of reinforcement used in the MSE wall design (Collin, 1986; Christopher et al., 1990; Allen et al., 2001). Consequently, the tensile force is a function of the modulus, extensibility, and density of the reinforcement. Since the MSE wall design required the reinforcement to be attached to an unyielding structure, an increase in the lateral earth pressure was considered. The actual soil pressure that results from material placed and compacted behind an unyielding structure was not well defined and investigating such a case was the objective of this research. FHWA GEC #11 (2009), acknowledges that “much higher” soil reinforcement tension develops when back-to-back walls are tied to each other. The added stress occurs because stress relief through minor deformation of the retaining structure that typically occurs in conventional construction, is prevented by connecting the walls. While GEC # 11 recognizes the problem, it does not provide a clear recommendation for the estimation of soil pressure of compacted soils, and simply states that higher stresses are to be expected at the connection. WSDOT (2010) states that the soil reinforcement for back-to-back MSE walls, where both faces are connected (i.e., continuous from one wall to the other), should be designed for double the loading which suggests  $k_r$  at 95% of  $T-180$  (similar value to  $k_0$ ) may be doubled and the horizontal stress may be similar to the vertical stress. Although, this may be a conservative approach, WSDOT (2010) provided the only quantifiable increase in stress found within the literature, for two walls tied together. However, based on the dimensions for when a tied together scenario would be implemented in practice ( $B/H = 0.3$ ), the lateral earth pressure

may be reduced due to the narrow condition as suggested by Spangler and Handy (1984; soil arching/silo effect).

The following was calculated at a depth of 8.61 ft below the top of the wall which was the deepest reinforcement level. The horizontal spacing ( $S_h$ ) and vertical spacing ( $S_v$ ) of the reinforcement were both set to 2.46 ft to provide a conservative design approach. The total unit weight of the soil was also used, rather than the dry unit weight, to provide a conservative design approach. Using the previously defined soil and loading parameters, the Simplified Method earth pressure coefficient, and AASHTO LRFD load factors, the following provides a sample calculation for the factored horizontal earth pressure and maximum factored load applied to the reinforcement for each state of soil density.

For 95% of T-180:

$$\gamma_r = 113.2 \text{ pcf}, Z = 8.61 \text{ ft}, k_r = 0.475, q_s = 2,603 \text{ psf}, \gamma_{EV-MAX} = 1.35, \gamma_{ES-MAX} = 1.50, S_v = S_h = 2.46'$$

$$\sigma_h = k_r[(\gamma_r Z)\gamma_{EV-MAX} + q_s\gamma_{ES-MAX}] \quad (3-13)$$

$$\sigma_h = 0.475[(113.2 \text{ pcf} \times 8.61 \text{ ft})1.35 + (2,603 \text{ psf})1.5] = 2,480 \text{ psf},$$

$$T_{max} = \sigma_h S_v S_h = 2,480 \text{ psf} \times 2.46 \text{ ft} \times 2.46 \text{ ft} = 15,008 \text{ lbf}, \quad (3-14)$$

For 104% of T-180:

$$\gamma_r = 123.9 \text{ pcf}, Z = 8.61 \text{ ft}, k_r = 0.308, q_s = 2,849 \text{ psf}, \gamma_{EV-MAX} = 1.35, \gamma_{ES-MAX} = 1.50, S_v = S_h = 2.46'$$

$$\sigma_h = k_r[(\gamma_r Z)\gamma_{EV-MAX} + q_s\gamma_{ES-MAX}]$$

$$\sigma_h = 0.308[(123.9 \text{ pcf} \times 8.61 \text{ ft})1.35 + (2,849 \text{ psf})1.5] = 1,760 \text{ psf},$$

$$T_{max} = \sigma_h S_v S_h = 1,760 \text{ psf} \times 2.46 \text{ ft} \times 2.46 \text{ ft} = 10,651 \text{ lbf}.$$

### 3.8.6 Nominal and Factored Long-term Tensile Resistance of Soil Reinforcements

The structural design properties of reinforcement materials are a function of geometric characteristics, strength and stiffness, durability, and material type (FHWA, 2009). The design life for steel reinforcement is estimated from a reduction of the cross-sectional area of the reinforcement used in design due to corrosion losses over the design life, Equation 3-15.

$$E_c = E_n - E_R \quad (3-15)$$

Where,

- $E_c$  is the thickness of the reinforcement at the end of the design life



- $E_n$  = the nominal thickness at construction
- $E_R$  = the sacrificial thickness of metal expected to be lost by uniform corrosion during the service life of the structure

The following corrosion rates for metallic reinforcement apply to permanent MSE Walls within non-corrosive environments only (FDOT Structures Design Guidelines (SDG) Section 3.13.2, Article J):

- Zinc (first 2 years) 0.58 mils/year (15  $\mu\text{m}/\text{year}$ )
- Zinc (subsequent years to depletion) 0.16 mils/year (4  $\mu\text{m}/\text{year}$ )
- Carbon Steel (after depletion of zinc to 75 years) 0.47 mils/year (12  $\mu\text{m}/\text{year}$ )
- Carbon Steel (75 to 100 years) 0.28 mils/year (7  $\mu\text{m}/\text{year}$ )

Table 3-9 indicates the soil properties of the select fill are non-corrosive. Therefore, based on the corrosion rates provided in the SDG for a design life of four years, the following corrosion is expected:

$$\text{Corrosion} = 2 \text{ years} \left( 15 \frac{\mu\text{m}}{\text{year}} \right) + 2 \text{ years} \left( 4 \frac{\mu\text{m}}{\text{year}} \right) = 38 \mu\text{m} \quad (3-16)$$

Table 3-9. O'steen Soil Electrochemical Properties with Acceptance Criteria.

Soil Properties	Electrochemical Properties for O'steen Soil				
	Measured	FDOT Acceptance Criteria		FHWA Acceptance Criteria	
pH	5.32	$5 < \text{pH} < 9$	FDOT FM 5-550	$5 < \text{pH} < 10$	AASHTO T-288
Resistivity ( $\Omega\text{-cm}$ )	58,900	$> 3,000$	FDOT FM 5-551	$> 3,000$	AASHTO T-289
Chloride (ppm)	54	$< 100$	FDOT FM 5-551	$< 100$	ASTM D4327
Sulfate (ppm)	6.5	$< 200$	FDOT FM 5-551	$< 200$	ASTM D4327
Organic Content (%)	0.3	$\leq 2$	FDOT FM 1-T267	$\leq 1$	AASHTO T-267

The RECo HA steel strips provide a zinc layer thickness of 86  $\mu\text{m}$  which indicates the zinc coating would not be depleted by the corrosion losses and the structural integrity of strips would not be affected. Therefore, the full cross-section of the steel strips is used to calculate the nominal tensile strength.

The nominal tensile strength for the steel reinforcement strips,  $T_{al}$ , is calculated as follows:

$$T_{al} = F_y A_{cs} = 65,000 \text{ psi} \times 0.31 \text{ in}^2 = 20,150 \text{ lbf} \quad (3-17)$$

Where,

- $F_y$  = yield stress of steel (Grade 65 steel, see Section 3.8.7)
- $A_{cs}$  = design cross sectional area of the steel strips = 50 mm x 4 mm = 200  $\text{mm}^2$  = 0.31  $\text{in}^2$

The resistance factors for tensile rupture of MSE wall soil reinforcements are summarized in Table 3-10.

Table 3-10. Resistance factors,  $\phi$ , for tensile and pullout resistance for MSE walls.

Reinforcement Type and Loading Condition		Resistance Factor	
Metallic reinforcement and connectors	Strip reinforcements <sup>(A)</sup>		
		Static loading	0.75
		Combined static/earthquake loading	1.00
		Combined static/traffic barrier impact <sup>(B)</sup>	1.00
	Grid reinforcements <sup>(A, C)</sup>		
		Static loading	0.65
		Combined static/earthquake loading	0.85
		Combined static/traffic barrier impact <sup>(B)</sup>	0.85
	Geosynthetic reinforcement and connectors		Static loading
		Combined static/earthquake loading	1.20
		Combined static/traffic barrier impact <sup>(B)</sup>	1.20
Pullout resistance of tensile reinforcement (metallic and geosynthetic)		Static loading	0.90
		Combined static/earthquake loading	1.20
		Combined static/traffic barrier impact <sup>(B)</sup>	1.00
Notes:			
A. Apply to gross cross-section less sacrificial area. For sections with holes, reduce gross area in accordance with AASHTO (2007) Article 6.8.3 and apply to net section less sacrificial area.			
B. Combined static/traffic barrier impact resistance factors are not presented in AASHTO.			
C. Applies to grid reinforcements connected to rigid facing element, e.g., a concrete panel or block. For grid reinforcements connected to a flexible facing mat or which are continuous with the facing mat, use the resistance factor for strip reinforcements.			

The factored tensile resistance,  $T_r$ , for static loading is equal to:

$$T_r = \Phi T_{al} = \Phi F_y A_{CS} = 0.75 \times 65,000 \text{ psi} \times 0.31 \text{ in}^2 = 15,113 \text{ lbf} \quad (3-18)$$

Therefore,

$$T_r = 15,113 \text{ lbf} > T_{max95\%} = 15,008 \text{ lbf} \rightarrow CDR = 1.01 \therefore \text{ok.}$$

$$T_r = 15,113 \text{ lbf} > T_{max104\%} = 10,651 \text{ lbf} \rightarrow CDR = 1.42 \therefore \text{ok.}$$

### 3.8.7 Grade of Soil Reinforcement and Number of Soil Reinforcement Elements

Standard RECo reinforcing strips are fabricated from hot rolled steel conforming to the physical and mechanical properties of ASTM A-572 Grade 65 or equivalent (compliant with FDOT

specs). The HA strips are 50 mm wide by 4 mm thick, Figure 3-19. After fabrication, the reinforcing strips are hot dip galvanized in accordance with ASTM A-123 (compliant with FDOT specs) which provides a minimum of 0.61 kg/m<sup>2</sup> (2.0 oz/ft<sup>2</sup>) of zinc (0.86 μm minimum thickness layer; RECo, 2001).

The number of strips required per tributary wall area for tensile capacity is calculated from the following equation:

$$N = \frac{(\sigma_h A_p)}{A_{cs}(0.55F_y)} \quad (3-19)$$

Where,

- N = number of strips per tributary wall area (round up to nearest integer)
- $\sigma_h$  = horizontal earth pressure at that level
- $A_p$  = tributary wall area
- $A_{cs}$  = cross sectional area of reinforcing strip (at end of service life)
- $F_y$  = yield strength of steel reinforcing strips

The tributary wall area used for calculation is 24.2 ft<sup>2</sup>. This corresponds to half a square panel high (2.46 ft) by two square panels wide (9.84 ft). The factored lateral earth pressures were previously determined in Section 3.8.5. The cross-sectional area of the strips is 0.31 in<sup>2</sup>. The yield strength of the reinforcement strips is  $F_y = 65$  ksi.

The number of reinforcement strips per tributary wall area was determined to be four to fit the instrumentation within the reinforced fill. Therefore, a different approach is taken for this stability check. For the research, the maximum factored horizontal earth pressure was determined based on  $N = 4$  steel strips per tributary wall area. The worst-case scenario (95% of T-180 @  $z = 8.61$  ft) is used in the calculation.

$$\sigma_h = \frac{N \times A_{cs} \times 0.55 \times F_y}{A_p} = \frac{4 \text{ strips} \times 0.31 \text{ in}^2 \times 0.55 \times 65,000 \text{ psi}}{24.2 \text{ ft}^2} = 1,832 \text{ psf}$$

The factored horizontal earth pressure of 1,832 psf corresponds to the maximum simulated surcharge that can be safely applied, which is the equivalent to 15 ft of overburden following the Simplified method. Following the Spangler and Handy method, the maximum surcharge height would be 20 ft. In either case, exceeding the simulated surcharge heights would cause the factored loads to exceed the factored resistance. However, live monitoring results received from the instrumentation inside the wall allowed the surcharge to be safely applied without exceeding the unfactored tensile capacity.

### 3.8.8 Connection Resistance at MSE Wall Facing

Metallic reinforcements for MSE wall segmental precast panels are structurally connected to the facing by either bolting the reinforcement to a tie strip cast in the panel or connected with a bar

connector to a suitable anchorage device in the panels (FHWA, 2009). For the research, embedded connections were used for both walls. RECo states that their connections embedded in the facing panels and the high strength nut/bolt/washer assembly (Figure 3-15) exceeds the requirements of AASHTO, and that the embedded connection is stronger than the steel soil reinforcement. Calculations are made for the following connection failure mechanisms corresponding to Figure 3-15:

- 2 tie strips tensile resistance (embedded connection – Section A-A)
- Tie strips tensile resistance at bolt hole (2 tie strips – Section B-B)
- Tie strips bolt hole bearing resistance (2 tie strips – Section B-B)
- Reinforcement strip tensile resistance (Section C-C)
- Reinforcement strip tensile resistance at bolt hole (Section B-B)
- Reinforcement strip bearing resistance at bolt hole (Section B-B)
- Bolt shear resistance (Section B-B)

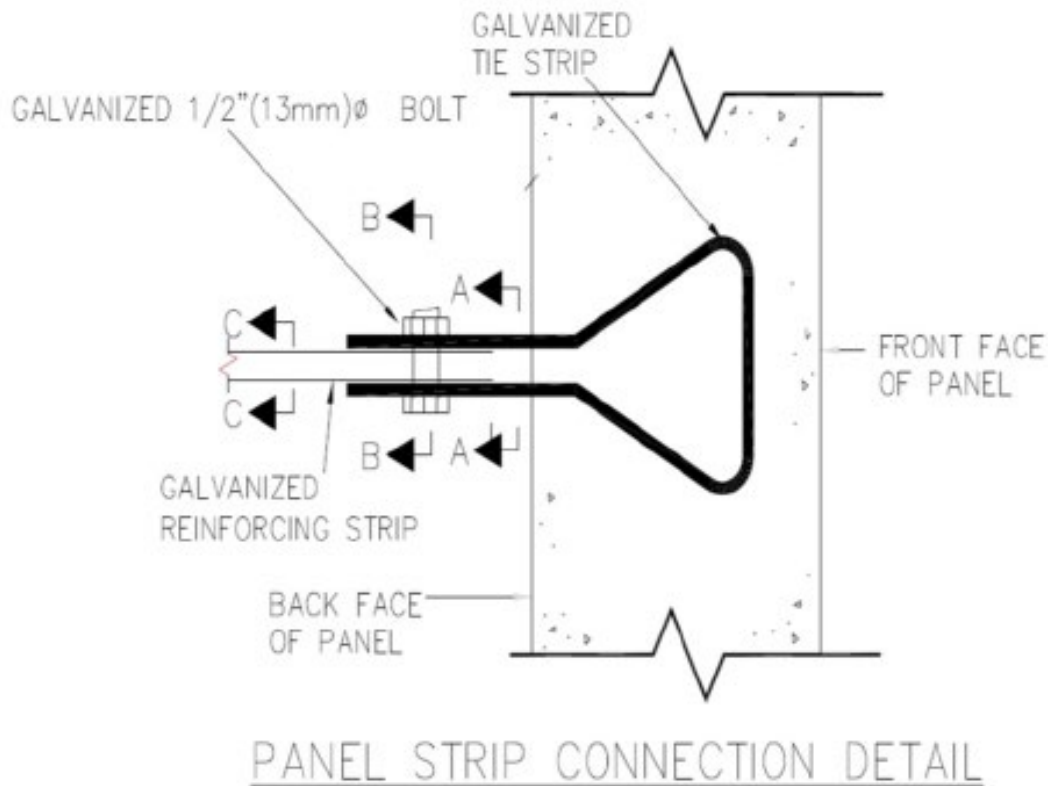


Figure 3-15. RECo panel strip connection detail.

Note:  $\phi = 0.75$  for tensile resistance of metallic reinforcements and connectors.

Table 3-11. Connection detail mechanical properties.

Mechanical Property	HA Strip	Tie Strip	Bolt Set
Thickness, t (mm)	4	3.42	N/A
Width, w (mm)	50	50	N/A
$F_u$ (ksi)	200	171	N/A
$F_y$ (ksi)	80	65	N/A
Bolt Diameter, d (in)	N/A	N/A	0.5
$F_u$ (ksi) – Bolt set	N/A	N/A	120
Bolt Hole Dia. (mm)	14.3	14.3	N/A

$$2 \text{ Tie Strip Tensile Resistance} = \phi F_y 2A_s$$

$$\therefore \phi F_y 2A_s = 0.75 \times 50 \text{ ksi} \times 2 \times 0.265 \text{ in}^2 = 19.88 \text{ kips}$$

$$2 \text{ Tie Strip Tensile Resistance at Bolt Hole} = \phi F_y 2A_s$$

$$\therefore \phi F_u 2A_s = 0.75 \times 65 \text{ ksi} \times 2 \times 0.189 \text{ in}^2 = 18.45 \text{ kips}$$

$$2 \text{ Tie Strip Bearing Resistance at Bolt Hole} = \phi(2.4 \times d \times 2t \times F_u)$$

$$\therefore \phi(2.4 \times d \times 2t \times F_u) = 0.75(2.4 \times 0.5 \text{ in} \times 2(0.135 \text{ in}) \times 65 \text{ ksi}) = 15.75 \text{ kips}$$

$$\text{Reinforcement Strip Tensile Resistance} = \phi F_y A_s$$

$$\therefore \phi F_y A_s = 0.75 \times 65 \text{ ksi} \times 0.310 \text{ in}^2 = 15.11 \text{ kips}$$

$$\text{Reinforcement strip tensile resistance at bolt hole} = \phi F_y A_s$$

$$\therefore \phi F_u A_s = 0.75 \times 80 \text{ ksi} \times 0.221 \text{ in}^2 = 13.28 \text{ kips}$$

$$\text{Reinforcement Strip Bearing Resistance at Bolt Hole} = \phi(2.4 \times d \times t \times F_u)$$

$$\therefore \phi(2.4 \times d \times t \times F_u) = 0.75(2.4 \times 0.5 \text{ in} \times 0.157 \text{ in} \times 80 \text{ ksi}) = 11.34 \text{ kips} \leftarrow \text{Controls}$$

$$\text{Bolt Shear Resistance} = \phi(0.48F_u A_b N_s)$$

$$\therefore \phi(0.48F_u A_b N_s) = 0.75(0.48 \times 120 \text{ ksi} \times 0.196 \text{ in}^2 \times 2 \text{ shear planes}) = 16.96 \text{ kips}$$

The following table provides a summary of the factored and unfactored resistance components.

Table 3-12. Resistance components summary.

Resistance Component	Resistance (kips)	
	Factored	Unfactored
2 Tie strips tensile resistance (embedded connection)	19.9	26.5
Tie Strips tensile resistance at bolt hole (2 tie strips)	18.5	24.6
Tie Strips bolt hole bearing resistance (2 tie strips)	15.8	21.0
Reinforcing strip tensile resistance	15.1	20.2
Reinforcing Strip tensile resistance at bolt hole	13.3	17.7
Reinforcing Strip bolt hole bearing resistance	11.3	15.1
Bolt shear resistance	17.0	22.6

Stability checks are then performed using five different earth pressure coefficients for each state of soil density, at each reinforcement level, with a surcharge equivalent to 23 feet of overburden.

Table 3-13. Connection strength stability check for 95% of T-180 (Simplified Method).

Depth (ft)	$\sigma_v$ (psf)	$\Delta\sigma_v$ (psf)	Simplified	$\sigma_h$ (psf)	Load Factors		$\sigma_h$ (psf)	Unfactored	Factored	Factored	Unfactored
			$k_{rs}$		Unfactored	$\gamma_{P-EV}$		$\gamma_{P-ES}$	Factored	$T_{max}$ (lbf)	$T_{max}$ (lbf)
1.23	139	2,603	0.534	1,465	1.35	1.5	2,187	8,866	13,232	11,340	15,120
3.69	418	2,603	0.515	1,554	1.35	1.5	2,299	9,407	13,915	11,340	15,120
6.15	696	2,603	0.495	1,633	1.35	1.5	2,397	9,881	14,509	11,340	15,120
8.61	974	2,603	0.475	1,700	1.35	1.5	2,481	10,289	15,012	11,340	15,120

Table 3-14. Connection strength stability check for 95% of T-180 (Coherent Gravity Method).

Depth (ft)	$\sigma_v$ (psf)	$\Delta\sigma_v$ (psf)	Coherent	$\sigma_h$ (psf)	Load Factors		$\sigma_h$ (psf)	Unfactored	Factored	Factored	Unfactored
			$k_{rCG}$		Unfactored	$\gamma_{P-EV}$		$\gamma_{P-ES}$	Factored	$T_{max}$ (lbf)	$T_{max}$ (lbf)
1.23	139	2,603	0.475	1,302	1.35	1.5	1,943	7,879	11,759	11,340	15,120
3.69	418	2,603	0.455	1,373	1.35	1.5	2,031	8,308	12,290	11,340	15,120
6.15	696	2,603	0.434	1,433	1.35	1.5	2,104	8,669	12,730	11,340	15,120
8.61	974	2,603	0.414	1,481	1.35	1.5	2,161	8,962	13,077	11,340	15,120

Table 3-15. Connection strength stability check for 95% of T-180 (At-rest condition).

Depth (ft)	$\sigma_v$ (psf)	$\Delta\sigma_v$ (psf)	At-Rest	$\sigma_h$ (psf)	Load Factors		$\sigma_h$ (psf)	Unfactored	Factored	Factored	Unfactored
			$k_0$		Unfactored	$\gamma_{P-EV}$		$\gamma_{P-ES}$	Factored	$T_{max}$ (lbf)	$T_{max}$ (lbf)
1.23	139	2,603	0.485	1,330	1.35	1.5	1,985	8,047	12,010	11,340	15,120
3.69	418	2,603	0.485	1,465	1.35	1.5	2,167	8,864	13,113	11,340	15,120
6.15	696	2,603	0.485	1,600	1.35	1.5	2,349	9,681	14,216	11,340	15,120
8.61	974	2,603	0.485	1,735	1.35	1.5	2,531	10,498	15,319	11,340	15,120

Table 3-16. Connection strength stability check for 95% of T-180 (Active state).

Depth (ft)	$\sigma_v$ (psf)	$\Delta\sigma_v$ (psf)	Active	$\sigma_h$ (psf)	Load Factors		$\sigma_h$ (psf)	Unfactored	Factored	Factored	Unfactored
			$k_a$		Unfactored	$\gamma_{P-EV}$		$\gamma_{P-ES}$	Factored	$T_{max}$ (lbf)	$T_{max}$ (lbf)
1.23	139	2,603	0.320	878	1.35	1.5	1,310	5,312	7,927	11,340	15,120
3.69	418	2,603	0.320	967	1.35	1.5	1,430	5,851	8,655	11,340	15,120
6.15	696	2,603	0.320	1,056	1.35	1.5	1,551	6,390	9,383	11,340	15,120
8.61	974	2,603	0.320	1,145	1.35	1.5	1,671	6,929	10,111	11,340	15,120

Table 3-17. Connection strength stability check for 95% of T-180 (Spangler and Handy Method).

Depth (ft)	$\sigma_v$ (psf)	$\Delta\sigma_v$ (psf)	S & H	$\sigma_h$ (psf)	Load Factors		$\sigma_h$ (psf)	Unfactored	Factored	Factored	Unfactored
			$k_{rSH}$		Unfactored	$\gamma_{P-EV}$		$\gamma_{P-ES}$	Factored	$T_{max}$ (lbf)	$T_{max}$ (lbf)
1.23	139	2,603	0.469	1,285	1.35	1.5	1,918	7,776	11,606	11,340	15,120
3.69	418	2,603	0.438	1,323	1.35	1.5	1,958	8,008	11,847	11,340	15,120
6.15	696	2,603	0.410	1,353	1.35	1.5	1,987	8,190	12,026	11,340	15,120
8.61	974	2,603	0.385	1,376	1.35	1.5	2,008	8,330	12,154	11,340	15,120

Table 3-18. Connection strength stability check for 104% of T-180 (Simplified Method).

Depth (ft)	$\sigma_v$ (psf)	$\Delta\sigma_v$ (psf)	Simplified	$\sigma_h$ (psf)	Load Factors		$\sigma_h$ (psf)	Unfactored	Factored	Factored	Unfactored
			$k_{rS}$		Unfactored	$\gamma_{P-EV}$		$\gamma_{P-ES}$	Factored	$T_{max}$ (lbf)	$T_{max}$ (lbf)
1.23	152	2,849	0.347	1,041	1.35	1.5	1,553	6,298	9,399	11,340	15,120
3.69	457	2,849	0.334	1,104	1.35	1.5	1,633	6,682	9,884	11,340	15,120
6.15	762	2,849	0.321	1,160	1.35	1.5	1,703	7,018	10,305	11,340	15,120
8.61	1,067	2,849	0.308	1,208	1.35	1.5	1,762	7,308	10,663	11,340	15,120

Table 3-19. Connection strength stability check for 104% of T-180 (Coherent Gravity Method).

Depth (ft)	$\sigma_v$ (psf)	$\Delta\sigma_v$ (psf)	Coherent	$\sigma_h$ (psf)	Load Factors		$\sigma_h$ (psf)	Unfactored	Factored	Factored	Unfactored
			$k_{rCG}$		Unfactored	$\gamma_{P-EV}$		$\gamma_{P-ES}$	Factored	$T_{max}$ (lbf)	$T_{max}$ (lbf)
1.23	152	2,849	0.336	1,007	1.35	1.5	1,503	6,096	9,097	11,340	15,120
3.69	457	2,849	0.319	1,054	1.35	1.5	1,559	6,379	9,437	11,340	15,120
6.15	762	2,849	0.302	1,091	1.35	1.5	1,602	6,601	9,693	11,340	15,120
8.61	1,067	2,849	0.285	1,117	1.35	1.5	1,630	6,761	9,865	11,340	15,120

Table 3-20. Connection strength stability check for 104% of T-180 (At-rest condition).

Depth (ft)	$\sigma_v$ (psf)	$\Delta\sigma_v$ (psf)	At-Rest	$\sigma_h$ (psf)	Load Factors		$\sigma_h$ (psf)	Unfactored	Factored	Factored	Unfactored
			$k_0$		Unfactored	$\gamma_{P-EV}$		$\gamma_{P-ES}$	Factored	$T_{max}$ (lbf)	$T_{max}$ (lbf)
1.23	152	2,849	0.344	1,032	1.35	1.5	1,541	6,248	9,324	11,340	15,120
3.69	457	2,849	0.344	1,137	1.35	1.5	1,682	6,882	10,181	11,340	15,120
6.15	762	2,849	0.344	1,242	1.35	1.5	1,824	7,517	11,037	11,340	15,120
8.61	1,067	2,849	0.344	1,347	1.35	1.5	1,965	8,151	11,893	11,340	15,120

Table 3-21. Connection strength stability check for 104% of T-180 (Active state).

Depth (ft)	$\sigma_v$ (psf)	$\Delta\sigma_v$ (psf)	Active	$\sigma_h$ (psf)	Load Factors		$\sigma_h$ (psf)	Unfactored	Factored	Factored	Unfactored
			$k_a$		Unfactored	$\gamma_{P-EV}$		$\gamma_{P-ES}$	Factored	$T_{max}$ (lbf)	$T_{max}$ (lbf)
1.23	152	2,849	0.208	623	1.35	1.5	930	3,773	5,630	11,340	15,120
3.69	457	2,849	0.208	687	1.35	1.5	1,016	4,156	6,148	11,340	15,120
6.15	762	2,849	0.208	750	1.35	1.5	1,101	4,539	6,665	11,340	15,120
8.61	1,067	2,849	0.208	813	1.35	1.5	1,187	4,922	7,182	11,340	15,120

Table 3-22. Connection strength stability check for 104% of T-180 (Spangler and Handy Method).

Depth (ft)	$\sigma_v$ (psf)	$\Delta\sigma_v$ (psf)	S & H	$\sigma_h$ (psf)	Load Factors		$\sigma_h$ (psf)	Unfactored	Factored	Factored	Unfactored
			$k_{rSH}$		Unfactored	$\gamma_{P-EV}$		$\gamma_{P-ES}$	Factored	$T_{max}$ (lbf)	$T_{max}$ (lbf)
1.23	152	2,849	0.336	1,008	1.35	1.5	1,504	6,098	9,100	11,340	15,120
3.69	457	2,849	0.320	1,058	1.35	1.5	1,565	6,402	9,470	11,340	15,120
6.15	762	2,849	0.305	1,102	1.35	1.5	1,618	6,669	9,793	11,340	15,120
8.61	1,067	2,849	0.291	1,141	1.35	1.5	1,665	6,904	10,073	11,340	15,120

As seen from all calculations, for certain earth pressure coefficients the factored loads exceed the controlling factored resistance (reinforcement strip bolt hole bearing resistance). However, these are conservative estimated loads and not representative of the true loading conditions. In all cases, the unfactored loads never exceed the ultimate strength ( $F_u$ ) or the yield strength ( $F_y$ ) of the metallic connection components. Therefore, implementing incremental surcharges provided a safe method of investigating this type of MSE wall as on-site data collected during each load increment provided guidance as to the true stresses being developed.

### *3.8.9 Estimated Lateral Wall Movement (at service limit state)*

Lateral wall movements in LRFD design are evaluated at the Service I limit state. Most internal deformations usually occur during construction. However, post-construction movement can occur due to post-construction surcharge loads, settlement of wall fill, or long-term settlement of the foundation soils. The latter was unlikely for the short design life of the proposed wall. The magnitude of the lateral displacement depends on fill placement techniques, compaction effects, reinforcement extensibility, reinforcement length, reinforcement-to-facing connection details, and details of the wall facing (FHWA, 2009). The estimated lateral wall movement should be less than 3/8" (See Section 3.1.6).

### *3.8.10 Vertical Movement and Bearing Pads*

Bearing pads are placed in the horizontal joints of the segmental precast concrete panels in order to allow the panel and reinforcement to move down with the reinforced fill as it is placed and settles, mitigating downdrag stress, and providing flexibility for differential foundation settlements (FHWA, 2009). Internal settlement within the reinforced mass is virtually immediate and often negligible for well graded, granular fill and external movement will usually control the compression pad requirements. The stiffness (axial and lateral), size, and number of bearing pads were checked with an assumed load at a given joint equal to 2 to 3 times the weight of the facing panels directly above that level. The final joint opening should be  $\frac{3}{4} \pm \frac{1}{8}$ -inch. Based on wall height and compaction requirements, the expected compression of bearing pads was on the order of 1/8" to 1/4" at each panel joint

## **3.9 Facing Elements**

Square facing panels were used for the research. The square panels were purchased from RECo. Typical designs for square wall panels, embedded strip connections, clip angle connections, and HA strips are provided in Figure 3-16 through Figure 3-19.



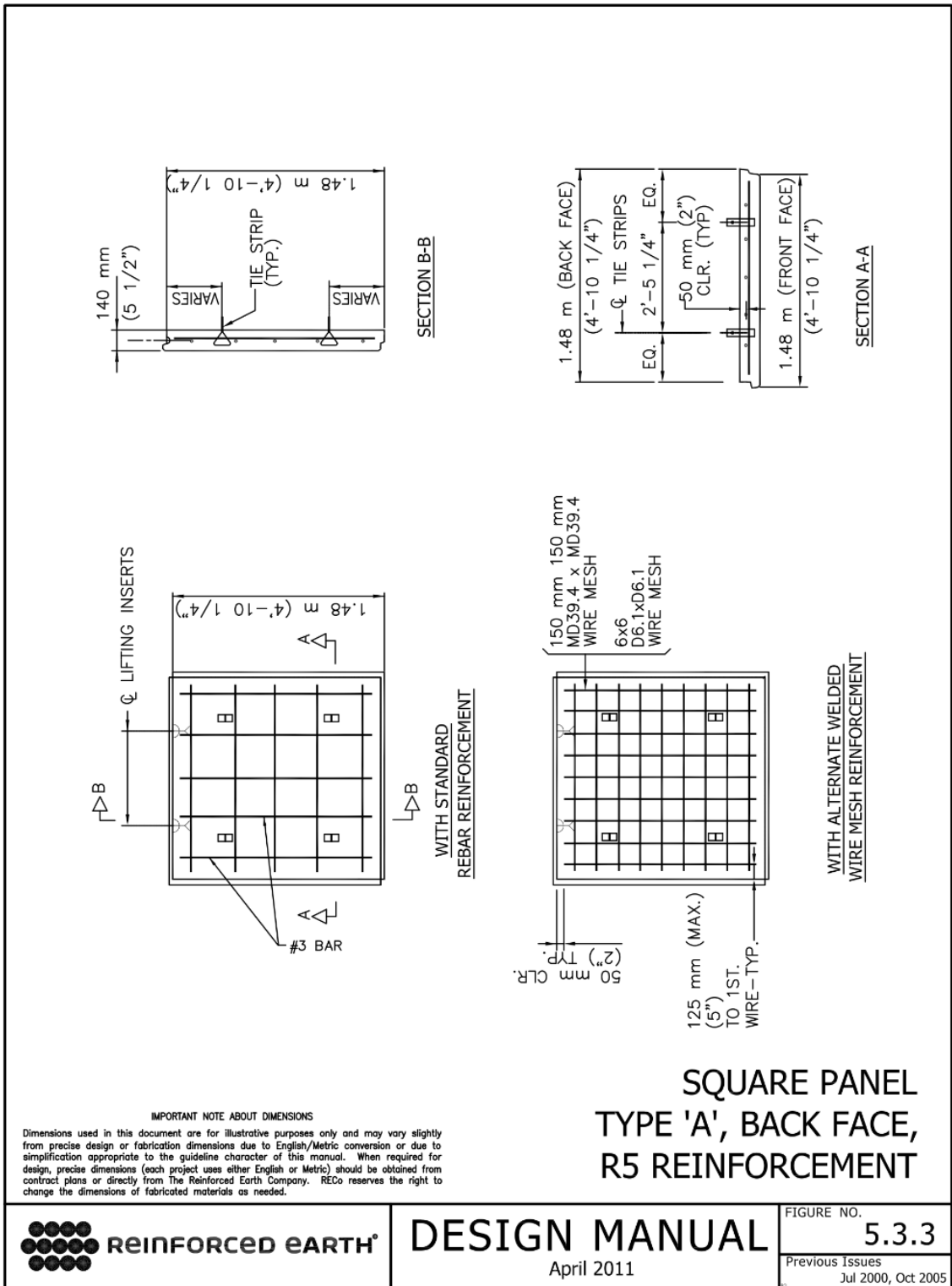


Figure 3-16. Square panel – Type A.

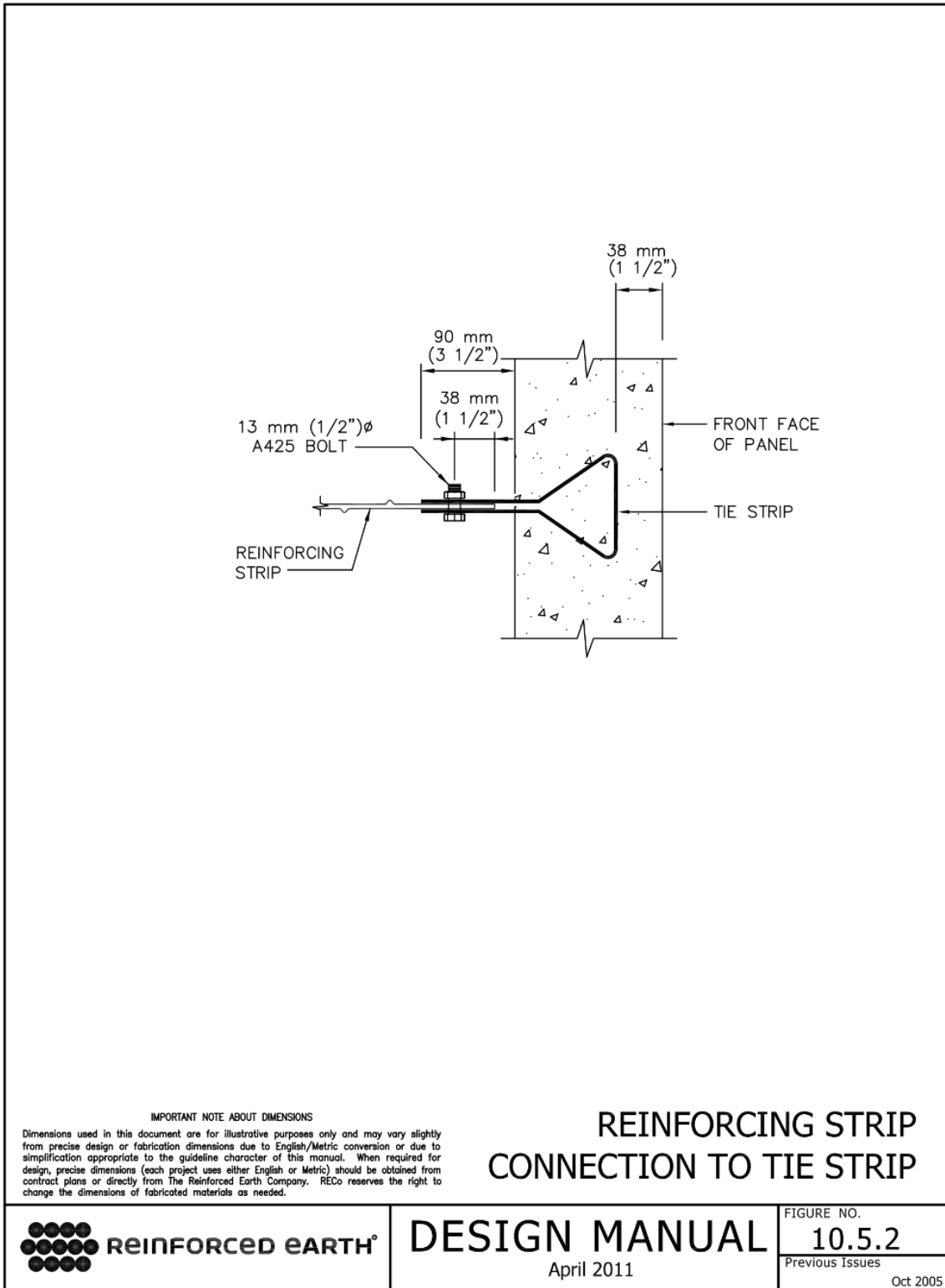


Figure 3-17. Reinforcing strip and connection to tie strip.

5/8" DIA. x 6" LONG HILTI HAS ANCHOR ROD / WITH HVA ADHESIVE ANCHOR EMBEDDED 4 1/2"

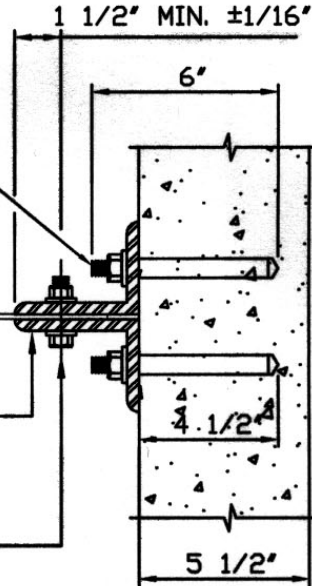
2 PER CONNECTION ASSEMBLY  
11/16" BOLT HOLE IN ANGLE

INSTALL IN ACCORDANCE WITH  
MANUFACTURERS RECOMENDATIONS

50mm X 4mm  
REINF. STRIP

4" x 3" x 3/8"  
3" LONG (GALV.) A36 STEEL  
2 PER CONNECTION

1/2" DIA. A325 BOLT 2" LONG  
W/WASHERS & NUT (GALVANIZED)  
9/16" Ø BOLT HOLE



## CLIP ANGLE DETAIL

SCALE: 3/16" = 1"

### MATERIAL PROPERTIES

1. CLIP ANGLE - A36 STEEL  
GALVANIZED PER ASTM A-123 OR AASHTO M111
2. 1/2" Ø BOLTS - A325 - GALVANIZED  
PER ASTM A-153
3. 50mm x 4mm R.S. - A-572 GRADE 65  
GALVANIZED PER ASTM A-123 OR AASHTO M111
4. HILTI COMPONENTS PER HILTI SPECS.




 <p>The Reinforced Earth Company 120 PARK STREET, NORTH READING MA 01864, (978) 864-2020</p>	PROJECT:	DATE:
	DESCRIPTION CLIP ANGLE DETAIL	JOB NO.
	SCALE AS SHOWN	

Figure 3-18. Clip angle details.

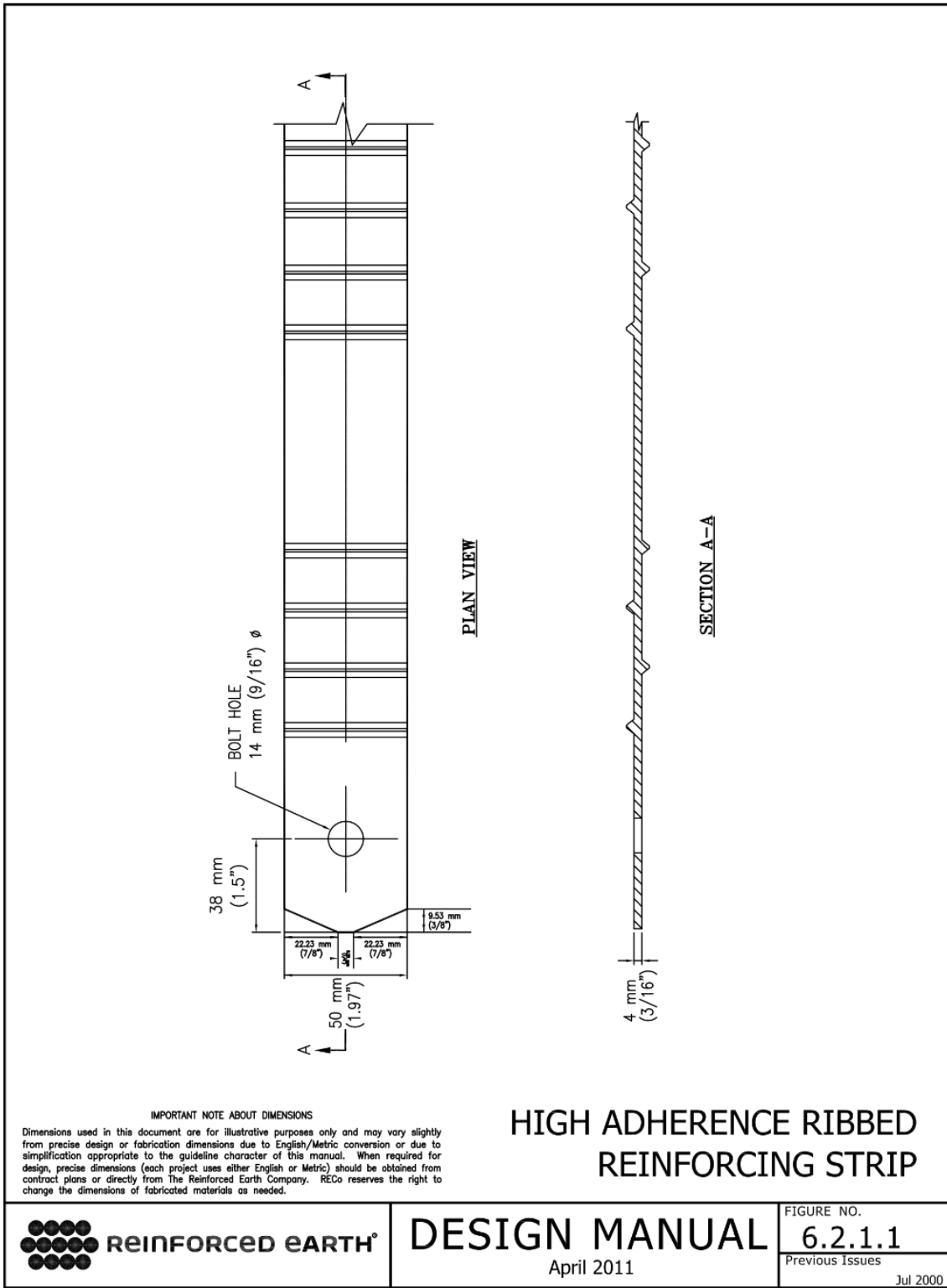


Figure 3-19. High adherence ribbed reinforcing strip.

### 3.10 Internal Overall/Global Stability

Overall/Global Stability is determined using rotational or wedge analysis to examine potential failure planes passing behind and under the reinforced zone (FHWA, 2009). The reinforced soil is assumed to behave as a rigid body and only failure surfaces completely outside the reinforced mass are considered for stability as depicted in Figure 3-20. Due to the unique research scenario where the wall was underlain by a concrete floor with no external forces generated from retained backfill, Global failure was unlikely (RECo agreed). Therefore, Global stability checks were not performed.

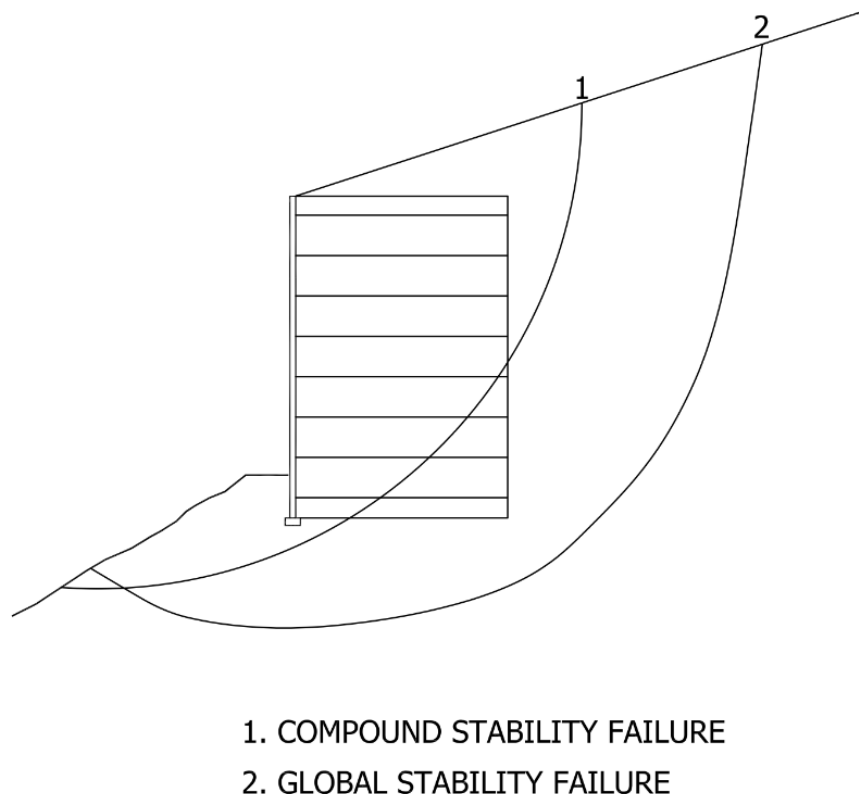


Figure 3-20. Global and compound stability (Figure 6.3.3; RECo, 2011).

### 3.11 Compound Stability

Compound stability is determined using rotational or wedge analysis to examine potential failure planes passing behind or under and through a portion of the reinforced zone as depicted in Figure 3-20. For simple structures with rectangular geometry, uniform reinforcement spacing, and a near vertical face (all characteristics of the research MSE wall), compound failures passing both through the unreinforced and reinforced zones will not generally be critical. Also, the research MSE wall was underlain by a concrete floor with no external forces generated from retained backfill and therefore compound stability became even less critical (RECo agreed). Therefore, compound stability checks were not performed.

### 3.12 Wall Drainage System

The MSE wall drainage system was comprised of a six inch layer of coarse aggregate encapsulated in a non-woven geotextile that routed water through three inch schedule 80 PVC pipes placed in each drainage port of the base soil concrete blocks as depicted in Figure 3-1 and Figure 3-4. Coarse aggregate comprised of natural stones meeting the requirements of FDOT (2017) Section 901 with a size distribution of No. 89 stone was used. The selected No. 89 stone was obtained from the FDOT approved Plant 214\_03400-Gainesville Terminal, Product GRAN-GA-CMK89-#89. The gradation provided in Table 3-23, provides the mean aggregate sizes from 30 tests conducted by the distributor. As seen in Table 3-23, the selected drainage aggregate meets the FDOT gradation specification.

Table 3-23. No. 89 Gradation summary comparing FDOT specifications with select aggregate.

Section 901-1.4 Gradation – Table 1 Summary for No. 89 Stone							
Amounts Finer than Each Laboratory Sieve (Square Openings), Weight Percent							
Size No.	3/4"	1/2"	3/8"	No. 4	No. 8	No. 16	No. 50
89 – Spec.	-	100	90 to 100	20 to 55	0 to 30	0 to 10	0 to 5
89 – Select	100	100	98.7	45.4	7.9	3.0	1.7

The geotextile encapsulating the coarse aggregate served as a separation layer between the coarse aggregate and base layer soil. FDOT Specification 985-4.1.1 indicates that for a separation geotextile, Type D-5 should be used. AASHTO (2006) recommends a Class 1 geotextile when heavy construction equipment is used and/or angular fill will be placed directly above or below the geotextile which is the case for the research. Table 3-24 provides the FDOT requirements, per Section 985-2.2 that must be satisfied for a Type D-5 separation geotextile and the criteria for an AASHTO Class 1 geotextile. Thrace-LINQ 180EX non-woven geotextile was selected for use in the drainage layer of the MSE wall due to the apparent opening size (AOS) of 100. Provided in Table 3-2, approximately 23% of the select reinforced fill has a particle size smaller than 0.150 mm (No. 100) and therefore a geotextile with a smaller AOS was ideal for the design (Note: All other vendors on the FDOT’s approved list provide an AOS = 80 for an 8 oz/sy non-woven geotextile). As seen in Table 3-24, the selected geotextile met all FDOT and AASHTO requirements.

Table 3-24. Geotextile test methods and requirements.

Test Methods and Requirements for Drainage Geotextiles			
Property/Test Method	FDOT Type D-5	AASHTO Class 1	Thrace- LINQ 180EX
Min. Permittivity (Sec <sup>-1</sup> ) ASTM D4491	0.5	N/A	1.5
Max. AOS (US Sieve No.) ASTM D4751	70	N/A	100
Min. Grab Tensile Strength (lbs) ASTM D4632	90	200	205
Mass per Unit Area (oz/sy) ASTM D5261	Test Result	N/A	8 oz/sy
Min. Puncture Strength (lbs) ASTM D6241	223	433	535
Min. Trapezoidal Tear (lbs) ASTM D4533	40	80	80
Min. UV Resistance ASTM D4355	50% @ 500 Hours	50% @ 500 Hours	70% @ 500 Hours

### 3.13 Simulated Surcharge Reaction Frame Design and Calculations

In order to provide the needed B/H ratio of 0.3, a simulated surcharge equivalent to 23 feet of overburden soil at each state of soil density was applied to each respective portion of the reinforced fill. This required a reaction frame to be designed using portions of UF's Soil Box and the Matjack-airbag system. Figure 3-21 through Figure 3-24 present the layout for the soil pates that rested just above the compacted reinforced fill, the soil areas attributed to each Matjack, and the Matjack-airbag configuration that induced the required simulated earth pressures. A layer of chain-link fencing was laid on top of the entire soil area before placing the soil plates. This helped to evenly distribute stress from individual soil plates on the soil and reduced the chances of soil plate edges getting caught under adjacent soil plates. Once the airbags were placed on each respective side of the reinforced fill, one soil box wall (approximately 8' by 11') was placed atop the airbags on each side of the separation boundary. Reaction girders were then placed atop the Soil Box walls and tied into threaded Dwyidag bars that tie into the Strong Floor (Figure 3-25).

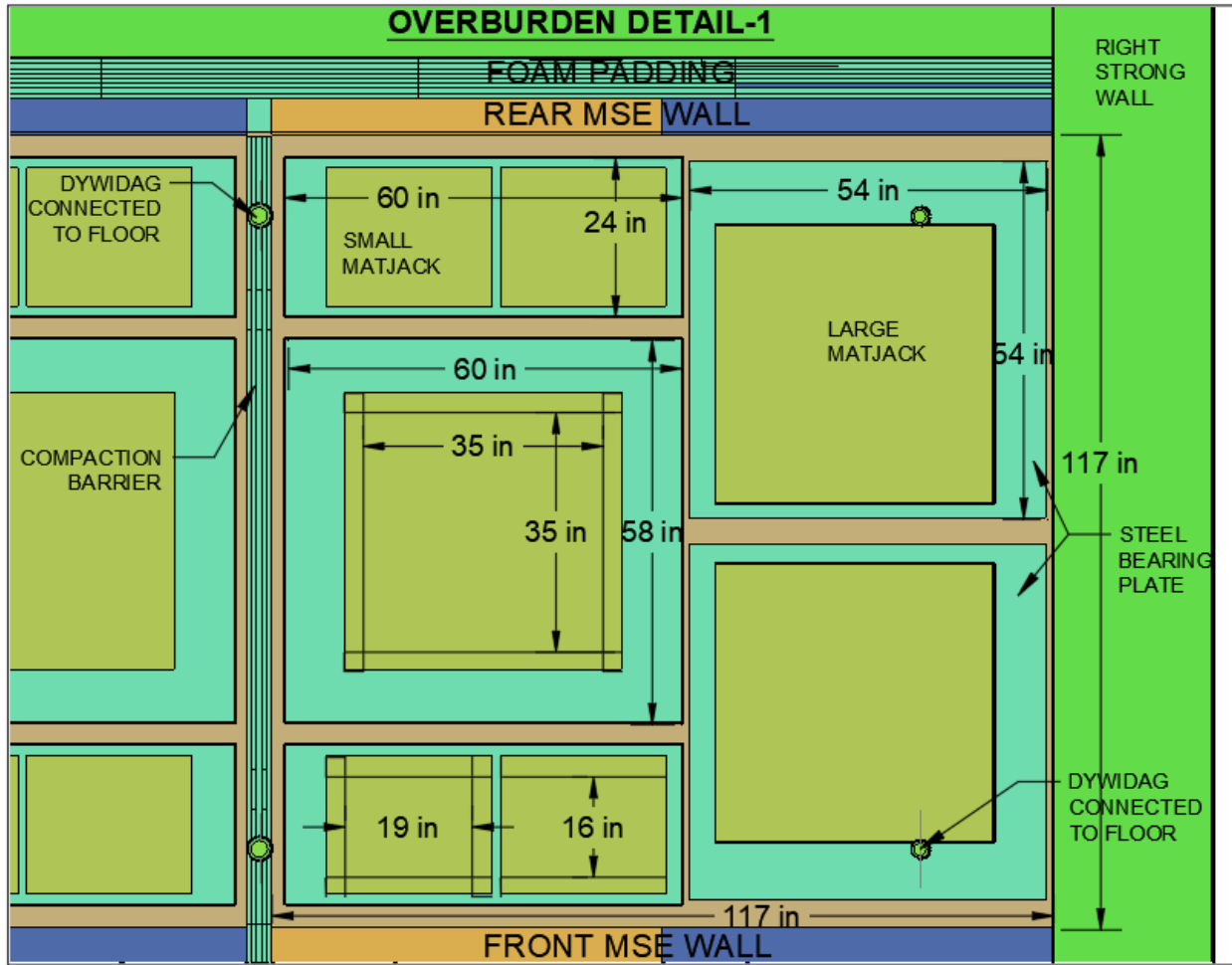


Figure 3-21. Matjack-airbag system, overburden detail 1.



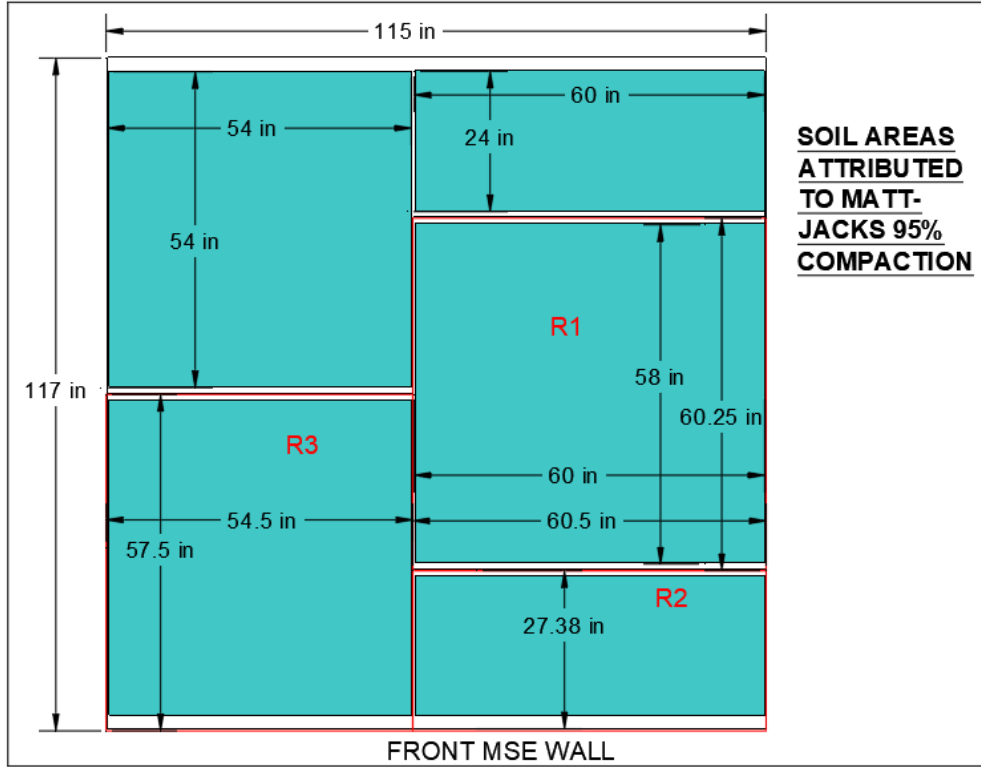


Figure 3-22. Soil areas attributed to Matjacks 95% compaction effort

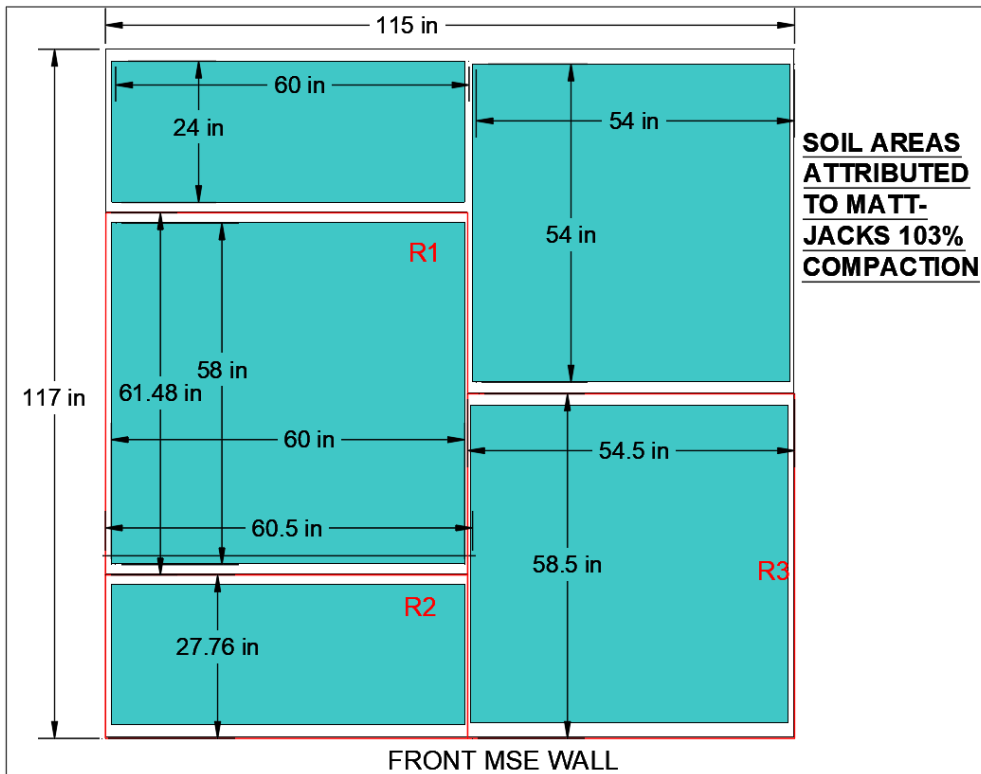


Figure 3-23. Soil areas attributed to Matjacks 103% compaction effort.

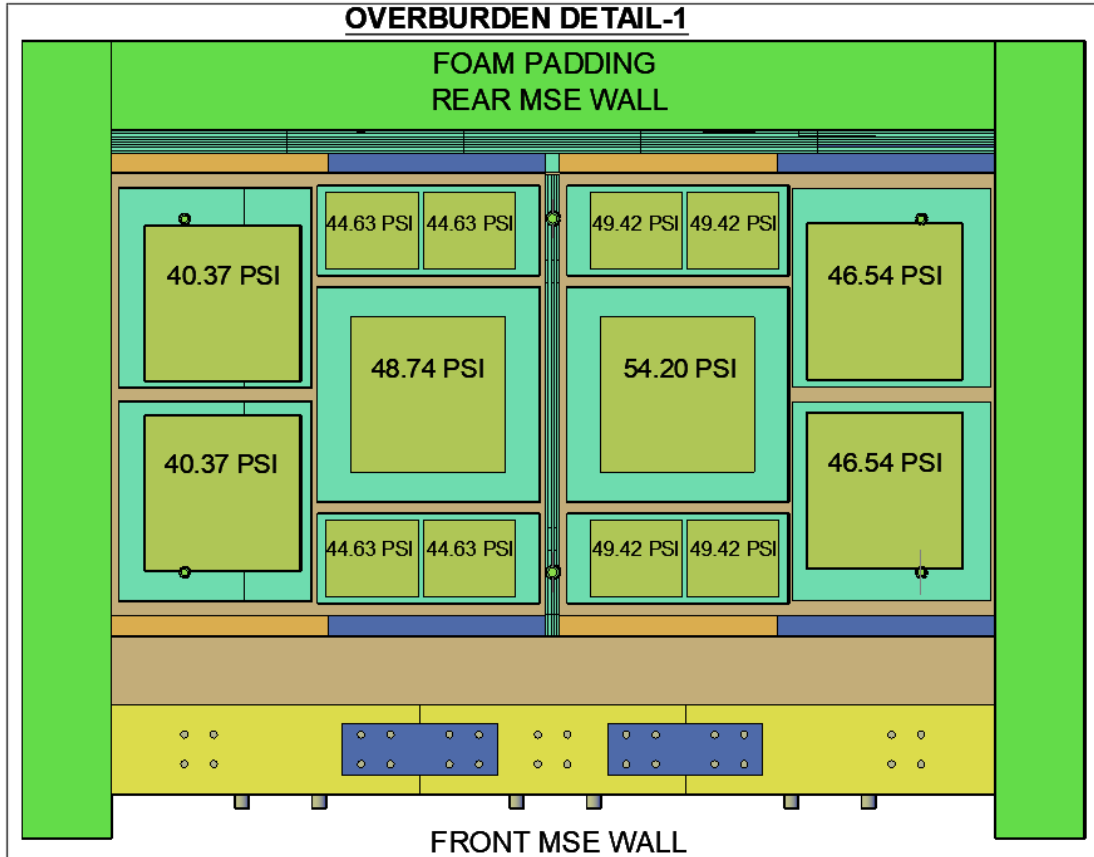


Figure 3-24. Calculated pressures for each Matjack to induce the required surcharge.

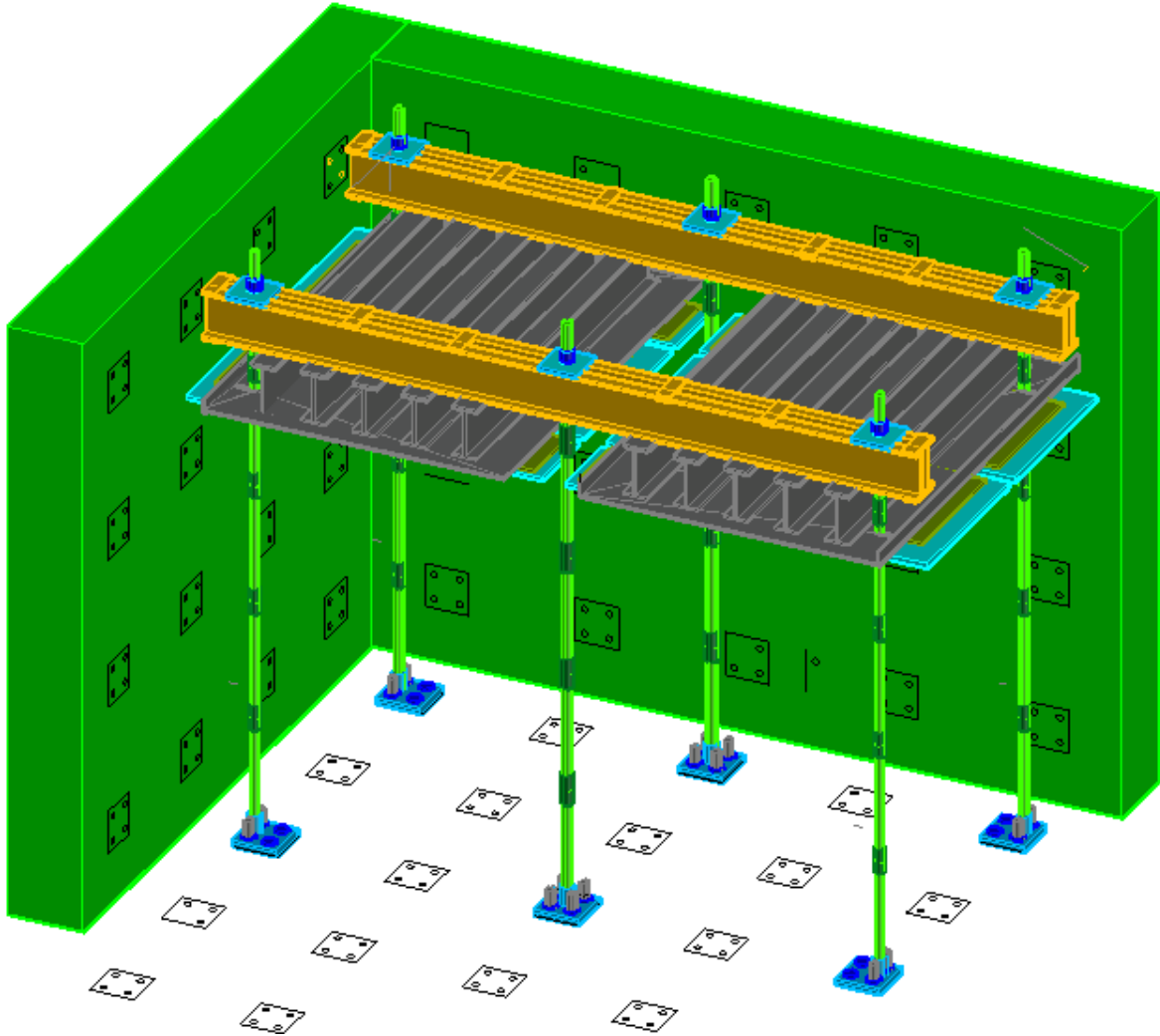


Figure 3-25. Reaction frame tied into Strong Floor.

Based on the defined areas (Figure 3-21 through Figure 3-24), the required Matjack pressures to induce the needed surcharge for each compaction effort were calculated.

**95% Compaction effort:**

$$23.3\text{ft} (101.26\text{pcf}) = 2,359.4 \text{ lbs./ft}^2 = 16.38\text{psi}$$

R1:

$$\text{Actual size of steel soil plate (R1)} = 60'' \times 58'' = (3,480 \text{ in}^2)$$

$$\text{Attributable soil area for plate (R1)} = 60.5 \times 60.25'' = (3,645.125 \text{ in}^2)$$

$$(3,645.125\text{in}^2) (16.38 \text{ psi}) = (59,707.07 \text{ lbs.}) \text{ total force}$$

Inflated area of Matjack in (R1) = 35"x35" = (1225 in<sup>2</sup>)

Therefore,

Required pressure in Matjack for plate (R1)

$$(59,707.07 \text{ lbs.}) / (1225 \text{ in}^2) = \mathbf{48.74 \text{ psi}}$$

R2:

Actual size of steel soil plate (R2) = 60" x 24" = (1,440 in<sup>2</sup>)

Attributable soil area for plate (R2) = 60.5 x 27.38" = (1,656.49 in<sup>2</sup>)

$$(1,656.49 \text{ in}^2) (16.38 \text{ psi}) = (27,133.31 \text{ lbs.}) \text{ total force}$$

Inflated area of Matjacks in (R2) = 19"x 16"x 2 = (608 in<sup>2</sup>)

Therefore,

Required pressure in Matjack for plate (R2)

$$(27,133.31 \text{ lbs.}) / (608 \text{ in}^2) = \mathbf{44.63 \text{ psi}}$$

R3:

Actual size of steel soil plate (R3) = 54" x 52" = (2,808 in<sup>2</sup>)

Attributable soil area for plate (R3) = 57.5 x 52.5" = (3,018.75 in<sup>2</sup>)

$$(3,018.75 \text{ in}^2) (16.38 \text{ psi}) = (49,447.13 \text{ lbs.}) \text{ total force}$$

Inflated area of Matjacks in (R3) = 35"x 35" = (1,225 in<sup>2</sup>)

Therefore,

Required pressure in Matjack for plate (R3)

$$(49,447.13 \text{ lbs.}) / (1,225 \text{ in}^2) = \mathbf{40.37 \text{ psi}}$$

**103% Compaction effort:**

$$23.3 \text{ ft} (108.53 \text{ pcf}) = 2,528.75 \text{ lbs./ft}^2 = 17.56 \text{ psi}$$

R1:

Actual size of steel soil plate (R1) = 60" x 58" = (3,480 in<sup>2</sup>)

Attributable soil area for plate (R1) = 61.48" x 61.5" = (3,781.02 in<sup>2</sup>)

(3,781.02 in<sup>2</sup>) (17.56 psi) = (66,394.71 lbs.) total force

Inflated area of Matjack in (R1) = 35"x35" = (1225 in<sup>2</sup>)

Therefore,

Required pressure in Matjack for plate (R1)

(66,394.71 lbs.) / (1225 in<sup>2</sup>) = **54.2 psi**

R2:

Actual size of steel soil plate (R2) = 60" x 24" = (1,440 in<sup>2</sup>)

Attributable soil area for plate (R2) = 61.5 x 27.76" = (1,707.24 in<sup>2</sup>)

(1,707.24 in<sup>2</sup>) (17.56 psi) = (30,047.42 lbs.) total force

Inflated area of Matjacks in (R2) = 19"x 16"x 2 = (608 in<sup>2</sup>)

Therefore,

Required pressure in Matjack for plate (R2)

(30,047.42 lbs.) / (608 in<sup>2</sup>) = **49.42 psi**

R3:

Actual size of steel soil plate (R3) = 54" x 54" = (2,916 in<sup>2</sup>)

Attributable soil area for plate (R3) = 58.5 x 55.5" = (3,246.75 in<sup>2</sup>)

(3,246.75 in<sup>2</sup>) (17.56 psi) = (57,012.93 lbs.) total force

Inflated area of Matjacks in (R3) = 35"x 35" = (1,225 in<sup>2</sup>)

Therefore,

Required pressure in Matjack for plate (R3)

(57,012.93 lbs.) / (1,225 in<sup>2</sup>) = **46.54 psi**

Next the loads induced on the Soil Box girders from the Matjacks were calculated using two different approaches. Method 1 assumed the load from the Matjacks translated only to the Soil Box I-beam tributary areas (Figure 3-26). Method 2 assumed the loads from the Matjacks were distributed equally into four quadrants of the Soil Box wall, and the Soil Box I-beams took a portion of the load from the quadrants they are in based on the I-beam tributary area (Figure 3-29).

### 3.13.1 Method 1

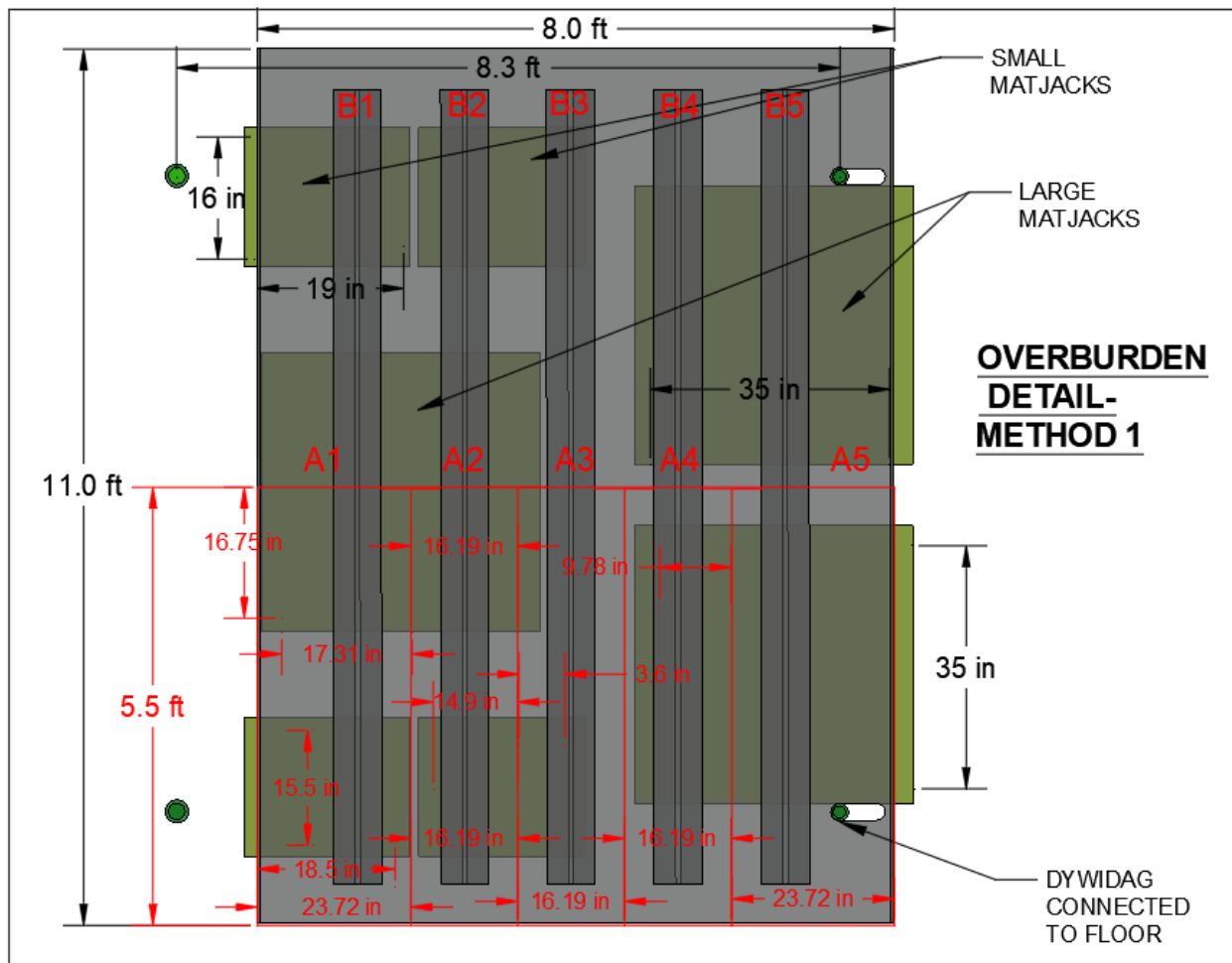


Figure 3-26. Method 1 – I-beam tributary areas.

### 3.13.2 Force from Soil Box I-beams to Perpendicular Girders (103% compaction)

$$A_1 \rightarrow \text{Area from Matjack} = 16.75'' \times 23.72'' = 397.31 \text{ in}^2$$

$$\text{Pressure on Matjack} = 54.20 \text{ psi}$$

$$\text{Area from Matjack} = 19'' \times 16'' = 304 \text{ in}^2$$

$$\text{Pressure on Matjack} = 49.42 \text{ psi}$$

$$\text{Force to B1} \rightarrow (397.31 \text{ in}^2 \times 54.20 \text{ psi}) + (304 \text{ in}^2 \times 49.42 \text{ psi}) = 36,557 \text{ lbs.} = \mathbf{36.56 \text{ kips}}$$

$$A_2 \rightarrow \text{Area from Matjack} = 16.75'' \times 16.19'' = 271.18 \text{ in}^2$$

$$\text{Pressure on Matjack} = 54.20 \text{ psi}$$

$$\text{Area from Matjack} = 15.15'' \times 16'' = 242.40 \text{ in}^2$$

$$\text{Pressure on Matjack} = 49.42 \text{ psi}$$

$$\text{Force to B2} \rightarrow (271.18 \text{ in}^2 \times 54.20 \text{ psi}) + (242.40 \text{ in}^2 \times 49.42 \text{ psi}) = 26,677 \text{ lbs} = \mathbf{26.67 \text{ kips}}$$

$$A_3 \rightarrow \text{Area from Matjack} = 16'' \times 3.85'' = 61.6 \text{ in}^2$$

$$\text{Pressure on Matjack} = 49.42 \text{ psi}$$

$$\text{Force to B3} \rightarrow (61.6 \text{ in}^2 \times 49.42 \text{ psi}) = 3,044 \text{ lbs} = \mathbf{3.04 \text{ kips}}$$

$$A_4 \rightarrow \text{Area from Matjack} = 35'' \times 11.28'' = 394.8 \text{ in}^2$$

$$\text{Pressure on Matjack} = 46.54 \text{ psi}$$

$$\text{Force to B4} \rightarrow 394.8 \text{ in}^2 \times 46.54 \text{ psi} = 18,372 \text{ lbs.} = \mathbf{18.37 \text{ kips}}$$

$$A_5 \rightarrow \text{Area from Matjack} = 35'' \times 23.72'' = 830.20 \text{ in}^2$$

$$\text{Pressure on Matjack} = 46.54 \text{ psi}$$

$$\text{Force to B5} \rightarrow 830.20 \text{ in}^2 \times 46.54 \text{ psi} = 38,637 \text{ lbs.} = \mathbf{38.64 \text{ kips}}$$

### 3.13.3 Force from Soil Box I-beams to Perpendicular Girders (95% compaction)

$$A_1 \rightarrow \text{Area from Matjack} = 16.75'' \times 23.72'' = 397.31 \text{ in}^2$$

$$\text{Pressure on Matjack} = 48.74 \text{ psi}$$

$$\text{Area from Matjack} = 19'' \times 16'' = 304 \text{ in}^2$$

$$\text{Pressure on Matjack} = 44.63 \text{ psi}$$

$$\text{Force to B1} \rightarrow (397.31 \text{ in}^2 \times 48.74 \text{ psi}) + (304 \text{ in}^2 \times 44.63 \text{ psi}) = 32,932 \text{ lbs} = \mathbf{32.93 \text{ kips}}$$

$$A_2 \rightarrow \text{Area from Matjack} = 16.75'' \times 16.19'' = 271.18 \text{ in}^2$$

$$\text{Pressure on Matjack} = 48.74 \text{ psi}$$

$$\text{Area from Matjack} = 15.15'' \times 16'' = 242.40 \text{ in}^2$$

$$\text{Pressure on Matjack} = 44.63 \text{ psi}$$

$$\text{Force to B2} \rightarrow (271.18 \text{ in}^2 \times 48.74 \text{ psi}) + (242.40 \text{ in}^2 \times 44.63 \text{ psi}) = 24,035 \text{ lbs} = \mathbf{24.03 \text{ kips}}$$

$$A_3 \rightarrow \text{Area from Matjack} = 16'' \times 3.85'' = 61.6 \text{ in}^2$$

$$\text{Pressure on Matjack} = 44.63 \text{ psi}$$

$$\text{Force to B3} \rightarrow (61.6 \text{ in}^2 \times 44.63 \text{ psi}) = 2,749 \text{ lbs.} = \mathbf{2.749 \text{ kips}}$$

$$A_4 \rightarrow \text{Area from Matjack} = 35'' \times 11.28'' = 394.8 \text{ in}^2$$

$$\text{Pressure on Matjack} = 40.37 \text{ psi}$$

$$\text{Force to B4} \rightarrow 394.8 \text{ in}^2 \times 40.37 \text{ psi} = 15,938 \text{ lbs.} = \mathbf{15.94 \text{ kips}}$$

$$A_5 \rightarrow \text{Area from Matjack} = 35'' \times 23.72'' = 830.20 \text{ in}^2$$

$$\text{Pressure on Matjack} = 40.37 \text{ psi}$$

$$\text{Force to B5} \rightarrow 830.20 \text{ in}^2 \times 40.37 \text{ psi} = 33,515 \text{ lbs.} = \mathbf{33.52 \text{ kips}}$$

With loads for each I-beam calculated, the reaction forces for each Dwyidag tie-in were calculated using Visual Analysis software. Note that it was assumed the front and rear girders experienced identical loads as the loading system layout was symmetric from front MSE wall to rear MSE wall.



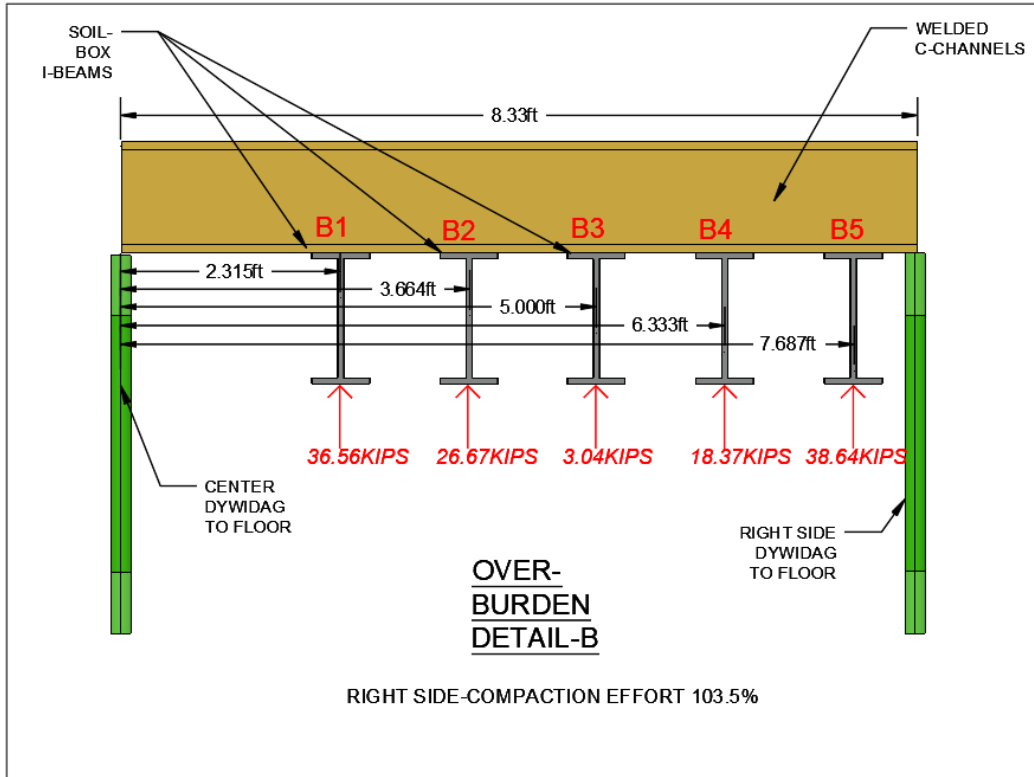


Figure 3-27. Calculated forces for right-side compaction of 103% (Method 1).

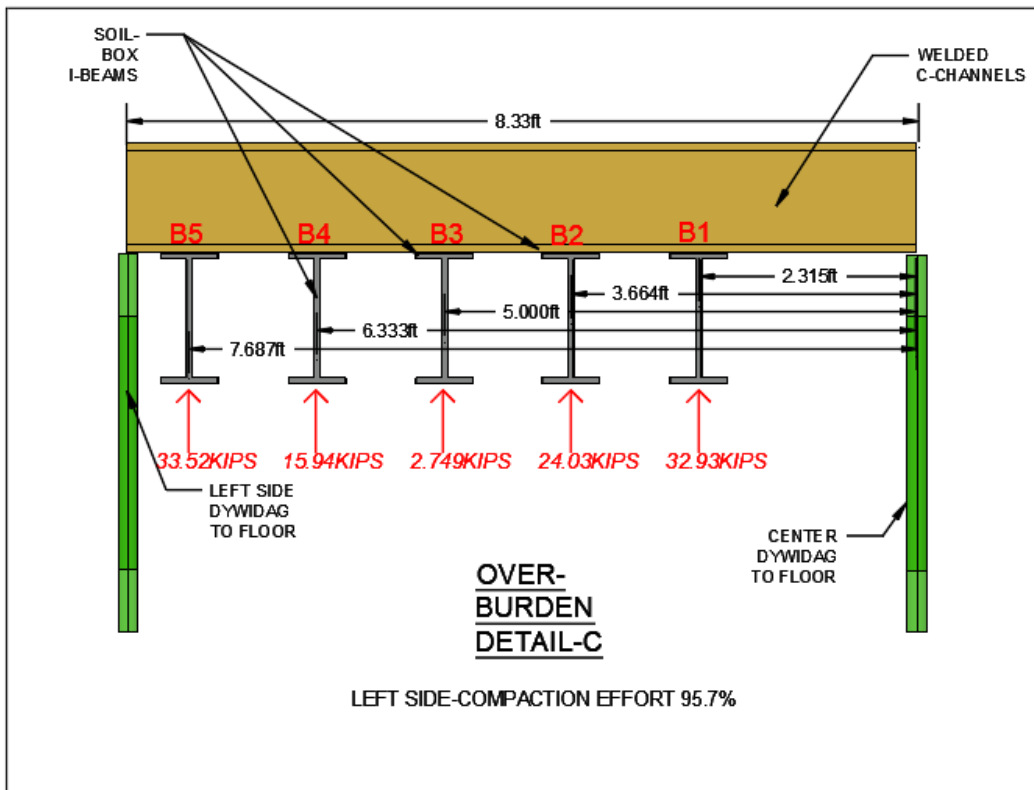


Figure 3-28. Calculated forces for left-side compaction of 95% (Method 1).

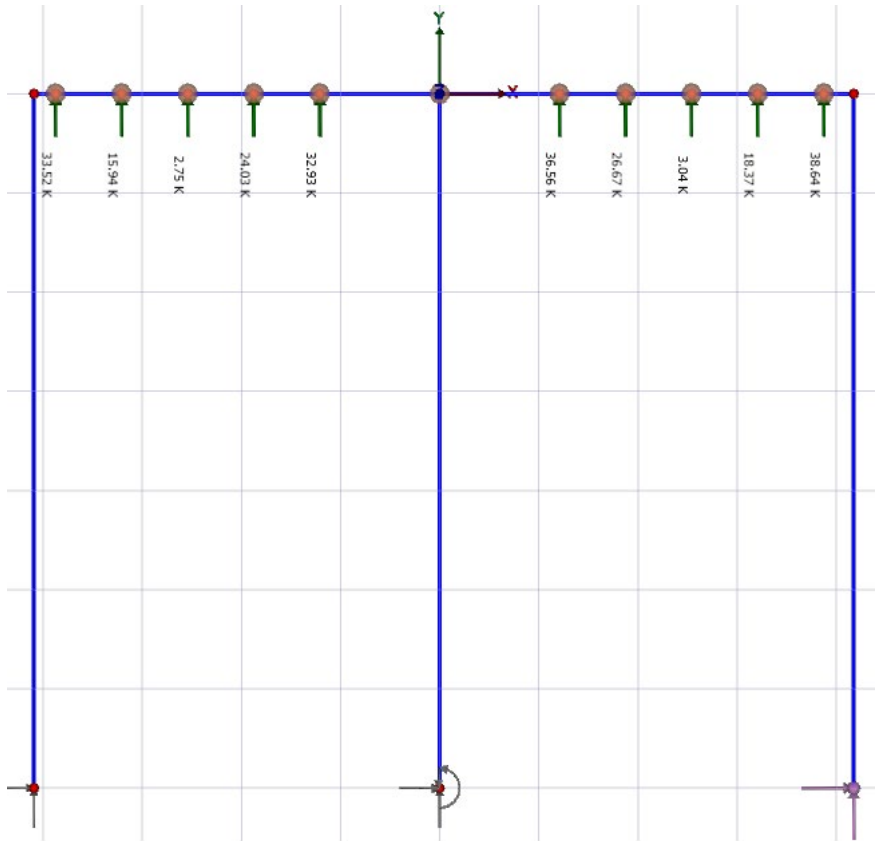


Figure 3-29. Visual Analysis with Matjack forces applied (Method 1).

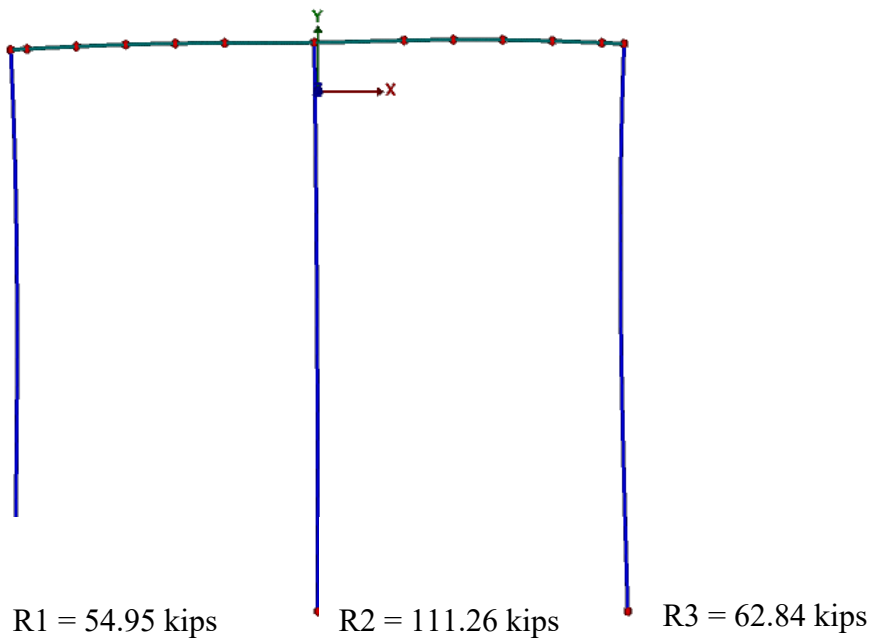


Figure 3-30. Visual Analysis reaction forces derived for Dwyidag tie-ins (Method 1).

### 3.13.4 Method 2

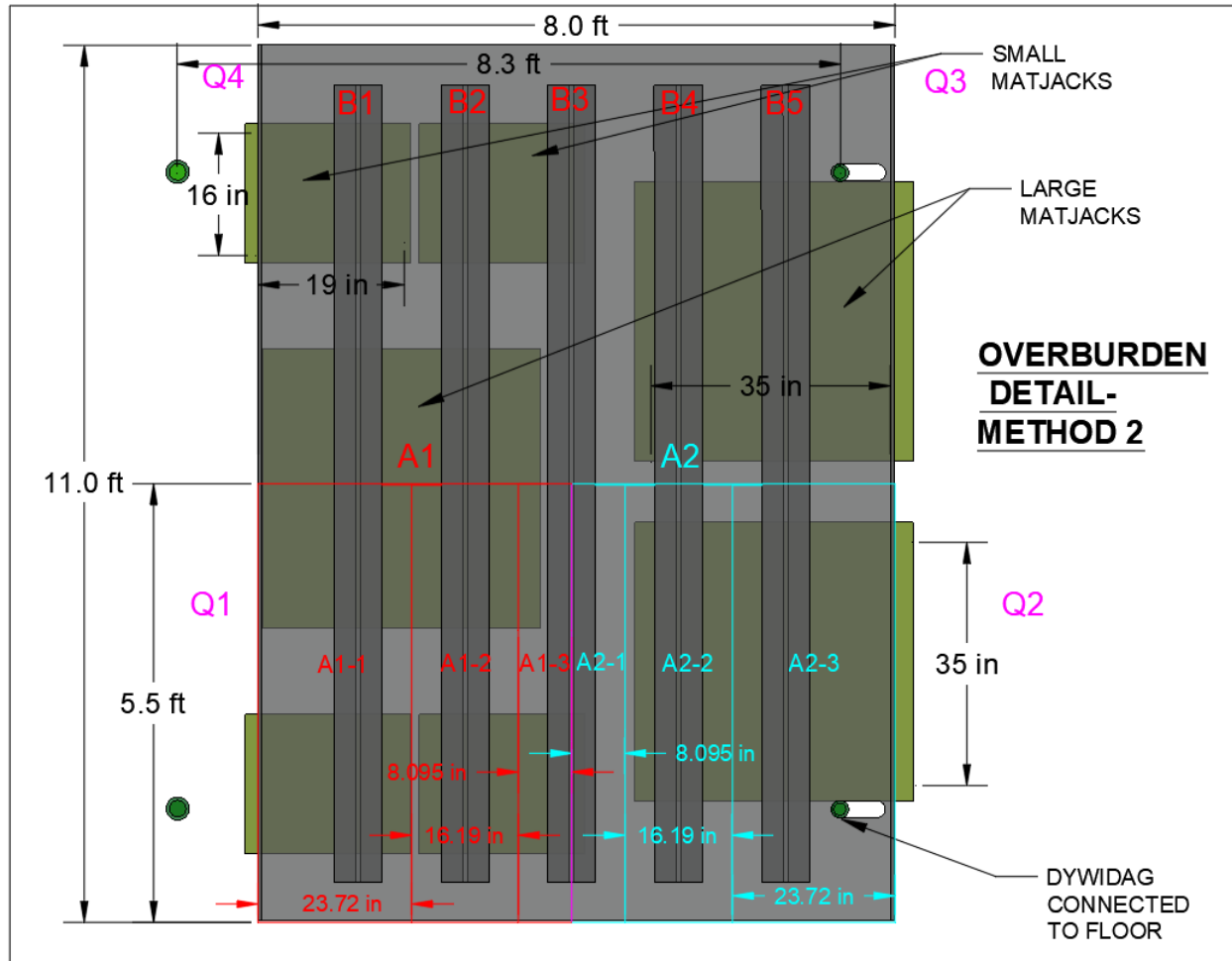


Figure 3-29. Method 2 – I-beam tributary areas.

### 3.13.5 Tributary Area for Soilbox I-Beams (Method 2)

$$A_1 = A_2 = 5.5\text{ft} \times 4\text{ft} = \mathbf{22\text{ft}^2}$$

$$A_{1-1} = 5.5\text{ft} \times [((8.94''/12) + 7.25'' + 12'')/12] = 10.87\text{ft}^2$$

$$A_{1-1} = \mathbf{49.4\%}$$
 total area of  $A_1$

$$A_{1-2} = 5.5\text{ft} \times [((8.94''/12) + 7.25'' + (8.94''/2))/12] = 7.42\text{ft}^2$$

$$A_{1-2} = \mathbf{33.73\%}$$
 total area of  $A_1$

$$A_{1-3} = 5.5\text{ft} \times [((8.94''/12) + (7.25''/2))/12] = 3.71\text{ft}^2$$

$A_{1-3}$ =**16.86%** total area of  $A_1$

$$A_{2-1} = 5.5\text{ft} \times [((8.94''/12) + (7.25''/2))/12] = 3.71\text{ft}^2$$

$A_{2-1}$ =**16.86%** total area of  $A_2$

$$A_{2-2} = 5.5\text{ft} \times [((8.94''/12) + 7.25'' + (8.94''/2))/12] = 7.42\text{ft}^2$$

$A_{2-2}$ =**33.73%** total area of  $A_2$

$$A_{2-3} = 5.5\text{ft} \times [((8.94''/12) + 7.25'' + 12'')/12] = 10.87\text{ft}^2$$

$A_{2-3}$ =**49.4%** total area of  $A_2$

### 3.13.6 Force from Soil Box I-beams to Perpendicular Girders (103% compaction)

Assume force from Matjacks (1/2 area of large Matjack + 2 small) to area  $A_1$  to be evenly distributed:

Force from large and small Matjacks to area  $A_1$ :  $(F_1) = 54.20 \text{ psi} [ \frac{1}{2} (1,225 \text{ in}^2) ] + 49.42 \text{ psi} \times [2(304\text{in}^2)] = \mathbf{63,245 \text{ lbs}}$

Assume force from Matjack to area  $A_2$  to be evenly distributed:

Force from large Matjack to area  $A_2$ :  $(F_2) = (46.54 \text{ psi} \times 1,225 \text{ in}^2) = \mathbf{57,012 \text{ lbs.}}$

$F_{B1} = (\% \text{ of } A_{1-1} \text{ to total area}) \times (F_1) = 49.4\% \times 63,245\text{lbs} = 31,243 \text{ lbs.} \text{ -----} \rightarrow \mathbf{31.24 \text{ kips}}$

$F_{B2} = (\% \text{ of } A_{1-2} \text{ to total area}) \times (F_1) = 33.73\% \times 63,245\text{lbs} = 21,332 \text{ lbs.} \text{ -----} \rightarrow \mathbf{21.33 \text{ kips}}$

$F_{B3} \text{ (from } A_{1-3}) = (\% \text{ of } A_{1-3} \text{ to total area}) \times (F_1) = 16.86\% \times 63,245\text{lbs} = 10,663 \text{ lbs.}$

$F_{B3} \text{ (from } A_{2-1}) = (\% \text{ of } A_{2-1} \text{ to total area}) \times (F_2) = 16.86\% \times 57,012 \text{ lbs.} = 9,612 \text{ lbs.}$

$F_{B3} = 10,663 \text{ lbs.} + 9,612 \text{ lbs} = 20,275 \text{ lbs.} \text{ -----} \rightarrow \mathbf{20.28 \text{ kips}}$

$F_{B4} = (\% \text{ of } A_{2-2} \text{ to total area}) \times (F_2) = 33.73\% \times 57,012 \text{ lbs.} = 19,230 \text{ lbs.} \text{ -----} \rightarrow \mathbf{19.23 \text{ kips}}$

$F_{B5} = (\% \text{ of } A_{2-3} \text{ to total area}) \times (F_2) = 49.4\% \times 57,012 \text{ lbs.} = 28,163 \text{ lbs.} \text{ -----} \rightarrow \mathbf{28.16 \text{ kips}}$

### 3.13.7 Force from Soil Box I-beams to Perpendicular Girders (95% compaction)

Assume force from Matjacks (1/2 area of large Matjack + 2 small) to area  $A_1$  to be evenly distributed:

Force from large and small Matjacks to area A<sub>1</sub>: (F<sub>1</sub>) = 48.74 psi [ ½ (1,225 in<sup>2</sup>)] + 44.63 psi x [2(304in<sup>2</sup>)] = **56,988 lbs.**

Assume force from Matjack to area A<sub>2</sub> to be evenly distributed:

Force from large Matjack to area A<sub>2</sub>: (F<sub>2</sub>) = (40.37 psi x 1,225 in<sup>2</sup>) = **49,453 lbs.**

**F<sub>B1</sub>** = (% of A<sub>1-1</sub> to total area) x (F<sub>1</sub>) = 49.4% x 56,988 lbs. = 28,152 lbs. -----→ **28.15 kips**

**F<sub>B2</sub>** = (% of A<sub>1-2</sub> to total area) x (F<sub>1</sub>) = 33.73% x 56,988 lbs. = 19,222 lbs. -----→ **19.22 kips**

**F<sub>B3</sub>** (from A<sub>1-3</sub>) = (% of A<sub>1-3</sub> to total area) x (F<sub>1</sub>) = 16.86% x 56,988 lbs. = 9,608 lbs.

**F<sub>B3</sub>** (from A<sub>2-1</sub>) = (% of A<sub>2-1</sub> to total area) x (F<sub>2</sub>) = 16.86% x 49,453 lbs. = 8,338 lbs.

**F<sub>B3</sub>** = 9,608 lbs. + 8,338 lbs. = 17,946 lbs.-----→ **17.95 kips**

**F<sub>B4</sub>** = (% of A<sub>2-2</sub> to total area) x (F<sub>2</sub>) = 33.73% x 49,453 lbs. = 16,680 lbs. -----→ **16.68 kips**

**F<sub>B5</sub>** = (% of A<sub>2-3</sub> to total area) x (F<sub>2</sub>) = 49.4% x 49,453 lbs. = 24,430 lbs. -----→ **24.43 kips**

With loads for each I-beam calculated, the reaction forces for each Dwyidag tie-in were calculated using Visual Analysis software.

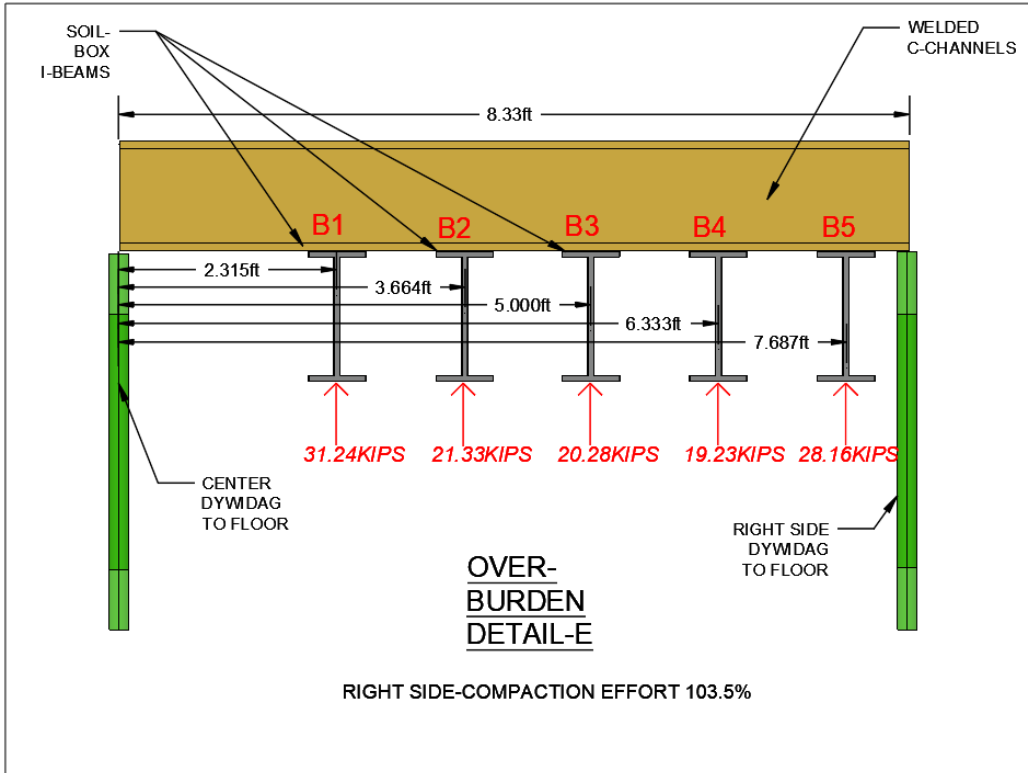


Figure 3-31. Calculated forces for right-side compaction of 103% (Method 2).

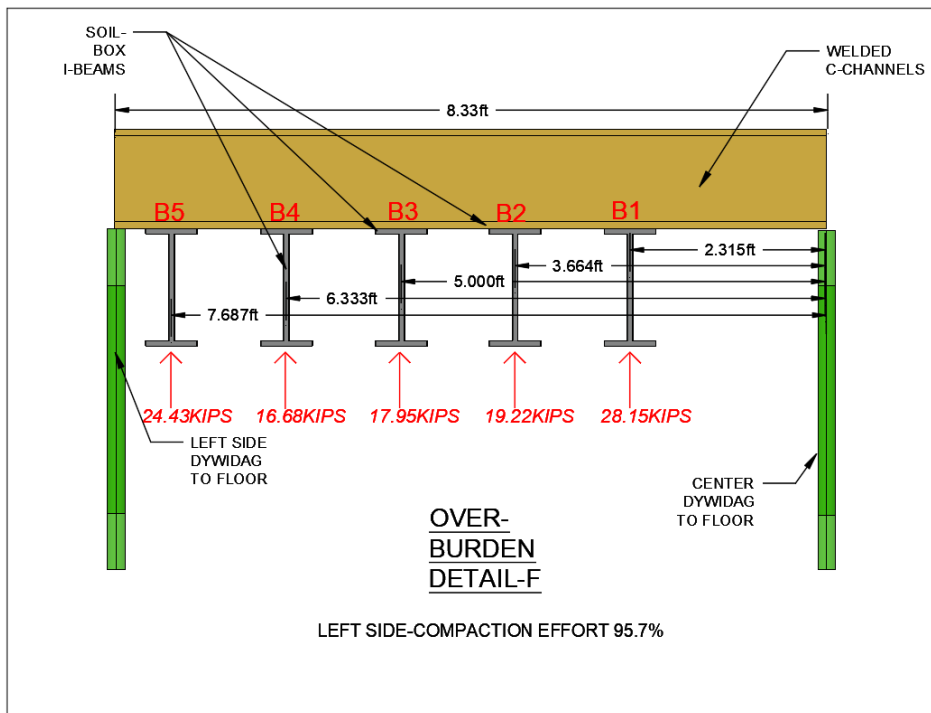


Figure 3-32. Calculated forces for right-side compaction of 95% (Method 2).

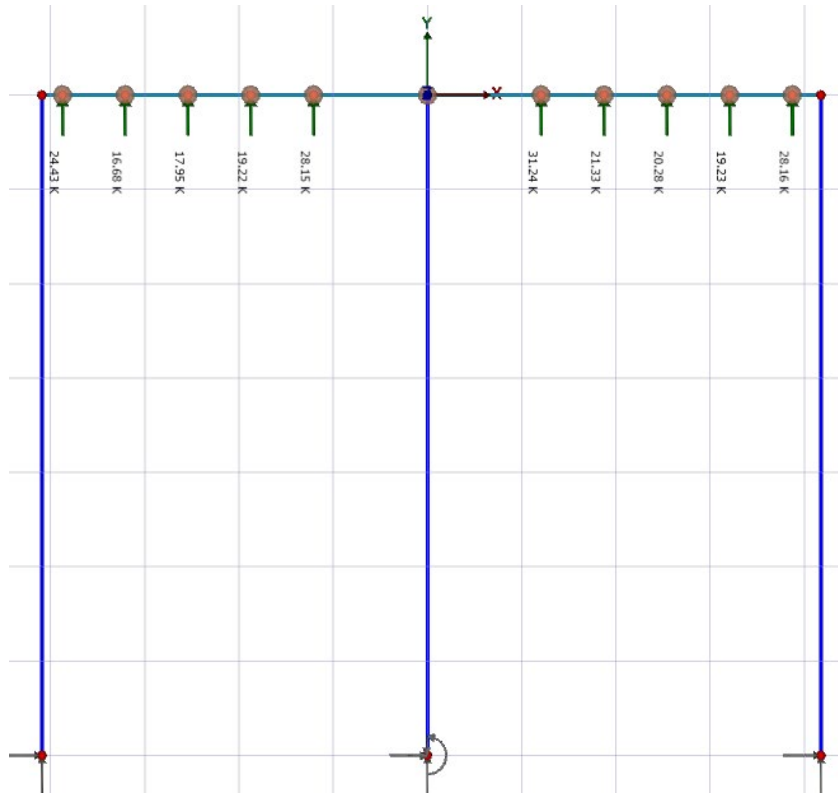


Figure 3-33. Visual Analysis with Matjack forces applied (Method 2).

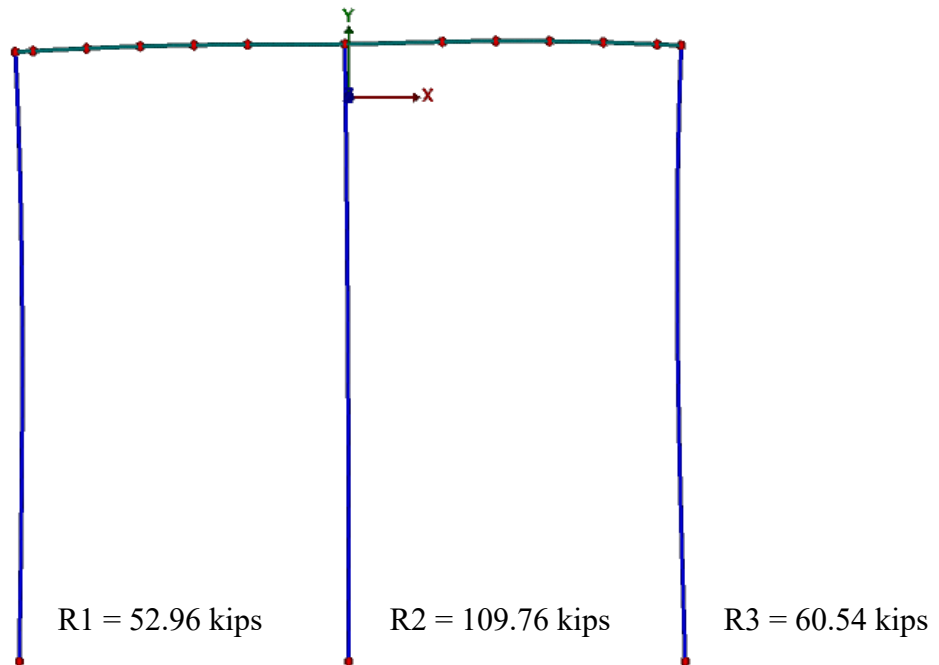


Figure 3-34. Visual Analysis reaction forces derived for Dwyidag tie-ins (Method 2).

### 3.13.8 Maximum Moments and Deflections

The maximum deflections and moments were then calculated for each compaction effort to select the girders that would tie into the Dwyidag thread bars and support the Soil Box Walls.

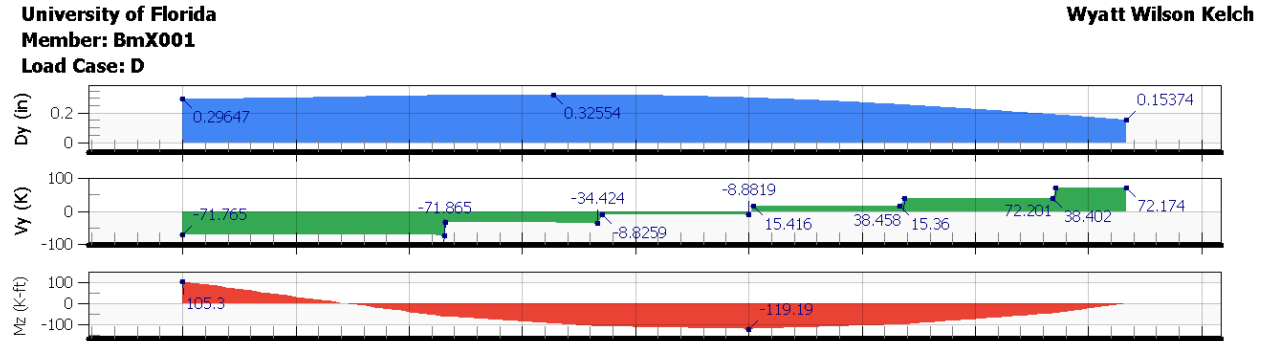


Figure 3-35. Moments and deflections for right-side compaction of 103%.

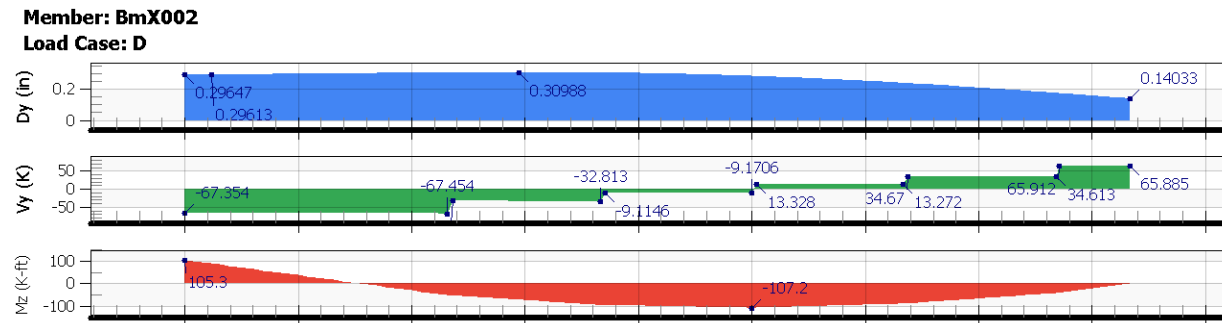


Figure 3-36. Moments and deflections for right-side compaction of 95%.

Maximum moment = 119.2 kip-ft (Use W12 x 30 I-beam).

### 3.13.9 Steel Selection and Connection Details

Following moment values (LRFD) from Steel Construction Manual from American Institute of Steel Construction 14<sup>th</sup> Edition; page 3-130, “Table 3-10 W-Shapes – Available Moment vs. Unbraced Length” for unbraced length of 8’-6” [Actual length = 8’-4”], W12 x 30 I-beams were sufficient to support the Soil Box walls and complete the reaction frame.



Table 3-25. W-Shapes – Available Moment vs. Unbraced Length of 8’-6”.

W- Shape	Max Moment (LRFD)
W10 x 30	120 K-ft
W12 x 26	121.5 K-ft
W16 x 26	125 K-ft
W8 x 35	126.5 K-ft
W10 x 33	139 K-ft
W12 x 30	143.5 K-ft
W8 x 40	145.5 K-ft
W14 x 30	155 K-ft
W12 x 33	173 K-ft

However, to connect the Dywidag thread bars to the steel girders as a pinned connection it was determined the Dywidag bars should run through the steel girders and bear on the top of them with a steel plate and bearing nut. Using experience from past load frames, it was decided that instead of one W12 x 30 I beam for each girder, the team would use two C-15 x 33.9 channels welded back-to-back with a 4” gap between them from web to web, (Figures 3-37, 3-38). The gap between C-channels allowed for the Dywidags to run through the center of the girders.

3.13.10 Reaction Frame Connection Details

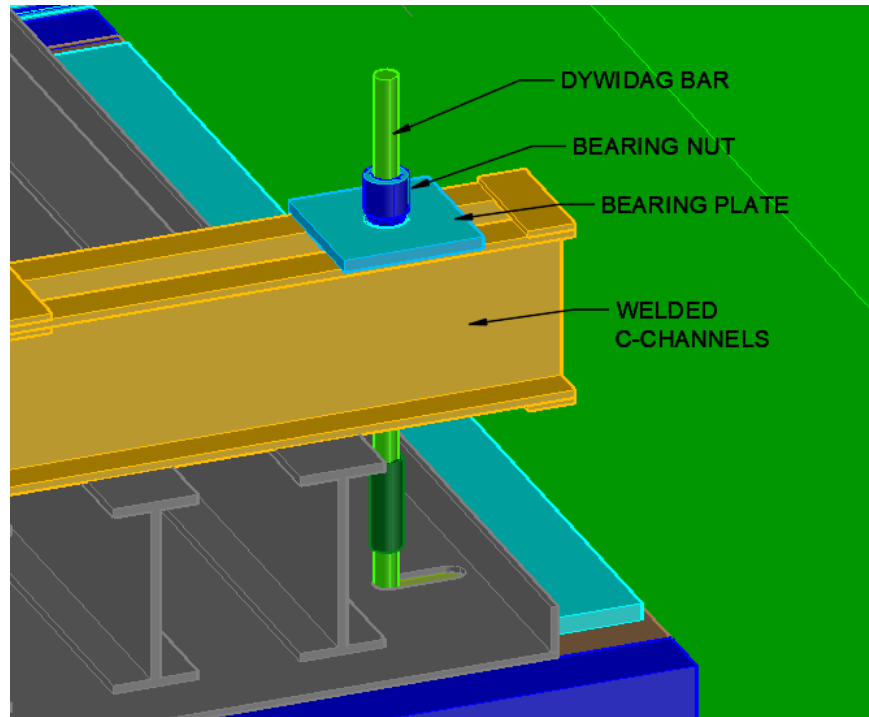


Figure 3-37. Side connections (non-moment connection).

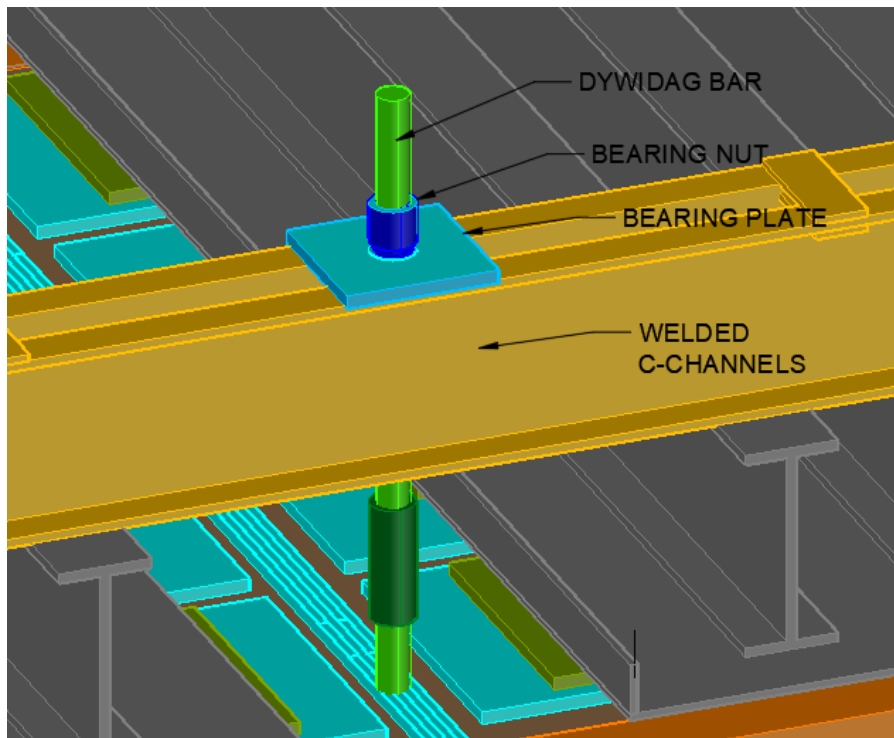


Figure 3-38. Center connections (non-moment connection).

- A 2" thick 12"x12" bearing plate was then placed around each Dwyidag and rested on the girders with a washer and nut locking them in place.
- This connection was designed to act as pinned to limit influence from moments.

### 3.13.11 Strong Floor Connection Details

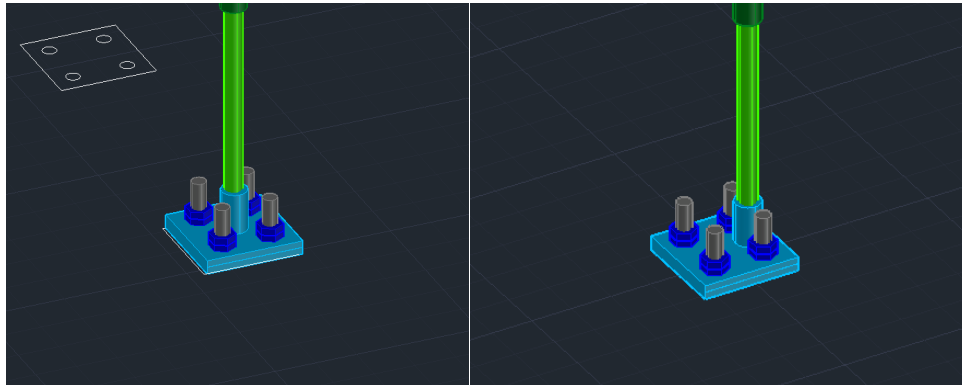


Figure 3-39. Steel plates and hardware for Strong Floor connections.

- Side plates: 1" thick x 14" x 14" with #14 Coupler
- Middle plates: 1" thick x 14" x 14" with #18 Coupler

### 3.13.12 Bolts Connecting Floor Plates

- 1.25" #7 Bolt for floor connections:
- 4 bolts per Dywidag floor connection = 24 bolts

3.13.13 Dwyidag Threaded Rod Selection

DYWIDAG-SYSTEMS INTERNATIONAL



**DYWIDAG THREADBAR® Properties – Reinforcing Steel per ASTM A615**

THREADBAR® Designation	Maximum THREADBAR® Diameter		Minimum Yield Stress (f <sub>y</sub> )		Nominal Cross Section Area (A <sub>s</sub> )		Minimum Yield Load (f <sub>y</sub> x A <sub>s</sub> )		Nominal Weight		
	[mm]	[in]	[mm]	[ksi]	[MPa]	[in²]	[mm²]	[kips]	[kN]	[lbs/ft]	[kg/m]
<b>GRADE 75, 80 THREADBAR®</b>											
#6	19	0.86	22	75	517	0.44	284	33.0	147	1.50	2.23
#7	22	0.99	25	75	517	0.60	387	45.0	200	2.04	3.04
#8	25	1.12	28	75	517	0.79	510	59.3	264	2.67	3.97
#9	29	1.26	32	75	517	1.00	645	75.0	334	3.40	5.06
#10	32	1.43	36	75	517	1.27	819	95.3	424	4.30	6.40
#11	36	1.61	41	75	517	1.56	1,006	117.0	520	5.31	7.90
#14	43	1.86	47	80	552	2.25	1,452	180.0	801	7.65	11.38
#18	57	2.50	64	80	552	4.00	2,581	320.0	1,423	13.60	20.24
#20	63	2.72	69	80	552	4.91	3,168	393.0	1,748	16.70	24.85
#24*	75	3.18	81	75	517	7.06	4,555	529.5	2,355	24.09	35.85
#28*	90	3.68	94	75	517	9.62	6,206	721.5	3,209	32.79	48.80

Figure 3-40. Dwyidag Threadbar Properties with #14 and #18 indicated.

Note: Maximum allowable temporary tension is 90% of minimum yield load.

- Middle use #18; Sides use #14
- $FS = (320\text{kips} - [320 \times 10\%]) / 148\text{kips} = 1.95$  (Middle Connection) → Floor Panel Controls
- Floor Panel has 200-kip limit →  $FS = 200 / 148 = 1.35$  (Middle Connection)
- $FS = (180\text{kips} - [180 \times 10\%]) / 67.5\text{kips} = 2.4$  (Side Connections)

## 4 MSE Wall Construction

### 4.1 Design Construction Sequencing

MSE wall construction began by developing a 2.5 foot tall base soil layer retaining area using large concrete blocks. This required custom formwork to be developed to ensure each concrete retaining block could be mechanically fastened to the strong floor tie-ins (Figure 4-1). Once the concrete blocks were in place, the treaded rod running through the concrete blocks, attached to the strong floor tie-ins, was tensioned to ensure the retaining blocks would not move under the anticipated loads.



Figure 4-1. Constructing forms to cast base layer retaining concrete blocks.

Figure 4-2 depicts the concrete blocks in place post tensioning. Also depicted in Figure 4-2, the concrete blocks had additional threaded rod that was not tied into the strong floor. These rods were strategically cast into the concrete blocks to serve as the loading point for the temporary bracing that was required to construct the wall. Also shown in Figures 4-2 and 4-3, the entire strong wall area had to be lined with EPDM rubber to safeguard the strong floor and strong wall tie-ins that would be exposed to water during soil placement and compaction. Each concrete retaining block also had openings cast into them at the base of the blocks. The openings allowed drains to be placed through the blocks to ensure the water added to the soil retainment area during compaction could properly drain out to represent actual construction conditions.



Figure 4-2. Retaining blocks mechanically fastened to strong floor.



Figure 4-3. EPDM rubber placed throughout the research area to protect metal tie-ins.

Once the blocks, EPDM rubber, and drains were in place, plastic sheeting was added to the side walls of the strong wall to reduce friction at the soil interface and a non-woven structural geotextile was placed to encapsulate the gravel drainage layer (Figure 4-4). After the geotextile

was in place, the reaction frame threaded rods were secured to the strong floor tie-ins. Next, select gravel was placed and compacted as depicted in Figures 4-4 and 4-5.



Figure 4-4. Structural geotextile placed and threaded rods mechanically fastened to strong floor.

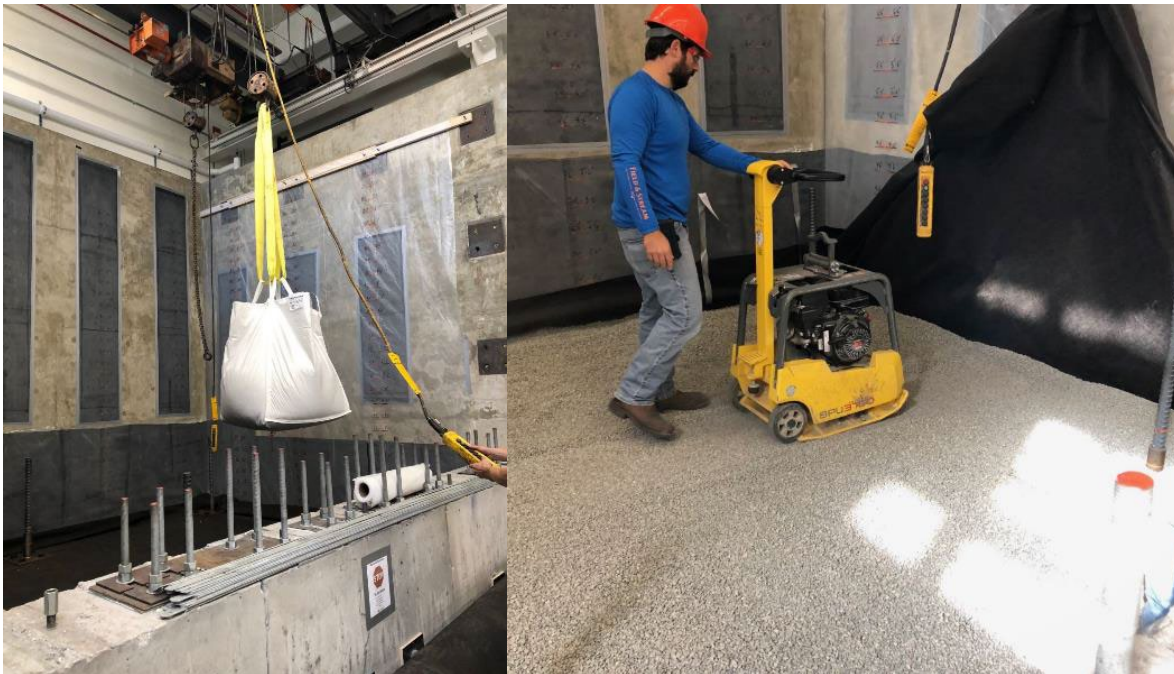


Figure 4-5. Crane lifting soil bags with gravel into the wall area and compacting the gravel layer.

After the gravel layer was placed, compacted, and encapsulated in the geotextile, soil was then added to the base layer (Figure 4-6). The soil was placed in six-inch lifts and compacted using a vibratory plate compactor (Figure 4-7). After each six-inch lift was completed, nuclear density testing was performed to ensure the proper degree of compaction had been achieved (Figure 4-7). This was conducted for every six-inch soil layer added throughout the entire construction process.



Figure 4-6. Base layer soil placement.





Figure 4-7. Base layer soil compaction and nuclear density testing.

Once the base layer was six inches from the reinforced soil zone (bottom of MSE wall, top of leveling pads), soil embedded earth pressure cells (EPCs) were placed in the soil to measure the earth pressure underneath each MSE wall leveling pad (Figure 4-8), and the wiring was run to the top of the wall area for later connection the data acquisition system (DAQ). For EPC placement, the soil was dug out six inches below the base of the leveling pad locations. The EPCs were then leveled and tested to ensure they were functioning and to get baseline readings prior to backfilling. Once the EPCs were in place, the soil was backfilled over them and hand compacted. A final six-inch lift of soil was then placed and compacted to complete the base layer.

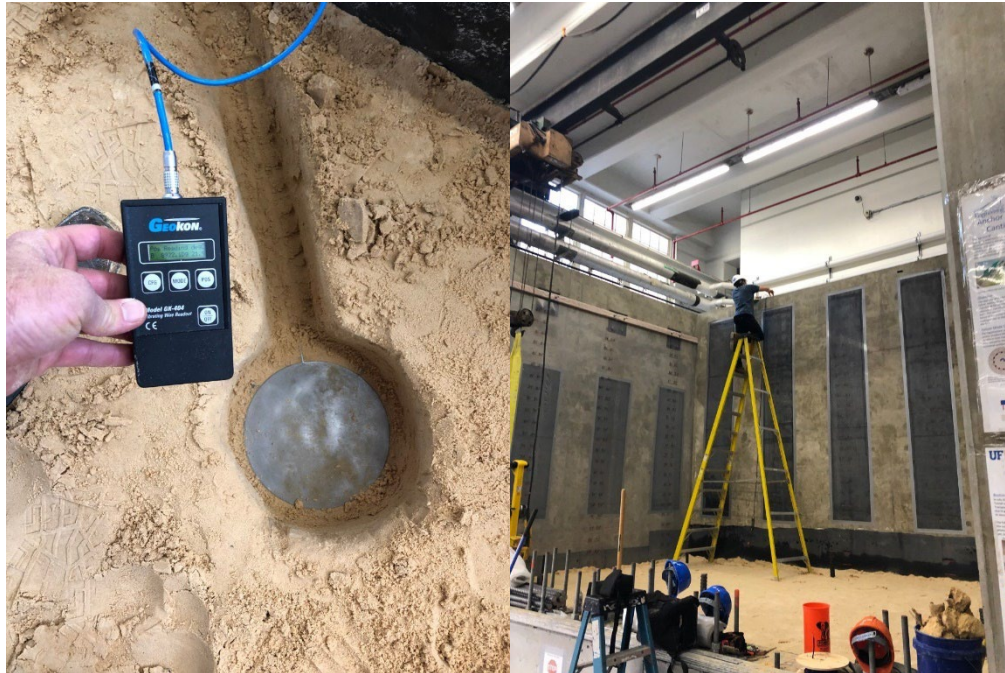


Figure 4-8. Placing EPCs under leveling pad locations and testing using handheld readout.

After the base layer was completed, leveling pad formwork was constructed, and the leveling pads were cast (Figure 4-9). Once the leveling pads were cured, they were then smoothed using a grinder to ensure they provided a uniform level bearing surface for the MSE wall panels (Figure 4-10). Once the leveling pads were complete, trenches were dug in the base layer soil for leveling pad placement (Figure 4-11). Surveying equipment was used during leveling pad placement to ensure the front and back MSE wall leveling pads were at the same elevation relative to the strong floor.



Figure 4-9. Building steel reinforced leveling pad forms and casting concrete.



Figure 4-10. Smoothing out imperfections on the leveling pads with a grinder.



Figure 4-11. Cutting trenches in the base layer for leveling pads and placing the leveling pads.

Next, the back strong wall was lined with the first course of high strength Styrofoam to provide clearance between the strong wall and back MSE wall. With the Styrofoam in place, the first course of MSE wall panels were placed and checked for plumbness (Figure 4-12). Once the proper vertical alignment was achieved, temporary bracing was added to ensure the wall panels remained in tolerance during construction (Figures 4-12 and 4-13). After the first course of MSE wall panels were secured in place using temporary bracing, the horizontal level of the wall panels was checked to ensure they were also in tolerance. This included checking each individual wall panel, the back MSE panels between the two compaction sides, the front MSE panels between the two compaction sides, and the level of the front and back MSE panels (Figures 4-14 through 4-16).

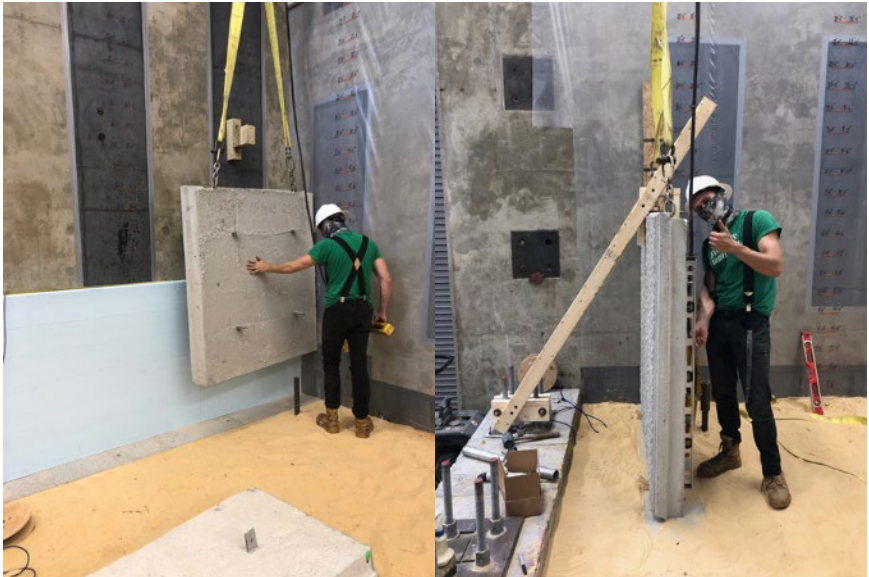


Figure 4-12. Placing first course of MSE wall panels, temporary bracing, and checking plumbness.

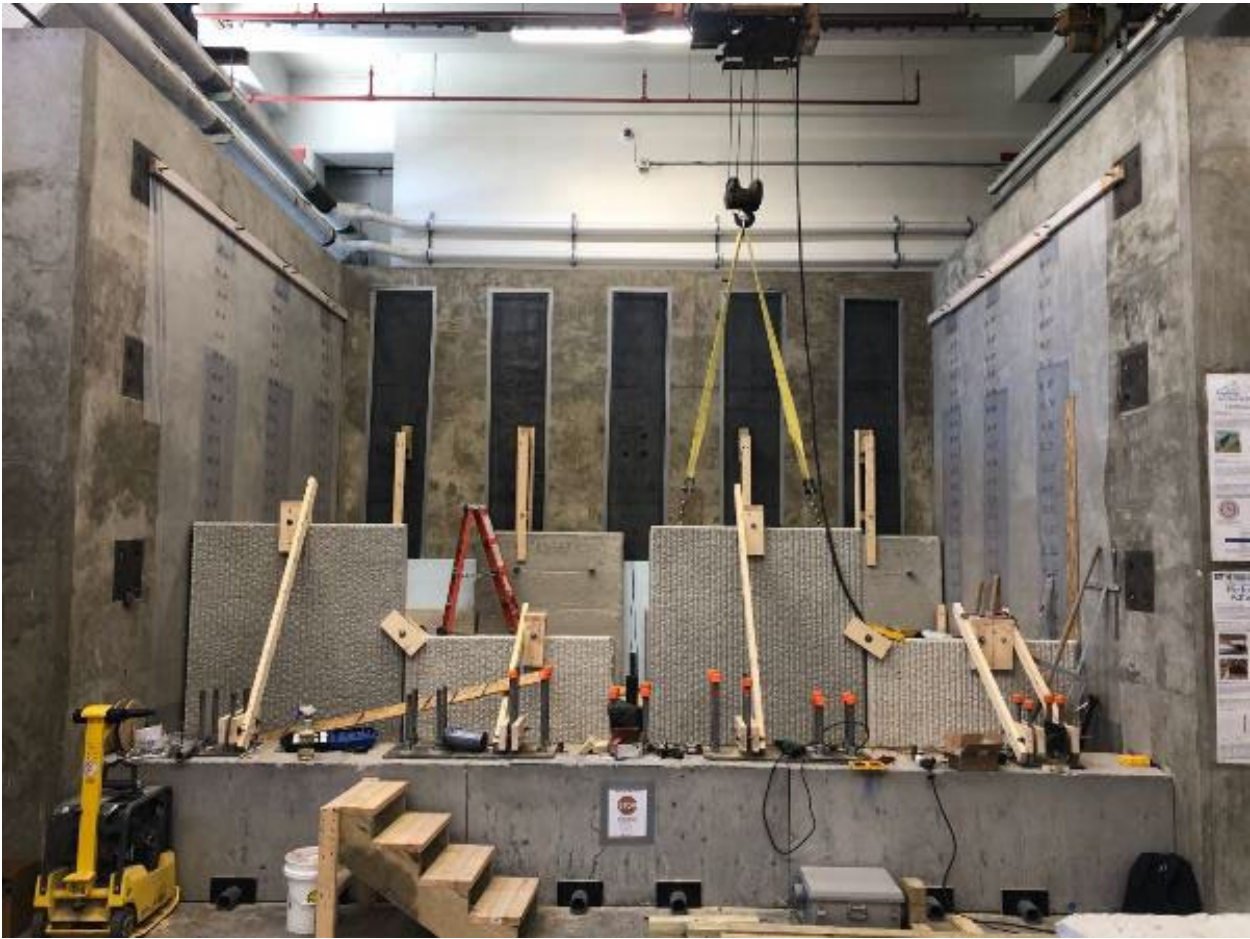


Figure 4-13. First course of MSE wall panels completed.

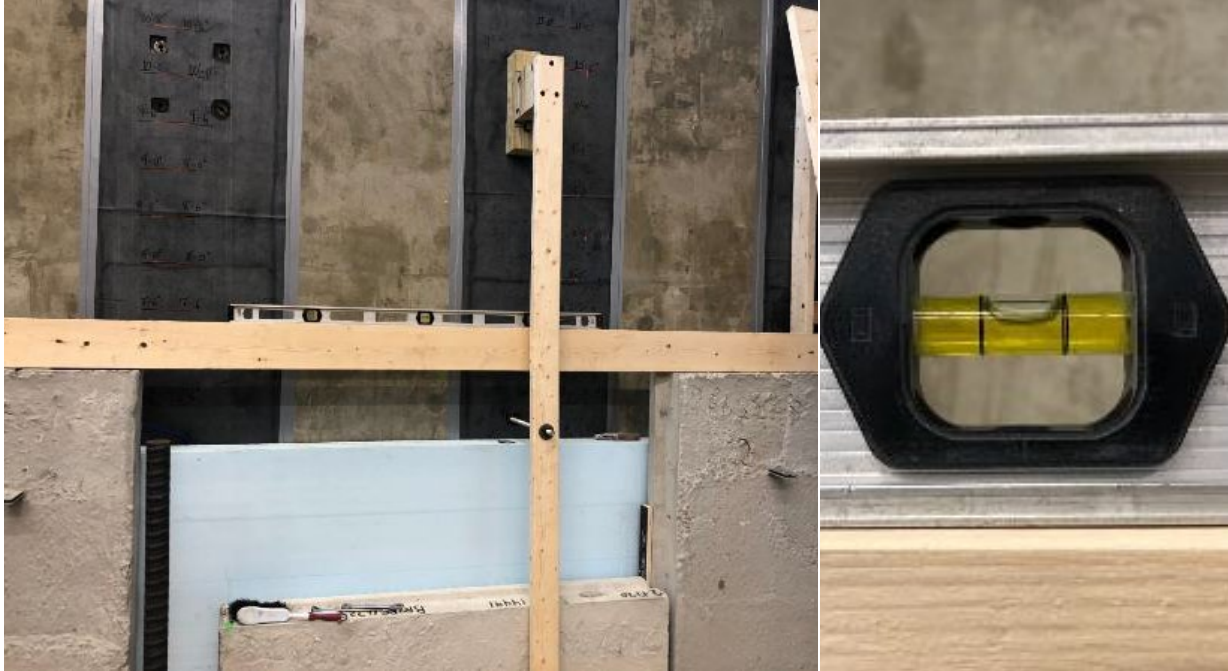


Figure 4-14. Checking the level of the backside MSE panels between the two compaction sides.



Figure 4-15. Checking the level of frontside MSE panels between the two compaction sides.



Figure 4-16. Checking the level of the front and back MSE panels.

After the first course of wall panels were secured in place and confirmed to be in tolerance, the first level of the divider wall to separate the two compaction efforts was constructed (Figures 4-17 and 4-18). Figures 4-19 and 4-20 depict the MSE wall reinforced soil zone prior to adding the first layer of soil above the base layer.



Figure 4-17. Constructing the frame for the compaction effort divider.

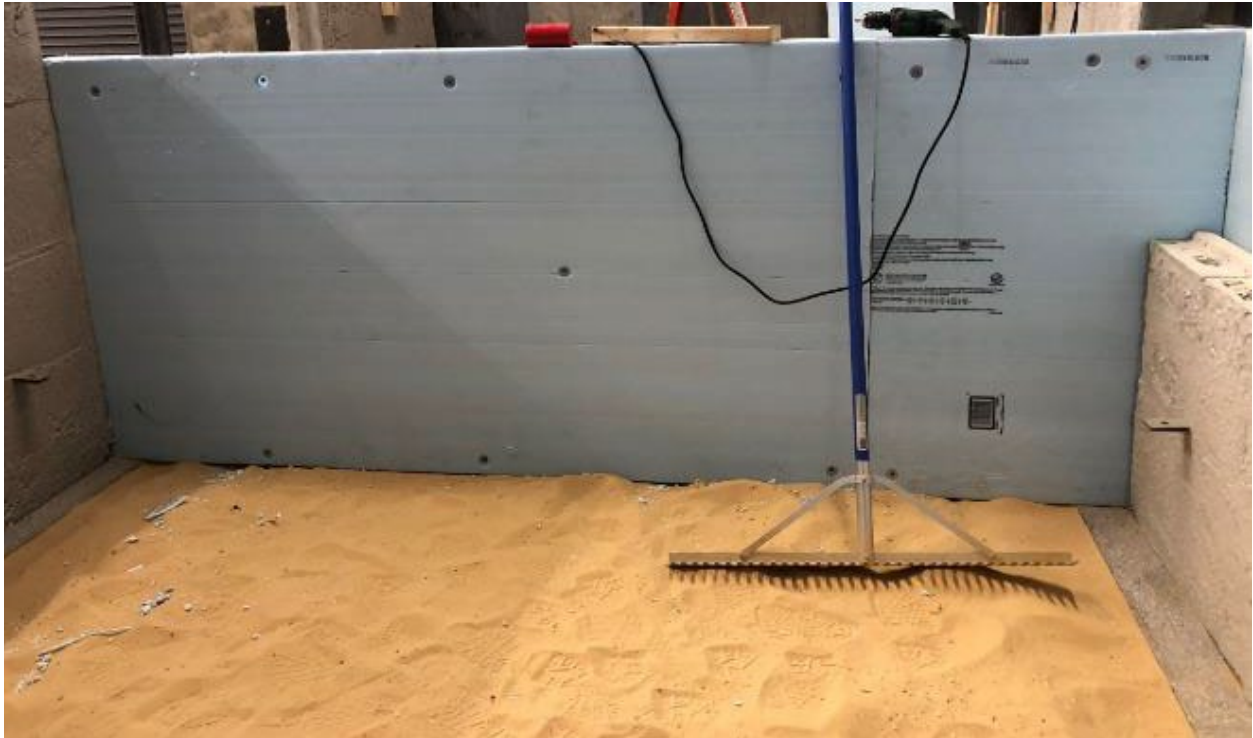


Figure 4-18. Compaction effort divider first level complete.





Figure 4-19. Back MSE wall prior to the first lift above the base layer.



Figure 4-20. Front MSE wall prior to the first lift above the base layer.

During construction of the reinforced soil zone, the initial layers were prevented from interacting with the wall panels until the first row of reinforcements were attached to the panels per construction specifications. This can be observed in Figures 4-21 and 4-22. Also, filter cloth was placed over the joints of the wall panels to retain the soil, and the reaction frame threaded rods were covered in plastic sheeting to reduce frictional effects within the reinforced zone as depicted in Figure 4-22.



Figure 4-21. Soil compaction prior to installing the first row of reinforcement strips.

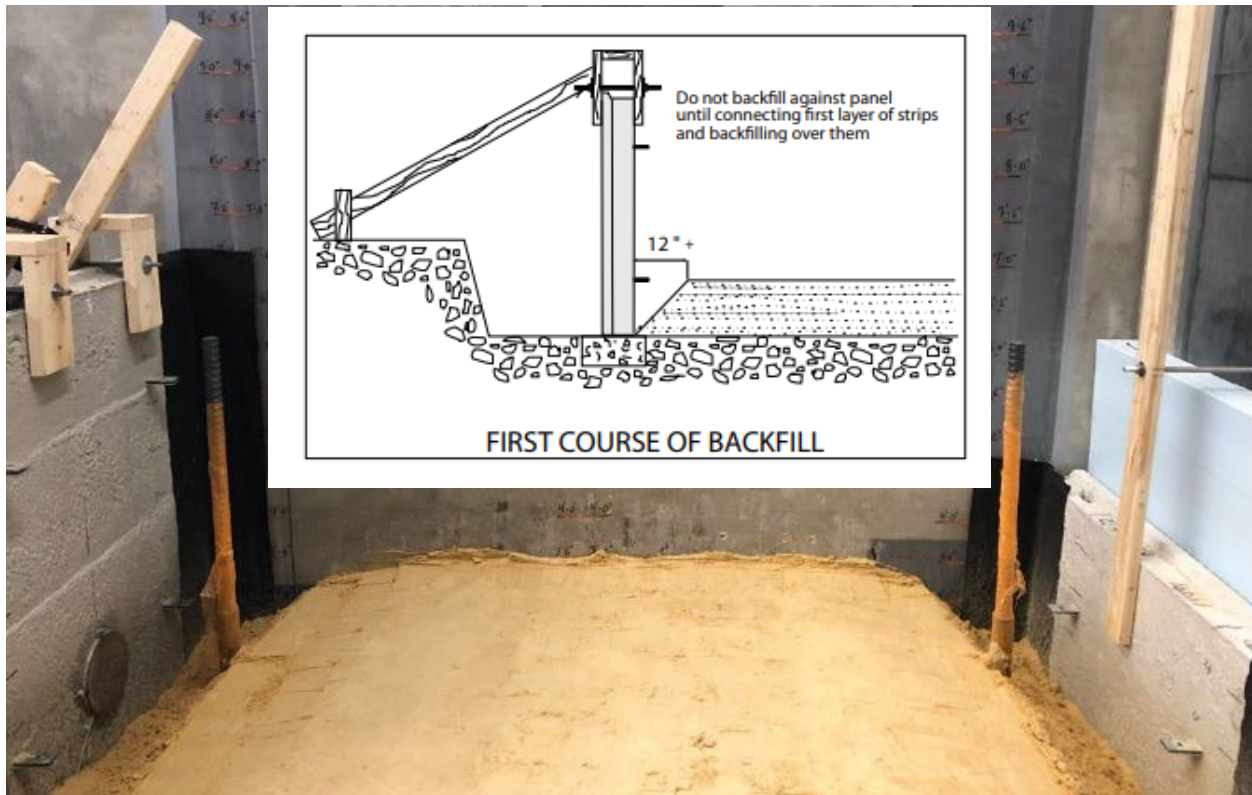


Figure 4-22. Soil compacted and leveled prior to installing the first row of reinforcement strips.

Once the reinforced zone soil layers reached the first level of MSE wall panel reinforcement connections, the reinforcement strips were connected and wall mounted EPCs were added to measure the horizontal earth pressure at the reinforcement level (Figures 4-23 and 4-24). Figures 4-25 and 4-26 depict the instrumentation wiring being routed out of the wall area and tied into designated multiplexers that are routed to the DAQ modules outside of the wall area for data collection. Each instrumentation wire was given its own code/label to ensure it was connected to the correct DAQ port. The next soil layer was added over the reinforcement layer and compacted while preventing the soil from interacting with the wall panels as was completed for the prior layers. EPCs were then placed as described in Figure 4-8 and backfilled prior to placement of the next soil layer. All layers after this lift were backfilled to the wall panels and soil was allowed to interact with the wall panels during compaction. Figures 4-27 and 4-28 depict the additional temporary bracing, spacers, wedges, and clamps that were placed during construction per construction specifications.



Figure 4-23. Frist row of reinforcement strips with filter cloth placed in the joints of wall panels.



Figure 4-24. Front MSE wall with fatback EPCs mounted to measure horizontal earth pressure.



Figure 4-25. Running instrumentation cables through the divider wall.

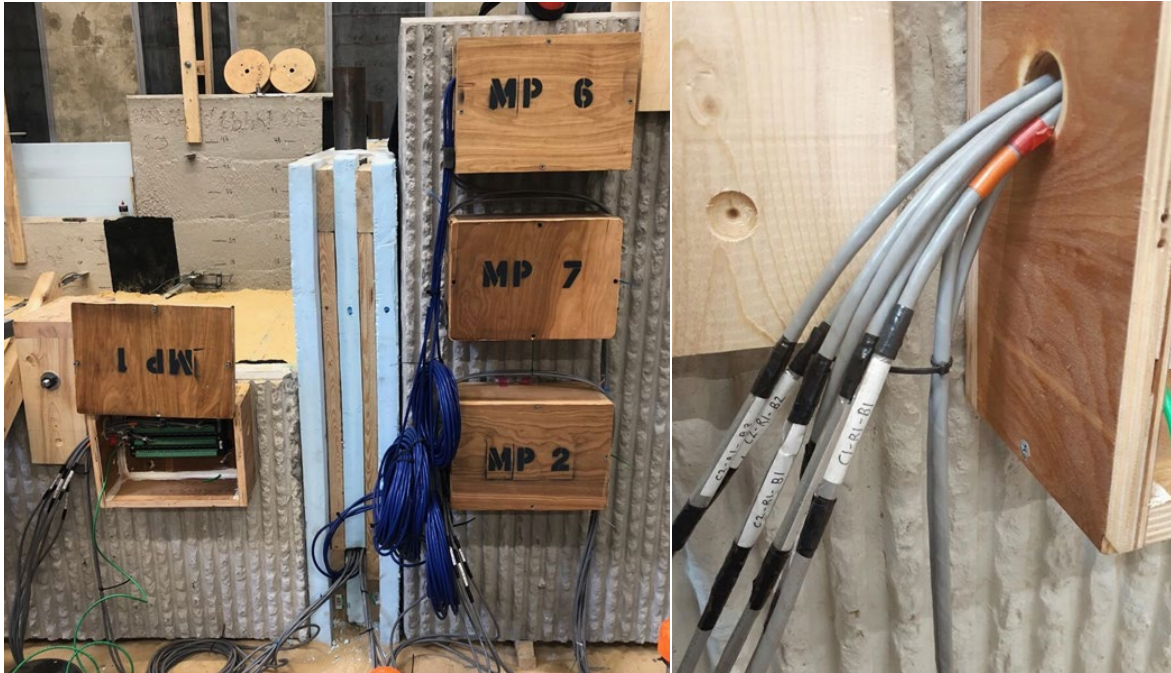


Figure 4-26. Labeled instrumentation cables running through the divider wall to the multiplexer.

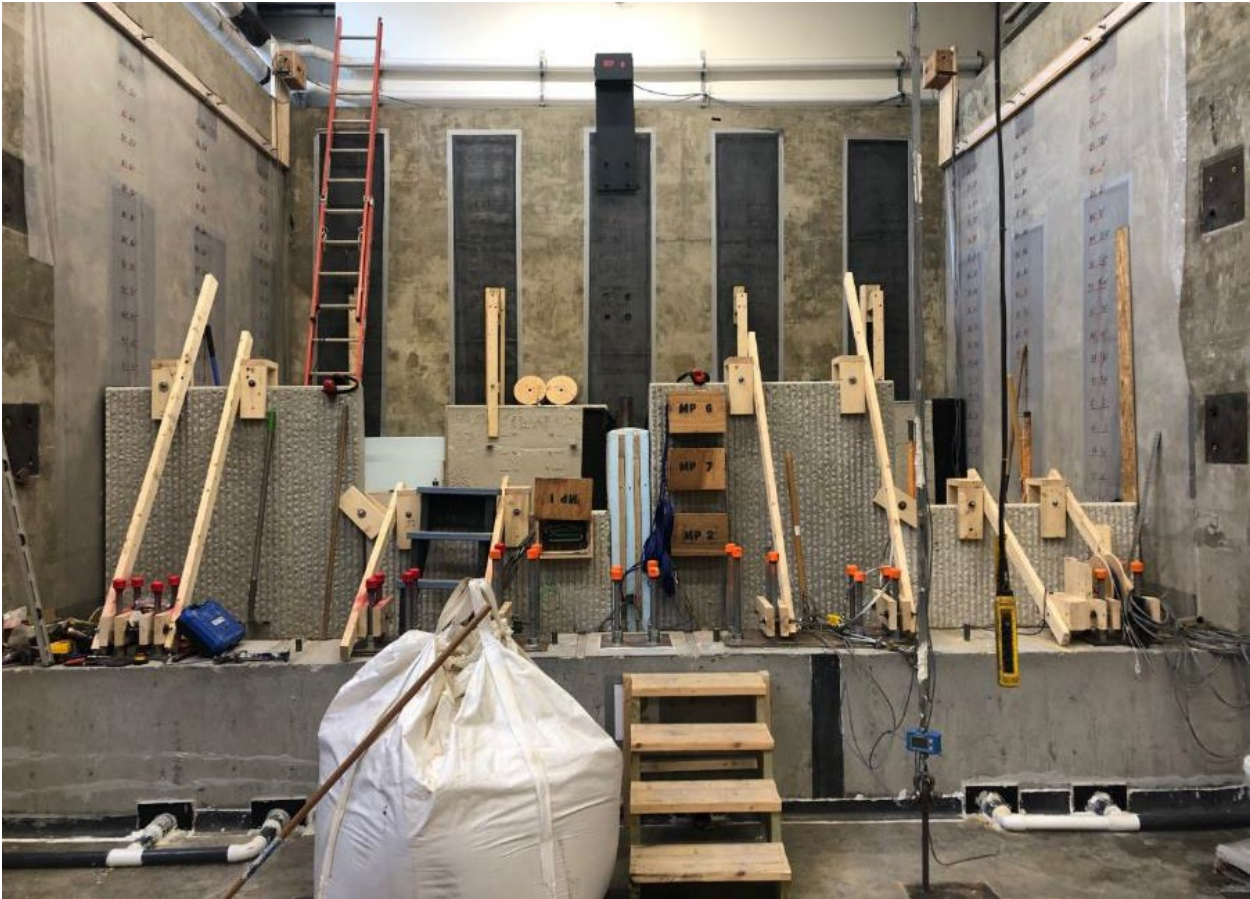


Figure 4-27. Additional temporary bracing added to control front MSE wall movement.



Figure 4-28. Temporary wall bracing, spacers, wedges, and clamps in place.

After the first course panels were secured in place, soil layers were added until the top of the first course half panels were reached. At this point, an OSHA approved safety harness system and a ladder to enter the reinforced soil area were put in place prior to adding the second course of panels. After the safety harness system was in place, bearing pads were placed on top of the first course half panels and the second course full panels were added to the wall. Once the panels were checked for vertical and horizontal leveling, temporary bracing and wall clamps were added prior to soil backfilling and compaction. Also added were temporary wood railings on top of the first course full panels for OSHA compliance. The soil was then backfilled and compacted in six-inch lifts until the second level of reinforcement tabs were reached. The reinforcement strips, wall mounted EPCS, and soil embedded EPCS were added as previously described. Construction proceeded in the same manner for the remainder of wall construction as depicted in Figures 4-29 through 4-33. Throughout this process, the OSHA safety system, temporary wall bracings, and ladder were routinely moved to accommodate wall construction while complying with OSHA regulations and square panel construction specifications.



Figure 4-29. Adding the second course of MSE wall panels.





Figure 4-30. Adding the third course of MSE wall panels.



Figure 4-31. Adding the final course of MSE wall panels.



Figure 4-32. Temporary wall bracing removed after completing wall construction.



Figure 4-33. Overview of MSE wall area.

Once the soil level reached the top of the MSE walls, the temporary bracing was removed, and steel chain link fence was placed atop the soil as depicted in Figure 4-33. The chain link fence was laid on top of the soil to assist in evenly distributing the surcharge load from the reaction system and to prevent the steel plates in which the air bags rest on from being pushed into the soil and possibly underneath one another. The steel plates were then laid on top of the chain link fence and each respective Matjack (airbag) was laid on top of the steel plates as depicted in Figures 4-34 and 4-35. Next, air hoses were connected to each Matjack, and wood spacers were placed around the Matjacks to ensure the soil box walls would not compromise the air hose connections during placement. As shown in Figures 4-36 and 4-37, the steel soil box walls were lifted into place using both overhead cranes in the UF laboratory. Once the soil box walls were in place, C-channels were added to the system and fastened into place using a large square steel washer and nut as depicted in Figure 4-38. Each threaded rod was instrumented with strain gauges in full bridge to monitor the reaction loads during surcharge loading. The instrumented rods allowed the UF research team to evenly tension each threaded connection to approximately 1,000 lbs prior to surcharge loading. This completed the MSE wall and reaction frame construction as depicted in Figure 4-39.

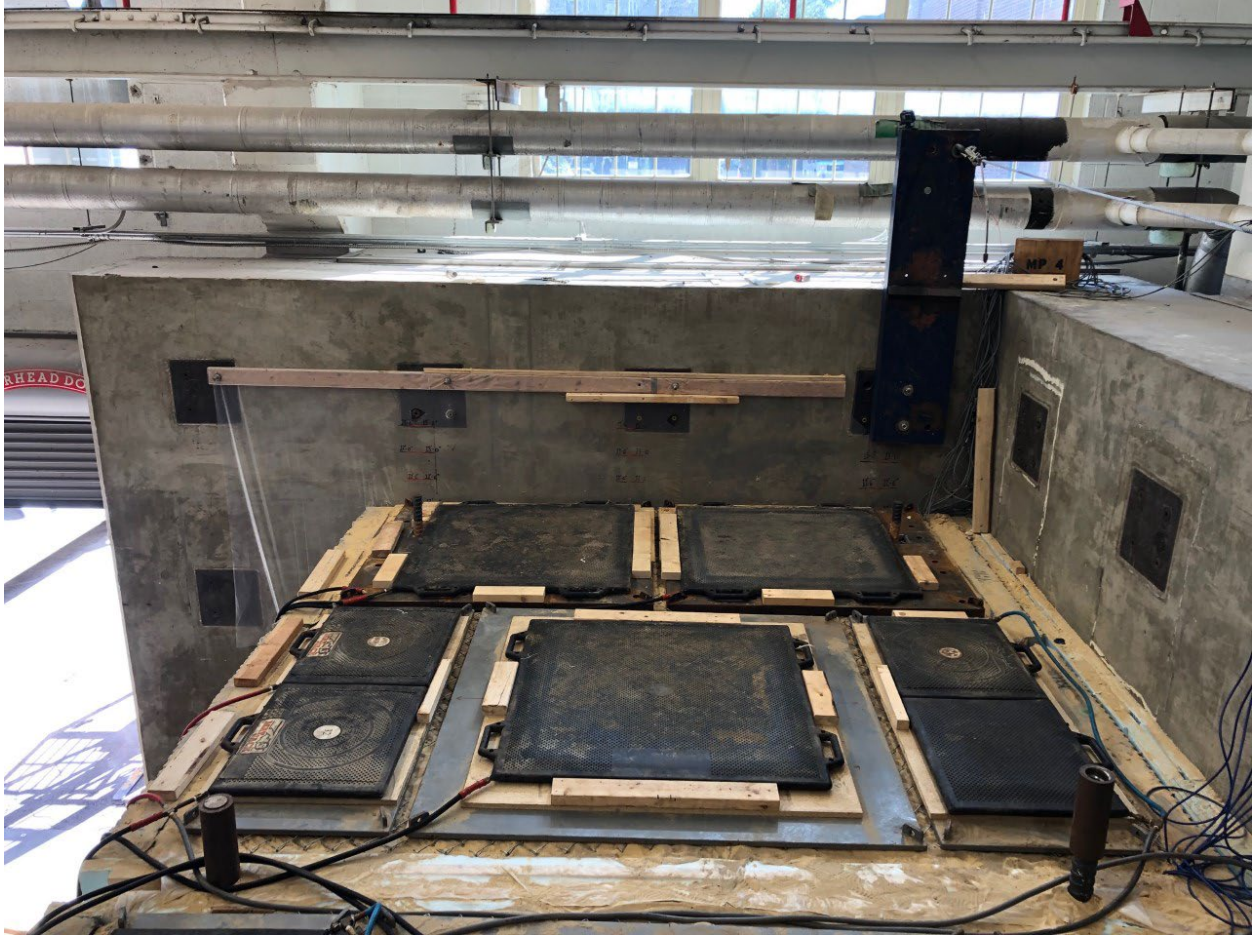


Figure 4-34. Matjack airbag system in place on the 95% compaction effort side.



Figure 4-35. Matjack airbag system in place on the 103% compaction effort side.



Figure 4-36. Crane lifting the first soil box wall in place.



Figure 4-37. First soil box wall in place, resting on matjack system.





Figure 4-38. C-channels added and secured in place to complete the matjack reaction frame.



Figure 4-39. MSE wall with reaction frame in place.

## 4.2 Instrumentation

Throughout the construction of the MSE walls, a significant amount of instrumentation was added within the investigated area to properly quantify the earth pressures that develop when typical MSE wall panels are mechanically fastened to an unyielding structure. During the research effort, 32 soil embedded EPCs were placed to measure the vertical earth pressure within the reinforced zone, 16 wall mounted EPCs were placed on the front MSE wall to measure the horizontal earth pressure that develops within the reinforced zone, 80 full bridge strain gauge locations were added to the reinforcement strips to measure the strip tension within the reinforced zone, 4 EPCs were placed underneath the leveling pads to quantify the down drag stresses that develop on the MSE wall panels from the confined loading, 2 draw wire sensors were attached to the exterior of the front MSE wall panels to monitor wall movement, and strain gauges were added to each of the six reaction frame threaded rods and set up in full bridge to monitor the reaction frame loads. In total, 140 instrumented/monitored locations were present within the investigated area. Each of these instruments were continuously logged after being added to the system. Additional instrumentation included digital pressure gauges placed in line with each of the six main Matjack air hose lines to properly control the surcharge loading.

Prior to adding the soil embedded EPCs, the length of the cables on the existing EPCs (used in prior FDOT/UF research) had to be increased which required splice kits to be added to 32 of the EPCs. The splice kits used can be seen in Figure 4-40. Once the splice kits were added, the EPCs then had to be tested and recalibrated. This required developing an “EPC loading system” which comprised a custom-built soil box as depicted in Figure 4-41, that could be installed and loaded in UF’s Instron load frame assembly as depicted in Figure 4-42. The EPC pressures were checked under each load using a handheld readout (Figure 4-42).



Figure 4-40. Geokon splice kit.



Figure 4-41. EPC test box for calibration after splicing was completed.



Figure 4-42. Load testing a soil embedded EPC for calibration.

As discussed, the extensible steel reinforcement strips were monitored in 80 locations using strain gauges set up in full bridge. In total, this required 320 individual strain gauges to be mounted on the reinforcement strips. The gauges were placed in strategic locations as discussed in Chapter 3. Each of the gauges from a single monitored location were then soldered to a terminal strip and shielded wire that attached to the DAQ for recording (Figure 4-43). Once the gauges were placed, a moisture protection coating and rugged coating were added to the gauge locations to ensure they could survive the construction process. After each step, gauge installation, moisture coating, and rugged coating, the strips were load tested under four tension loads to develop individual calibration curves for each monitored location (Figures 4-44 through 4-46). Load tests were conducted after each step to ensure the gauges were not affected by the application of the coatings. In total, over 320 load tests were conducted on the strips as some strip locations had to be modified due to malfunction.

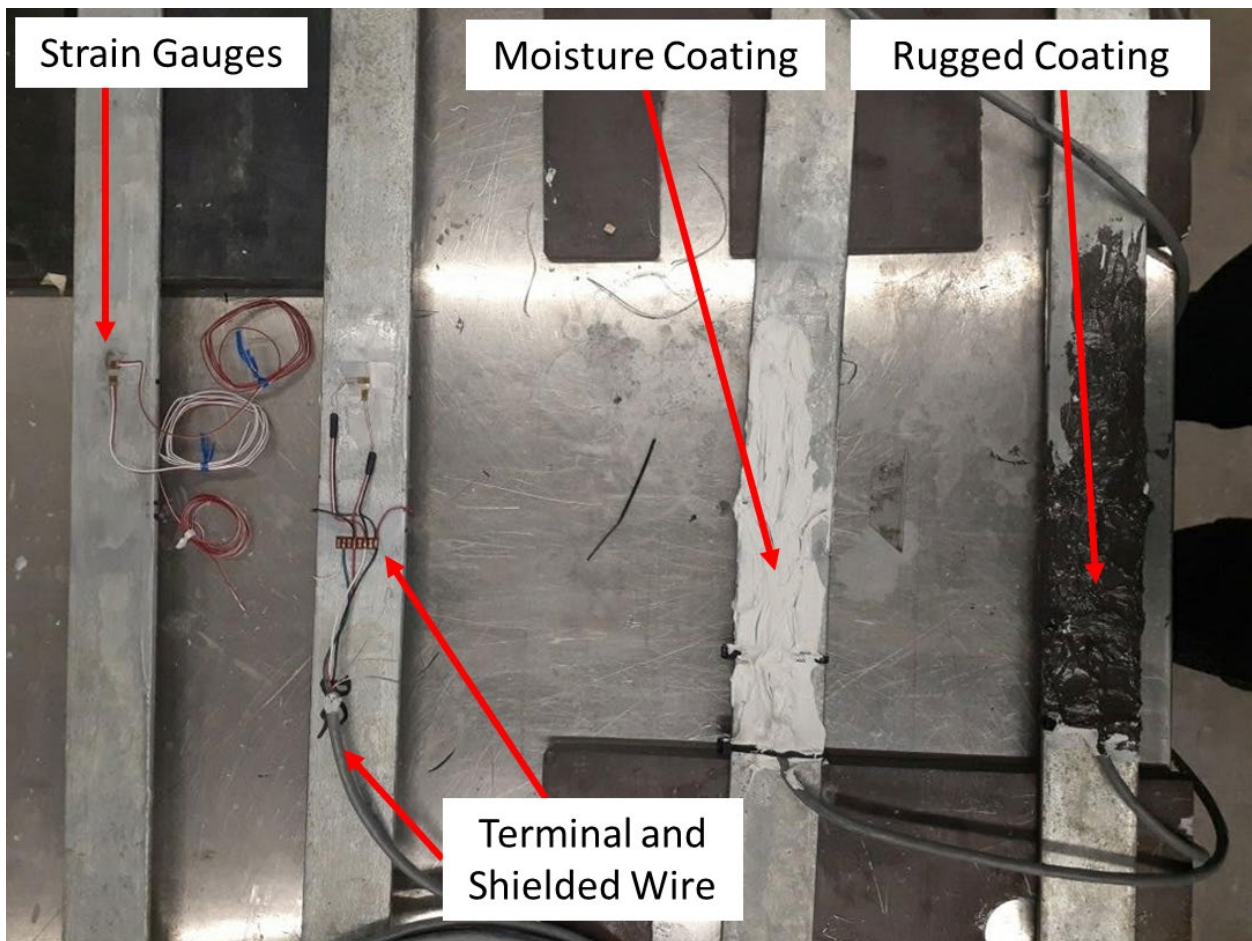


Figure 4-43. Installing strain gauges, moisture coating, and rugged coating on reinforcement strips.



Figure 4-44. Load testing reinforcement strips to develop individual calibration curves.

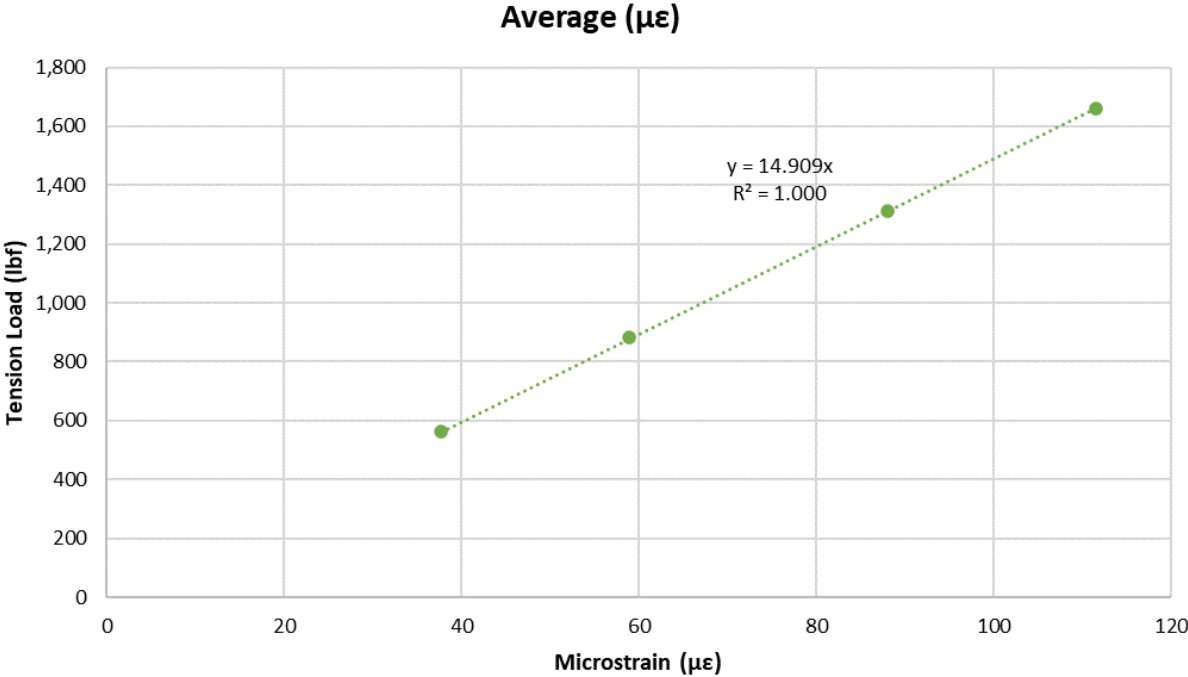


Figure 4-45. Calibration curves prior to adding moisture and protective coating.

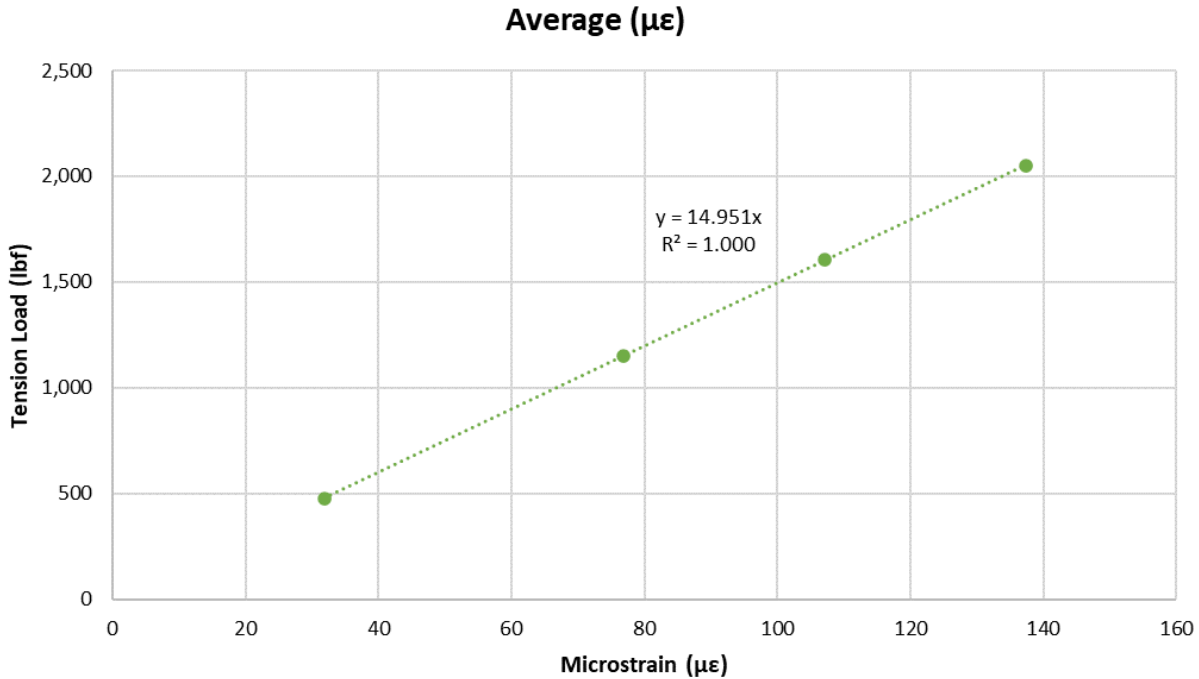


Figure 4-46. Calibration curves after adding moisture and protective coating.

Once the reinforcement strips were fully instrumented, they were systematically added to the MSE walls as construction progressed. Due to the large amount of instrumentation within the investigated wall area, the instrumentation first had to be routed to a series of eight multiplexers prior to reaching the Campbell Scientific CR6 data acquisition module for recording. Multiplexers are network devices that allow one or more analog or digital input signal to travel together over the same communication transmission link. The intent is to combine and transmit signals over a shared medium in order to optimize efficiency and decrease the total cost of communication. Unfortunately, the CR6 was unable to accommodate the large amount of instrumentation when each of the multiplexers were directly routed to the CR6. This was discovered after the first row of instrumented reinforcement strips was added to the MSE wall prior to loading being introduced. In Figure 4-47, the five monitored locations on the single strip should have produced a nearly identical signal. However, due to the voltage settling times available on the CR6, residual voltage would build up within the system and cause random gauge locations to begin “walking off” their baseline values. Shown in Figure 4-48, voltage settling tests were conducted to quantify these effects. In Figure 4-48, it is observed that the voltage never stabilized which resulted in the residual voltage buildup. Consequently, a complex tiered multiplexer system had to be developed. The wiring diagram for the tiered system is provided in Figure 4-49. Displayed in Figure 4-49, each of the eight multiplexers originally used are first routed to an intermediate multiplexer in Tier 1. The Tier 1 multiplexer is then wired into the CR6 for data collection. Once the tiered system was in place, the voltage settling tests were conducted again. Figure 4-50 shows the results from the tiered system test where it can be observed that the input voltage quickly stabilized which allowed accurate results to be measured as indicated in Figure 4-51. Figure 4-51 shows the strip tension versus time using the tiered multiplexer system

prior to loading. The gauges were now stable with negligible fluctuation from their initial baseline values (Note: some fluctuation is observed due to thermal effects).

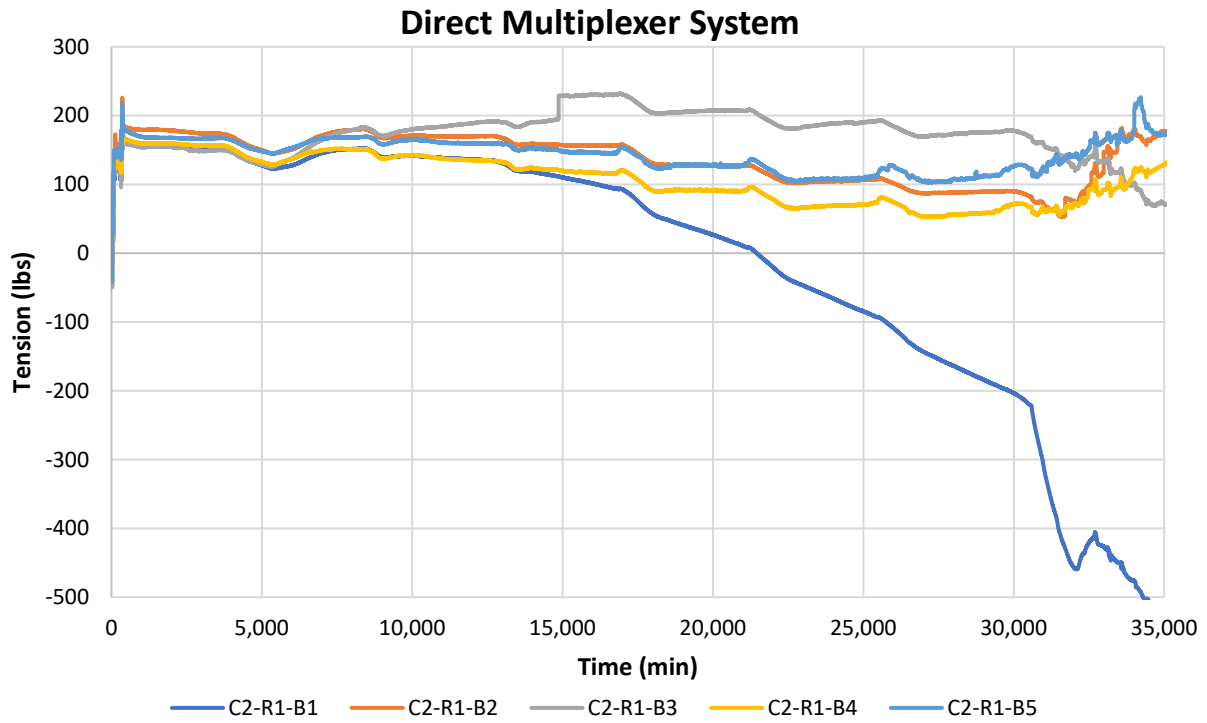


Figure 4-47. Strip tension vs. time using direct multiplexer system prior to loading.



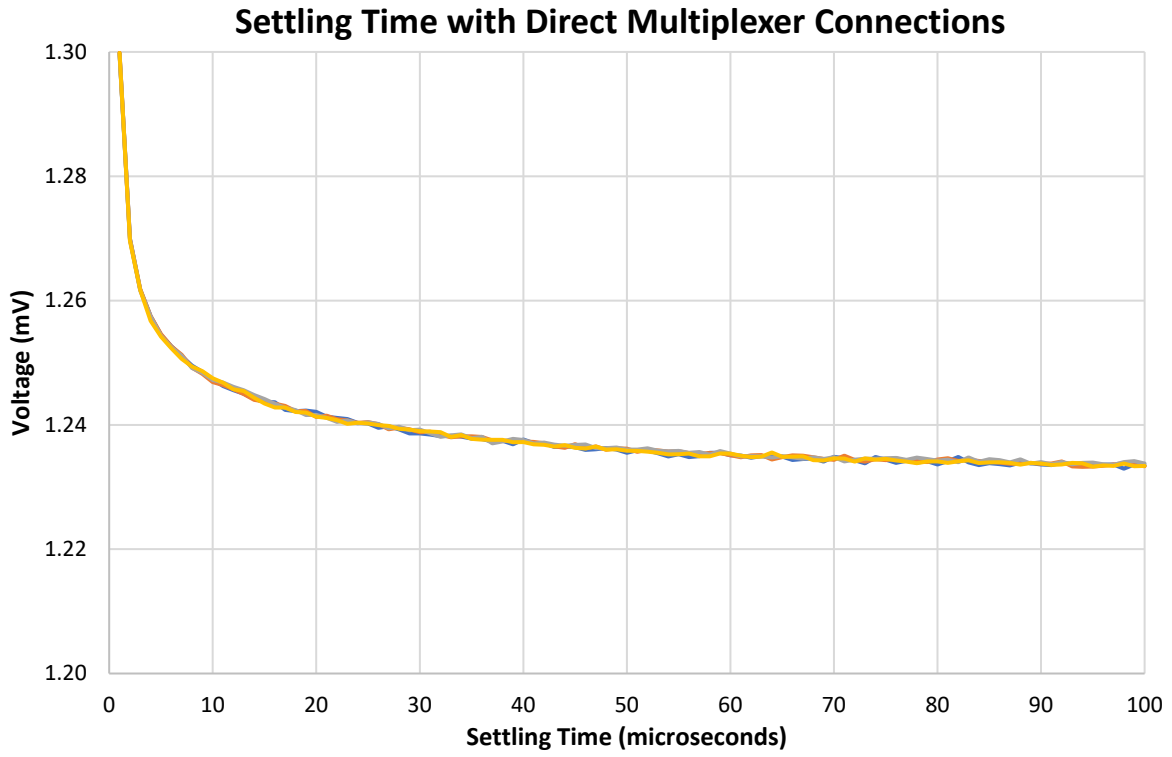


Figure 4-48. Voltage vs. settling time indicating stabilization was never achieved.

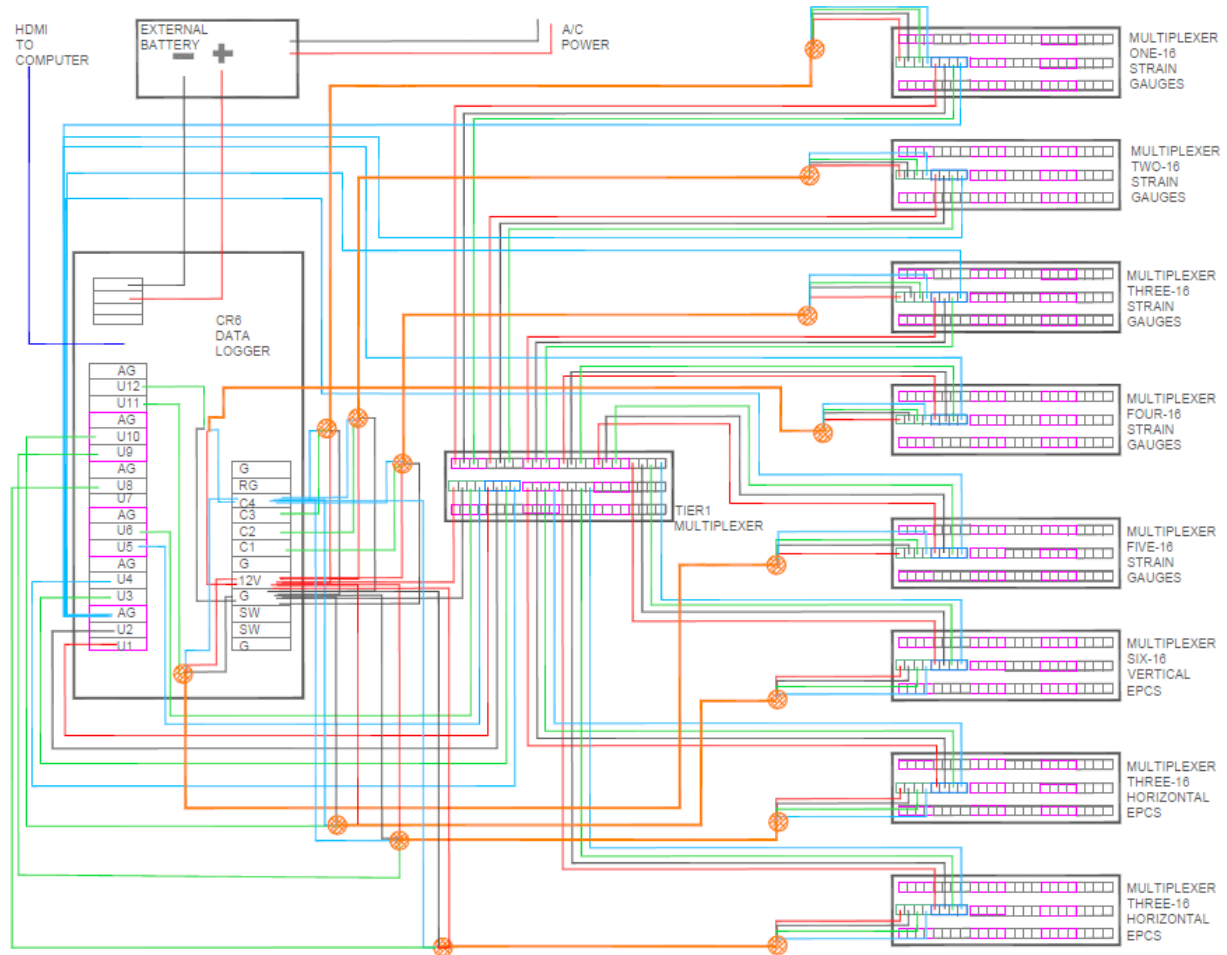


Figure 4-49. CR6 tiered multiplexer wiring diagram to resolve voltage settling issues.

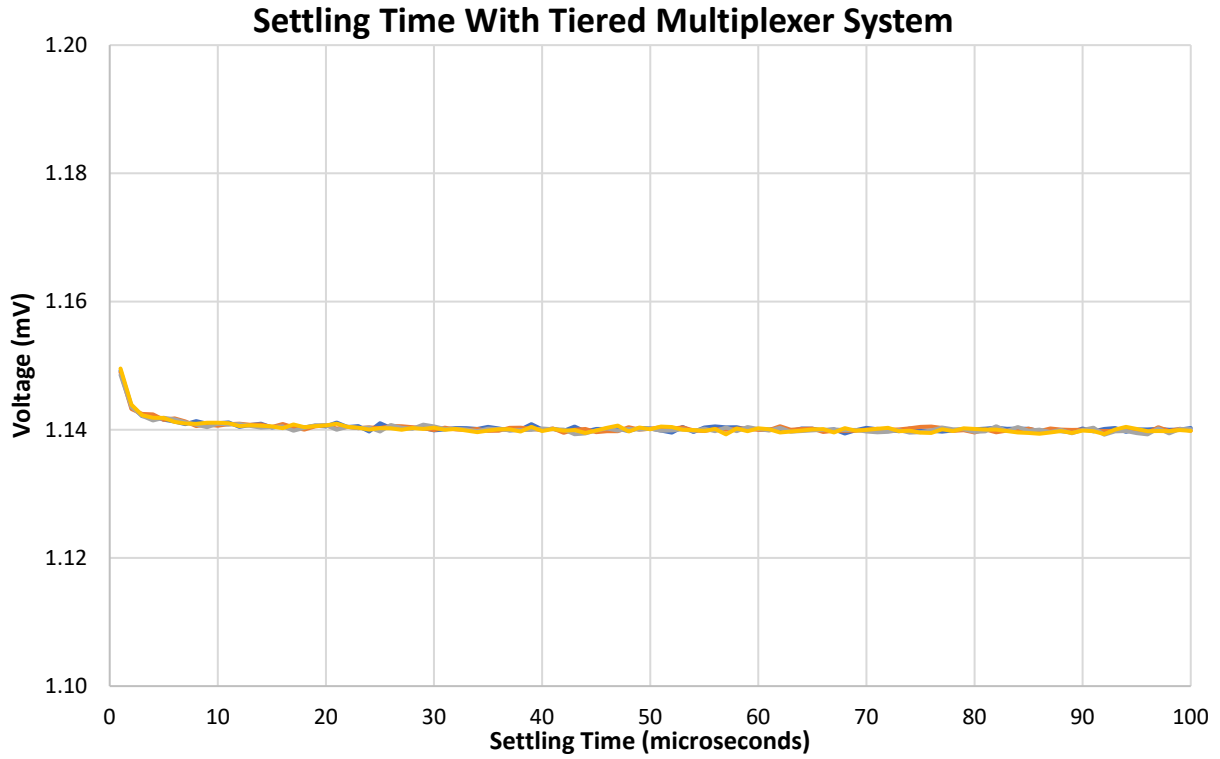


Figure 4-50. Voltage vs. settling time indicating stabilization was achieved using tiered system.

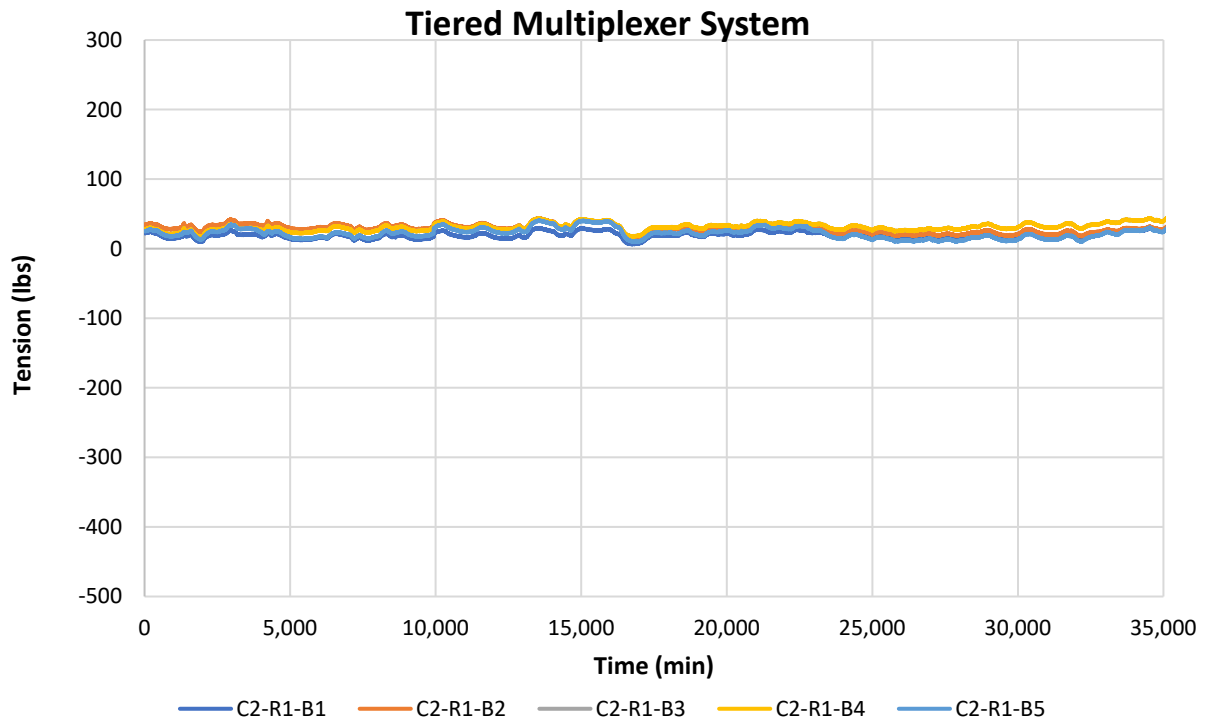


Figure 4-51. Strip tension vs. time using tiered multiplexer system prior to loading.

Even with the tiered multiplexer system developed, the CR6 was unable to accommodate all the instrumentation utilized. This required an additional DAQ to be added to the system, a CR10x. The CR10x was used to monitor the EPCs under the leveling pads, the draw wire sensors, and the reaction frame threaded rod strain gauges. The wiring diagram for the CR10x is provided in Figure 4-52 (Note: The instrumented threaded rod wiring is not displayed). The draw wire sensors used to monitor wall displacement are depicted in Figures 4-53 and 4-54.

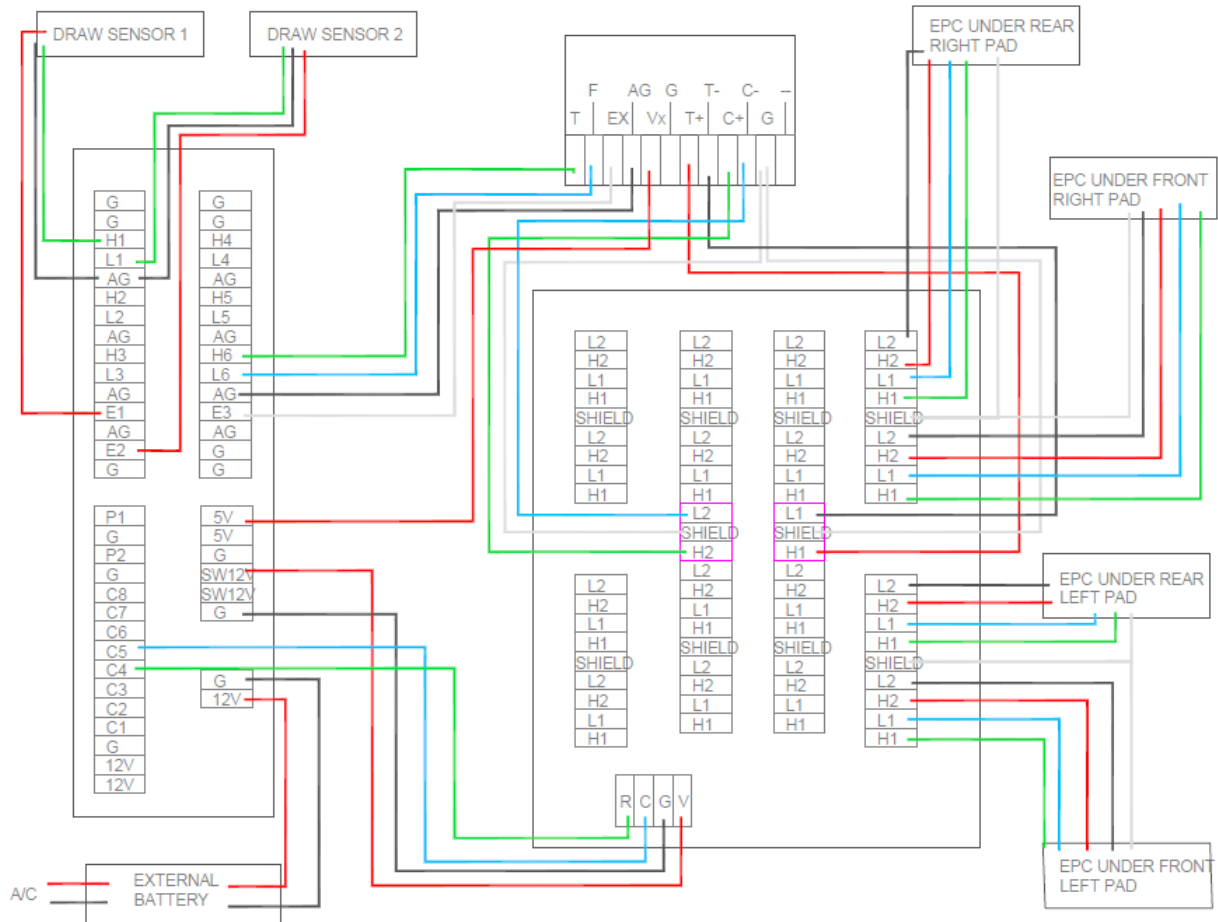


Figure 4-52. CR10x wiring diagram.



Figure 4-53. Draw wire sensor attached to base MSE wall panel to measure wall movement.

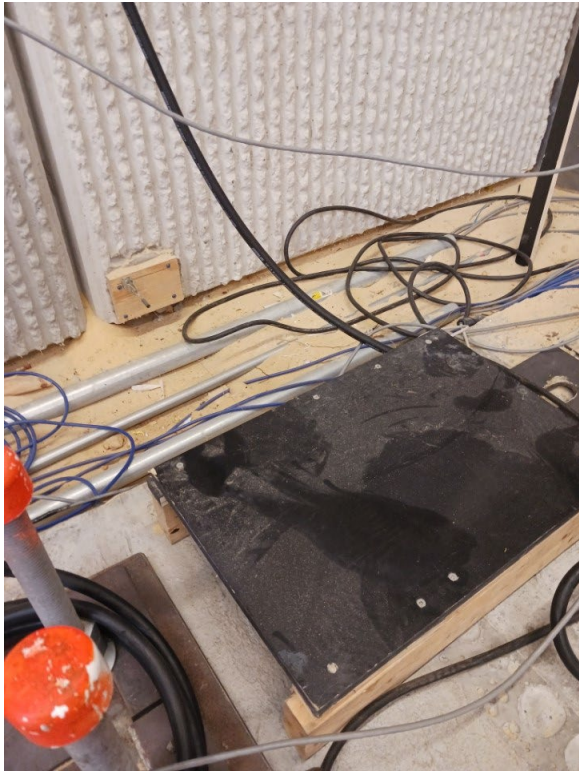


Figure 4-54. Draw wire sensor protective enclosure.

## 5 Construction Analysis

### 5.1 Nuclear Density Results

As discussed, nuclear density testing was performed for every six-inch soil lift added within the investigated area. Figure 5-1 displays the quadrants in which each nuclear density test was routinely performed. As seen in Figure 5-1, each compaction effort was tested for density in two locations. The results of all nuclear density tests are provided in Tables 5-1 through 5-22. Figures 5-2 and 5-3 display the soil density as a function of soil height for both compaction efforts.

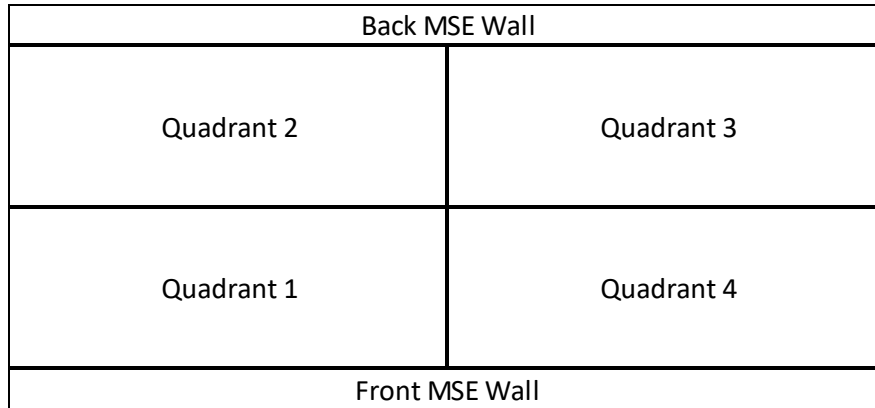


Figure 5-1. MSE wall area plan view of quadrants for nuclear density testing.

Table 5-1. Nuclear density results for soil lift 1 located in the base layer.

Lift 1 (6"-12")					
Location	$\gamma_d$ (pcf)	$\gamma_t$ (pcf)	$\gamma_w$ (pcf)	$w$ (%)	Relative Compaction (%)
1	109.4	118.7	9.4	8.6	103.5
2	109.5	120.3	10.9	9.9	103.6
3	109.8	118.8	8.9	8.1	103.9
4	109.5	118.9	9.4	8.5	103.6

Table 5-2. Nuclear density results for soil lift 2 located in the base layer.

Lift 2 (12"-18")					
Location	$\gamma_d$ (pcf)	$\gamma_t$ (pcf)	$\gamma_w$ (pcf)	$w$ (%)	Relative Compaction (%)
1	109.3	119.8	10.6	9.7	103.4
2	109.4	119.2	9.8	8.9	103.5
3	108.1	117.9	9.8	9.0	102.3
4	109.7	119.5	9.9	9.0	103.8

Table 5-3. Nuclear density results for soil lift 3 located in the base layer.

Lift 3 (18"-24")					
Location	$\gamma_d$ (pcf)	$\gamma_t$ (pcf)	$\gamma_w$ (pcf)	w (%)	Relative Compaction (%)
1	108.7	118.6	9.9	9.1	102.8
2	108.6	118.9	10.2	9.4	102.7
3	108.4	118.4	10.0	9.2	102.6
4	109.6	119.3	9.7	8.9	103.7

Table 5-4. Nuclear density results for soil lift 4 located in the reinforced zone of the soil.

Lift 4 (24"-30")					
Location	$\gamma_d$ (pcf)	$\gamma_t$ (pcf)	$\gamma_w$ (pcf)	w (%)	Relative Compaction (%)
1	106.2	110.4	4.2	4.0	100.5
2	105.3	109.6	4.4	4.1	99.6
3	108.3	114.1	5.8	5.3	102.5
4	107.8	113.2	5.4	5.0	102.0

Table 5-5. Nuclear density results for soil lift 5 located in the reinforced zone of the soil.

Lift 5 (30"-36")					
Location	$\gamma_d$ (pcf)	$\gamma_t$ (pcf)	$\gamma_w$ (pcf)	w (%)	Relative Compaction (%)
1	103.5	107.6	4.1	3.9	97.9
2	100.6	104.4	3.8	3.8	95.2
3	109.1	117.5	8.5	7.8	103.2
4	109.0	117.2	8.1	7.5	103.1

Table 5-6. Nuclear density results for soil lift 6 located in the reinforced zone of the soil.

Lift 6 (36"-42")					
Location	$\gamma_d$ (pcf)	$\gamma_t$ (pcf)	$\gamma_w$ (pcf)	w (%)	Relative Compaction (%)
1	103.3	107.1	3.8	3.7	97.7
2	101.3	105.4	4.1	4.0	95.8
3	108.0	113.4	5.3	4.9	102.2
4	108.1	113.7	5.6	5.2	102.3

Table 5-7. Nuclear density results for soil lift 7 located in the reinforced zone of the soil.

Lift 7 (42"-48")					
Location	$\gamma_d$ (pcf)	$\gamma_t$ (pcf)	$\gamma_w$ (pcf)	w (%)	Relative Compaction (%)
1	101.5	106.4	4.9	4.9	96.0
2	100.4	104.8	4.4	4.4	95.0
3	108.3	115	6.8	6.3	102.5
4	107.7	113.5	5.8	5.4	101.9

Table 5-8. Nuclear density results for soil lift 8 located in the reinforced zone of the soil.

Lift 8 (48"-54")					
Location	$\gamma_d$ (pcf)	$\gamma_t$ (pcf)	$\gamma_w$ (pcf)	w (%)	Relative Compaction (%)
1	101.8	109	7.2	7.1	96.3
2	102.0	108.3	6.3	6.2	96.5
3	108.0	121.5	13.5	12.5	102.2
4	107.7	120.1	12.4	11.5	101.9

Table 5-9. Nuclear density results for soil lift 9 located in the reinforced zone of the soil.

Lift 9 (54"-60")					
Location	$\gamma_d$ (pcf)	$\gamma_t$ (pcf)	$\gamma_w$ (pcf)	w (%)	Relative Compaction (%)
1	101.5	104.8	3.3	3.2	96.0
2	100.6	104.0	3.5	3.5	95.2
3	108.3	118.1	9.8	9.1	102.5
4	108.1	117.5	9.4	8.7	102.3

Table 5-10. Nuclear density results for soil lift 10 located in the reinforced zone of the soil.

Lift 10 (60"-66")					
Location	$\gamma_d$ (pcf)	$\gamma_t$ (pcf)	$\gamma_w$ (pcf)	w (%)	Relative Compaction (%)
1	100.6	104.1	3.5	3.5	95.2
2	102.1	106.7	4.6	4.5	96.6
3	108.4	118.5	10.0	9.3	102.6
4	108.3	121.5	13.2	12.2	102.5



Table 5-11. Nuclear density results for soil lift 11 located in the reinforced zone of the soil.

Lift 11 (66"-72")					
Location	$\gamma_d$ (pcf)	$\gamma_t$ (pcf)	$\gamma_w$ (pcf)	w (%)	Relative Compaction (%)
1	100.5	107.0	6.6	6.5	95.1
2	100.7	106.2	5.5	5.5	95.3
3	108.8	119.5	10.6	9.8	102.9
4	108.4	118.0	9.7	8.9	102.6

Table 5-12. Nuclear density results for soil lift 12 located in the reinforced zone of the soil.

Lift 12 (72"-78")					
Location	$\gamma_d$ (pcf)	$\gamma_t$ (pcf)	$\gamma_w$ (pcf)	w (%)	Relative Compaction (%)
1	101.4	107	5.6	5.5	95.9
2	100.2	104.7	4.4	4.4	94.8
3	107.9	118.2	10.3	9.5	102.1
4	108.2	118.1	9.9	9.1	102.4

Table 5-13. Nuclear density results for soil lift 13 located in the reinforced zone of the soil.

Lift 13 (78"-84")					
Location	$\gamma_d$ (pcf)	$\gamma_t$ (pcf)	$\gamma_w$ (pcf)	w (%)	Relative Compaction (%)
1	100.3	107.7	7.4	7.4	94.9
2	100.3	111.6	11.3	11.3	94.9
3	108.3	117.4	9.1	9.4	102.5
4	109.0	118.1	9.1	8.3	103.1

Table 5-14. Nuclear density results for soil lift 14 located in the reinforced zone of the soil.

Lift 14 (84"-90")					
Location	$\gamma_d$ (pcf)	$\gamma_t$ (pcf)	$\gamma_w$ (pcf)	w (%)	Relative Compaction (%)
1	100.3	106.1	5.8	5.8	94.9
2	101.8	107.5	5.7	5.6	96.3
3	108.8	115.1	6.2	5.7	102.9
4	109.4	115.3	6.0	5.5	103.5

Table 5-15. Nuclear density results for soil lift 15 located in the reinforced zone of the soil.

Lift 15 (90"-96")					
Location	$\gamma_d$ (pcf)	$\gamma_t$ (pcf)	$\gamma_w$ (pcf)	w (%)	Relative Compaction (%)
1	101.5	106.4	4.9	4.8	96.0
2	100.7	106.4	5.6	5.6	95.3
3	109.7	115.8	6.2	5.6	103.8
4	109.3	116	6.7	6.1	103.4

Table 5-16. Nuclear density results for soil lift 16 located in the reinforced zone of the soil.

Lift 16 (96"-102")					
Location	$\gamma_d$ (pcf)	$\gamma_t$ (pcf)	$\gamma_w$ (pcf)	w (%)	Relative Compaction (%)
1	102.2	107.5	5.4	5.3	96.7
2	102.2	107.5	5.3	5.2	96.7
3	109.0	115.3	6.3	5.8	103.1
4	109.4	115.8	6.4	5.8	103.5

Table 5-17. Nuclear density results for soil lift 17 located in the reinforced zone of the soil.

Lift 17 (102"-108")					
Location	$\gamma_d$ (pcf)	$\gamma_t$ (pcf)	$\gamma_w$ (pcf)	w (%)	Relative Compaction (%)
1	100.7	106.6	5.9	5.9	95.3
2	100.7	106.4	5.7	5.6	95.3
3	110.1	116.9	6.8	6.2	104.2
4	109.4	116	6.6	6.0	103.5

Table 5-18. Nuclear density results for soil lift 18 located in the reinforced zone of the soil.

Lift 18 (108"-114")					
Location	$\gamma_d$ (pcf)	$\gamma_t$ (pcf)	$\gamma_w$ (pcf)	w (%)	Relative Compaction (%)
1	102.0	106.1	4.2	4.1	96.5
2	101.0	105.1	4.1	4.0	95.6
3	107.8	113.6	5.8	5.4	102.0
4	107.8	112.8	5.1	4.7	102.0

Table 5-19. Nuclear density results for soil lift 19 located in the reinforced zone of the soil.

Lift 19 (120"-126")					
Location	$\gamma_d$ (pcf)	$\gamma_t$ (pcf)	$\gamma_w$ (pcf)	w (%)	Relative Compaction (%)
1	101.9	106.3	4.4	4.3	96.4
2	102.3	106.8	4.5	4.4	96.8
3	108.5	120.6	12.1	11.1	102.6
4	109.2	121.2	12.1	11.1	103.3

Table 5-20. Nuclear density results for soil lift 20 located in the reinforced zone of the soil.

Lift 20 (126"-132")					
Location	$\gamma_d$ (pcf)	$\gamma_t$ (pcf)	$\gamma_w$ (pcf)	w (%)	Relative Compaction (%)
1	101.6	107.3	5.7	5.6	96.1
2	101.7	107.3	5.6	5.5	96.2
3	108.5	118	9.6	8.8	102.6
4	108.1	118.3	10.2	9.4	102.3

Table 5-21. Nuclear density results for soil lift 21 located in the reinforced zone of the soil.

Lift 21 (132"-138")					
Location	$\gamma_d$ (pcf)	$\gamma_t$ (pcf)	$\gamma_w$ (pcf)	w (%)	Relative Compaction (%)
1	100.8	108.5	7.7	7.7	95.4
2	101.8	709.7	7.9	7.7	96.3
3	110.2	120.7	10.6	9.6	104.3
4	109.1	120.6	11.5	10.5	103.2

Table 5-22. Nuclear density results for soil lift 22 located in the reinforced zone of the soil.

Lift 22 (132"-138")					
Location	$\gamma_d$ (pcf)	$\gamma_t$ (pcf)	$\gamma_w$ (pcf)	w (%)	Relative Compaction (%)
1	101	105.3	4.3	4.3	95.6
2	101	105.7	4.7	4.6	95.6
3	109.8	119.8	10.0	9.1	103.9
4	110.4	119.9	9.6	8.7	104.4

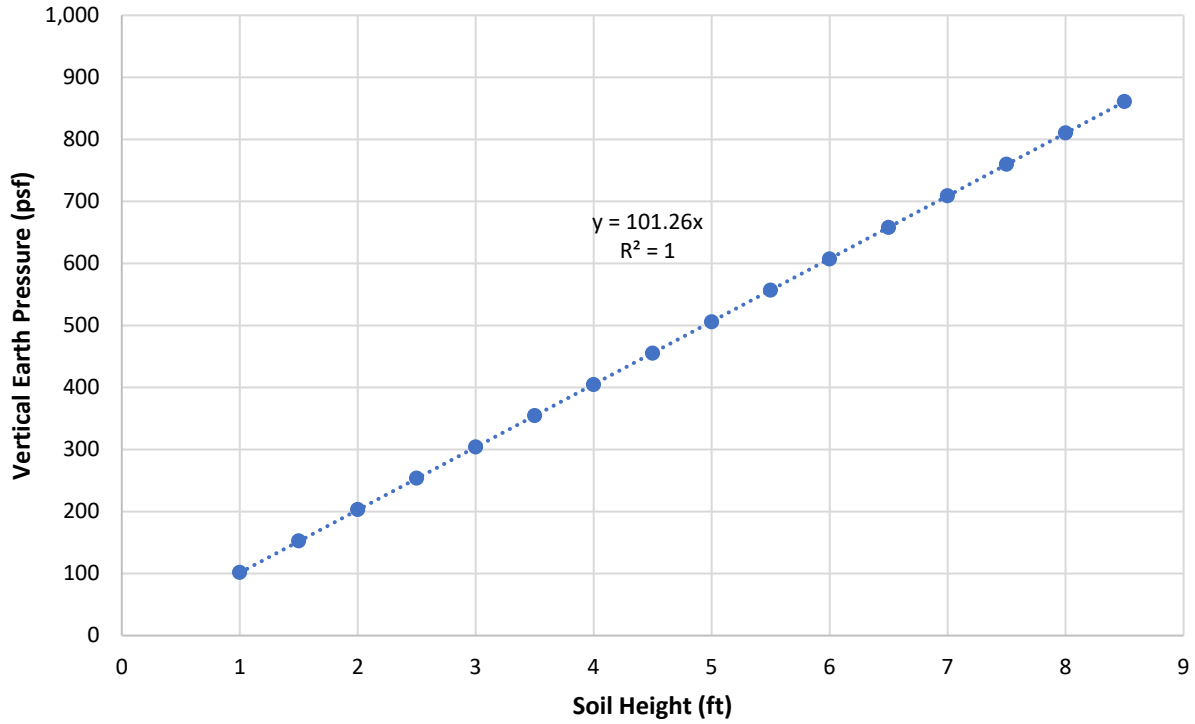


Figure 5-2. Nuclear density vertical earth pressure vs. soil height for 95% compaction effort side.

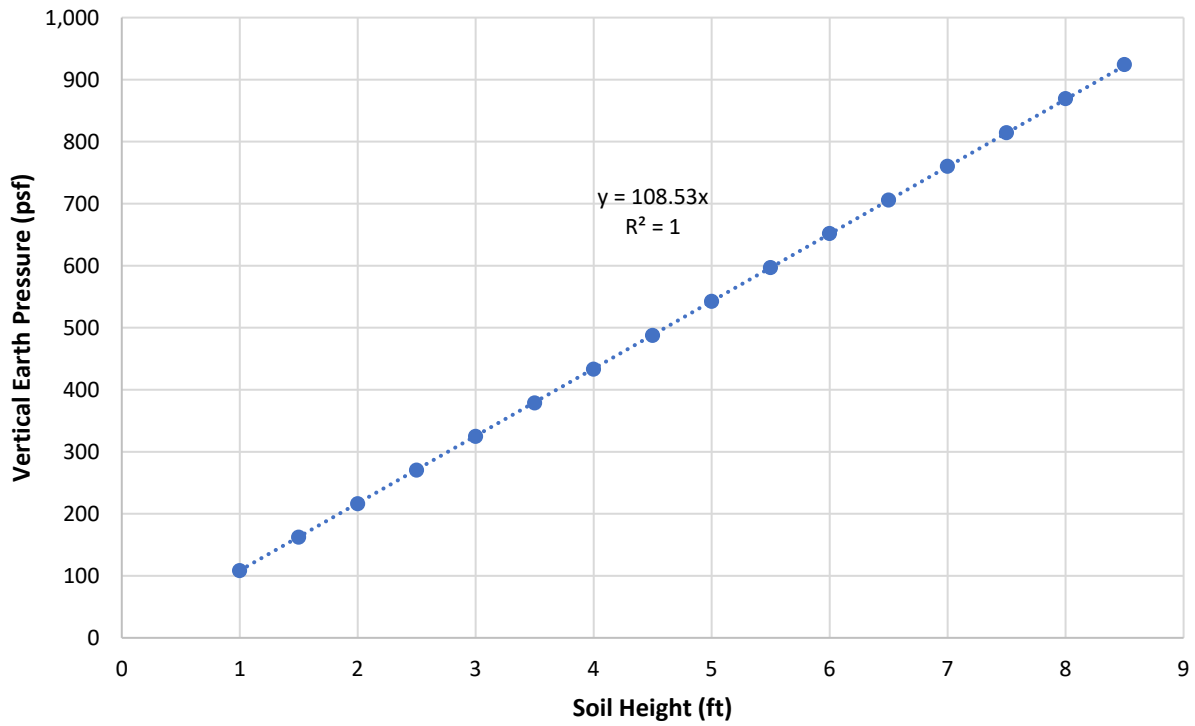


Figure 5-3. Nuclear density vertical earth pressure vs. soil height for 103% compaction effort side.

When the research began, the relative compaction targets were 95% of T-180 in the under-compact side and 103% of T-180 in the over-compact side. From the results of all nuclear density testing, the average relative compaction in the under-compact side was 95.8% of T-180 and the average relative compaction in the over-compact side was 102.8% of T-180. For the over-compact side, it was found that achieving the target compaction effort between reinforcement levels 1 and 2 was the most difficult as indicated in Table 5-23. UF researchers suspect this was due to the specified construction method of not backfilling the soil to the MSE wall panels until six inches above the first level of reinforcement was achieved. Consequently, the vibratory compaction effort delivered to the soil layers directly above the first reinforcement level was also distributed to the layers underlying the first reinforcement level where soil was only placed against the wall panels after the first row of reinforcements were secured in place. Once the second level of reinforcements were secured to the wall panels, compacting the soil to 103% of T-180 was more easily achieved, as indicated by the results displayed in Table 5-23. Interestingly, the specified construction method appeared to have negligible effect on the under-compact side as 95% of T-180 was routinely achieved in each layer.

Table 5-23. Summary of average soil compaction between MSE wall reinforcement levels.

Layers	Soil Height (ft)		95% of T-180		103% of T-180	
	Bottom	Top	$\gamma_d$ (pcf)	R.C. (%)	$\gamma_d$ (pcf)	R.C. (%)
Base Layer	0.0	1.5	109.2	103.3%	109.2	103.3%
Base Layer to Row 1	1.5	2.5	103.9	98.3%	108.6	102.7%
Row 1 to Row 2	2.5	5.0	101.5	96.0%	108.1	102.3%
Row 2 to Row 3	5.0	7.5	100.8	95.3%	108.8	102.9%
Row 3 to Row 4	7.5	10.0	101.6	96.1%	108.8	102.9%
Above Row 4	10.0	11.2	101.2	95.7%	109.9	103.9%

Note: R.C. is relative compaction.

## 5.2 Construction Analysis

Once the MSE walls were fully constructed, the data collected were analyzed prior to adding the reaction frame. The analysis was conducted by first analyzing each row (level) where reinforcements were attached to the wall panels, EPCs were embedded in the soil, and EPCs were attached to the wall panels. For each monitored level, four EPCs were embedded in the soil per compaction side, two instrumented reinforcement strips were attached to the wall panels per compaction side, and two wall mounted EPCs were attached to the wall panels per compaction side. Therefore, all measurements were recorded at the same height relative to the base layer of soil (datum) for each monitored row. After analyzing each row individually, the data was then analyzed as a whole to determine the earth pressure coefficients that developed during the construction phase of the research.

## 5.3 Row 1 Construction Analysis

To begin the individual row analysis, the vertical earth pressures recorded by each of the four EPCs embedded in the soil for each compaction side are first presented for Row 1 (Figures 3-4

and 3-5). Figure 3-4 indicates that three of the four EPCs in the under-compact (95%) side shared a very similar linear trend with the EPC X1-Y1R indicating a dissimilar linear trend. UF researchers suspect this EPC malfunctioned and did not represent the actual earth pressure applied in this portion of the Row 1 soil area. Figure 3-5 provides the over-compact (103%) vertical earth pressures in which all EPCs displayed a similar linear trend.

Note: The designations for each EPC are coded as follows: X = column (horizontal location), Y = Row (vertical location), F = quadrant closest to the front wall, and R = quadrant closest to the rear wall. Columns 1 and 2 are on the 95% side and Columns 3 and 4 are on the 103% side.

### 5.3.1 Row 1 Vertical Earth Pressure

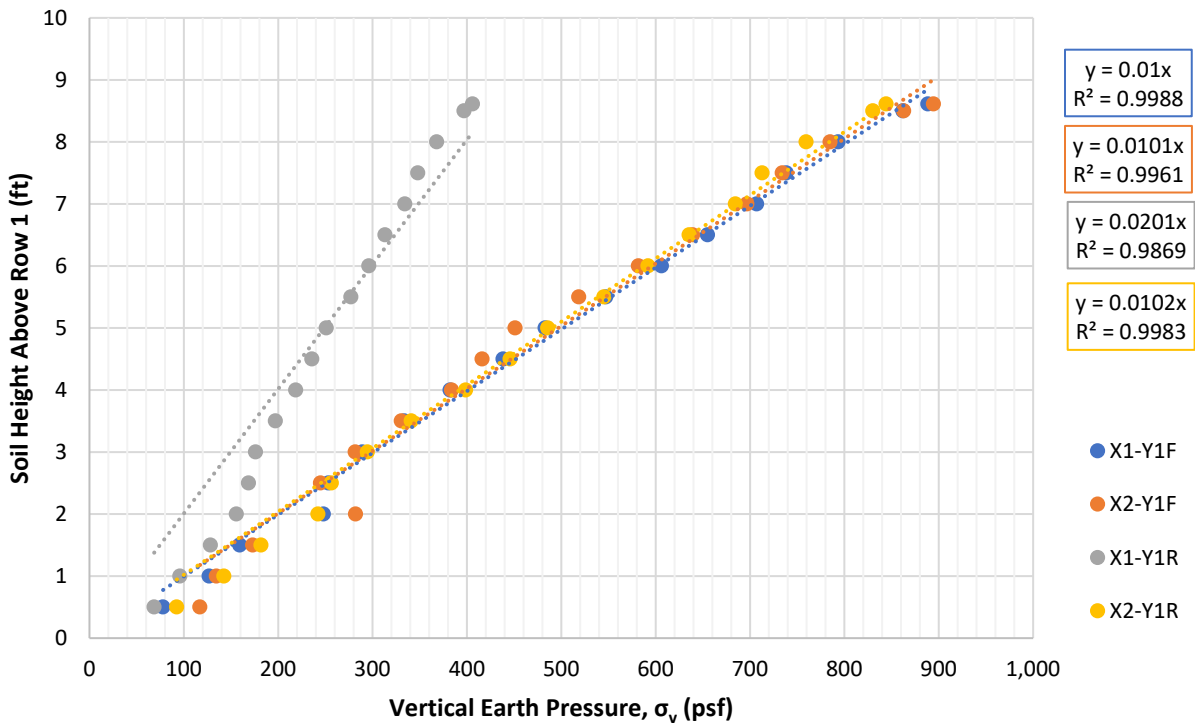


Figure 5-4. Row 1 – 95% compaction EPC vertical earth pressure vs. depth.

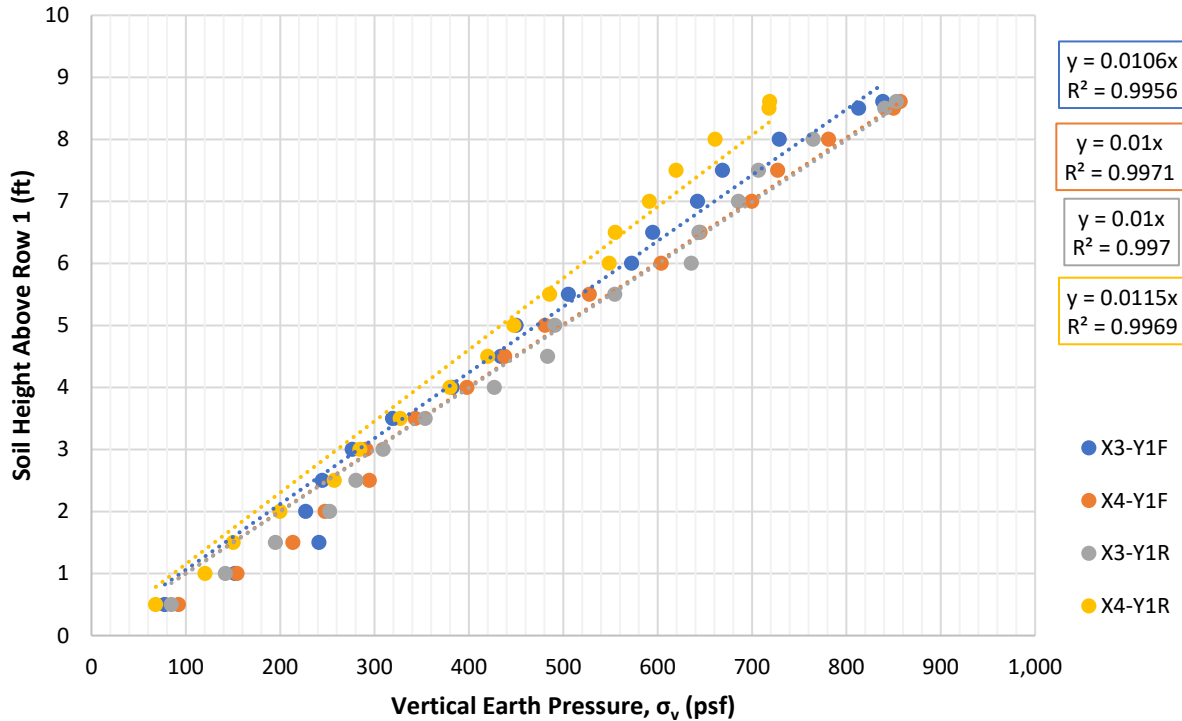


Figure 5-5. Row 1 – 103% compaction EPC vertical earth pressure vs. depth.

Next, the average earth pressures measured by the EPCs were compared to the nuclear density results. Figure 5-6 indicates that the EPC earth pressures, and nuclear density (ND) earth pressures are in good agreement for the under compact side (Note: EPC X1-Y1R was not used to derive the 95% average). Figure 5-7 provides the comparison between the EPCs and ND for the over compact side. For the over compact side, it is observed that below a depth of 2.5 feet the EPC vertical earth pressure began to decrease compared to the ND vertical earth pressure. This was the point at which the second level of reinforcements were attached to the wall panels and the compaction effort began to improve as previously discussed. This suggests that due to the higher compaction effort, down drag stresses began to increase at the soil-MSE wall interface. This observation is also supported by the earth pressures that developed underneath the leveling pads, which will be discussed later.

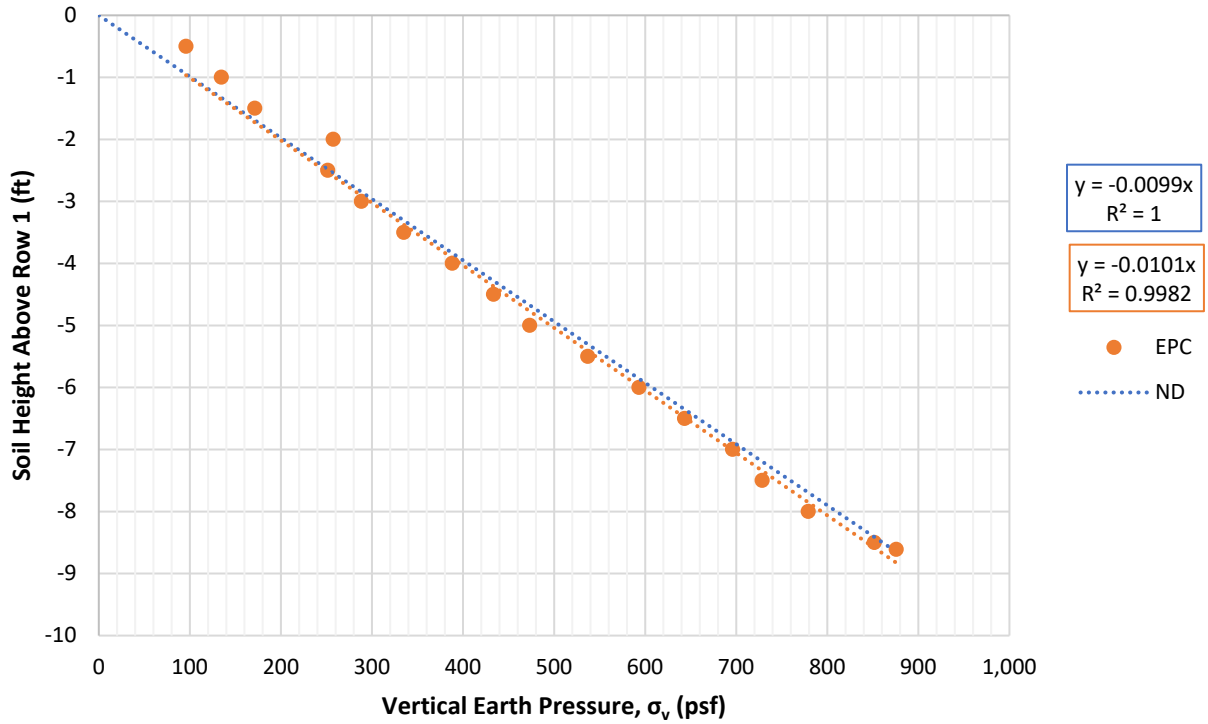


Figure 5-6. Row 1 – 95% compaction EPC earth pressure compared to nuclear density.

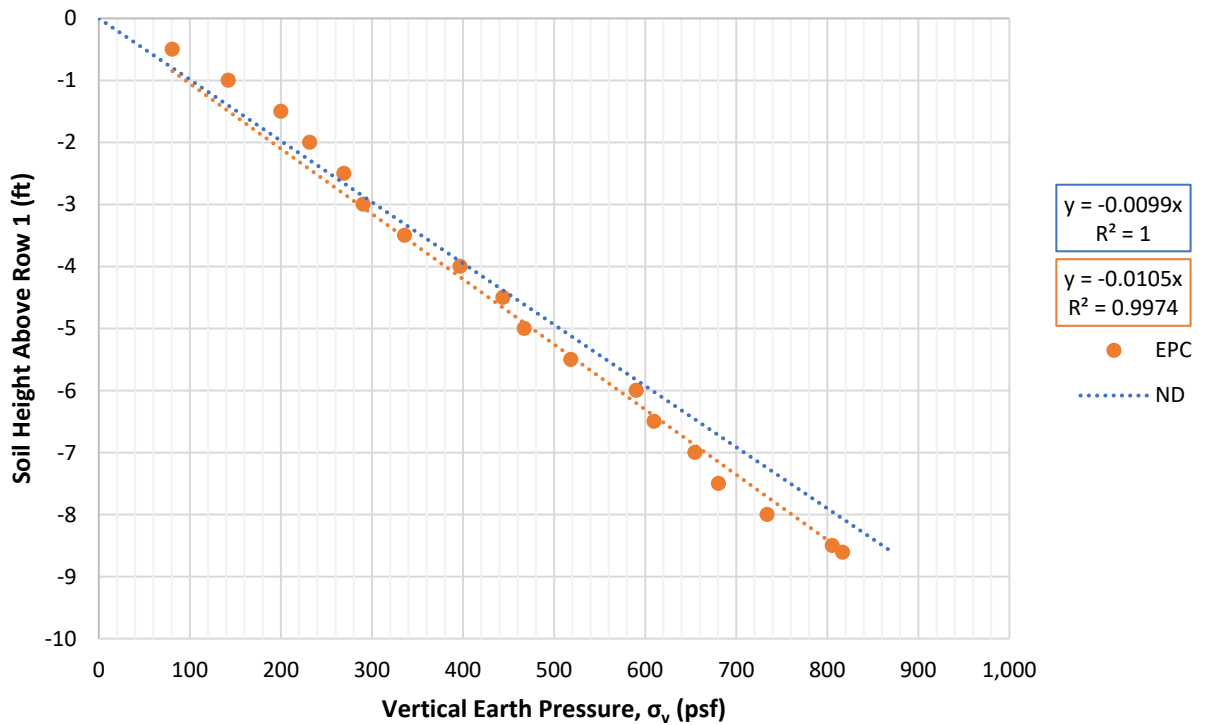


Figure 5-7. Row 1 – 103% compaction EPC earth pressure compared to nuclear density.



### 5.3.2 Row 1 Horizontal Earth Pressure

Next, the Row 1 horizontal earth pressures that developed during construction are presented in Figures 5-8 and 5-9 for each compaction effort. As observed in both figures, higher earth pressures developed early on with respect to the vertical earth pressures but then declined until a depth of approximately 2.5 feet was reached. This was the depth in which the Row 2 reinforcements were attached to the wall panels. It is observed that for the over-compact side in Figure 5-9, the high early horizontal earth pressure peaked earlier compared to the under-compact side before declining. The depth at which this peak occurred was when the second course of full sized panels were added to the walls. Beyond this depth, a linear increase was observed for both compaction efforts until the final data point collected at 8.61 feet of depth which is when the soil reached the top of the MSE walls. UF researchers believe the reduction in horizontal earth pressure was due to removing the temporary bracing which alleviated a small amount of confining pressure and possibly shifted the wall panels.

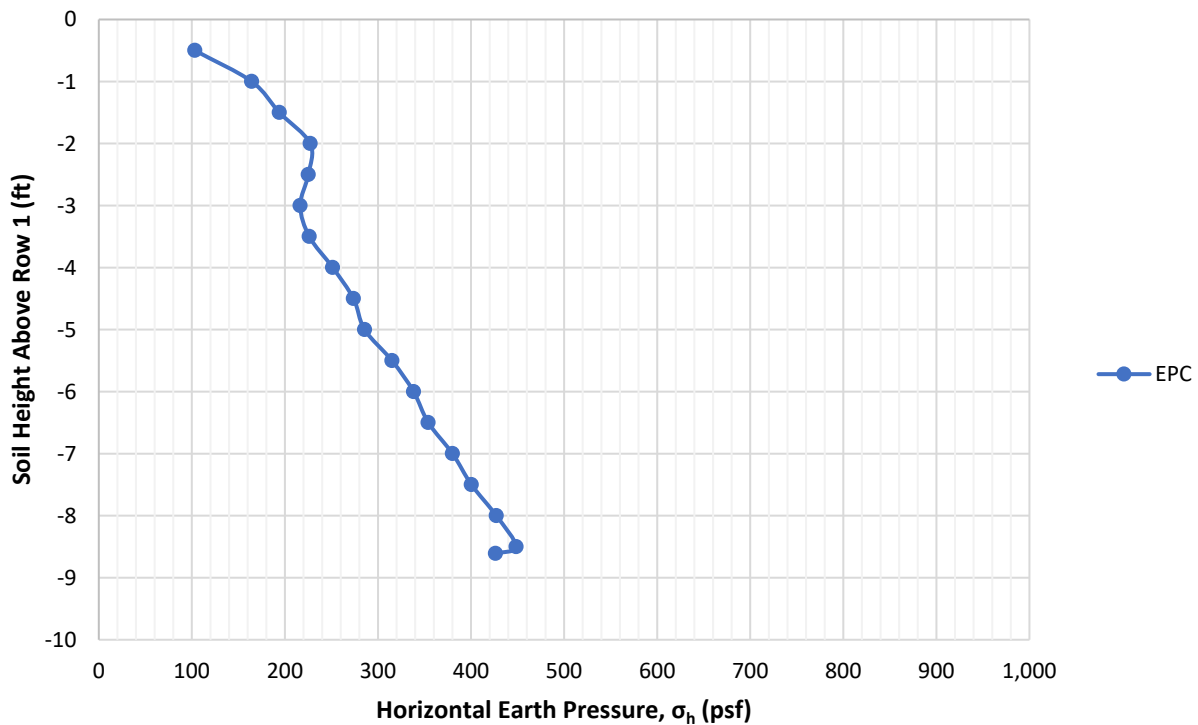


Figure 5-8. Row 1 – 95% compaction EPC horizontal earth pressure vs. depth.

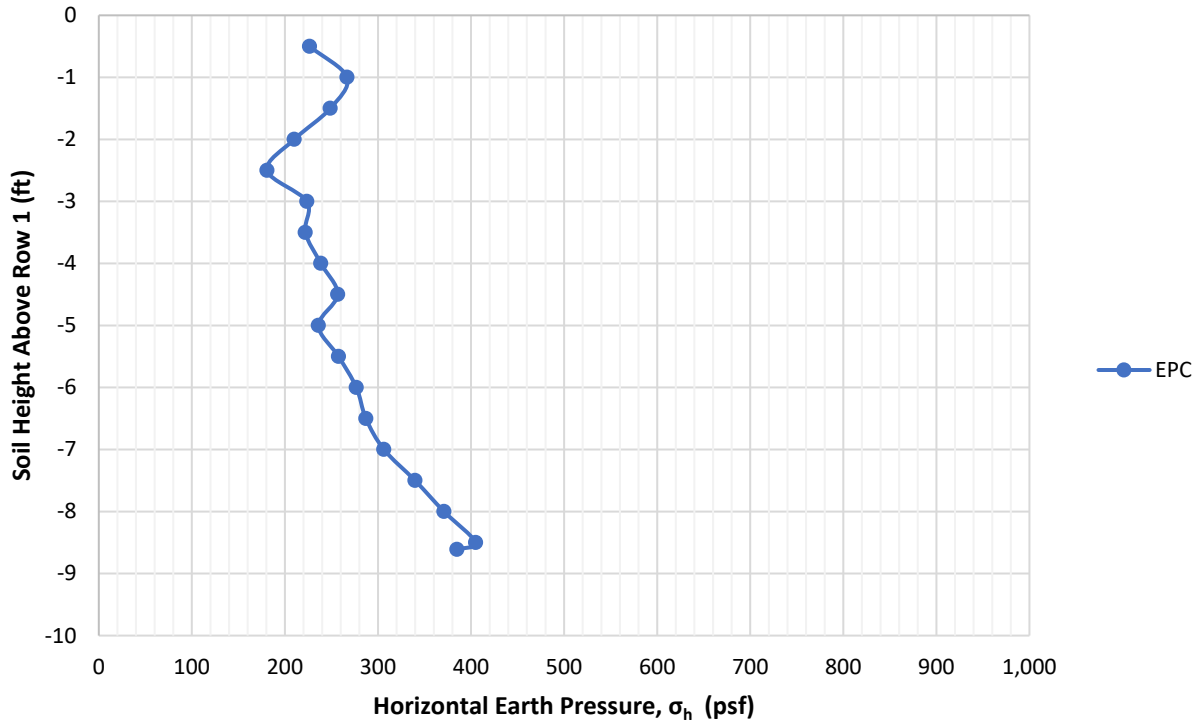


Figure 5-9. Row 1 – 103% compaction EPC horizontal earth pressure vs. depth.

### 5.3.3 Row 1 Reinforcement Strip Tension

Next, the strain gauge data collected for each instrumented reinforcement strip was analyzed (Figures 5-10 through 5-15). During the design phase it was assumed that similar tension would develop over the full length of the inextensible reinforcements. However, in both compaction efforts it was observed that stress concentrations developed over the length each strip. UF researchers believe the stress concentrations were due to the moisture and rugged coatings that were applied to the strips to protect the strain gauges. The coatings produced a raised, roughed surface in which passive earth pressures likely developed and created the stress concentrations. This also indicates that stress concentrations likely developed in soil that translated to the instrumented strips. In the 95% side, the stress concentrations began to develop at 2.5 feet which is when the second row of reinforcements were attached. In the 103% side, the stress concentrations began to develop at 1.5 feet which is when the second course full panels were added to the walls and braced at the top. For an unyielding condition, this suggests that when the wall panels are essentially locked in place, by adding an additional row of strips or securing a new wall panel in place, stress concentrations will develop in the soil because an active state of lateral earth pressure is prevented.

Note: the designations for the strain gauges in each figure are as follows: C = column (horizontal location), R = Row (vertical location), and B = location from front MSE wall panels (i.e., B-1 is the closest to the front MSE wall and B-5 is the furthest away from the front MSE wall). An average strip tension is then listed as “C# AVG”

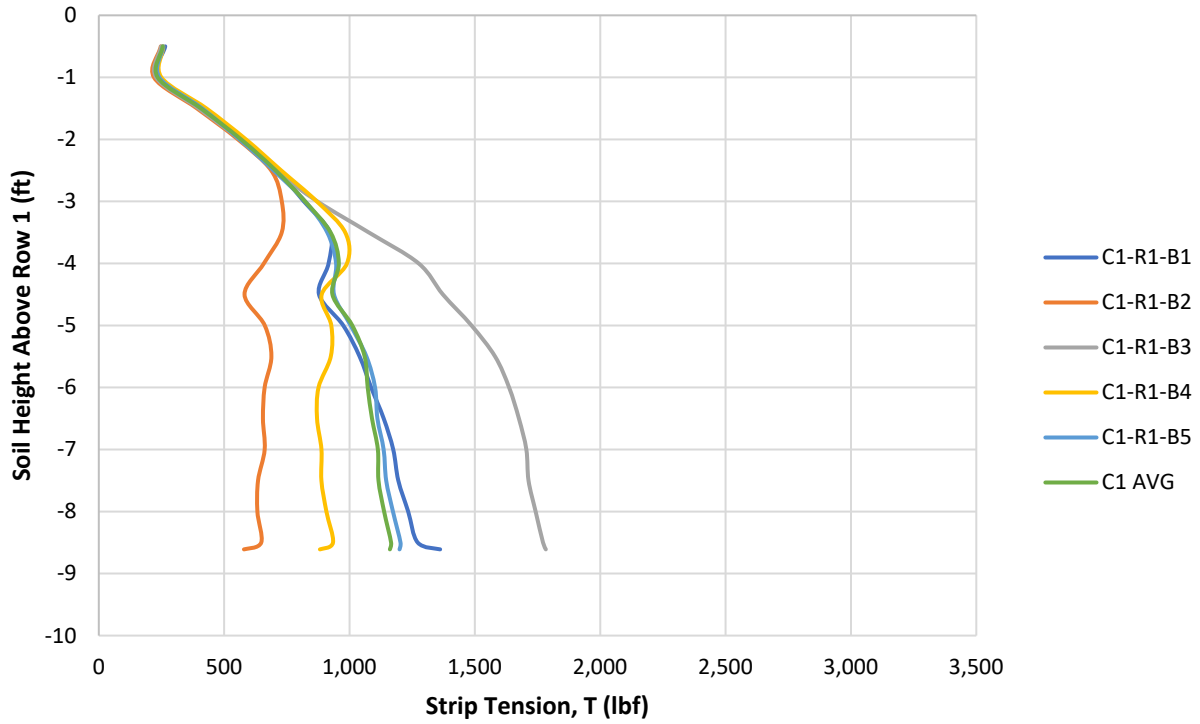


Figure 5-10. Row 1 – Column 1 - 95% compaction reinforcement strip tension vs. depth.

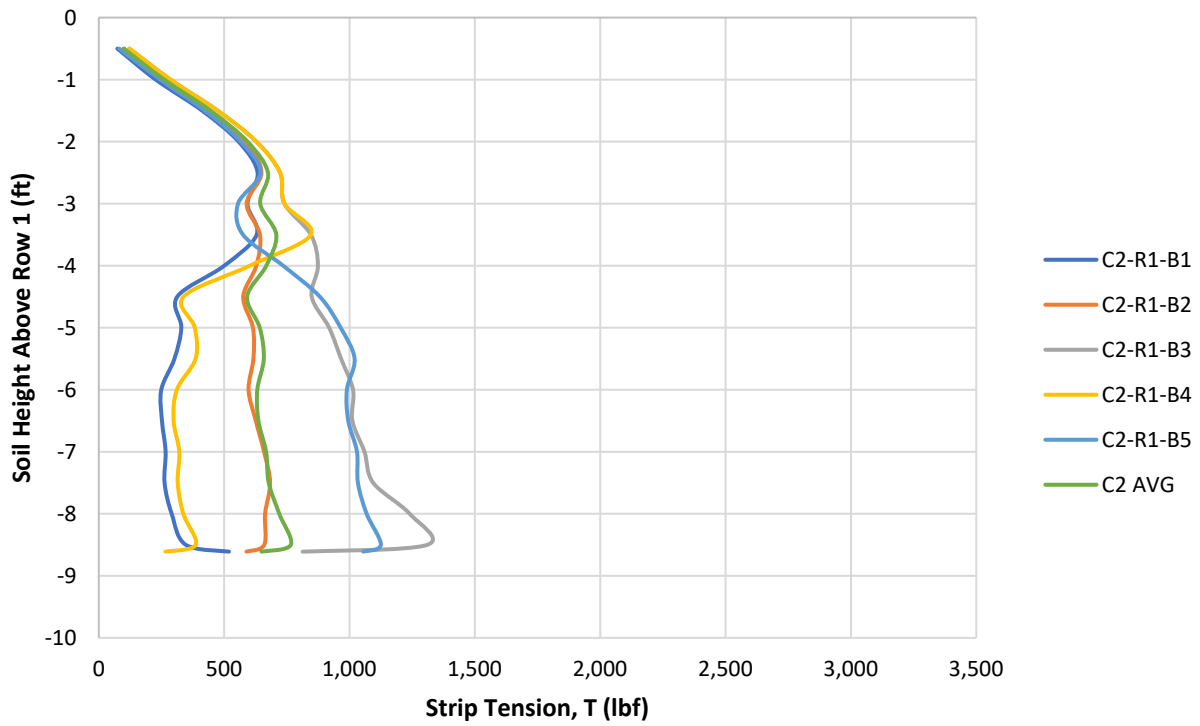


Figure 5-11. Row 1 – Column 2 - 95% compaction reinforcement strip tension vs. depth.

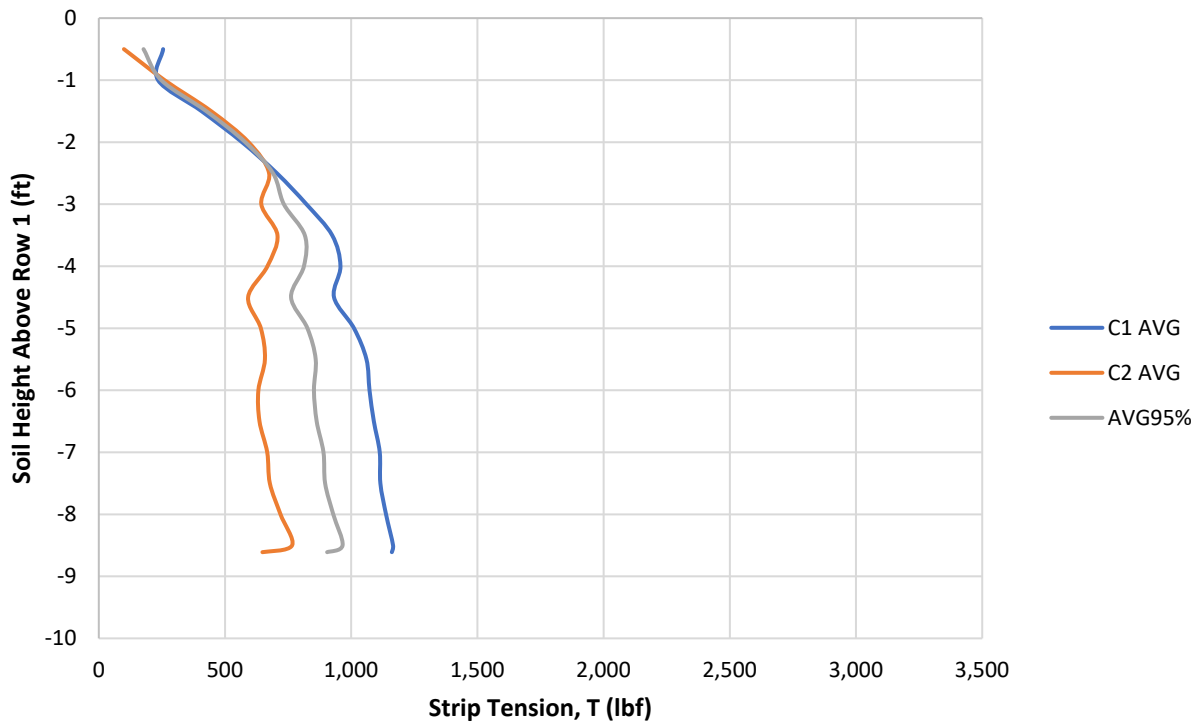


Figure 5-12. Row 1 – 95% compaction average reinforcement strip tension vs. depth.

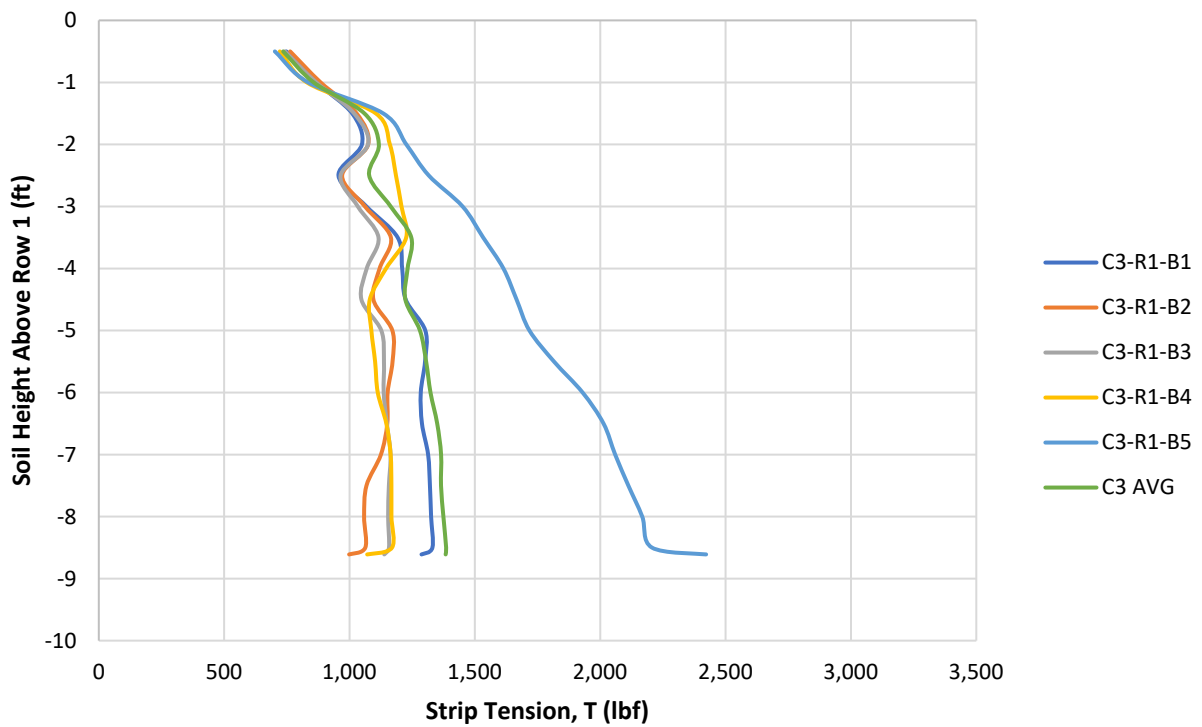


Figure 5-13. Row 1 – Column 3 - 103% compaction reinforcement strip tension vs. depth.

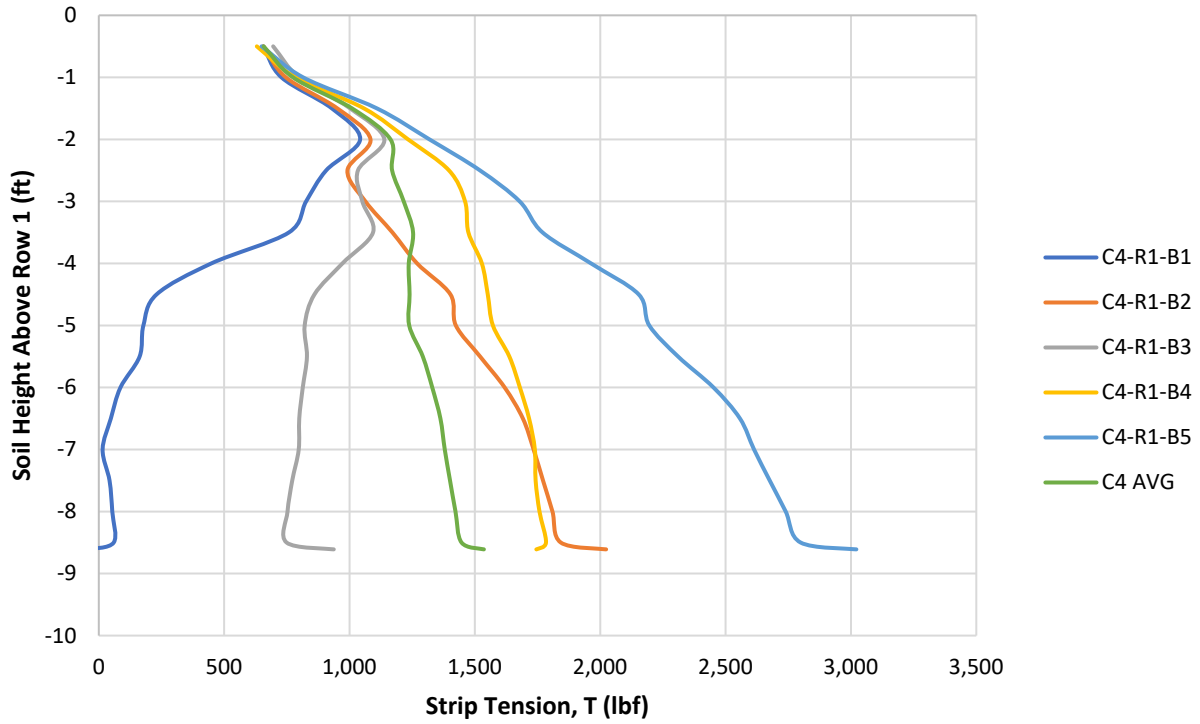


Figure 5-14. Row 1 – Column 4 - 103% compaction reinforcement strip tension vs. depth.

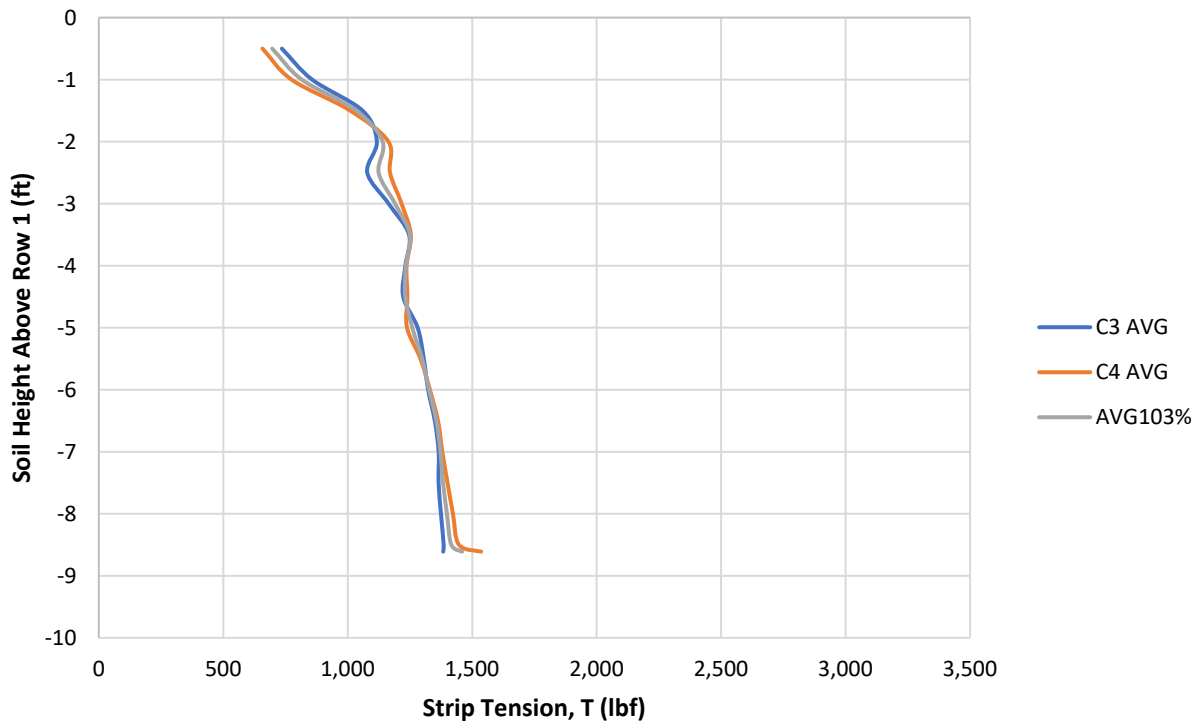


Figure 5-15. Row 1 – 103% compaction average reinforcement strip tension vs. depth.

### 5.3.4 Row 1 Average Earth Pressures and Strip Tension

Figures 5-16 and 5-17 provide the average vertical earth pressure, lateral earth pressure, and strip tension versus depth for both compaction efforts, respectively. Averages are used to account for the possible research induced effects. To clarify, for both compaction efforts one side of the reinforced zone was in contact with an unyielding strong wall whereas the other side of the reinforced zone was in contact with the divider wall that can slightly compress. Therefore, the intent of the averaging is to balance the influence of different interfaces on each side of the reinforced zone. The averages were derived for the vertical earth pressure, lateral earth pressure, and strip tension using the four soil embedded EPCs, two wall mounted EPCs, and the average strip tensions from both reinforced strips, respectively. The average values were the used during construction earth pressure coefficient analyses.

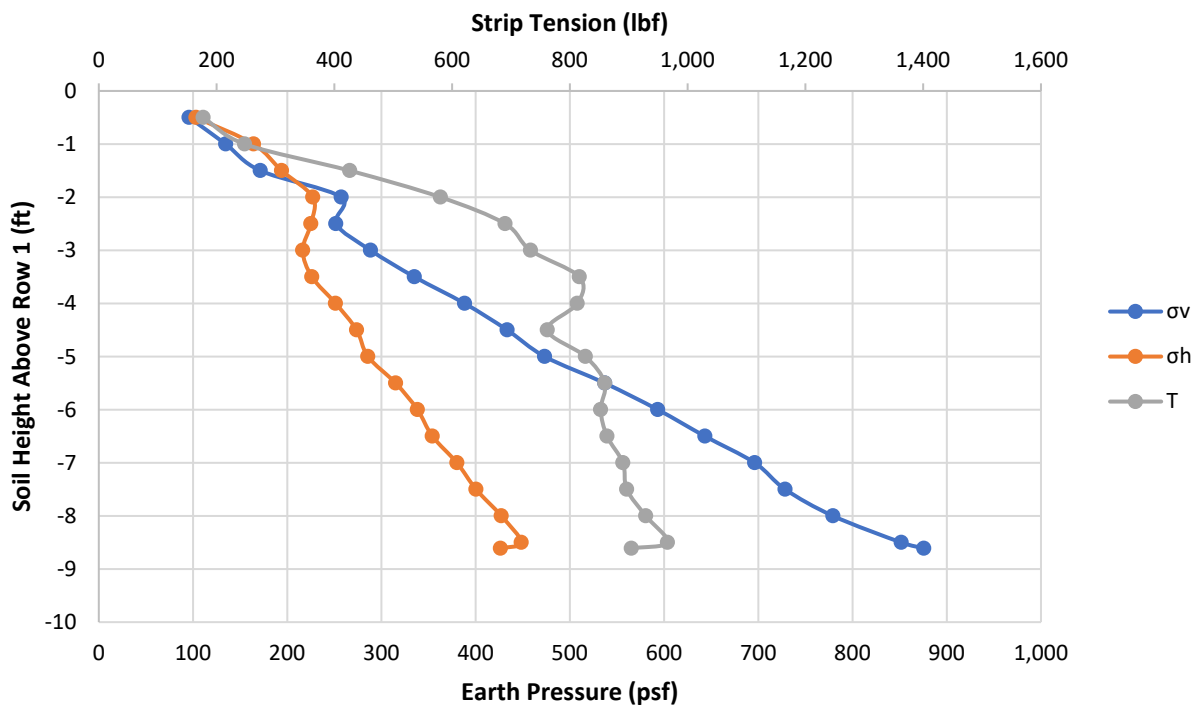


Figure 5-16. Row 1 – 95% compaction vertical and horizontal stress and strip tension vs. depth.

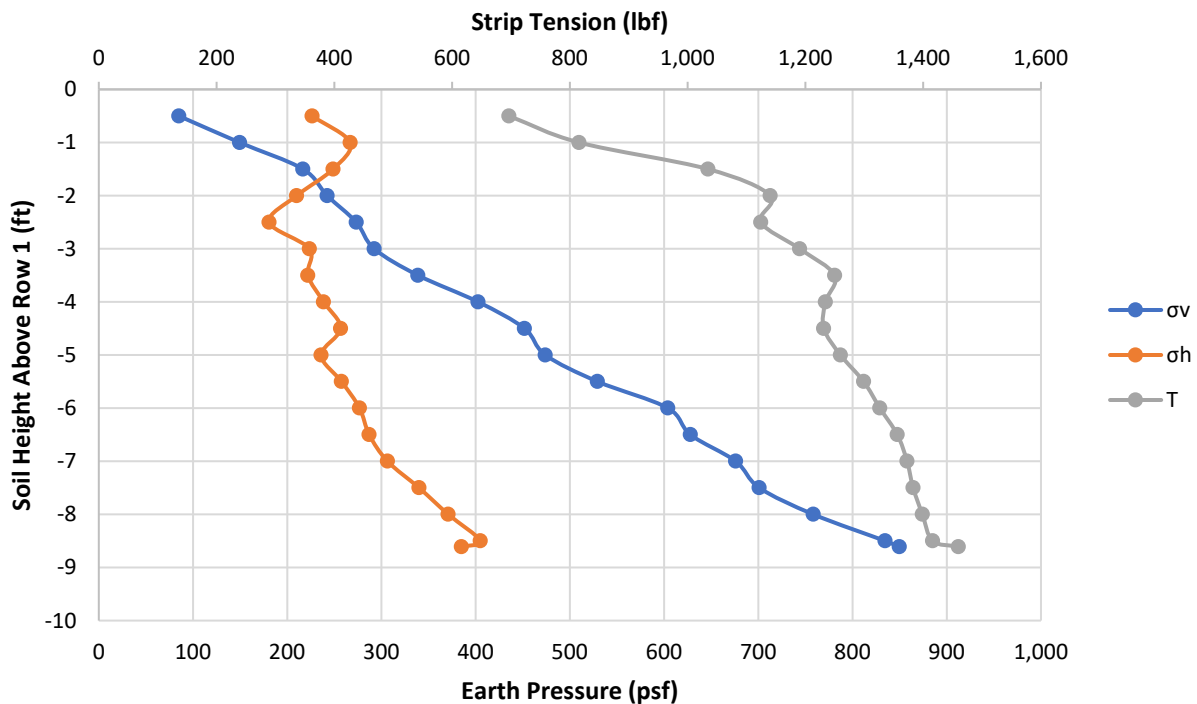


Figure 5-17. Row 1 – 103% compaction vertical and horizontal stress and strip tension vs. depth.

### 5.3.5 Row 1 Construction Earth Pressure Coefficient Analysis – 95% of T-180

For the construction earth pressure coefficients analyses, four methods of analysis were investigated. Method 1 considered the wall mounted EPC horizontal earth pressure divided by the soil embedded EPC and nuclear density vertical pressures as depicted in Figure 5-18. Method 2 considered the horizontal earth pressure derived from the average strip tension divided by the tributary wall area that was subsequently divided by the soil embedded EPC and nuclear density vertical earth pressures as presented in Figure 5-19. Method 3 compared the wall mounted EPC lateral earth pressure and reinforcement strip lateral earth pressure divided by the soil embedded EPC vertical earth pressure as presented in Figure 5-20. Finally, Method 4 compared the wall mounted EPC lateral earth pressure and reinforcement strip lateral earth pressure divided by the nuclear density vertical earth pressure as presented in Figure 5-21. Methods 1 and 2 both indicated that below a depth of 2.5 feet, where the second level of reinforcement was added, the lateral earth pressure began to stabilize and slightly decline with depth. Methods 3 and 4 both indicated that for the 95% side, the EPC lateral earth pressure was higher than the reinforcement strip lateral earth pressure. This indicates that the reinforcement strips were likely never fully engaged during construction and that the MSE will likely shift outward during surcharge loading due to the loosened state of the reinforcement strips.

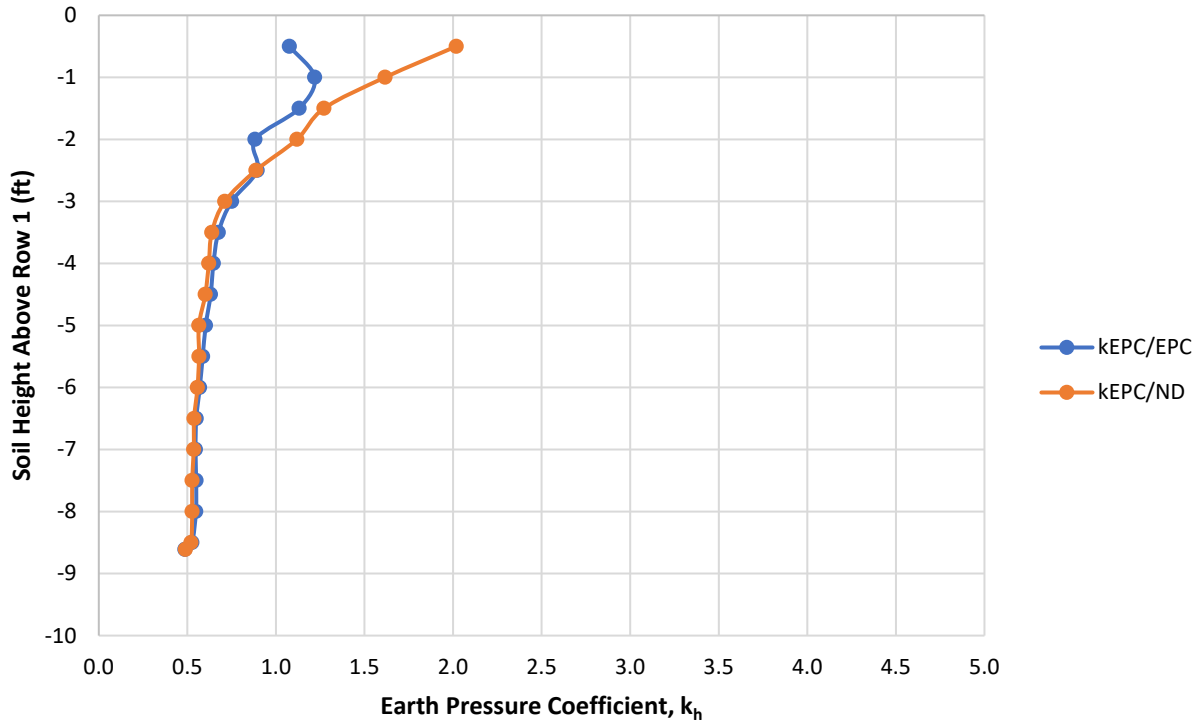


Figure 5-18. Row 1 – 95% compaction earth pressure coefficients from EPCs.

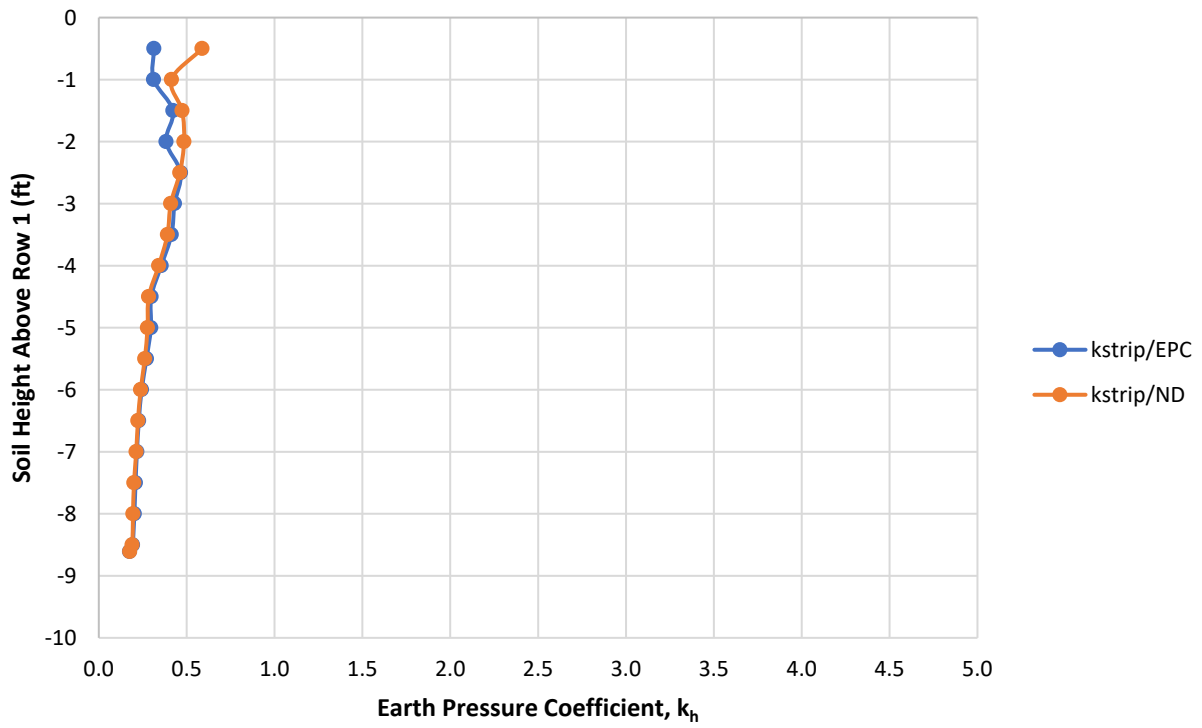


Figure 5-19. Row 1 – 95% compaction earth pressure coefficients from reinforcement strips.



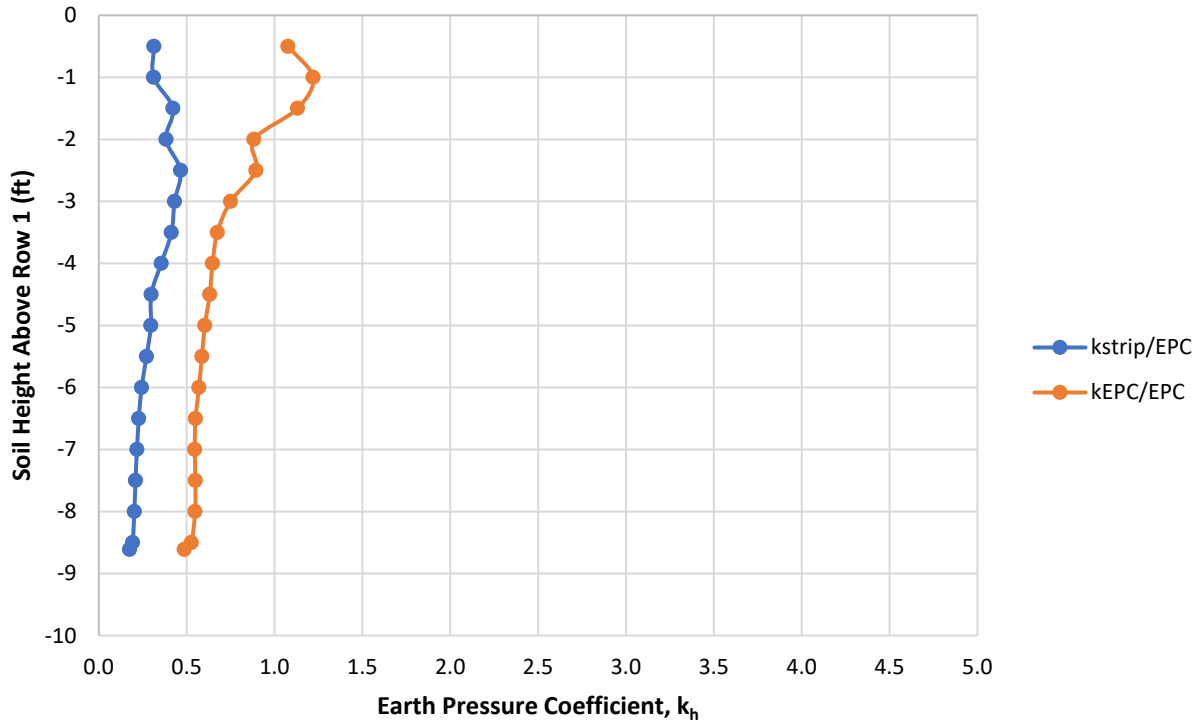


Figure 5-20. Comparing Row 1 – 95% compaction  $k_h$  using vertical stress from EPCs.

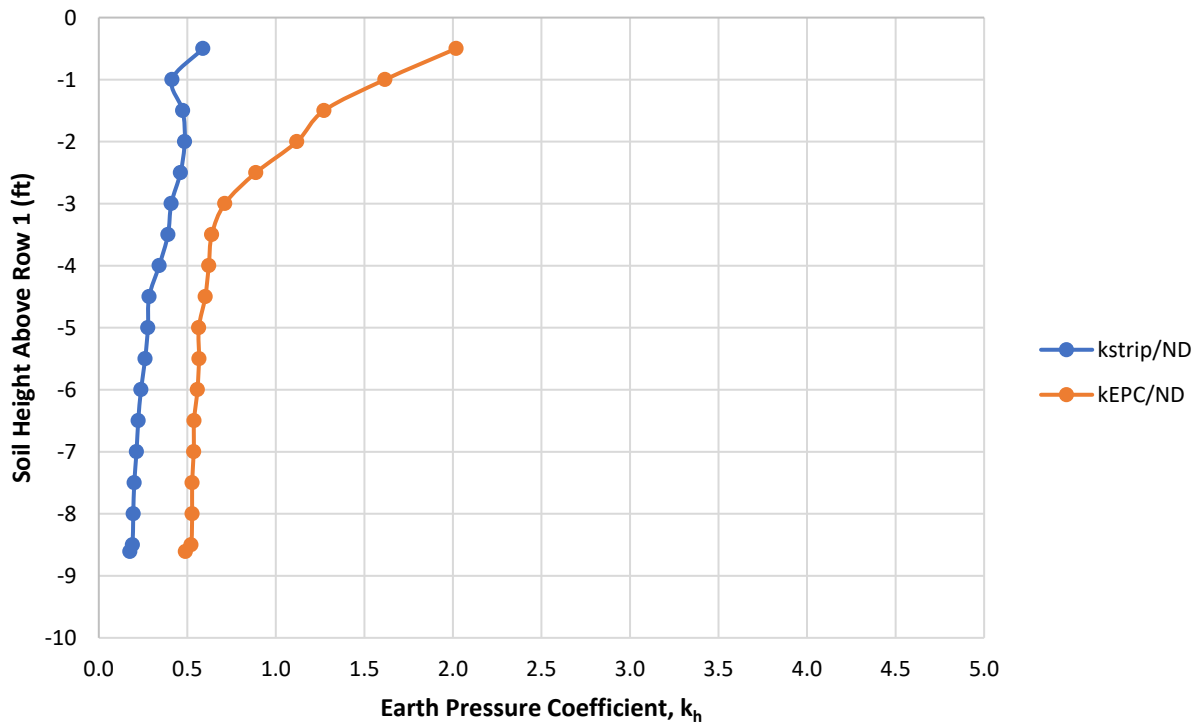


Figure 5-21. Comparing Row 1 – 95% compaction  $k_h$  using vertical stress from nuclear density.

### 5.3.6 Row 1 Construction Earth Pressure Coefficient Analysis – 103% of T-180

The same four methods of analysis were conducted for the 103% side as presented in Figures 5-22 to 5-25. A similar observation was made that below 2.5 feet, where the second row of reinforcements were added, the lateral earth pressure began to stabilize and slightly decline with depth. However, much higher earth pressure was observed above the 2.5-foot mark compared to the 95% side. This ultimately translated into increased strip tension as the strip reinforcement lateral earth pressure was much more similar to the EPC lateral earth pressure as illustrated in Figures 5-24 and 5-25.

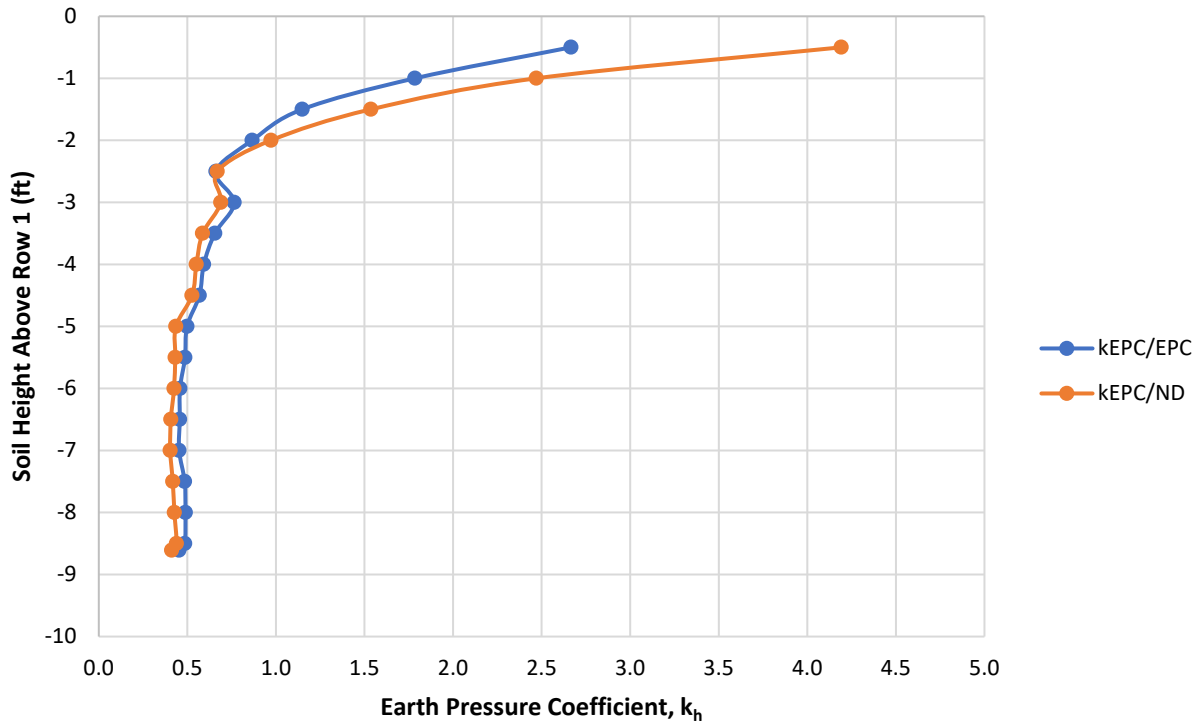


Figure 5-22. Row 1 – 103% compaction earth pressure coefficients from EPCs.

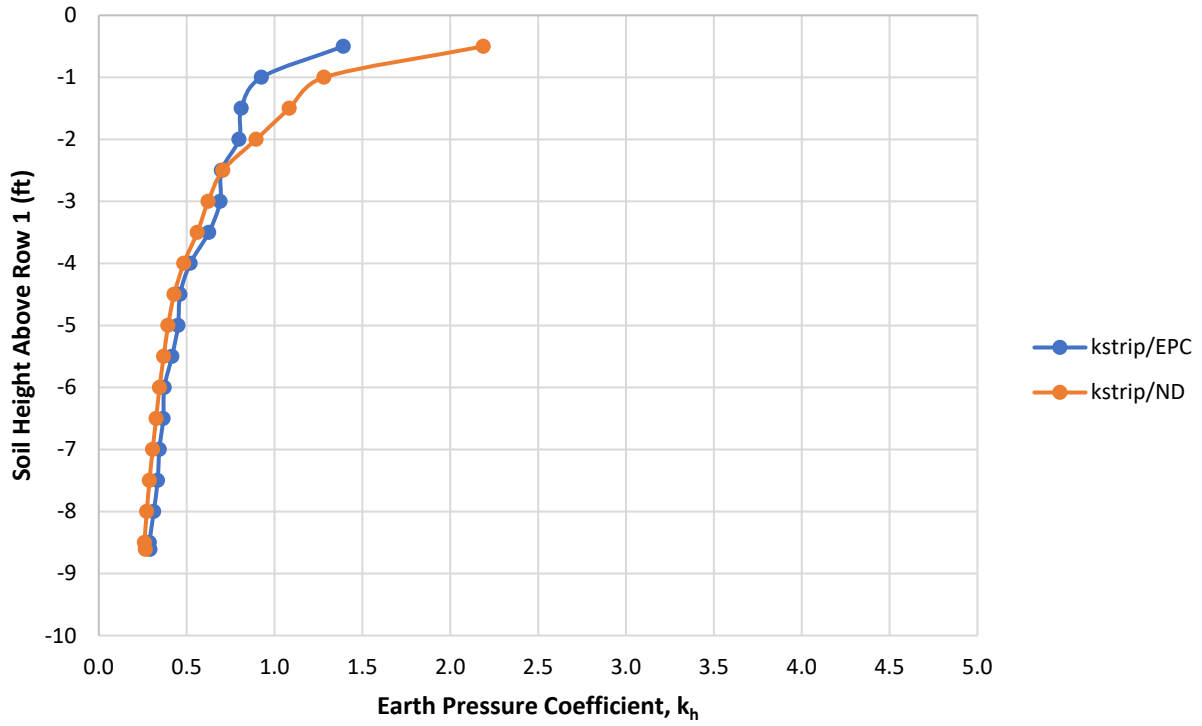


Figure 5-23. Row 1 – 103% compaction earth pressure coefficients from reinforcement strips.

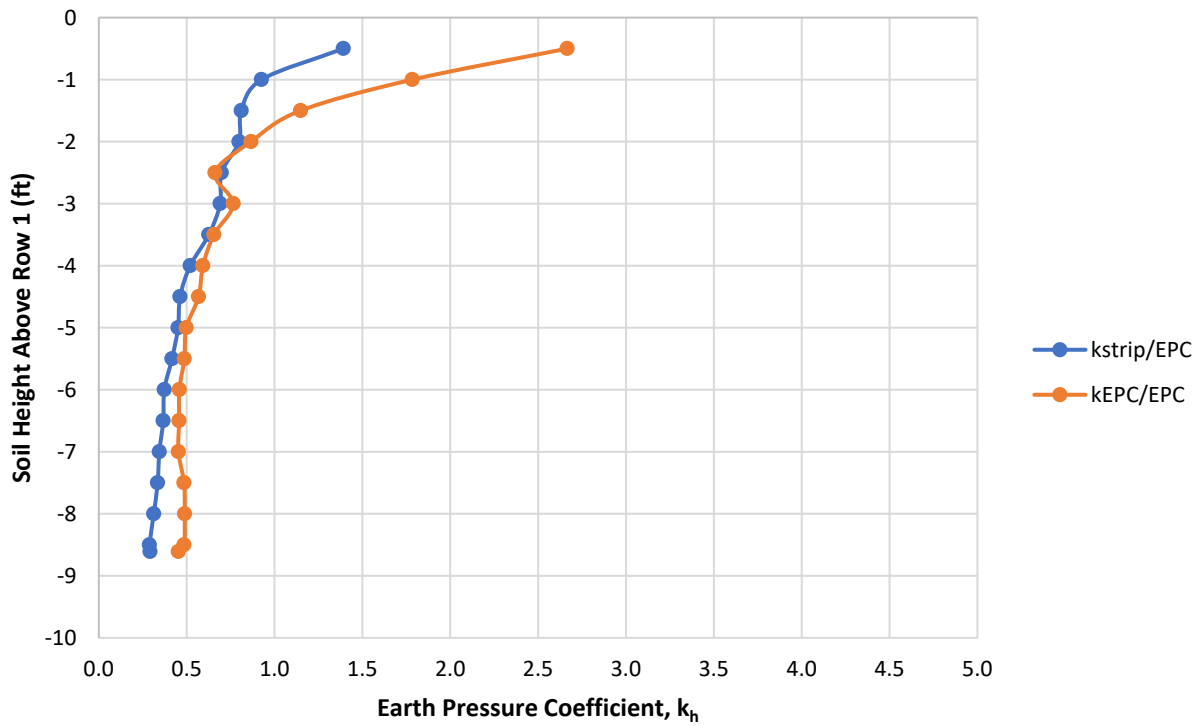


Figure 5-24. Comparing Row 1 – 103% compaction  $k_h$  using vertical stress from EPCs.

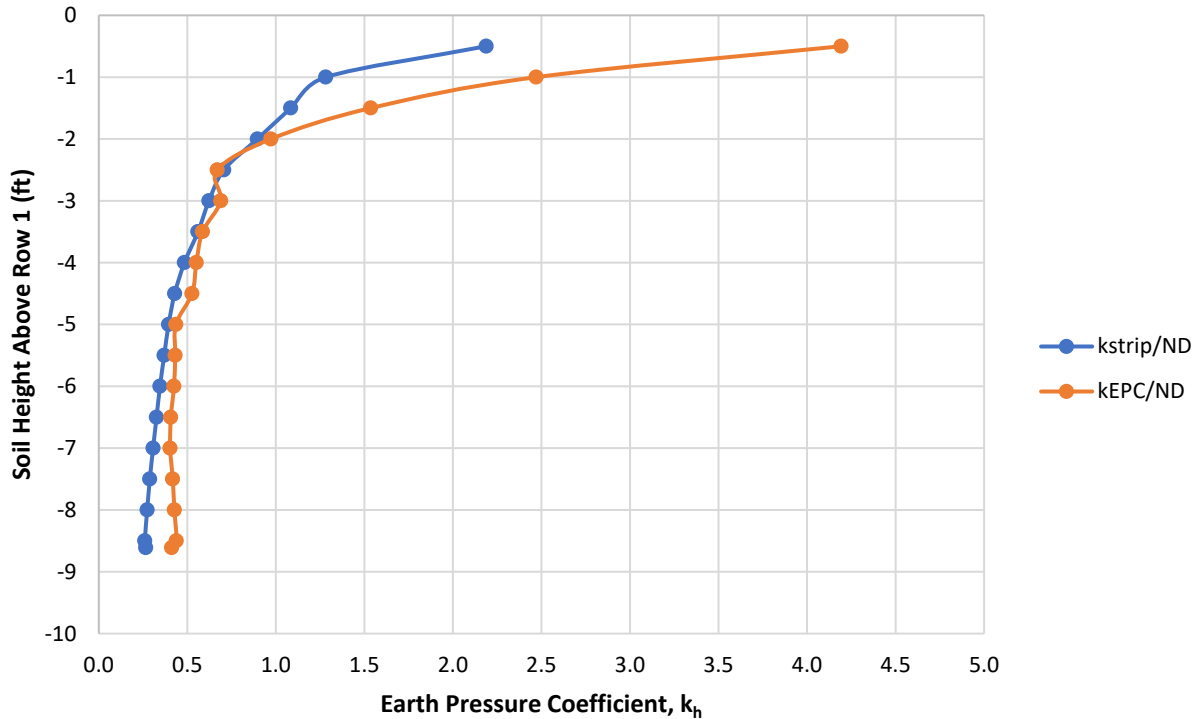


Figure 5-25. Comparing Row 1 – 103% compaction  $k_h$  using vertical stress from nuclear density.

The analyses for the remaining rows were conducted in the same way as Row 1 and therefore limited discussion is presented. However, some important observations are pointed out:

- The behavior of the soil in the 95% side was fairly consistent for each row, whereas far more variability in the soil behavior was observed in the 103% side;
- For the 103% side, the results of the analyses for Row 2 were quite similar to the Row 1 results. Increased lateral earth pressure was observed above the 2.5 feet mark which is when the next level of reinforcements was added, and below this mark, the lateral earth pressure began to stabilize and slightly decline with depth. However, Rows 3 and 4 produced much higher lateral earth pressure above the 2.5 foot mark compared to Rows 1 and 2, and lateral earth pressure stabilization never occurred (Note: Row 4 never reached a depth of 2.5 feet due to its location being 1.23 from the top of the wall). This suggests that higher earth pressure may develop in Rows 3 and 4 with respect to the surcharge height compared to Rows 1 and 2;
- One noticeable difference between Row 1 and all remaining rows, for both compaction efforts, was that the linear trends of vertical earth pressure versus depth for each soil embedded EPC from Rows 2 through 4 displayed more deviation compared to Row 1. This further suggests that stress concentrations were developing in the reinforced zone as more reinforcement levels were added, which likely contributed to the Row 1 strip tension stress concentrations. Row 2 strip tension also experienced more variability over the length of the strips compared to Rows 3 and 4.
- Strain gauge location C2-R2-B4 malfunctioned throughout testing and was discounted.

## 5.4 Row 2 Construction Analysis

### 5.4.1 Row 2 Vertical Earth Pressure

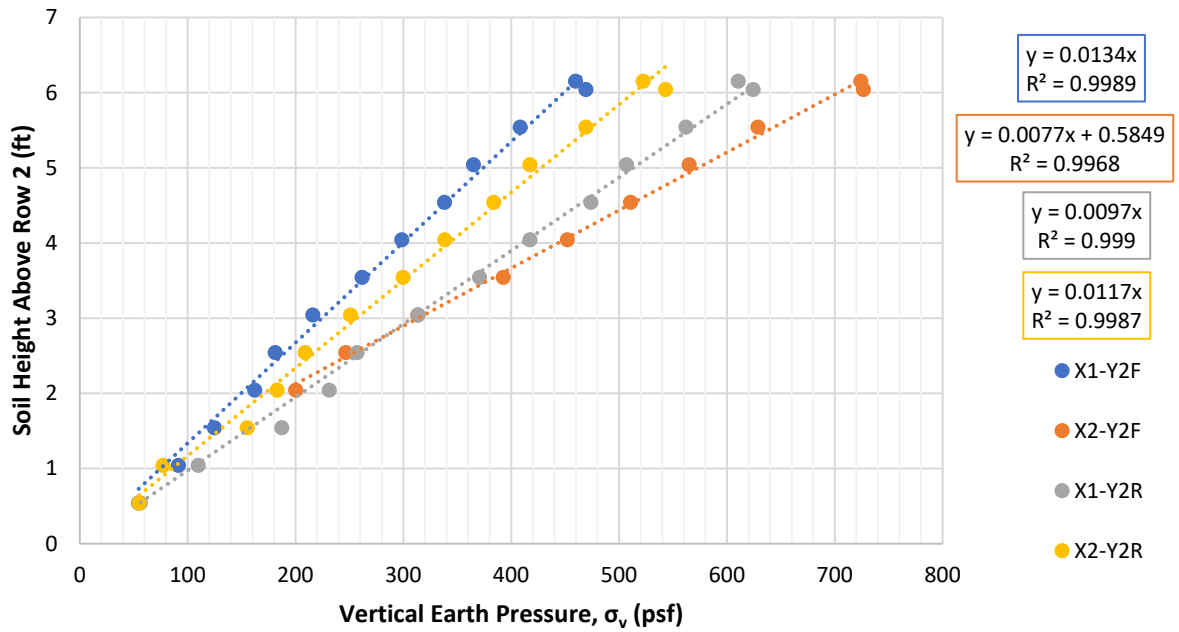


Figure 5-26. Row 2 – 95% compaction EPC vertical earth pressure vs. depth.

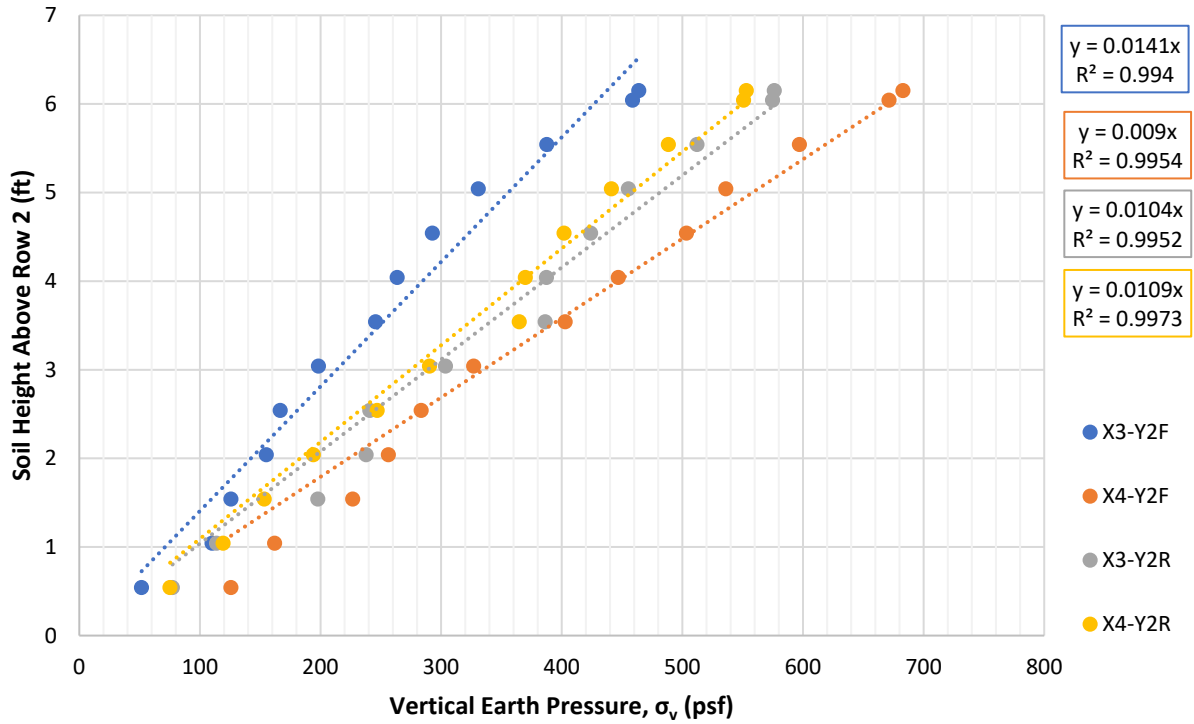


Figure 5-27. Row 2 – 103% compaction EPC vertical earth pressure vs. depth.

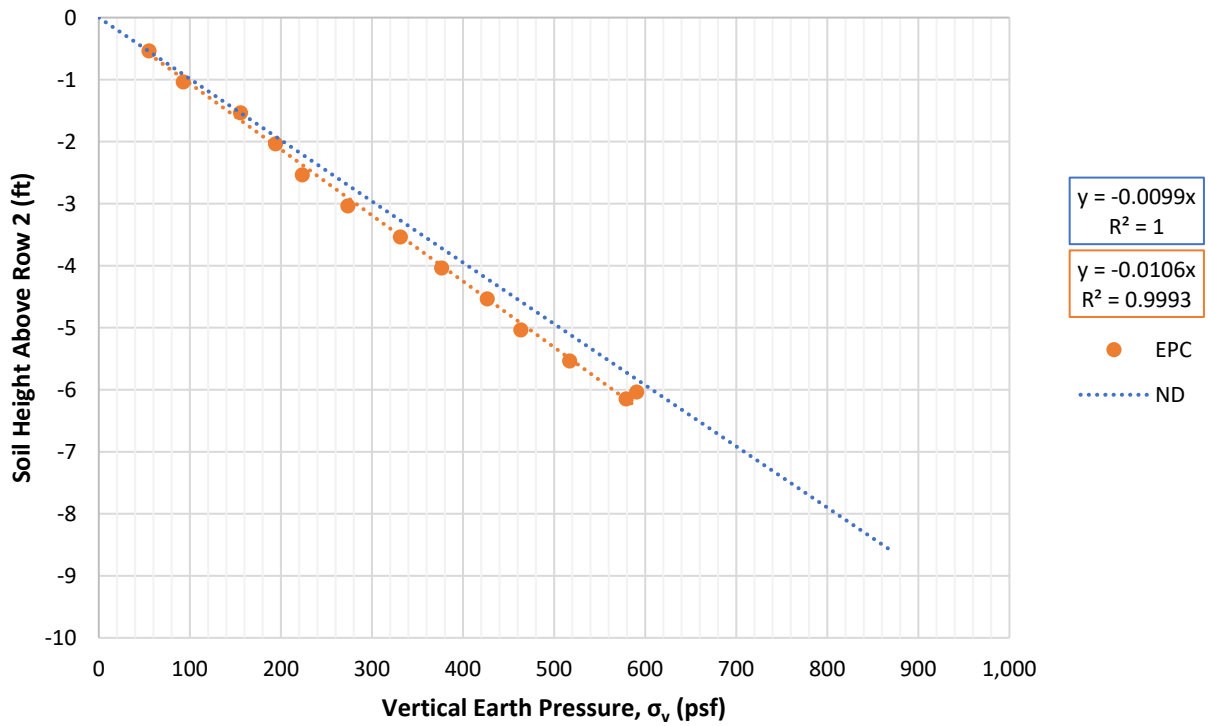


Figure 5-28. Row 2 – 95% compaction EPC earth pressure compared to nuclear density.

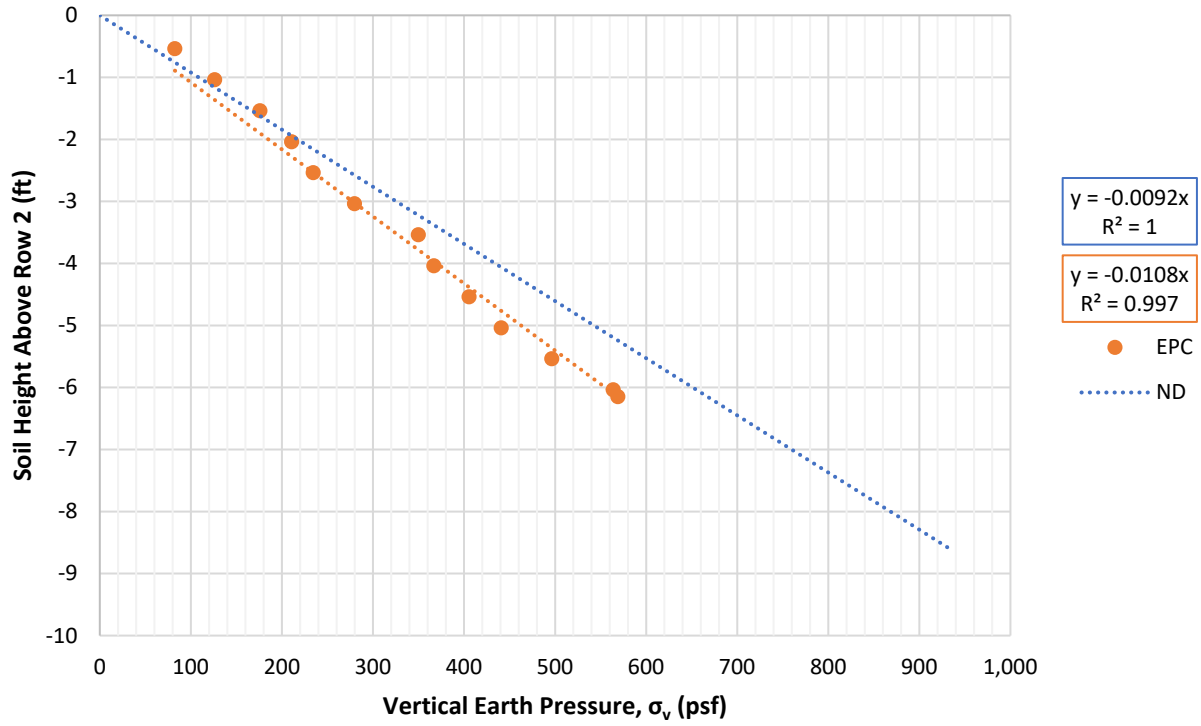


Figure 5-29. Row 2 – 103% compaction EPC earth pressure compared to nuclear density.

5.4.2 Row 2 Horizontal Earth Pressure

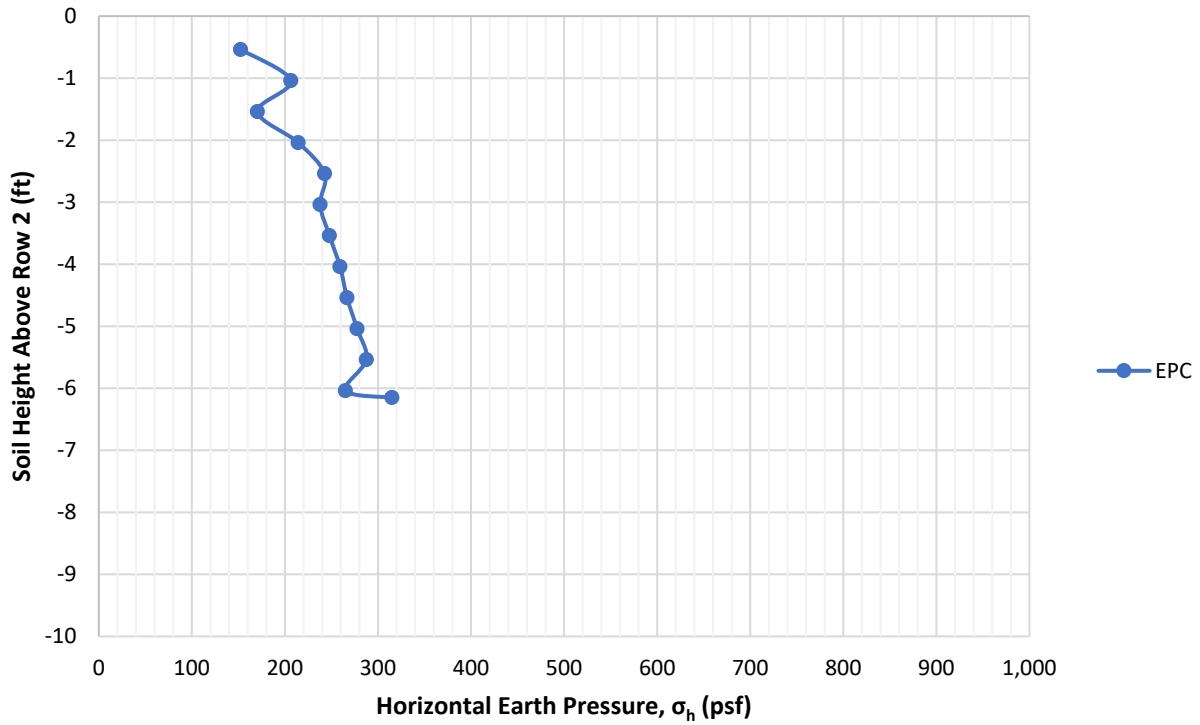


Figure 5-30. Row 2 – 95% compaction EPC horizontal earth pressure vs. depth.

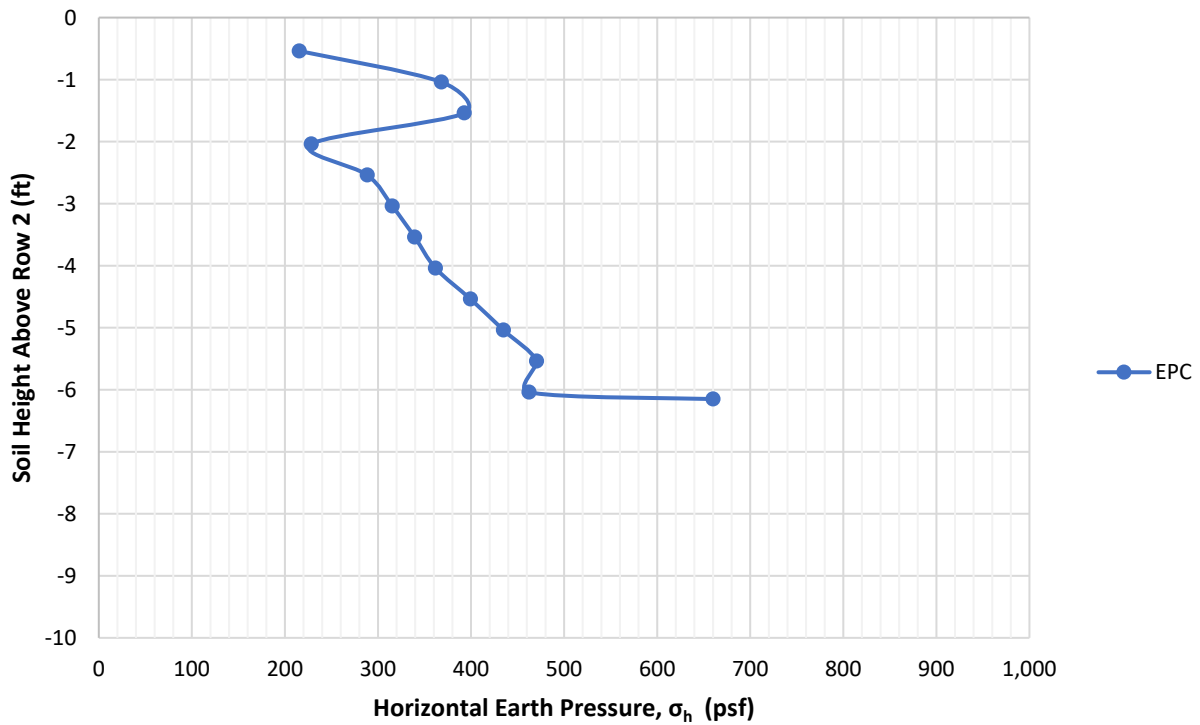


Figure 5-31. Row 2 – 103% compaction EPC horizontal earth pressure vs. depth.



### 5.4.3 Row 2 Reinforcement Strip Tension

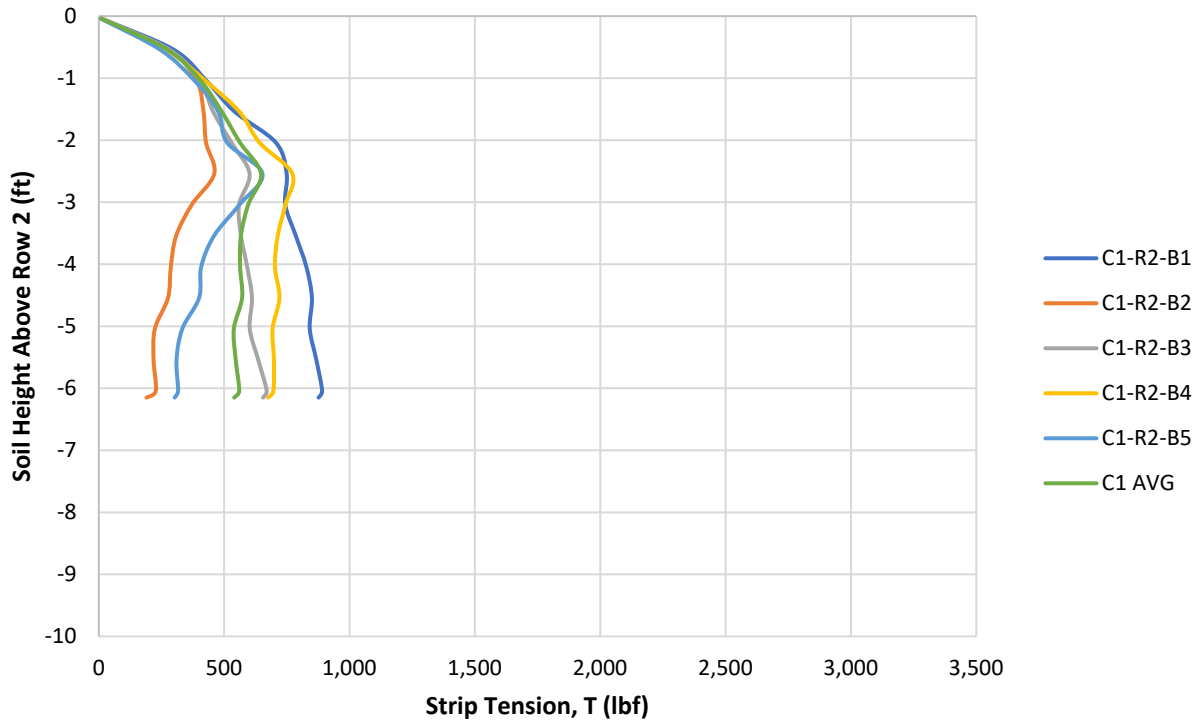


Figure 5-32. Row 2 – Column 1 - 95% compaction reinforcement strip tension vs. depth.

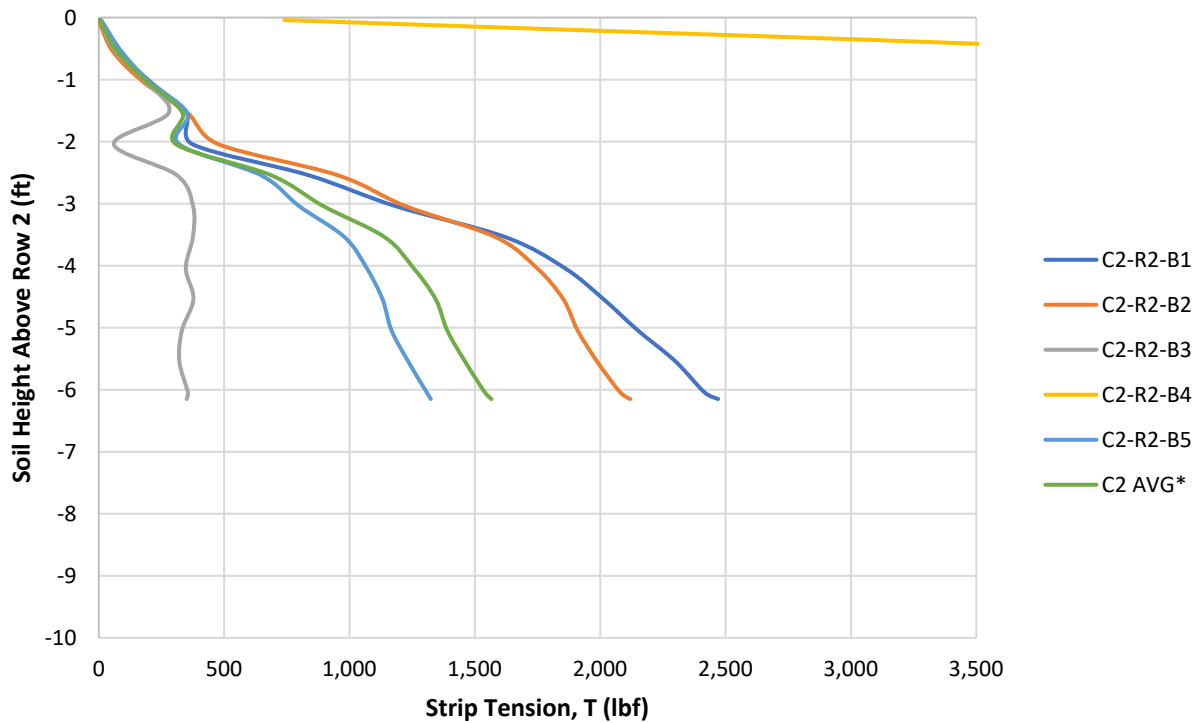


Figure 5-33. Row 2 – Column 2 - 95% compaction reinforcement strip tension vs. depth.

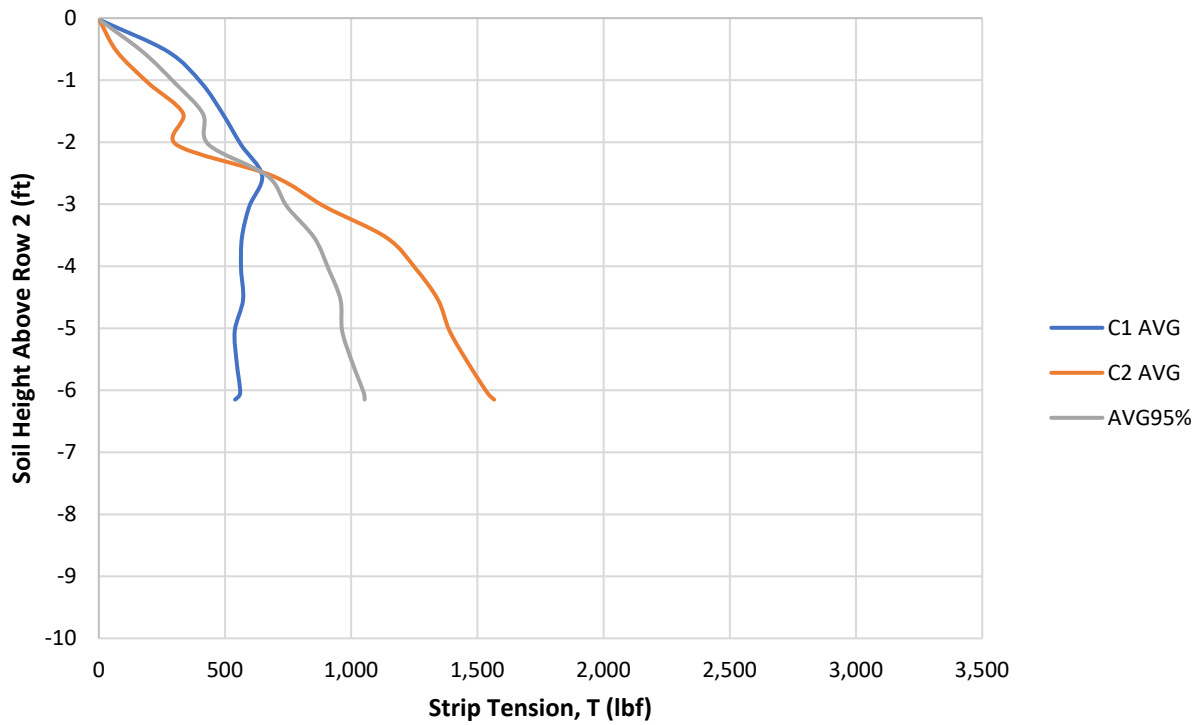


Figure 5-34. Row 2 – 95% compaction average reinforcement strip tension vs. depth.

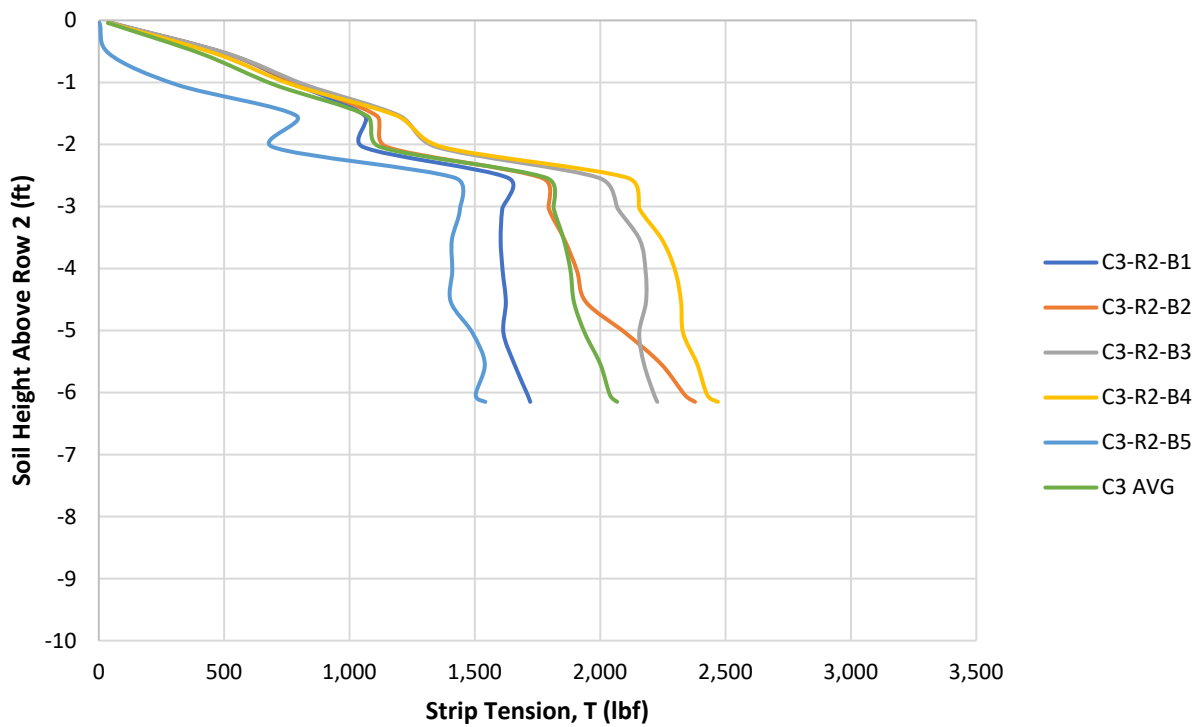


Figure 5-35. Row 2 – Column 3 - 103% compaction reinforcement strip tension vs. depth.

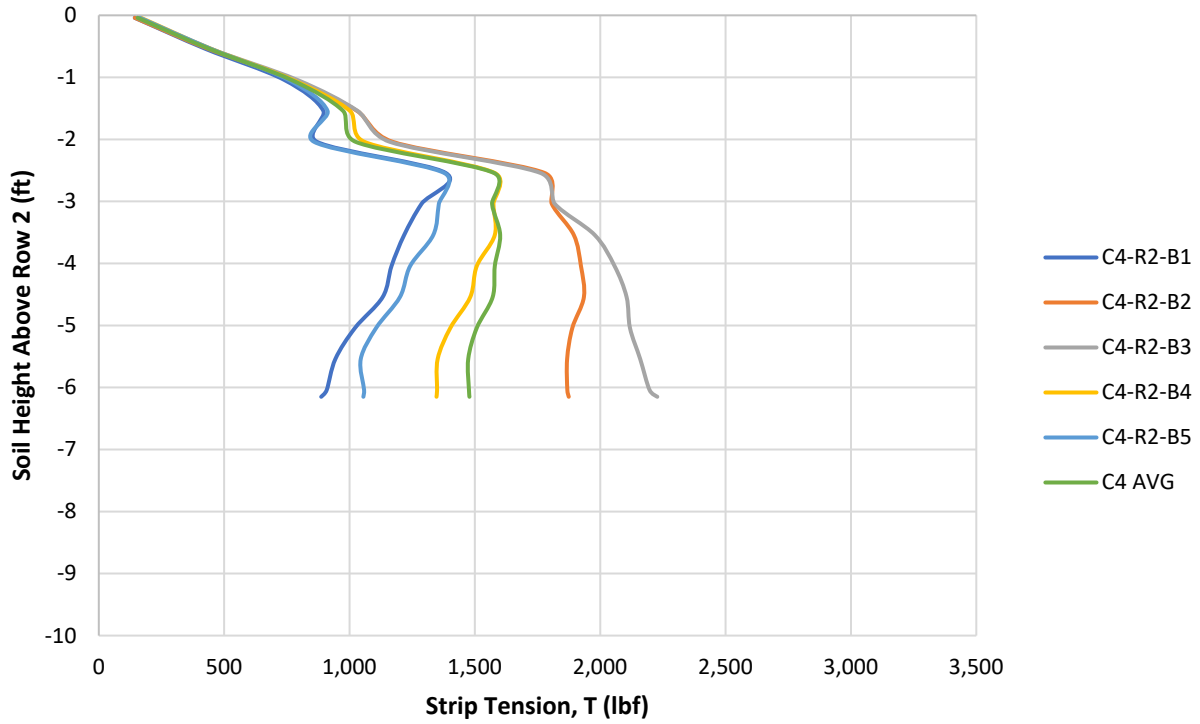


Figure 5-36. Row 2 – Column 4 - 103% compaction reinforcement strip tension vs. depth.

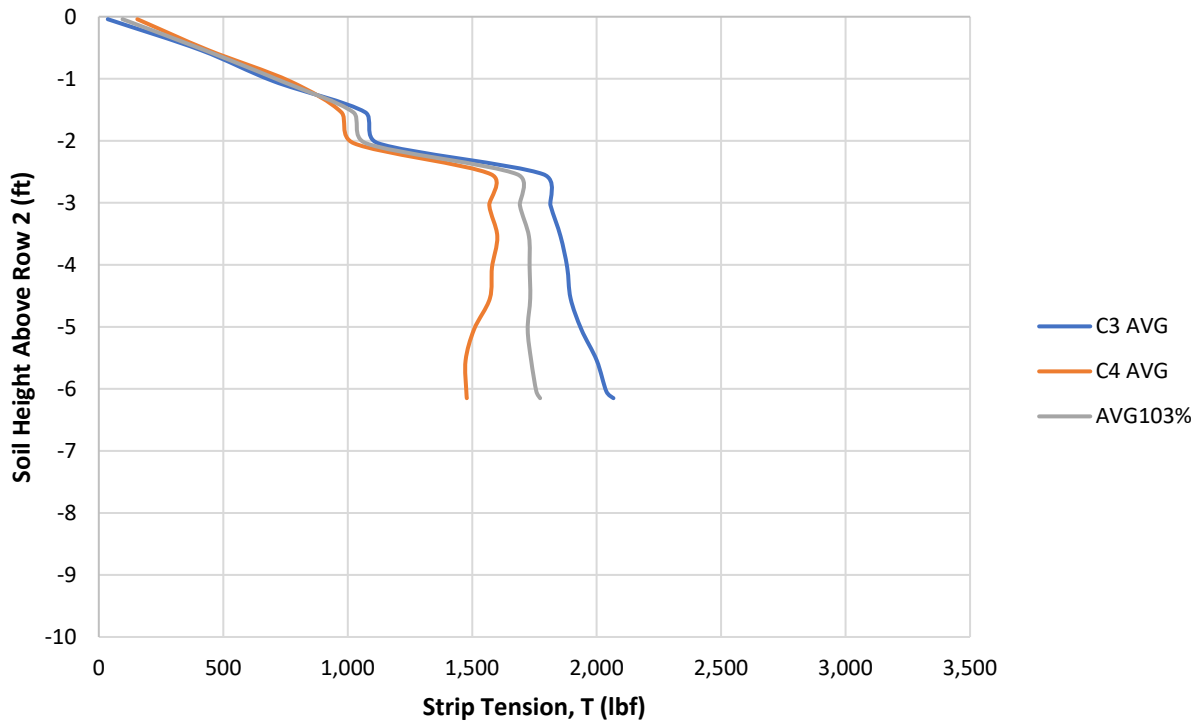


Figure 5-37. Row 2 – 103% compaction average reinforcement strip tension vs. depth.

5.4.4 Row 2 Average Earth Pressures and Strip Tension

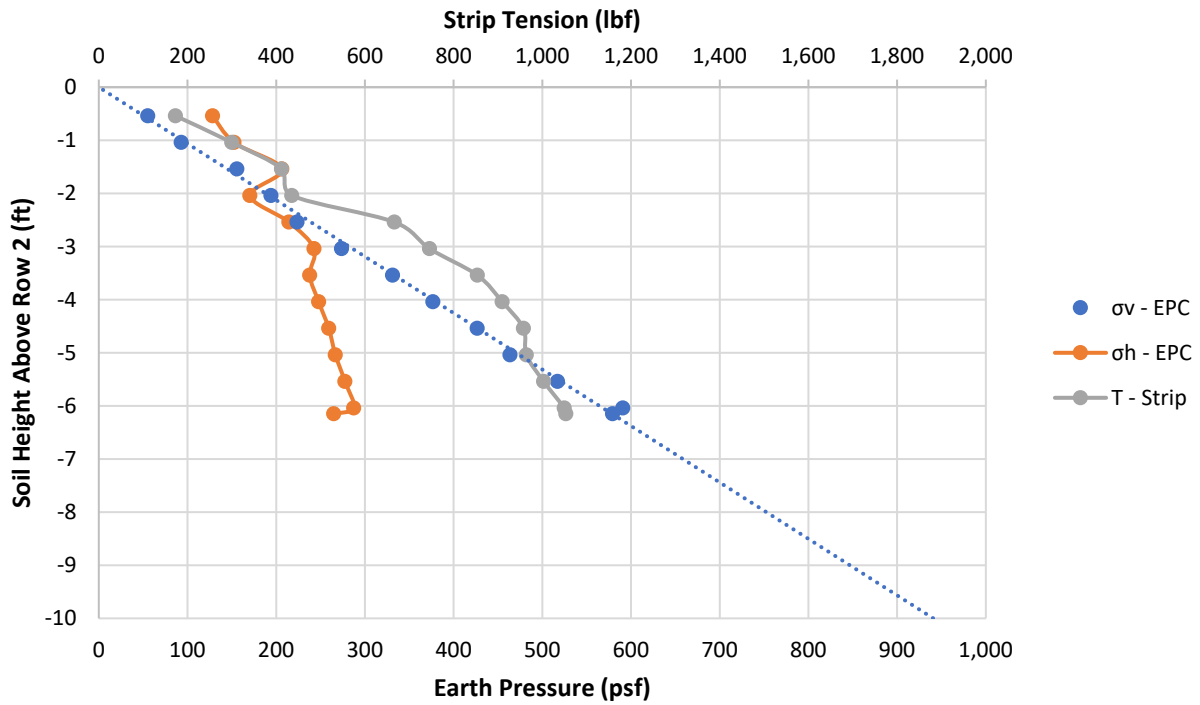


Figure 5-38. Row 2 – 95% compaction vertical and horizontal stress and strip tension vs. depth.

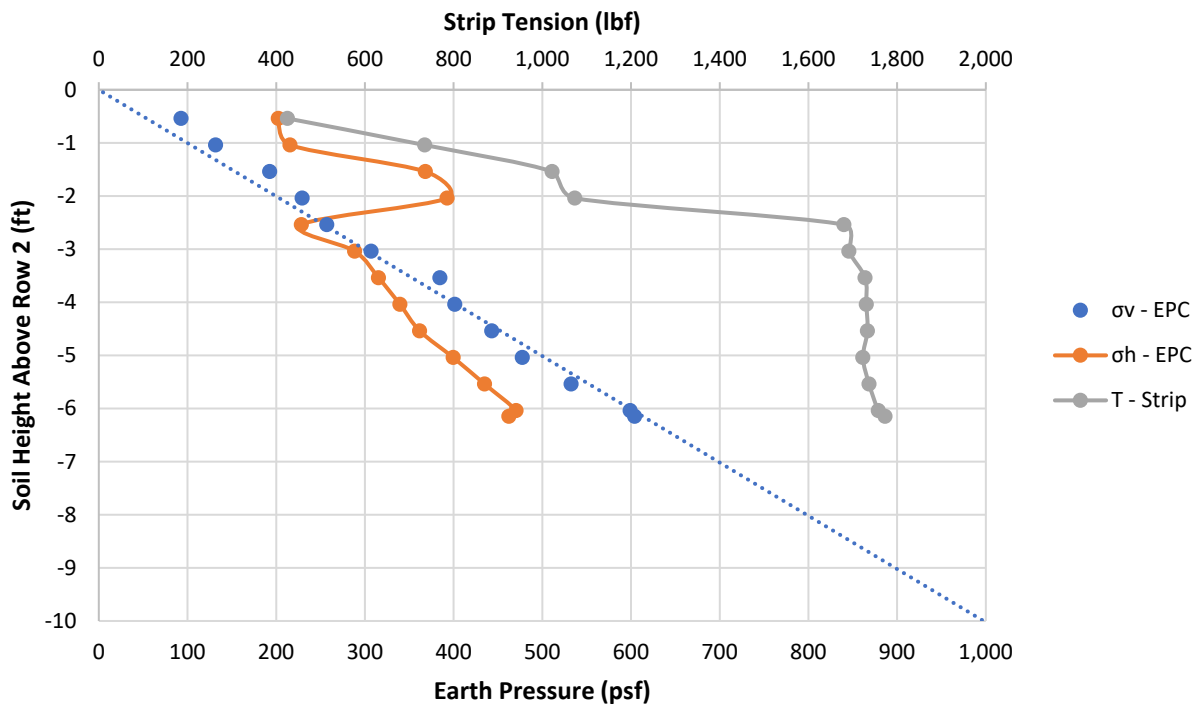


Figure 5-39. Row 2 – 103% compaction vertical and horizontal stress and strip tension vs. depth.

5.4.5 Row 2 Construction Earth Pressure Coefficient Analysis – 95% of T-180

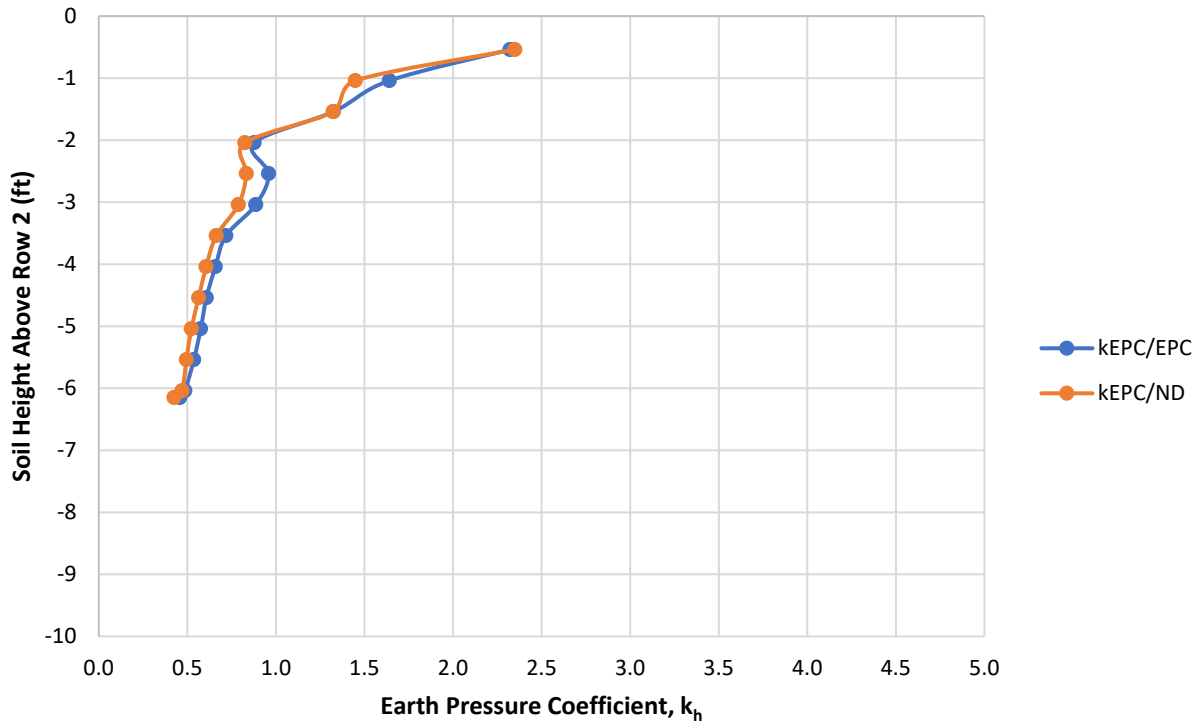


Figure 5-40. Row 2 – 95% compaction earth pressure coefficients from EPCs.

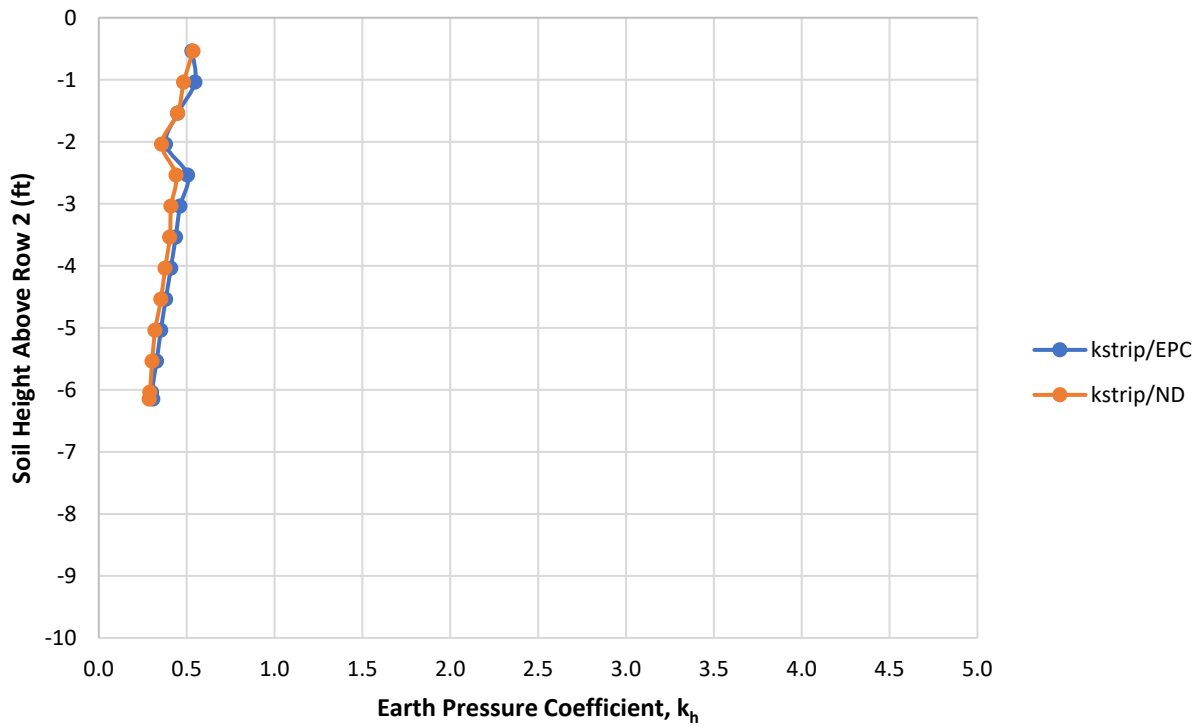


Figure 5-41. Row 2 – 95% compaction earth pressure coefficients from reinforcement strips.

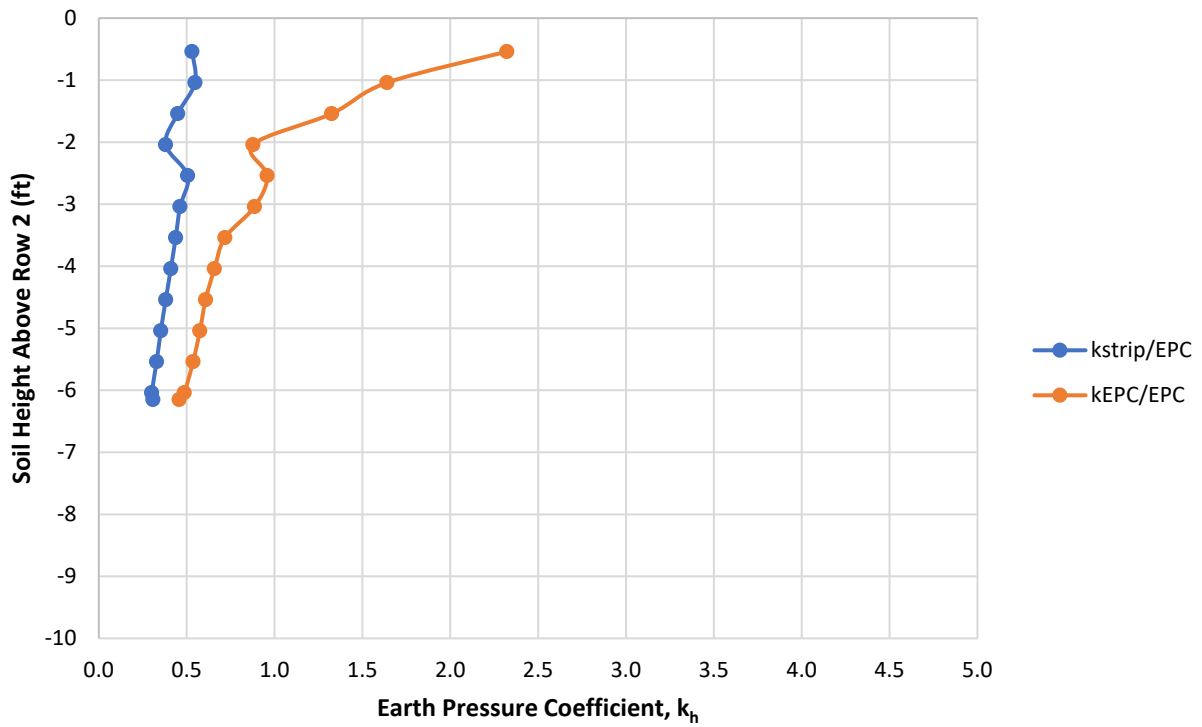


Figure 5-42. Comparing Row 2 – 95% compaction  $k_h$  using vertical stress from EPCs.

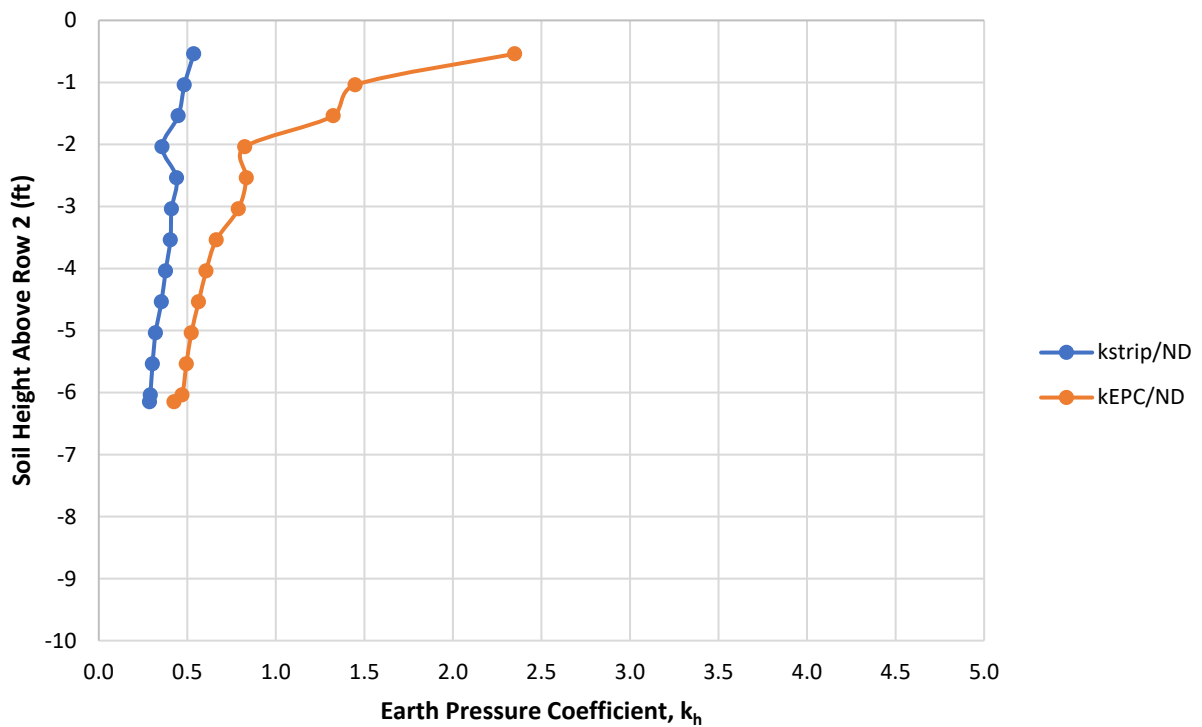


Figure 5-43. Comparing Row 2 – 95% compaction  $k_h$  using vertical stress from nuclear density.

5.4.6 Row 2 Construction Earth Pressure Coefficient Analysis – 103% of T-180

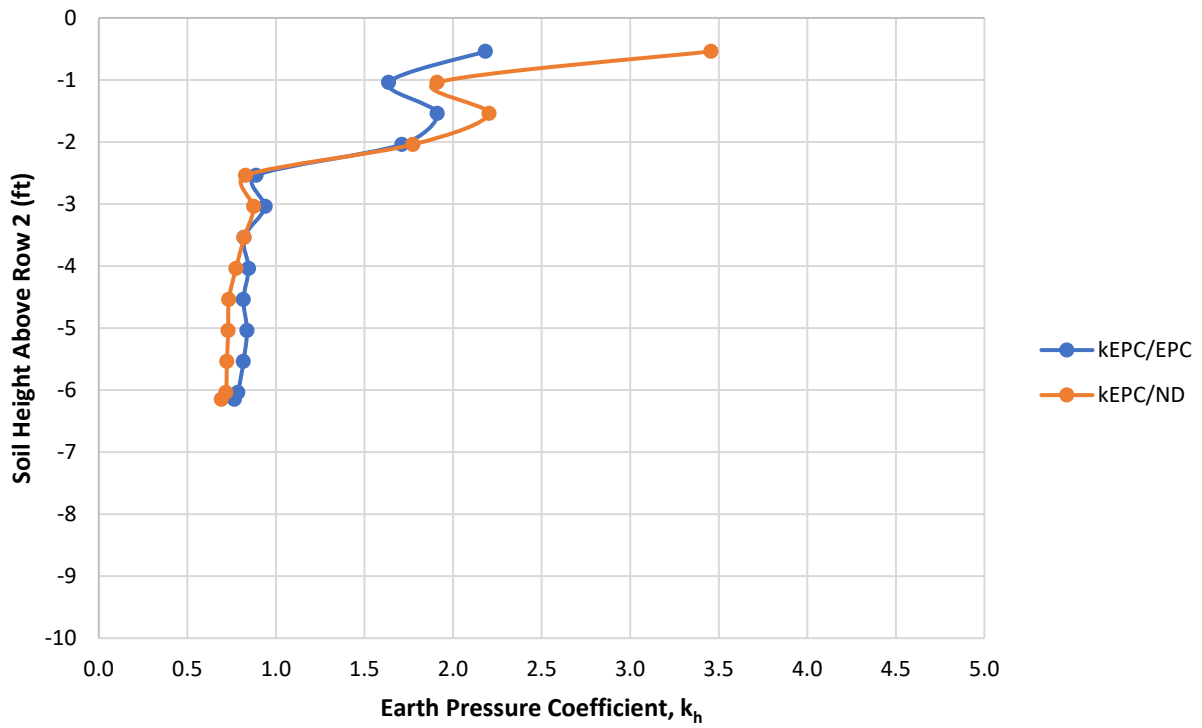


Figure 5-44. Row 2 – 103% compaction earth pressure coefficients from EPCs.

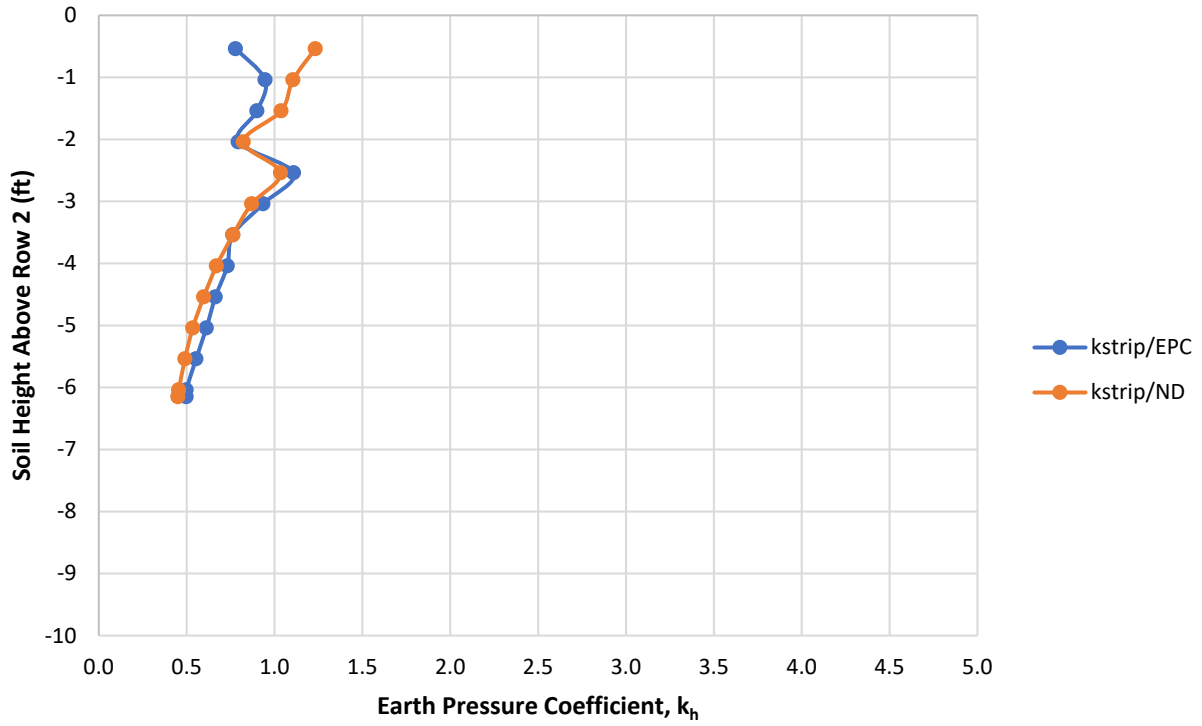


Figure 5-45. Row 2 – 103% compaction earth pressure coefficients from reinforcement strips.

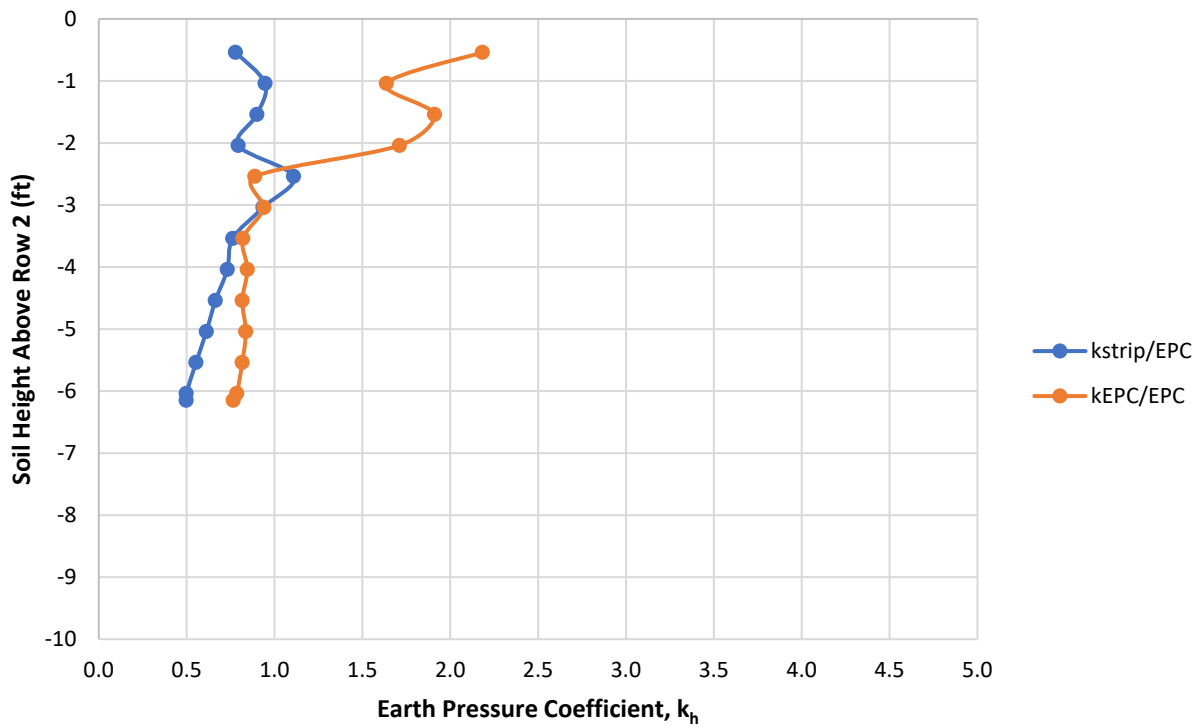


Figure 5-46. Comparing Row 2 – 103% compaction  $k_h$  using vertical stress from EPCs.



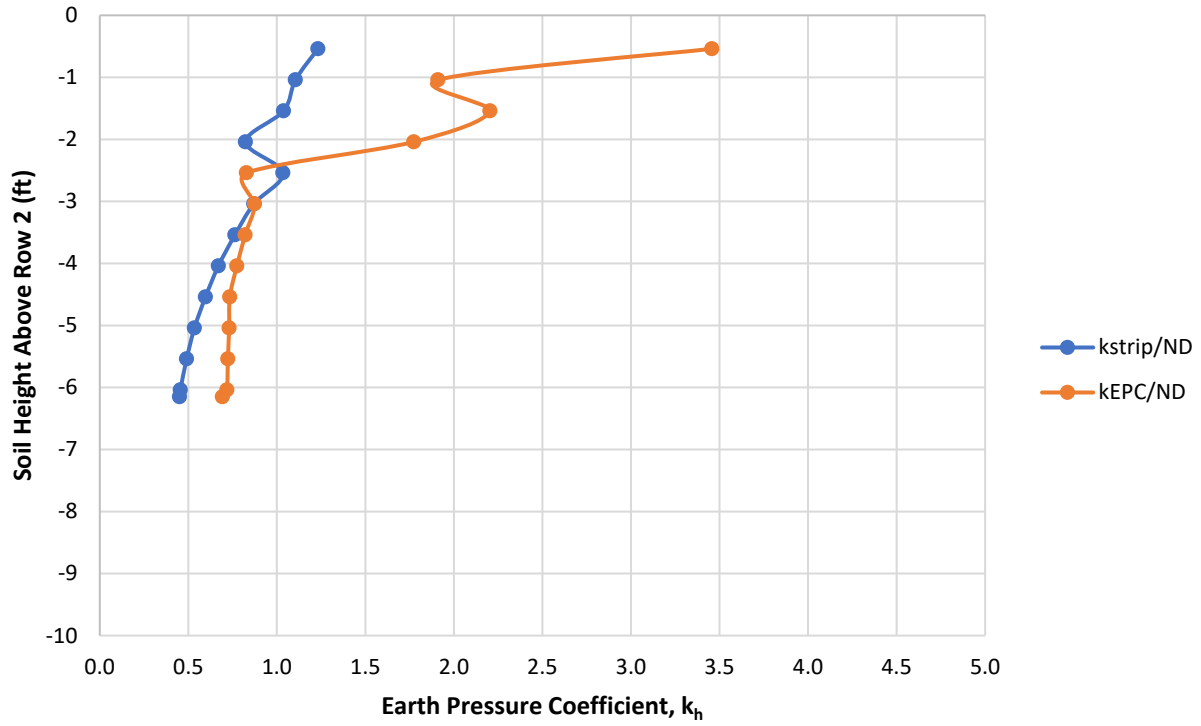


Figure 5-47. Comparing Row 2 – 103% compaction  $k_h$  using vertical stress from nuclear density.

## 5.5 Row 3 Construction Analysis

### 5.5.1 Row 3 Vertical Earth Pressure

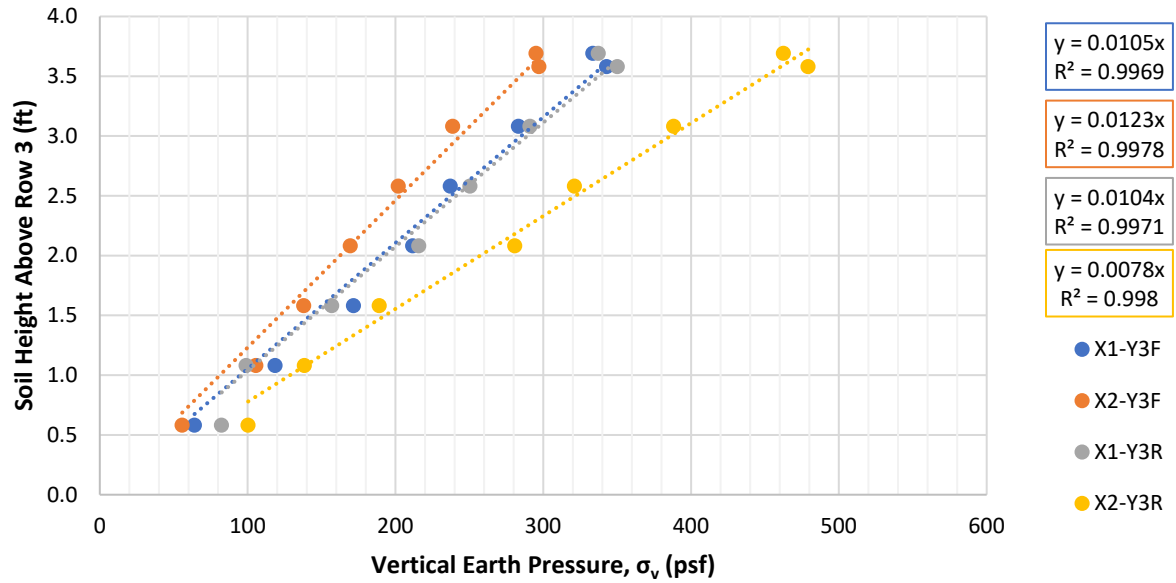


Figure 5-48. Row 3 – 95% compaction EPC vertical earth pressure vs. depth.

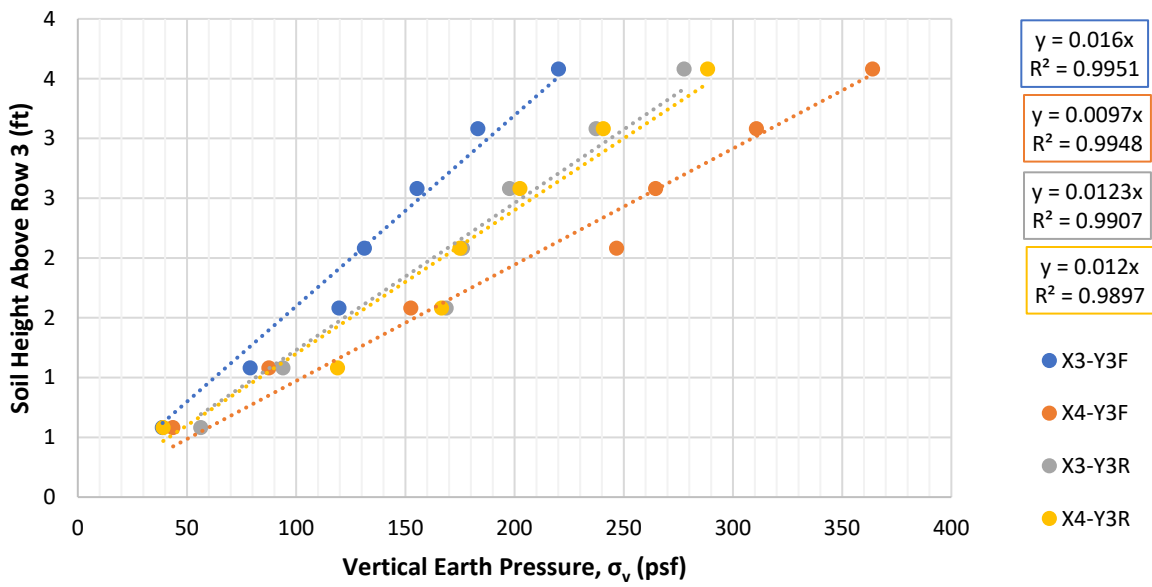


Figure 5-49. Row 3 – 103% compaction EPC vertical earth pressure vs. depth.

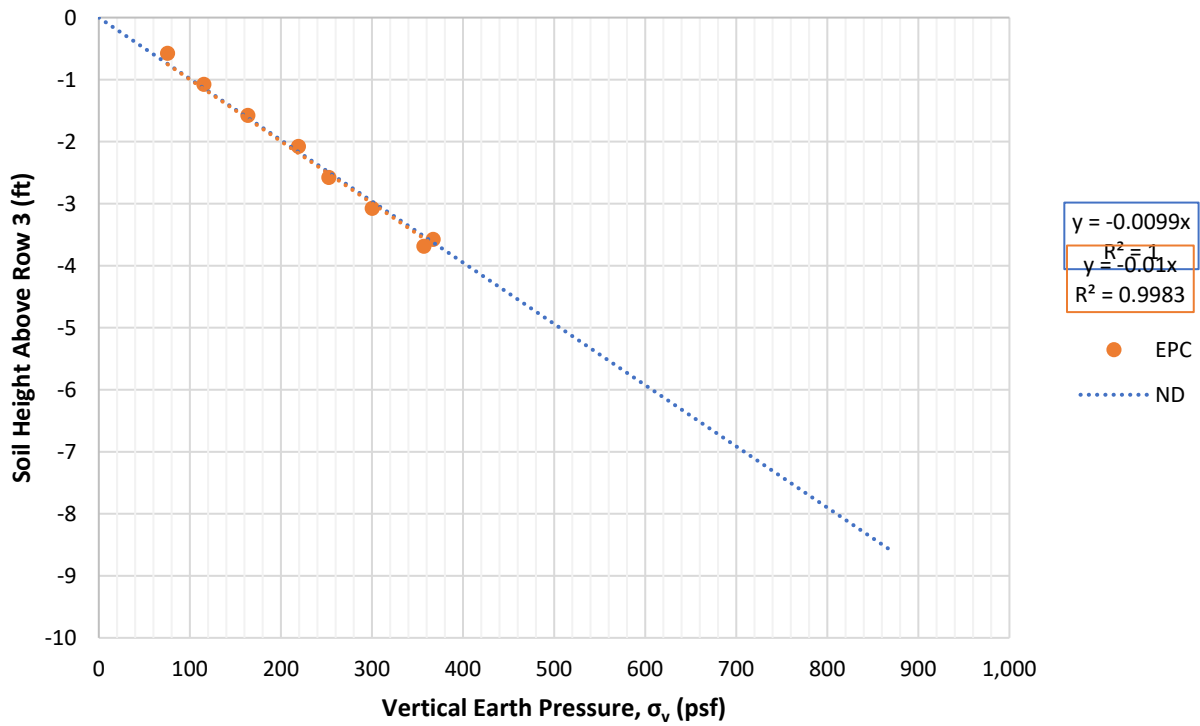


Figure 5-50. Row 3 – 95% compaction EPC earth pressure compared to nuclear density.

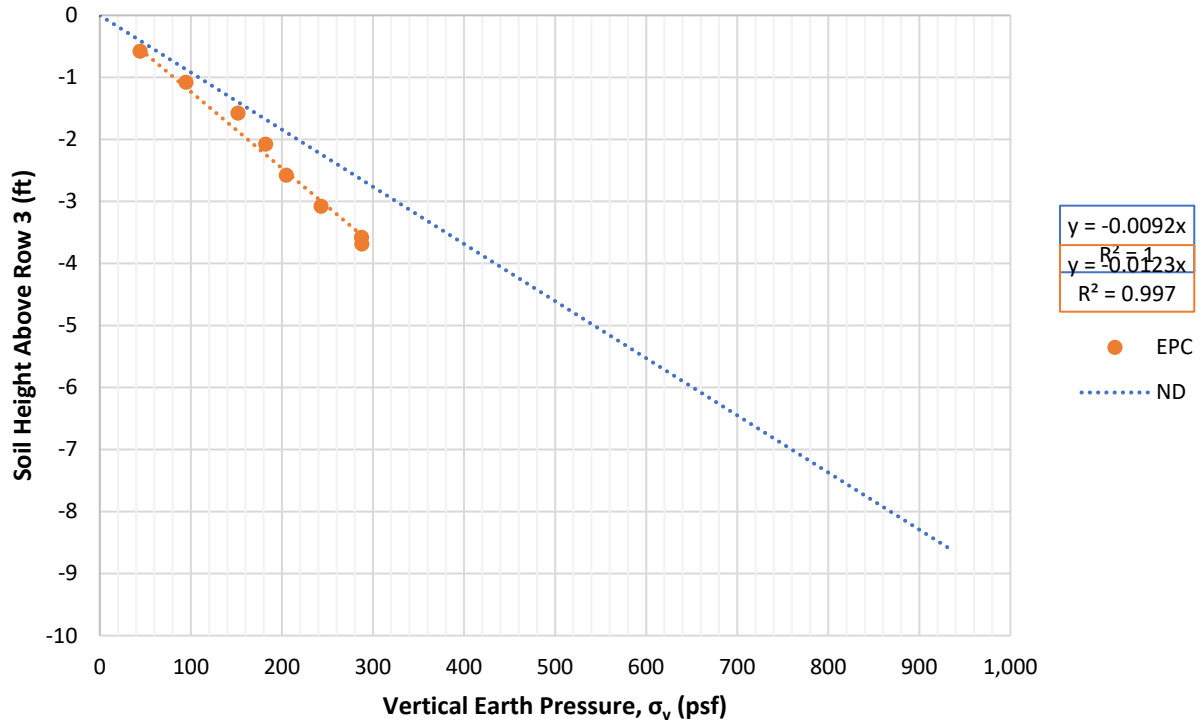


Figure 5-51. Row 3 – 103% compaction EPC earth pressure compared to nuclear density.

5.5.2 Row 3 Horizontal Earth Pressure

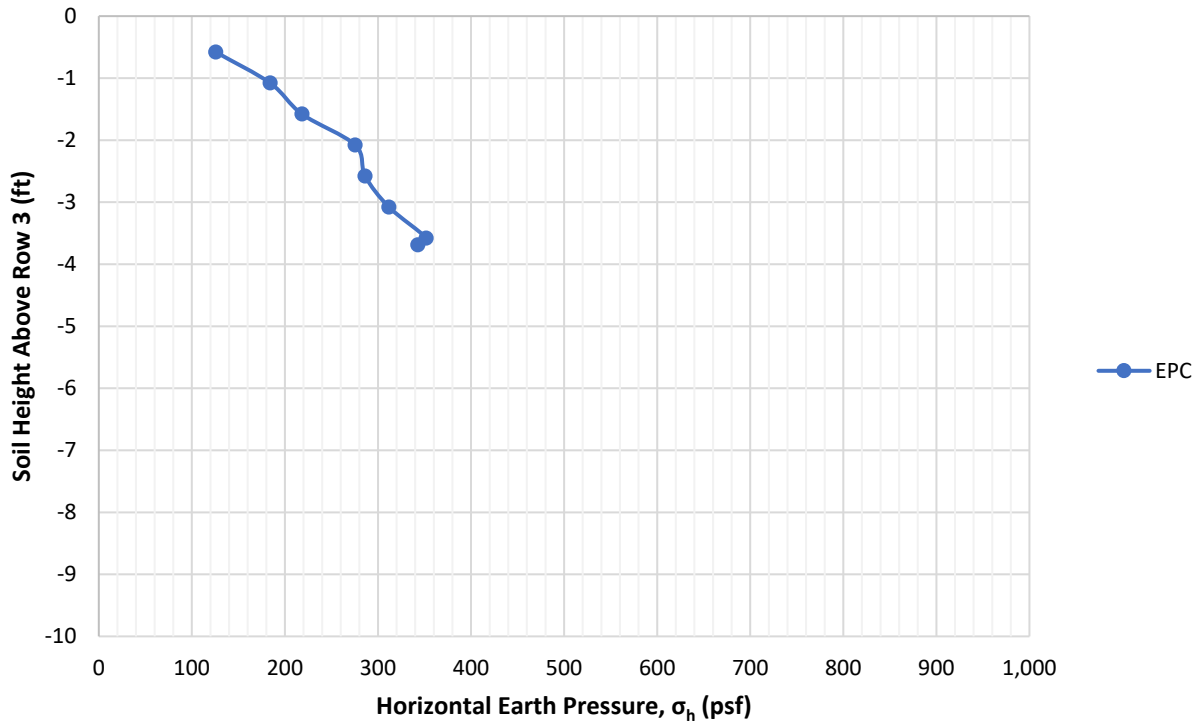


Figure 5-52. Row 3 – 95% compaction EPC horizontal earth pressure vs. depth.

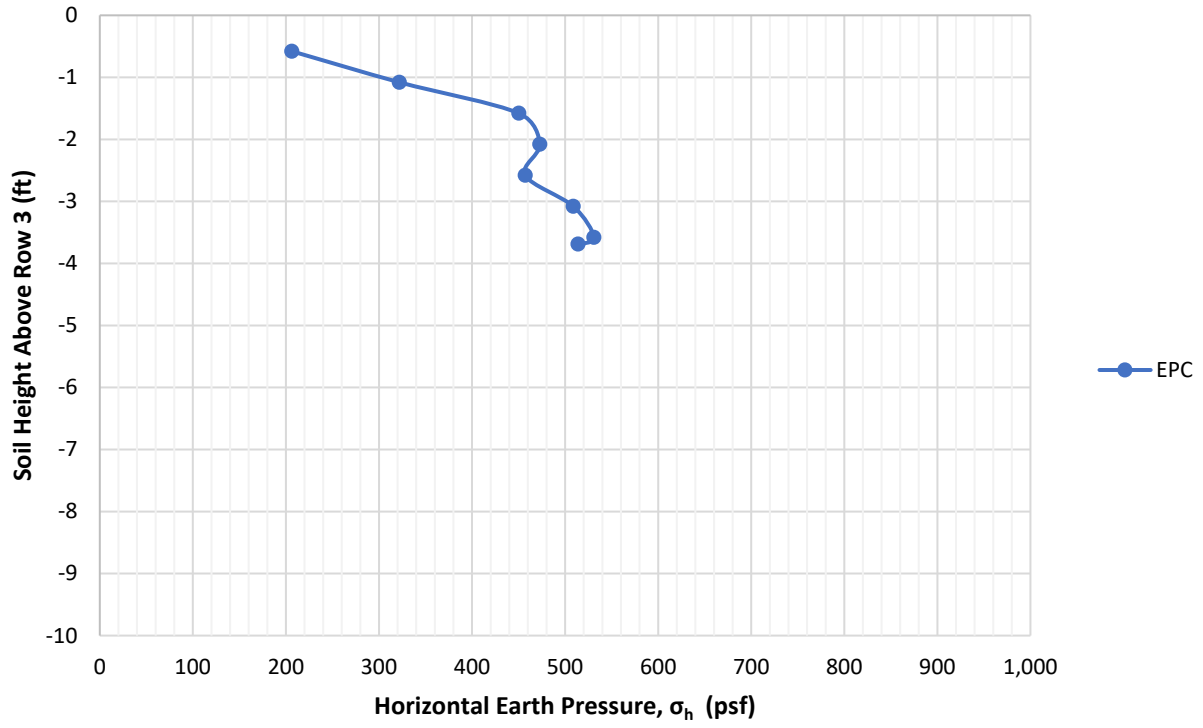


Figure 5-53. Row 3 – 103% compaction EPC horizontal earth pressure vs. depth.

### 5.5.3 Row 3 Reinforcement Strip Tension

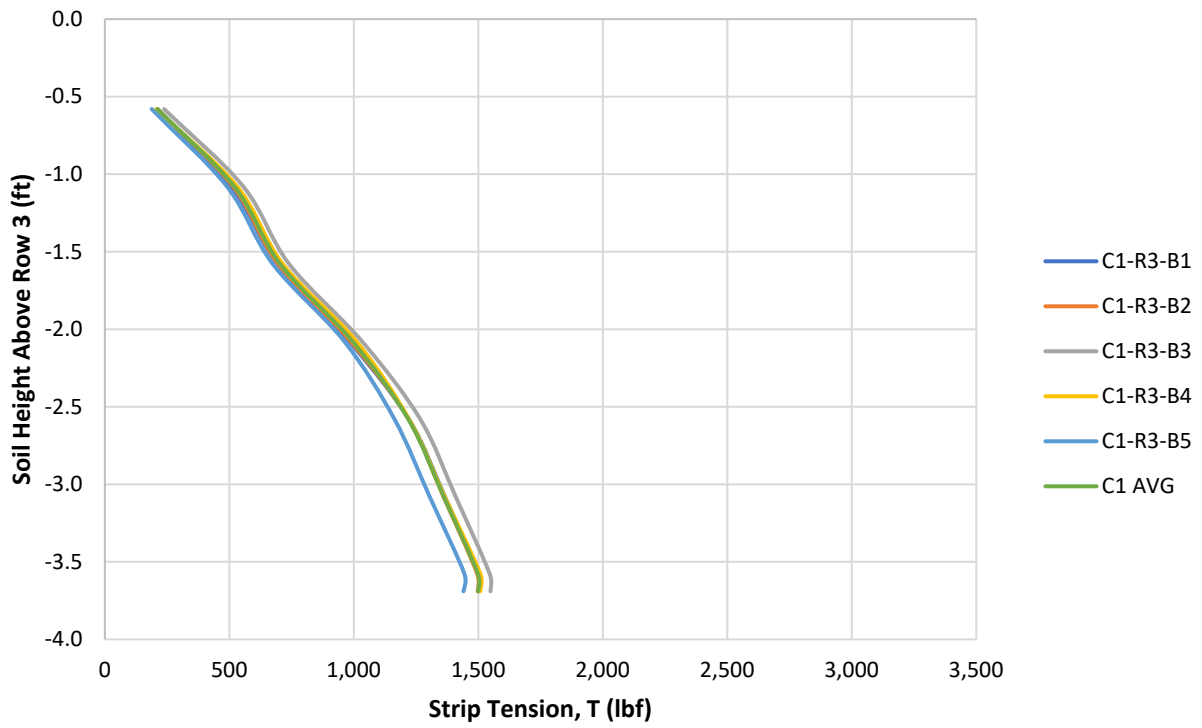


Figure 5-54. Row 3 – Column 1 - 95% compaction reinforcement strip tension vs. depth.

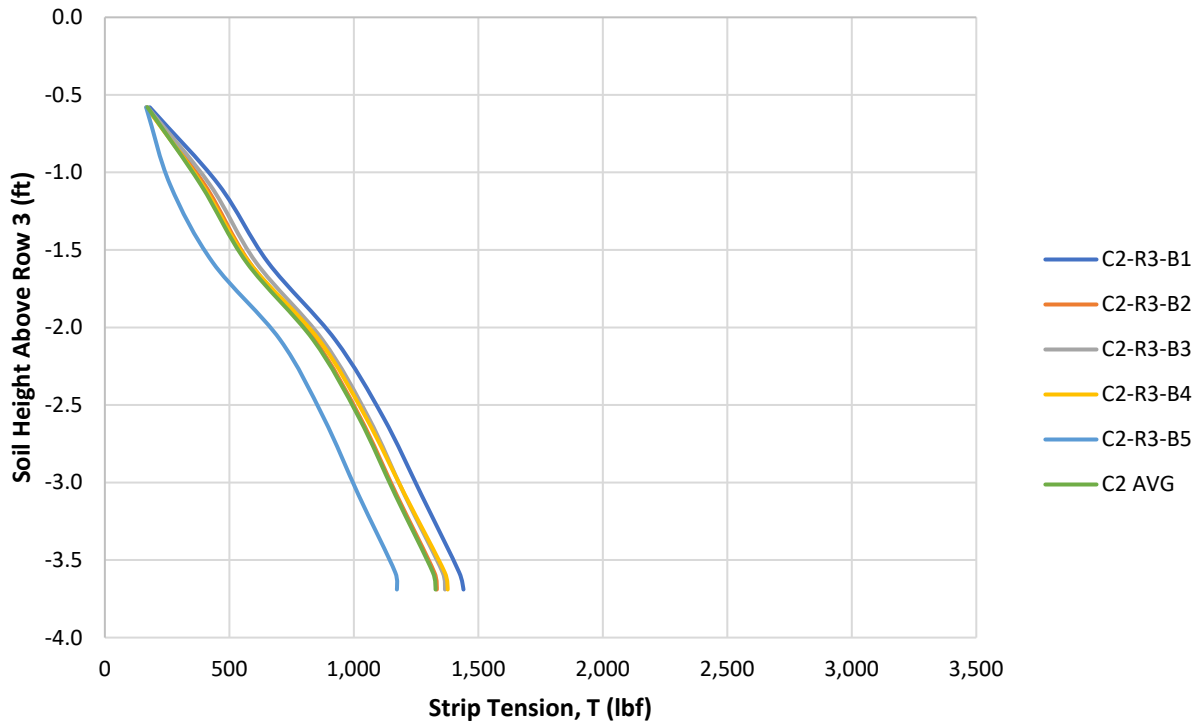


Figure 5-55. Row 3 – Column 2 - 95% compaction reinforcement strip tension vs. depth.

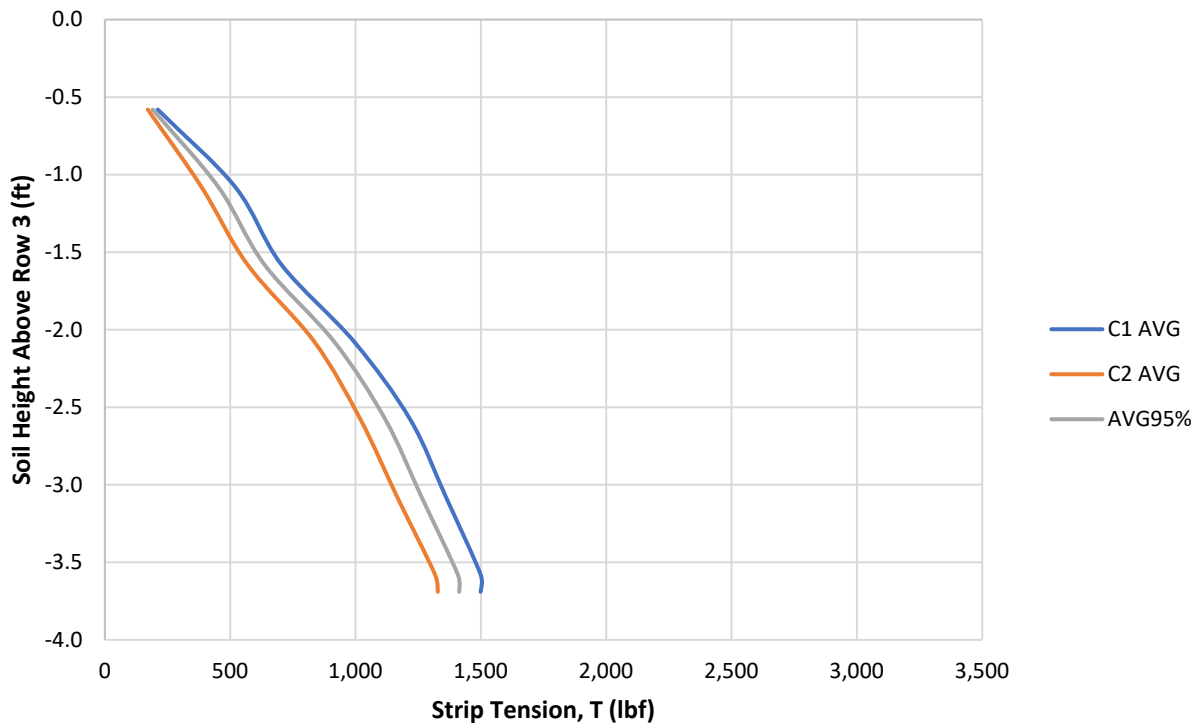


Figure 5-56. Row 3 – 95% compaction average reinforcement strip tension vs. depth.



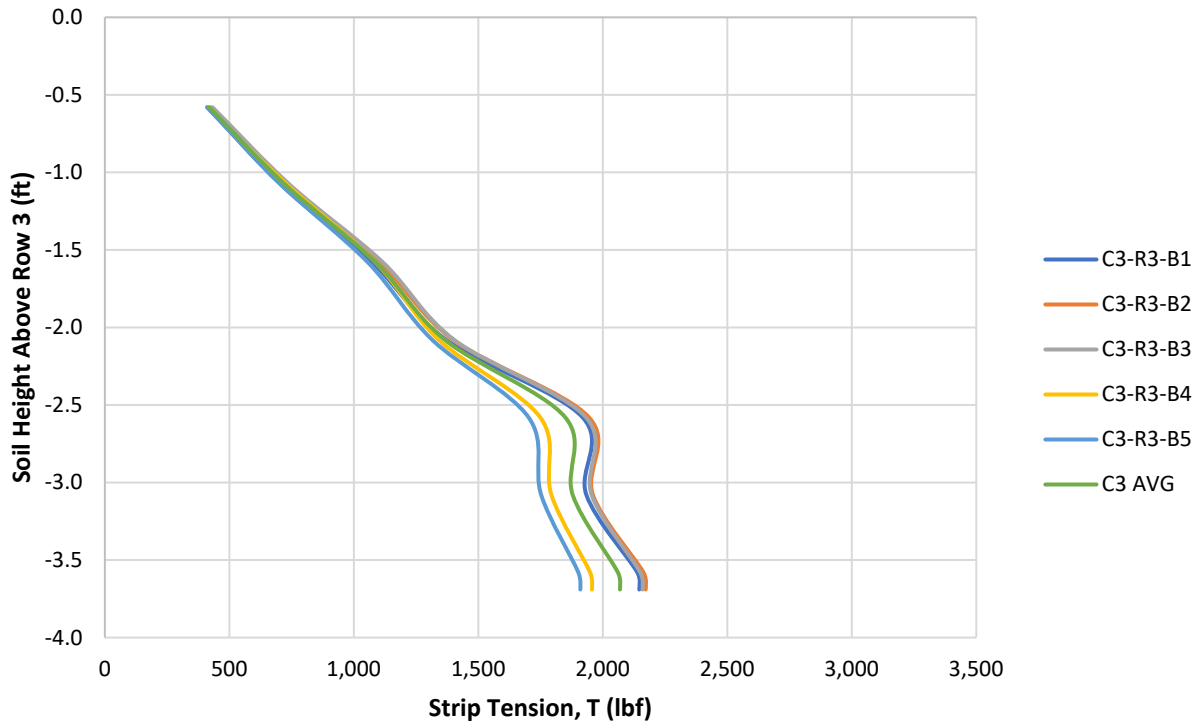


Figure 5-57. Row 3 – Column 3 - 103% compaction reinforcement strip tension vs. depth.

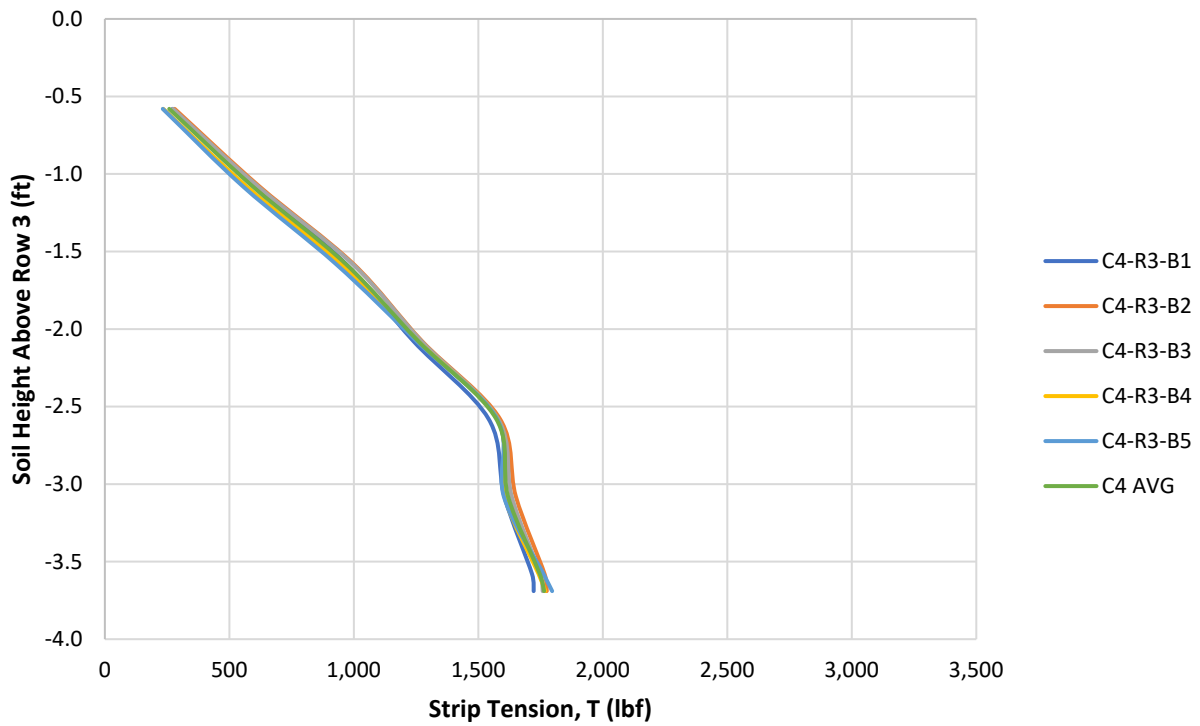


Figure 5-58. Row 3 – Column 4 - 103% compaction reinforcement strip tension vs. depth.

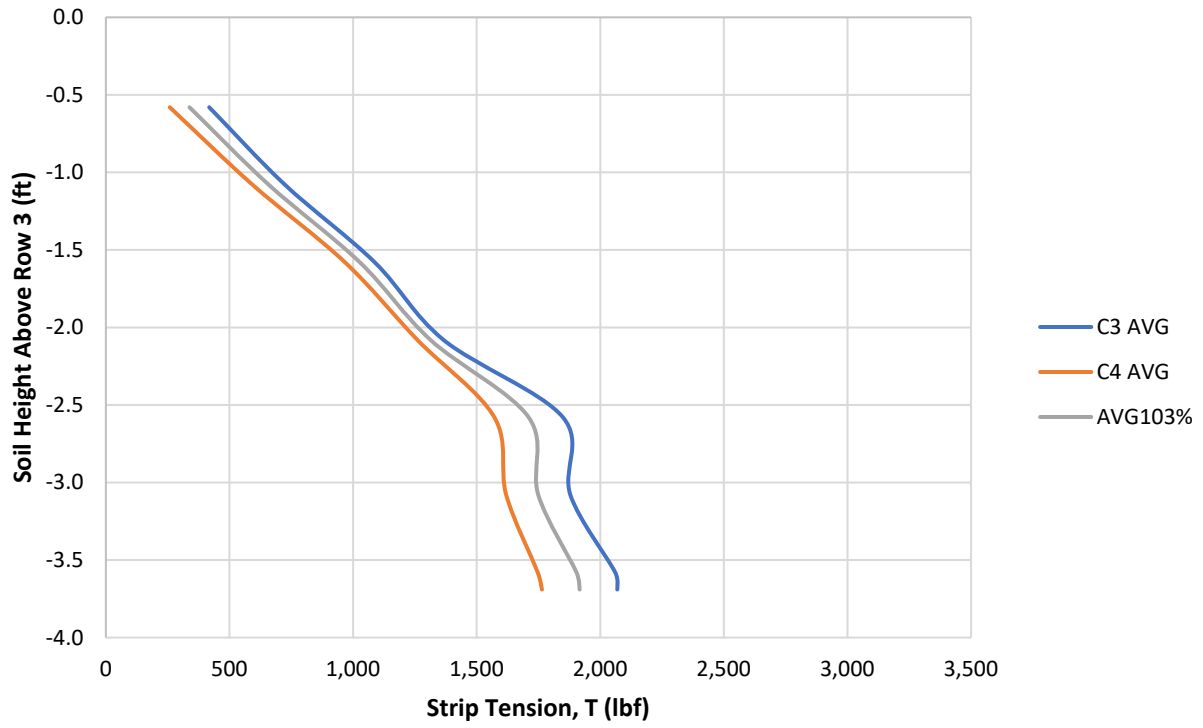


Figure 5-59. Row 3 – 103% compaction average reinforcement strip tension vs. depth.

5.5.4 Row 3 Average Earth Pressures and Strip Tension

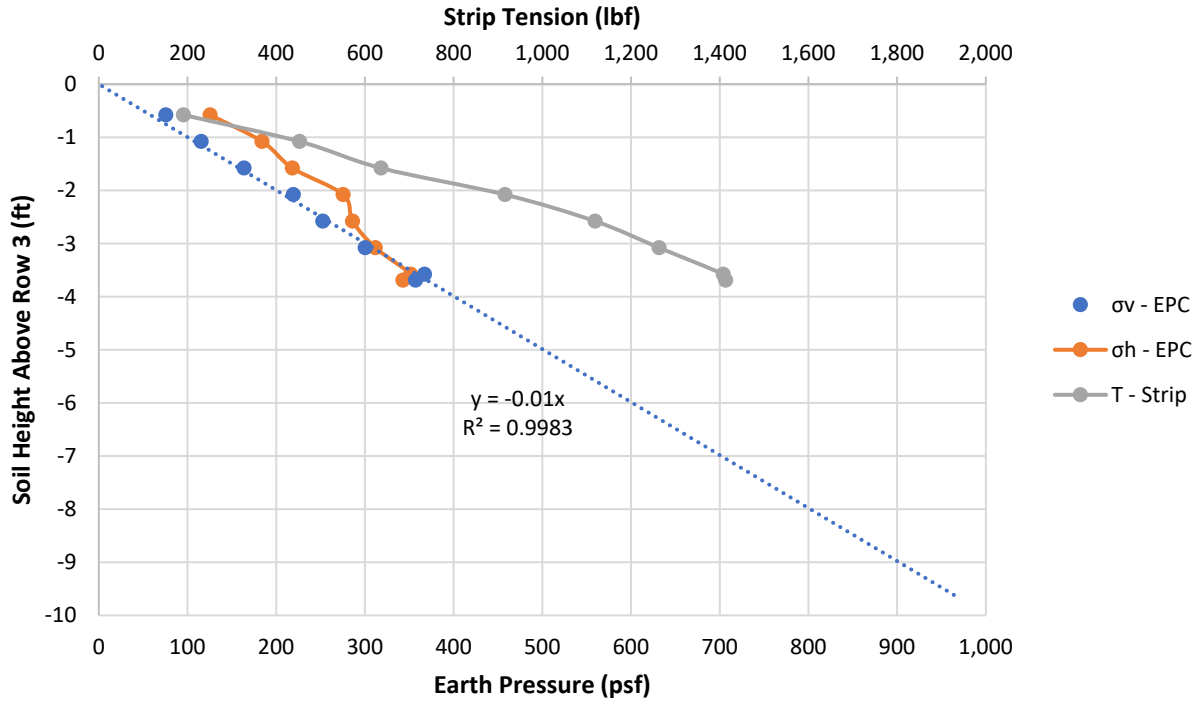


Figure 5-60. Row 3 – 95% compaction vertical and horizontal stress and strip tension vs. depth.

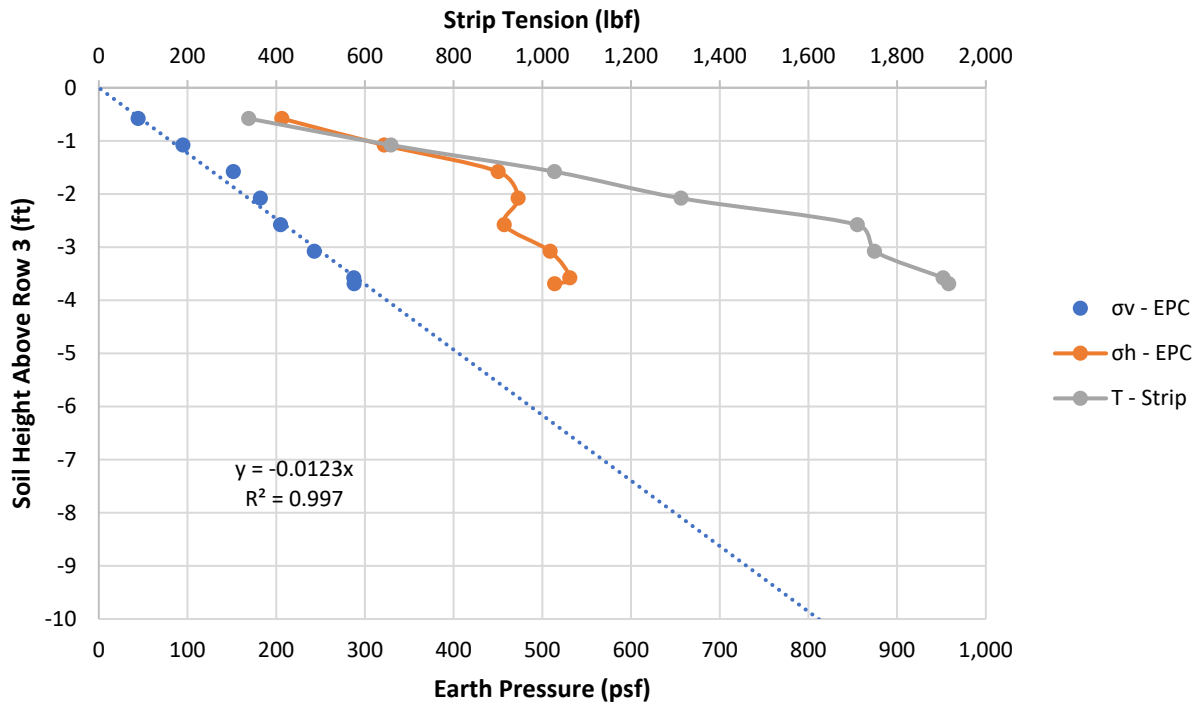


Figure 5-61. Row 3 – 103% compaction vertical and horizontal stress and strip tension vs. depth.

5.5.5 Row 3 Construction Earth Pressure Coefficient Analysis – 95% of T-180

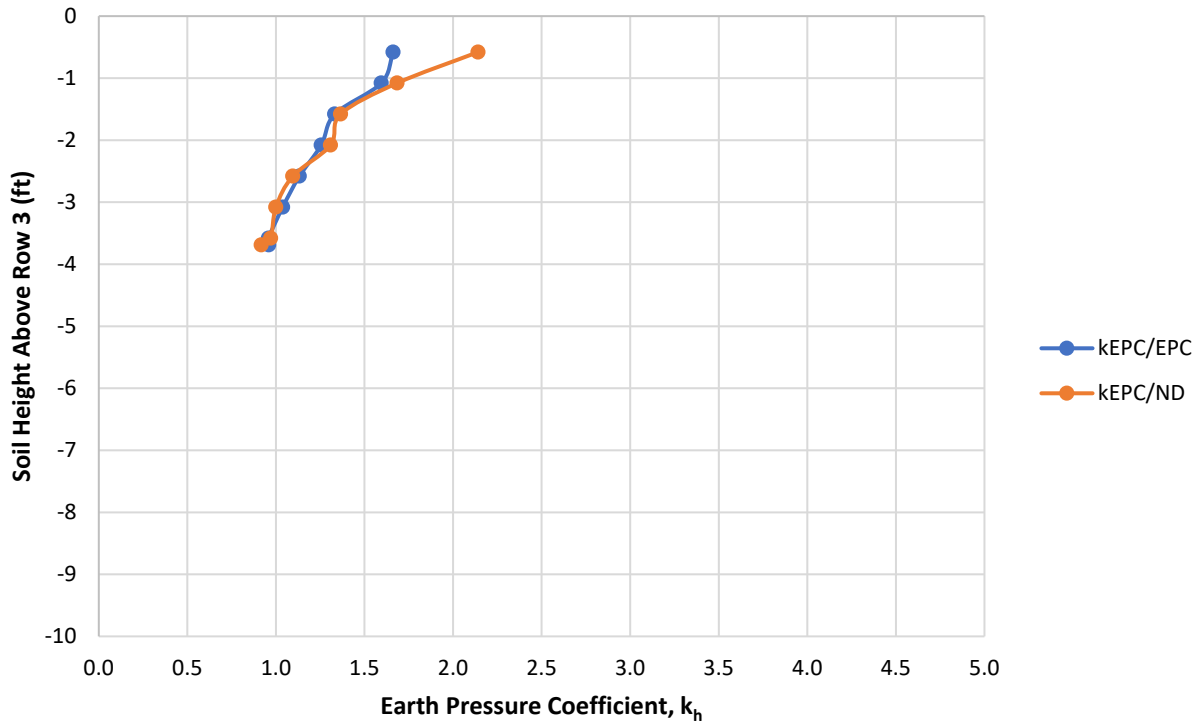


Figure 5-62. Row 3 – 95% compaction earth pressure coefficients from EPCs.

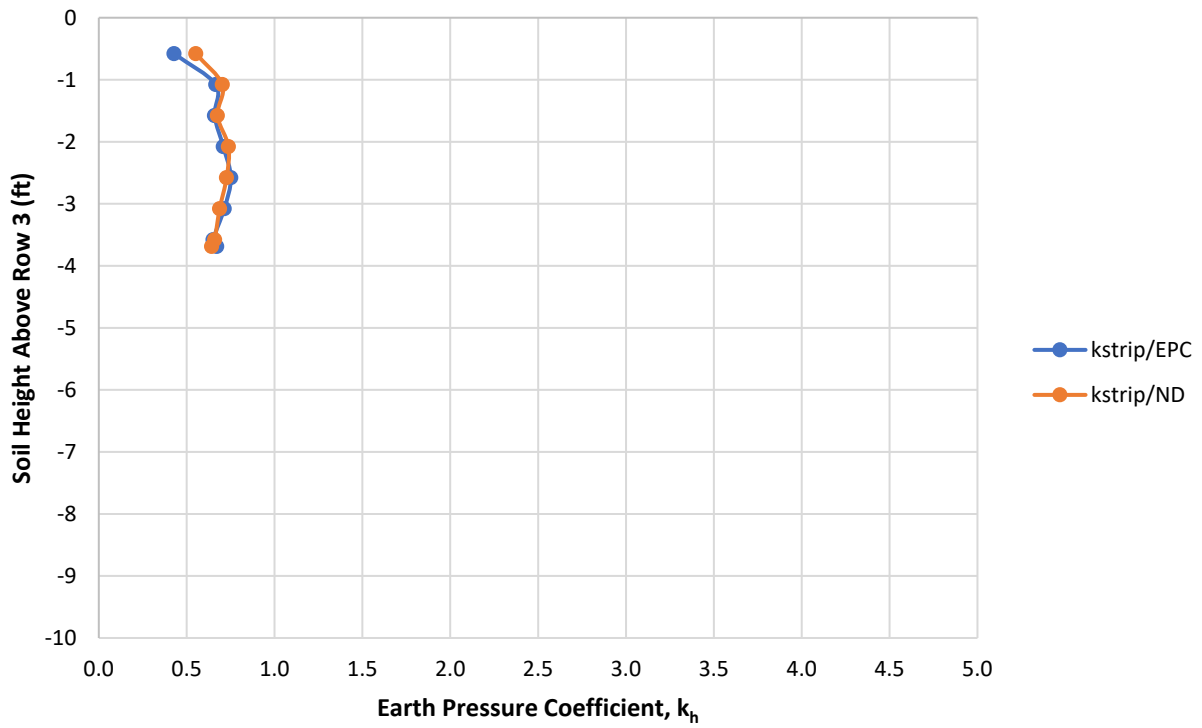


Figure 5-63. Row 3 – 95% compaction earth pressure coefficients from reinforcement strips.

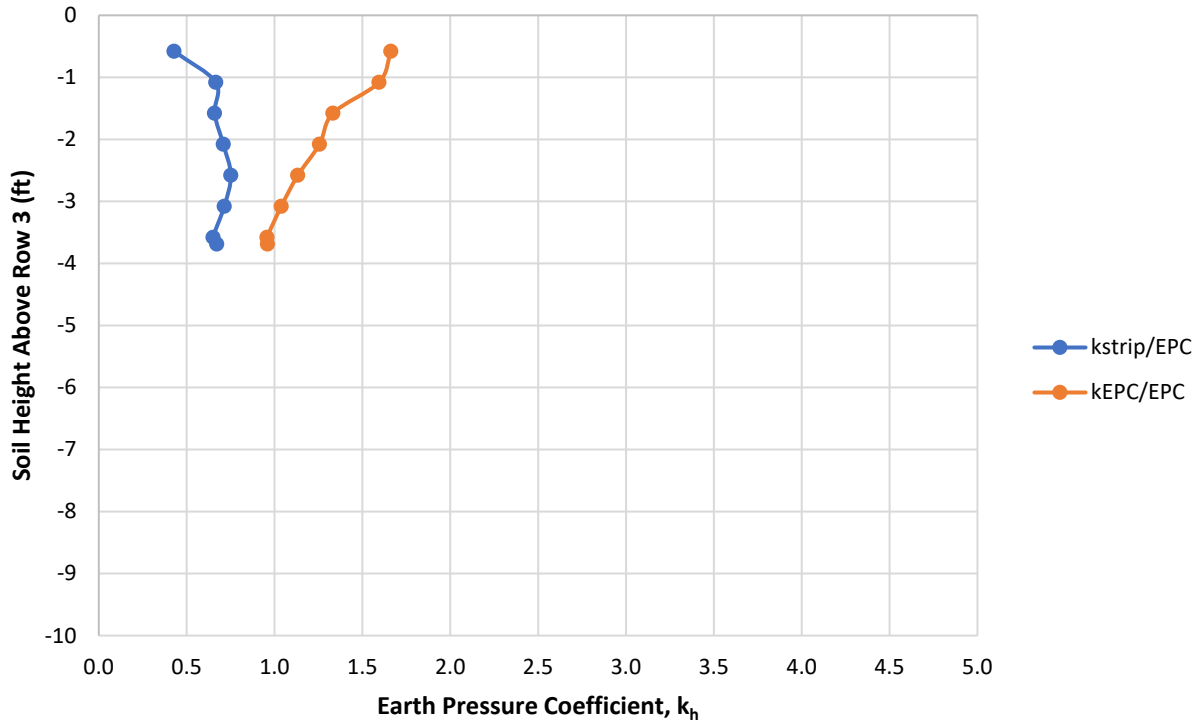


Figure 5-64. Comparing Row 3 – 95% compaction  $k_h$  using vertical stress from EPCs.

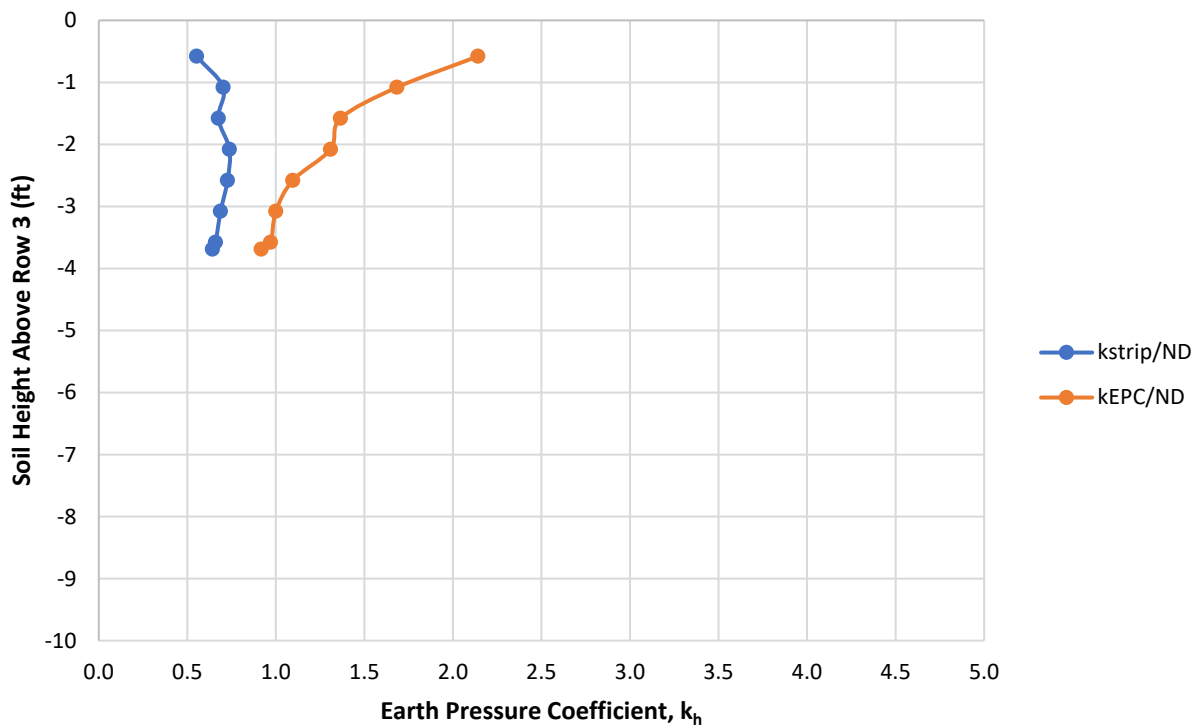


Figure 5-65. Comparing Row 3 – 95% compaction  $k_h$  using vertical stress from nuclear density.

5.5.6 Row 3 Construction Earth Pressure Coefficient Analysis – 103% of T-180

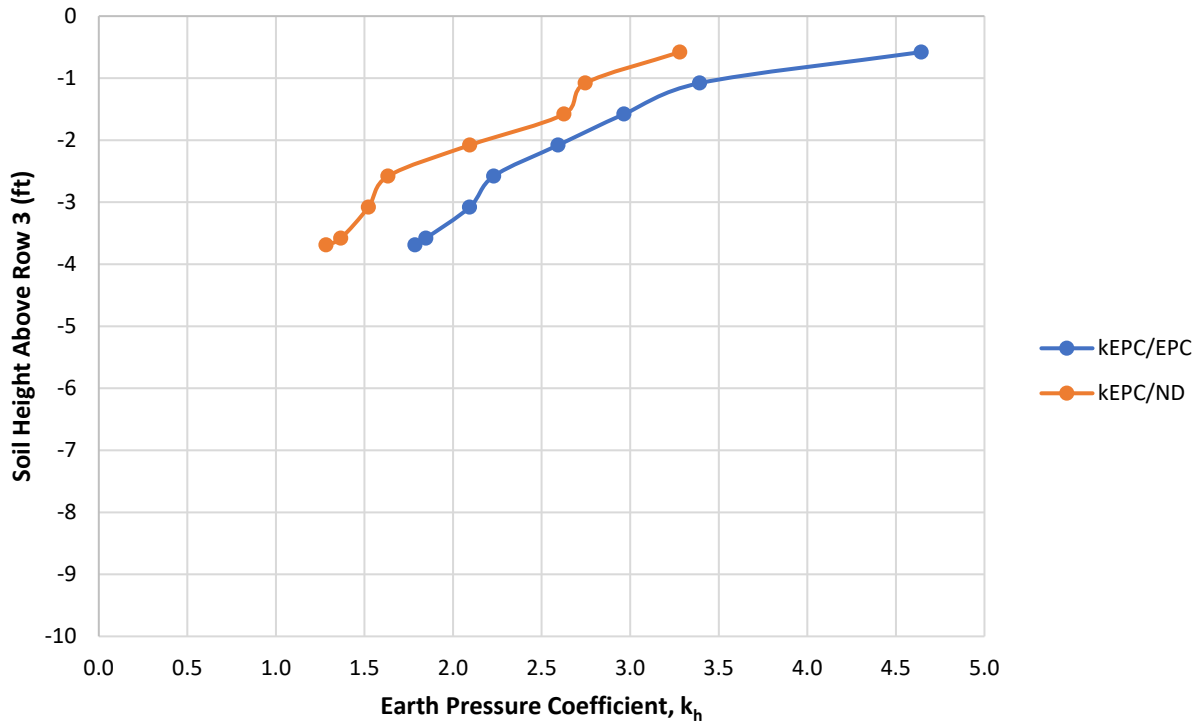


Figure 5-66. Row 3 – 103% compaction earth pressure coefficients from EPCs.

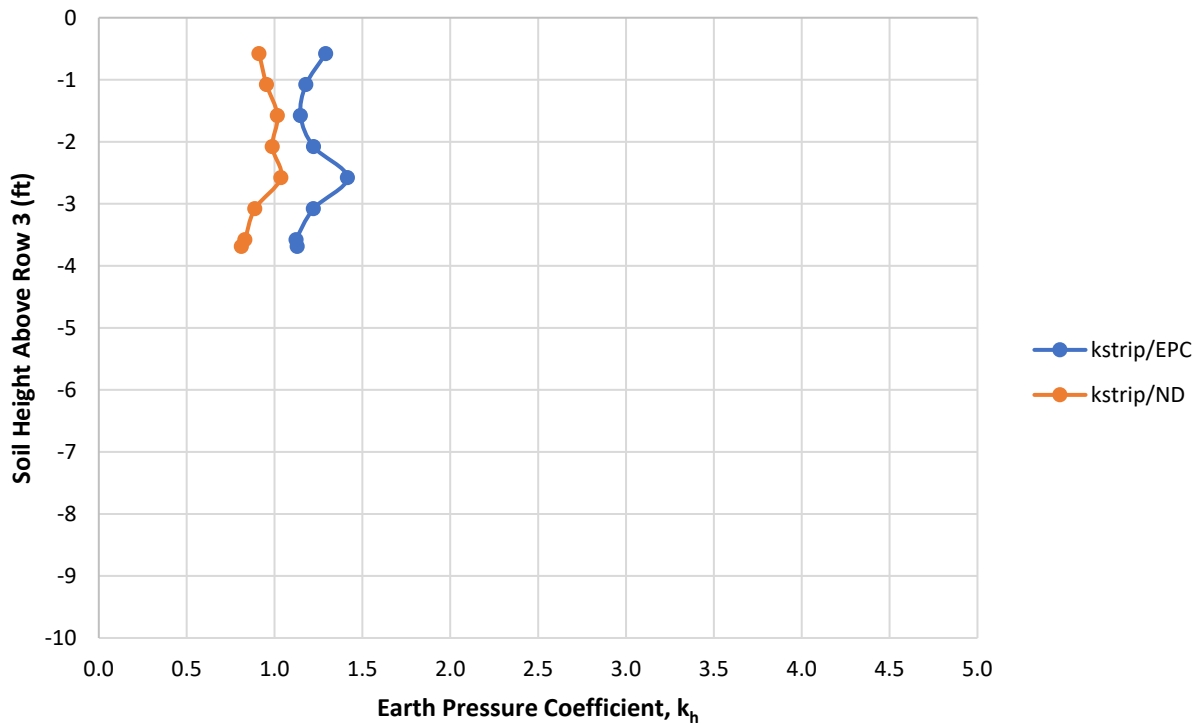


Figure 5-67. Row 3 – 103% compaction earth pressure coefficients from reinforcement strips.

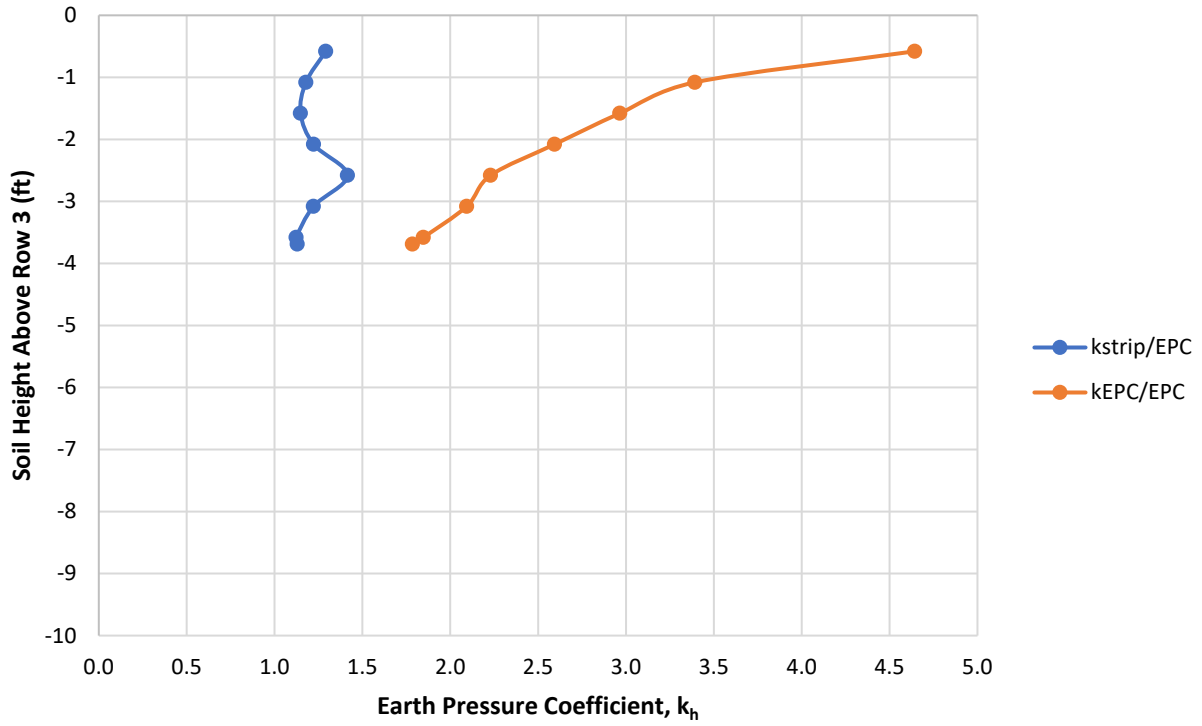


Figure 5-68. Comparing Row 3 – 103% compaction  $k_h$  using vertical stress from EPCs.

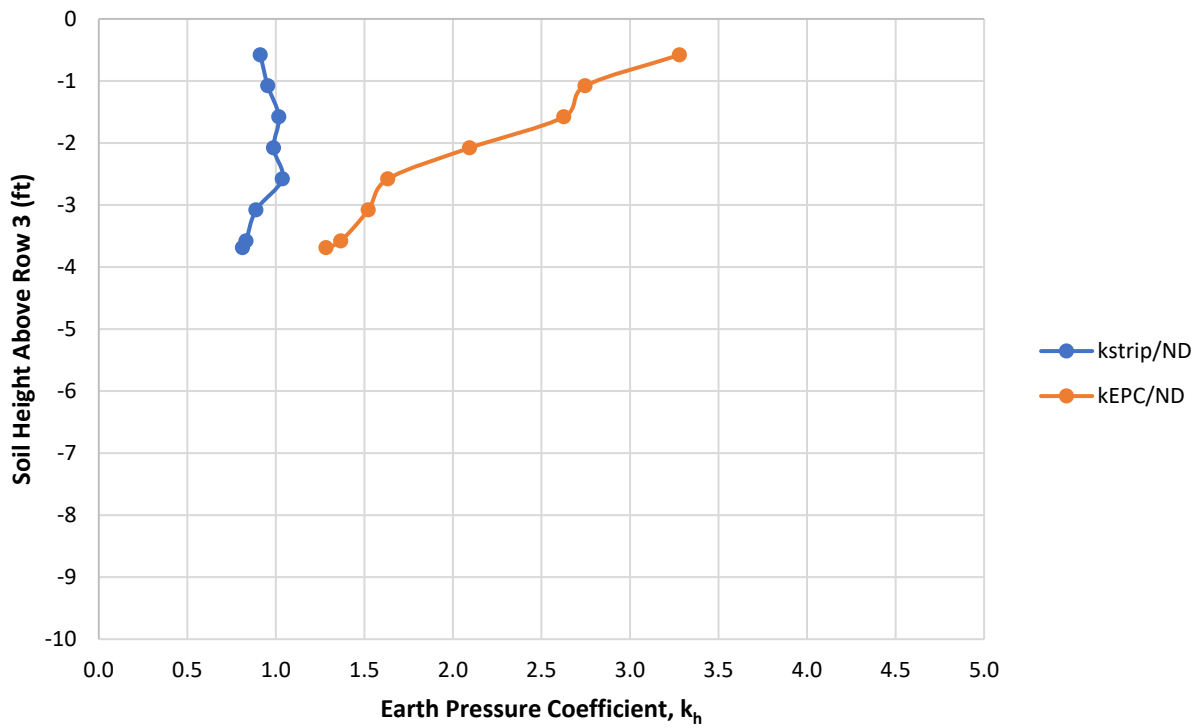


Figure 5-69. Comparing Row 3 – 103% compaction  $k_h$  using vertical stress from nuclear density.

## 5.6 Row 4 Construction Analysis

### 5.6.1 Row 4 Vertical Earth Pressure

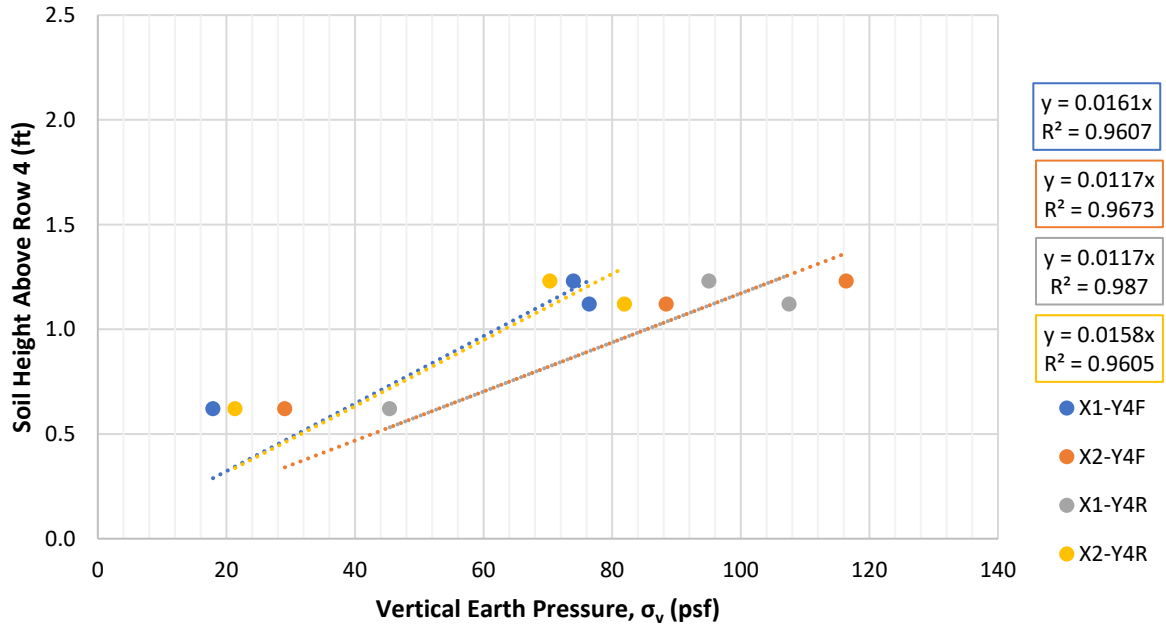


Figure 5-70. Row 4 – 95% compaction EPC vertical earth pressure vs. depth.



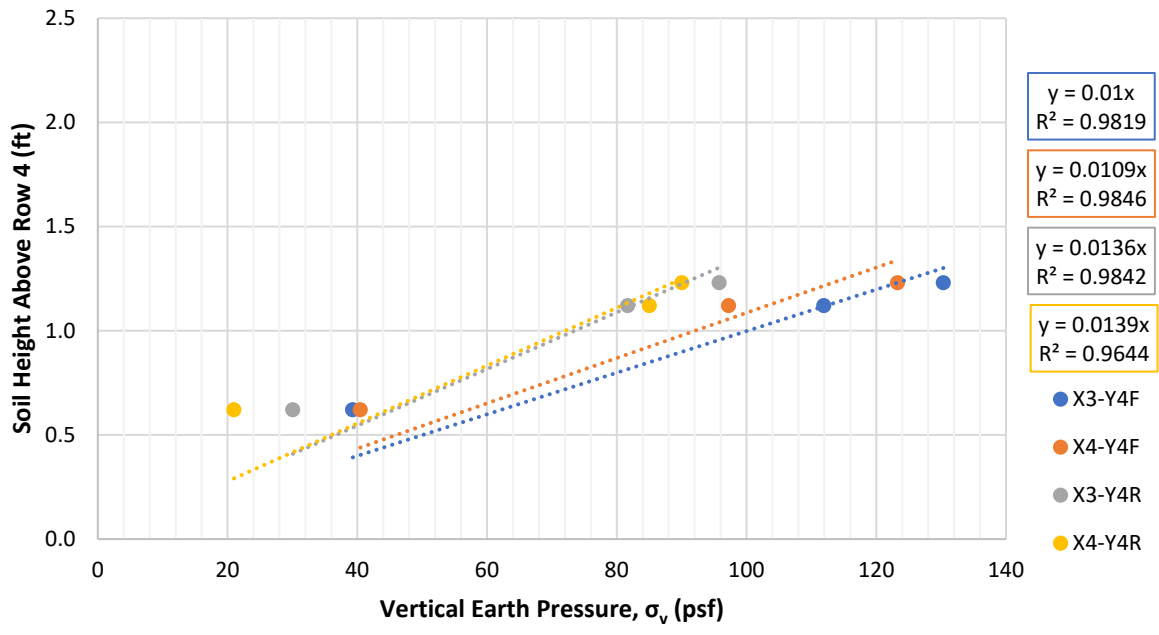


Figure 5-71. Row 4 – 103% compaction EPC vertical earth pressure vs. depth.

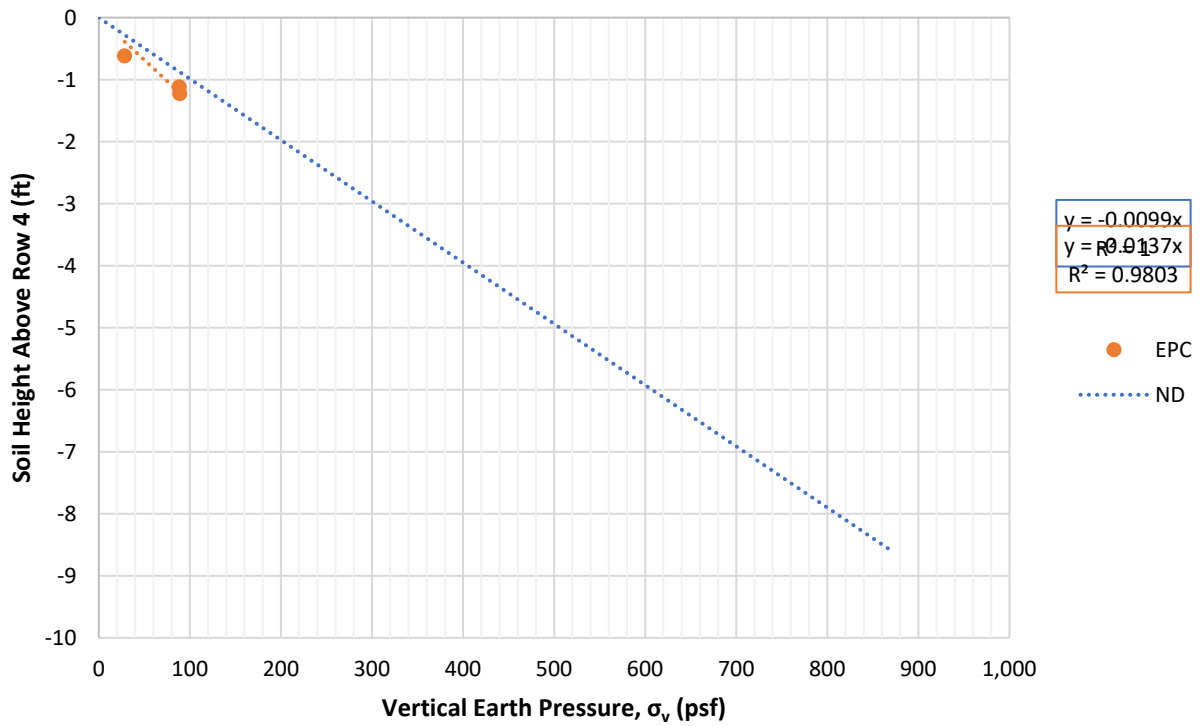


Figure 5-72. Row 4 – 95% compaction EPC earth pressure compared to nuclear density.

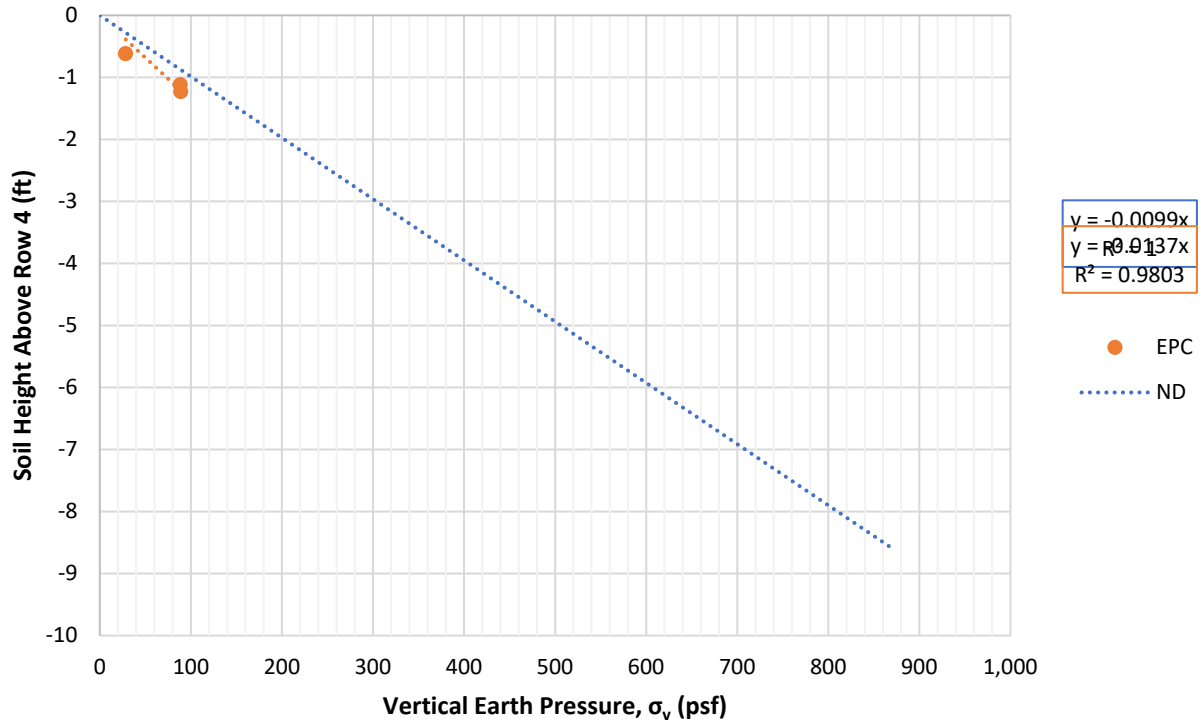


Figure 5-73. Row 4 – 103% compaction EPC earth pressure compared to nuclear density.

5.6.2 Row 4 Horizontal Earth Pressure

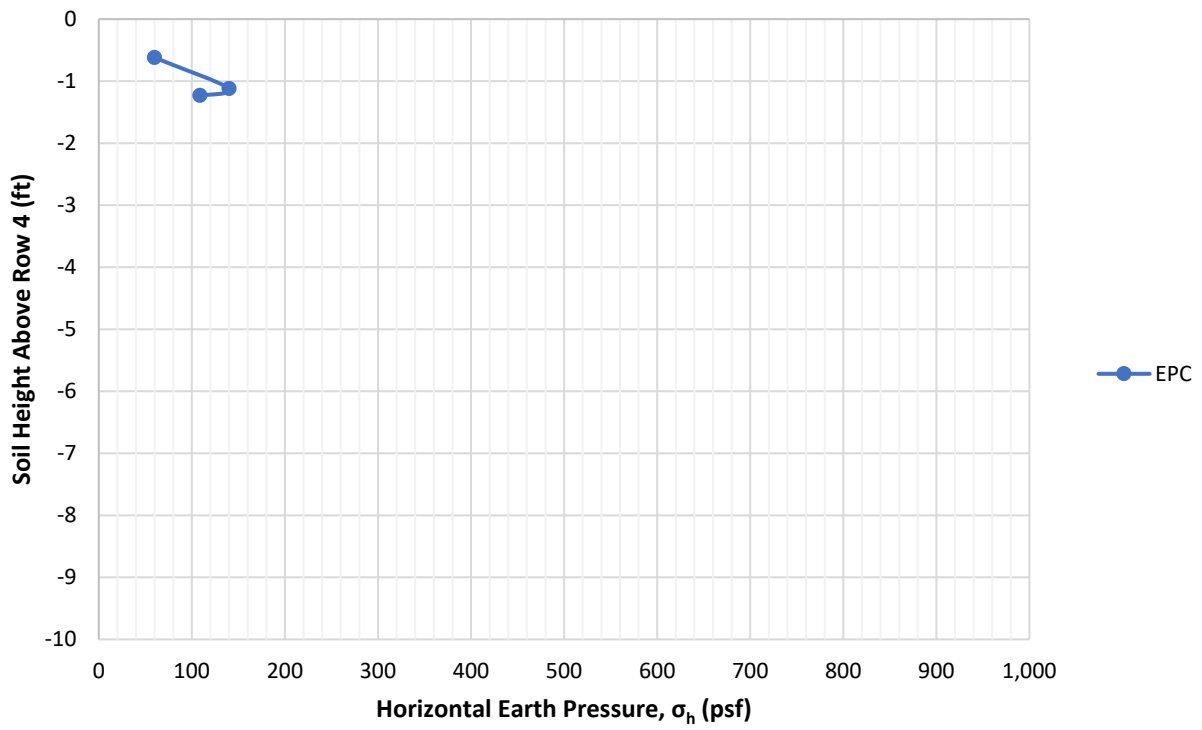


Figure 5-74. Row 4 – 95% compaction EPC horizontal earth pressure vs. depth.

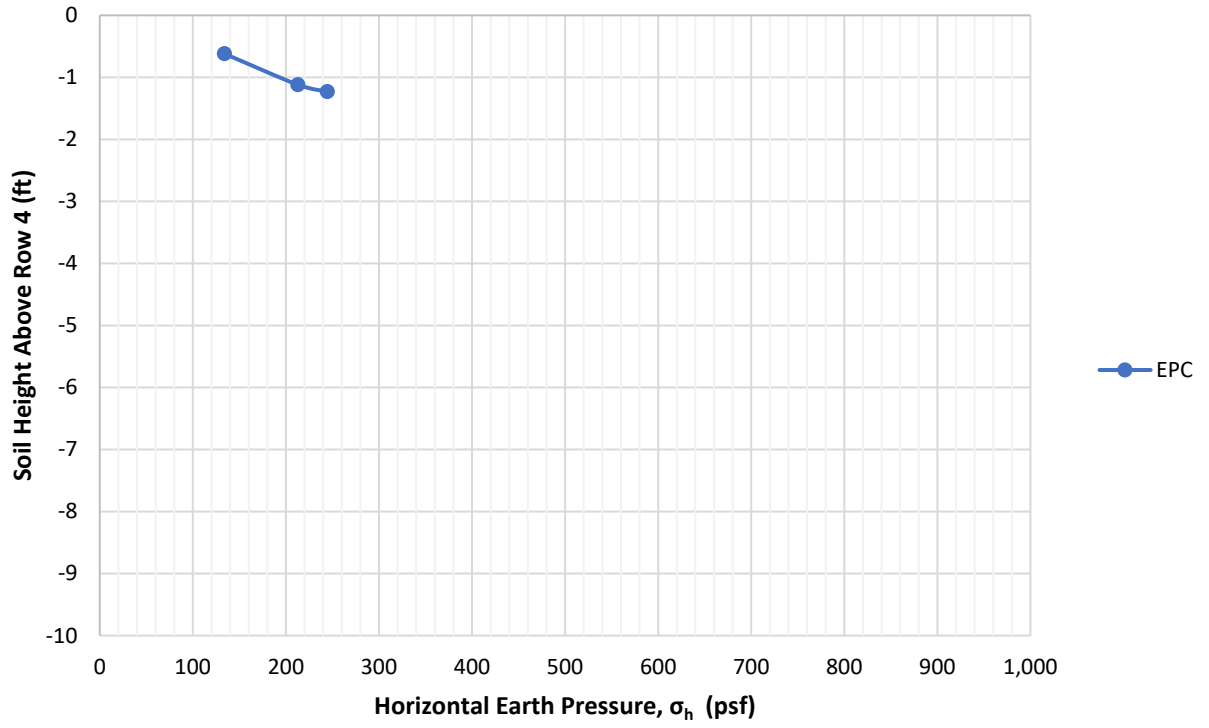


Figure 5-75. Row 4 – 103% compaction EPC horizontal earth pressure vs. depth.

### 5.6.3 Row 4 Reinforcement Strip Tension

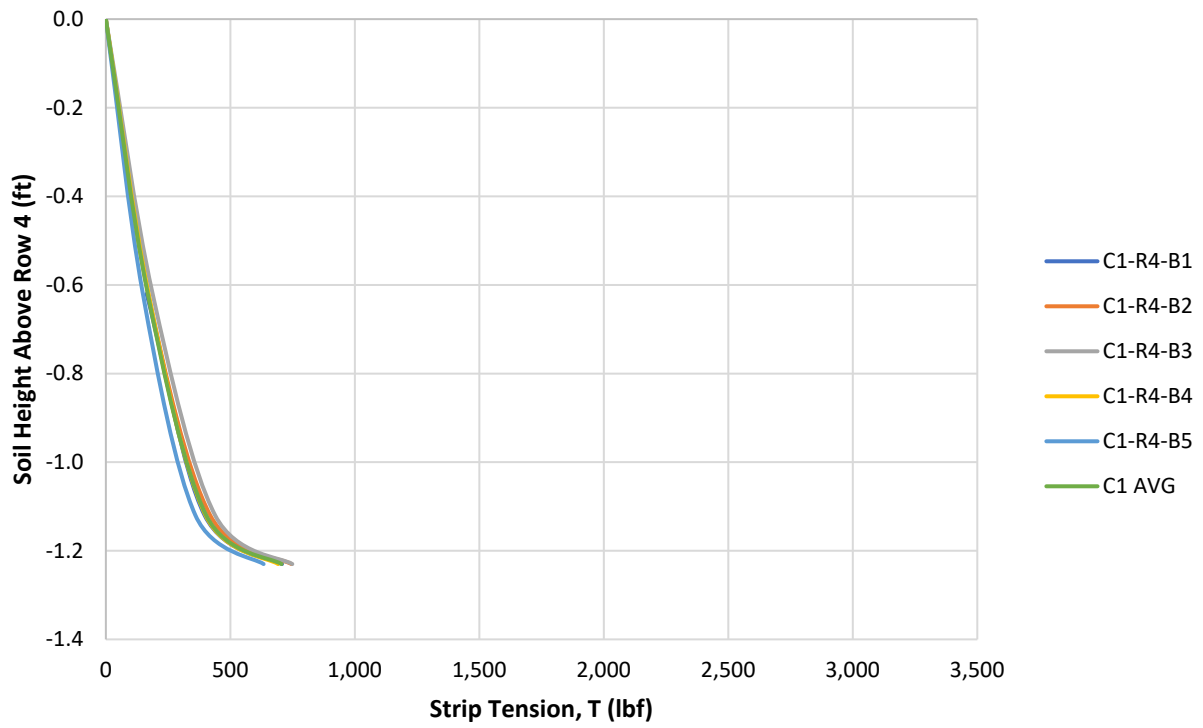


Figure 5-76. Row 4 – Column 1 - 95% compaction reinforcement strip tension vs. depth.

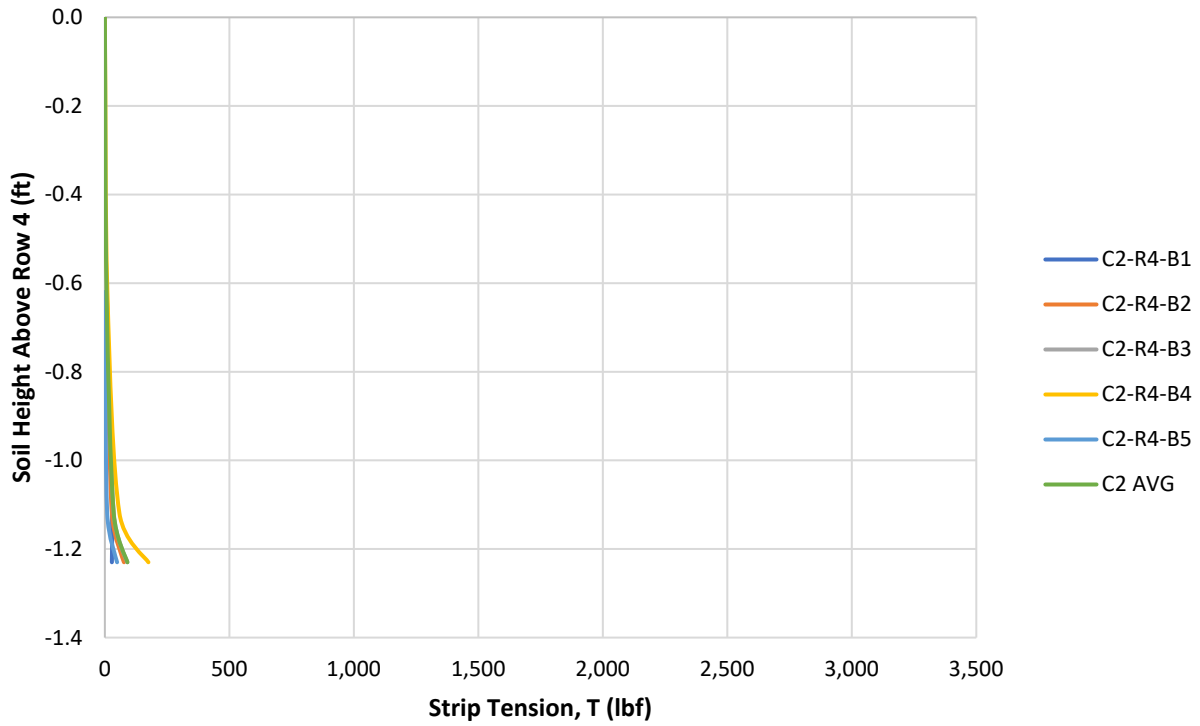


Figure 5-77. Row 4 – Column 2 - 95% compaction reinforcement strip tension vs. depth.

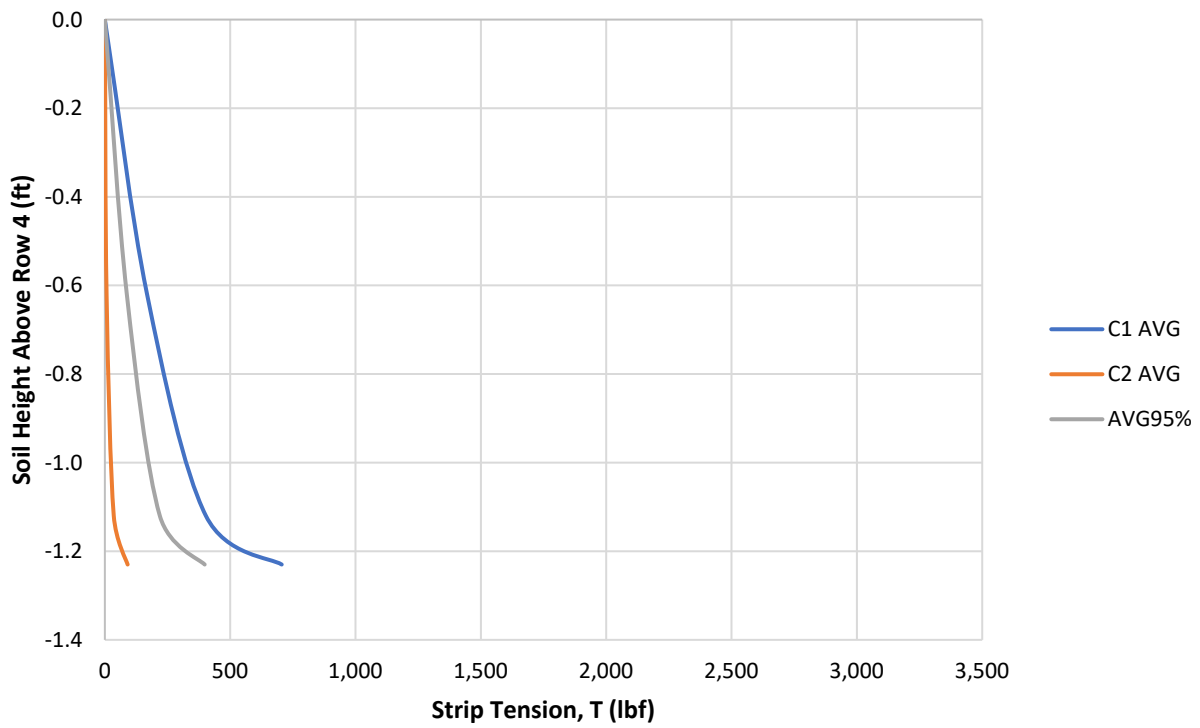


Figure 5-78. Row 4 – 95% compaction average reinforcement strip tension vs. depth.

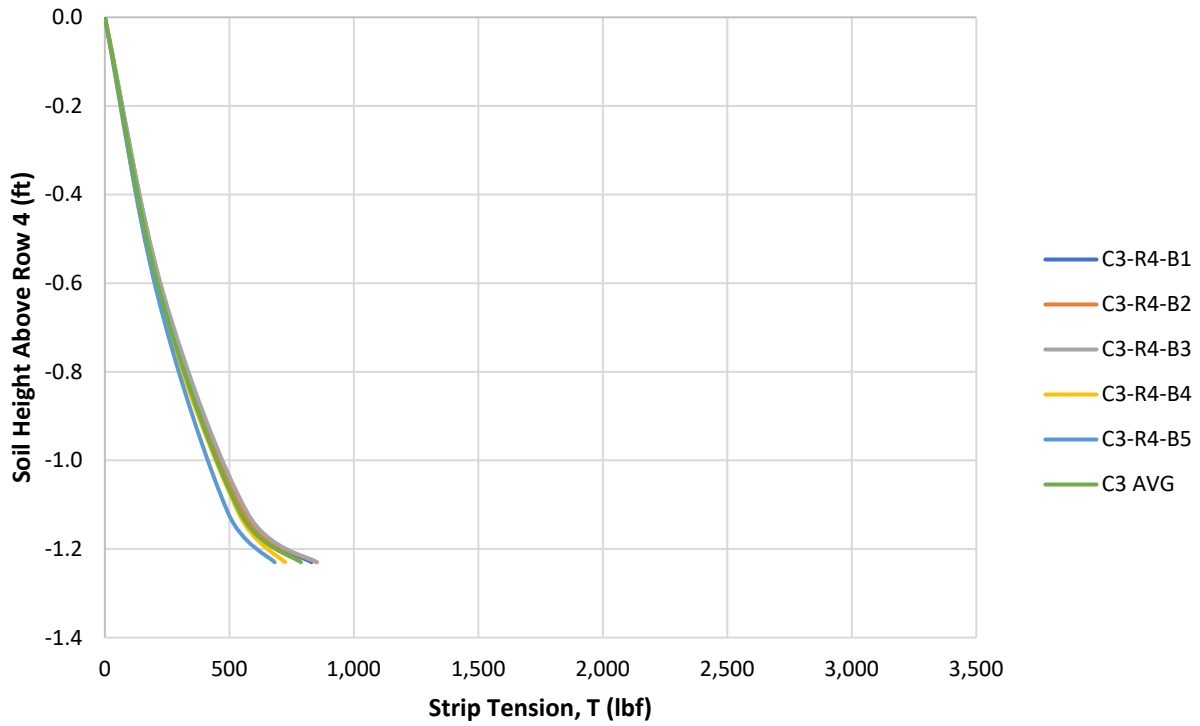


Figure 5-79. Row 4 – Column 3 - 103% compaction reinforcement strip tension vs. depth.

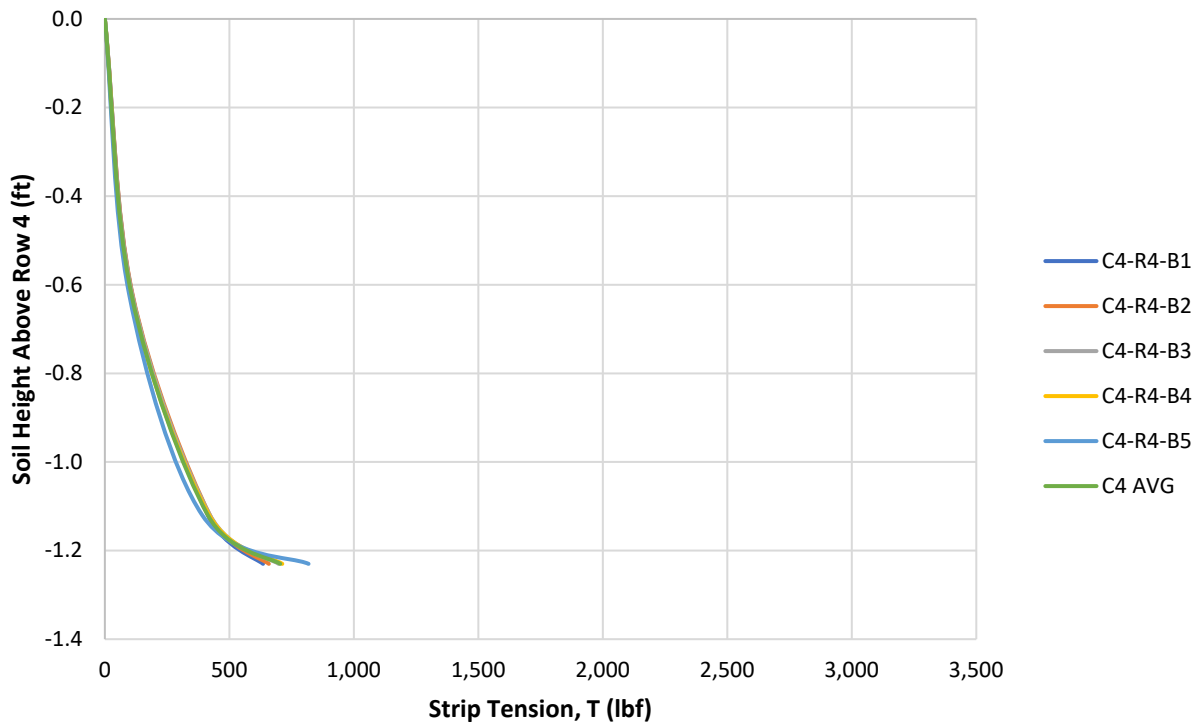


Figure 5-80. Row 4 – Column 4 - 103% compaction reinforcement strip tension vs. depth.

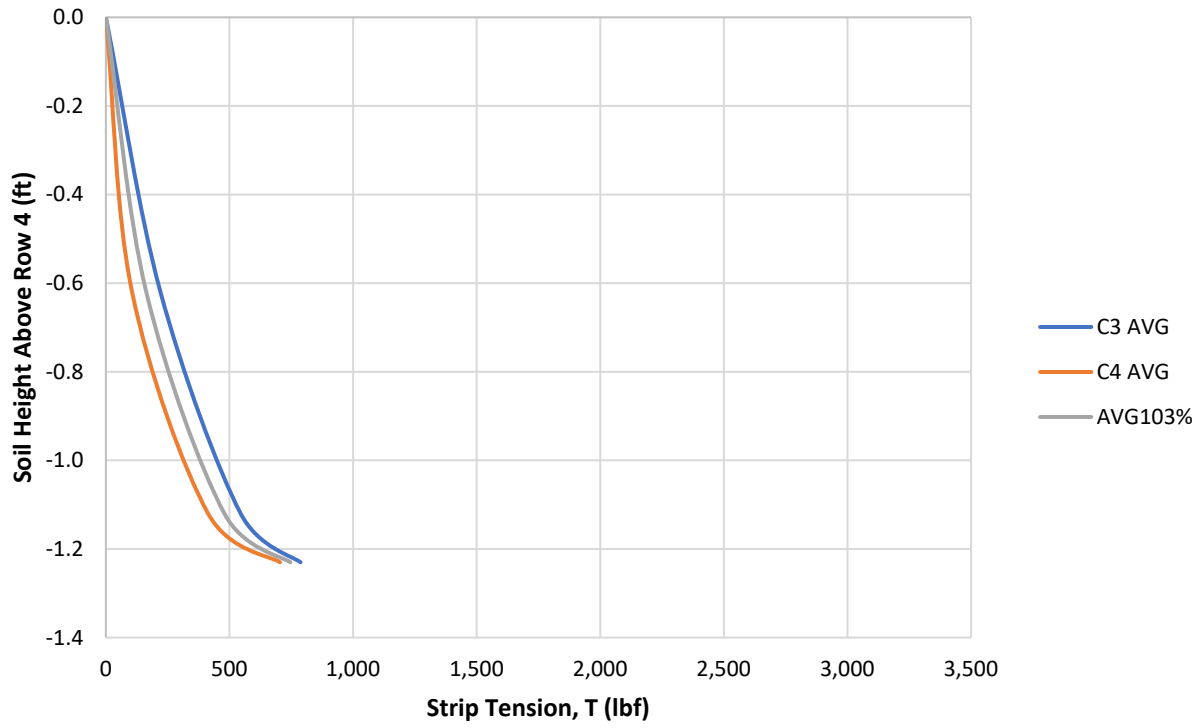


Figure 5-81. Row 4 – 103% compaction average reinforcement strip tension vs. depth.



5.6.4 Row 4 Average Earth Pressures and Strip Tension

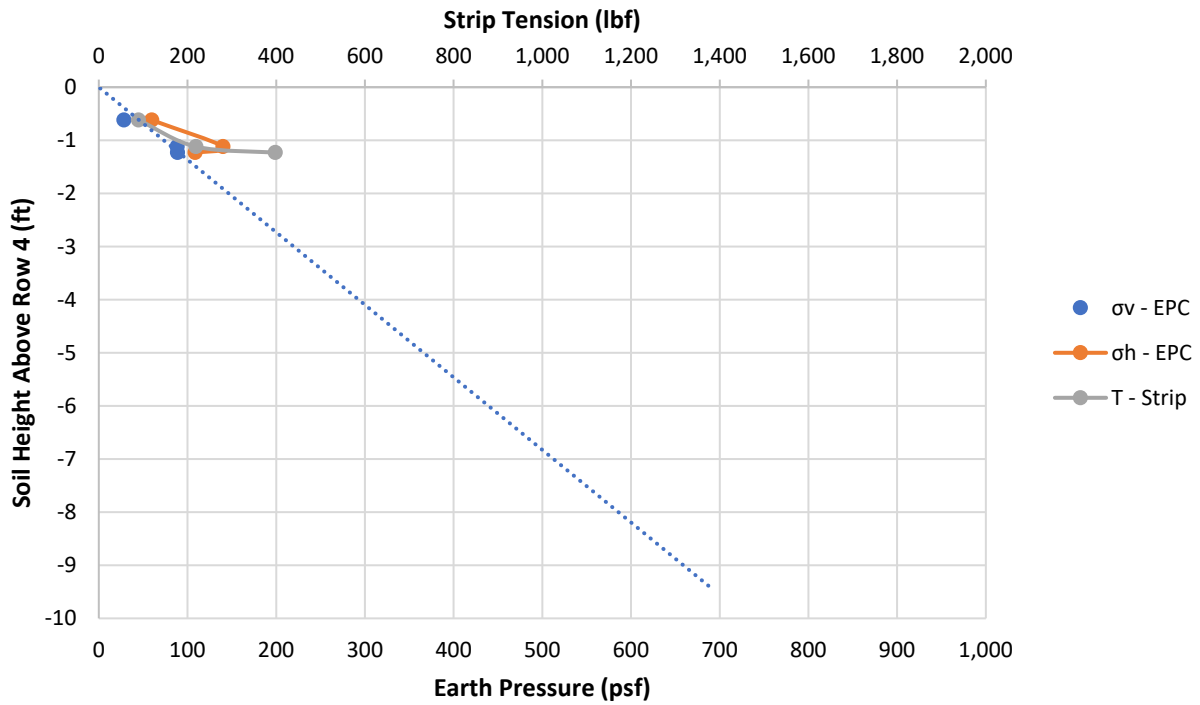


Figure 5-82. Row 4 – 95% compaction vertical and horizontal stress and strip tension vs. depth.

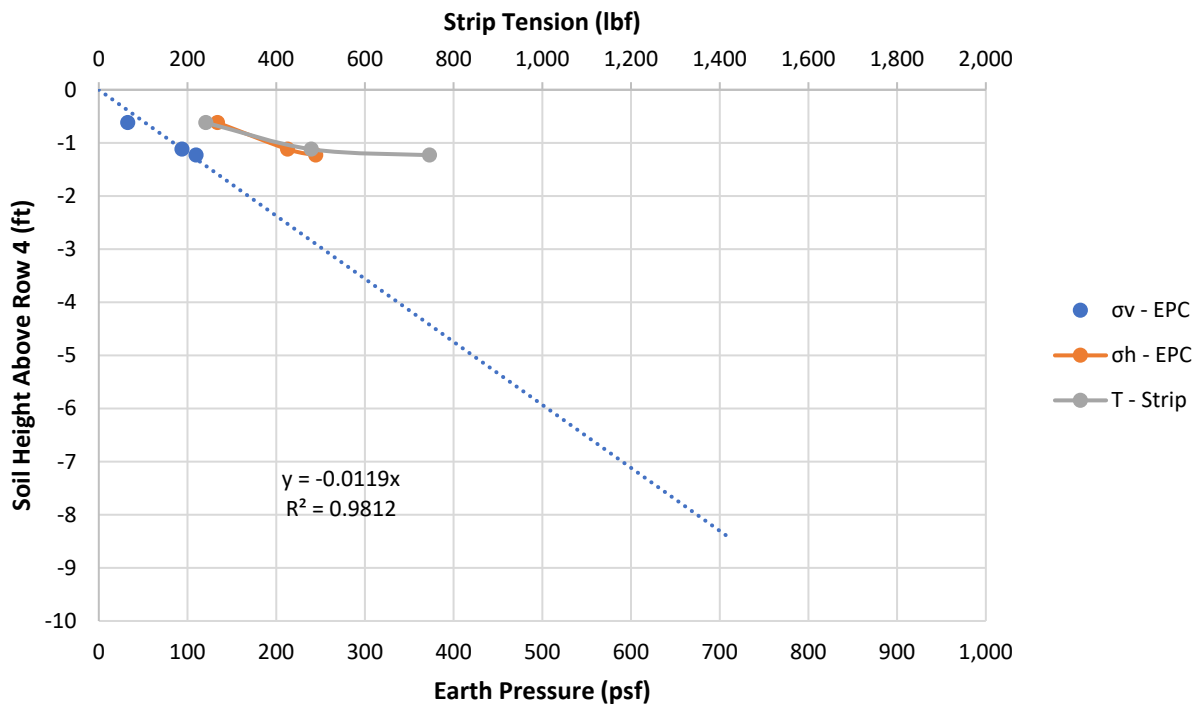


Figure 5-83. Row 4 – 103% compaction vertical and horizontal stress and strip tension vs. depth.

5.6.5 Row 4 Construction Earth Pressure Coefficient Analysis – 95% of T-180

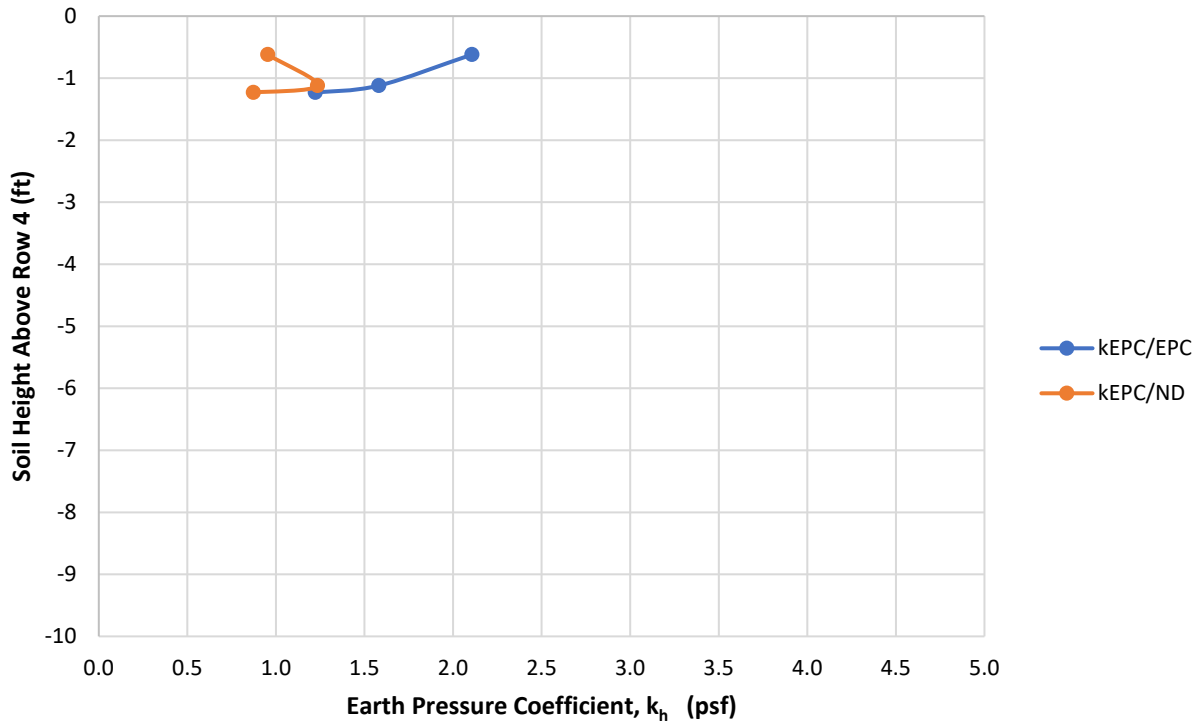


Figure 5-84. Row 4 – 95% compaction earth pressure coefficients from EPCs.

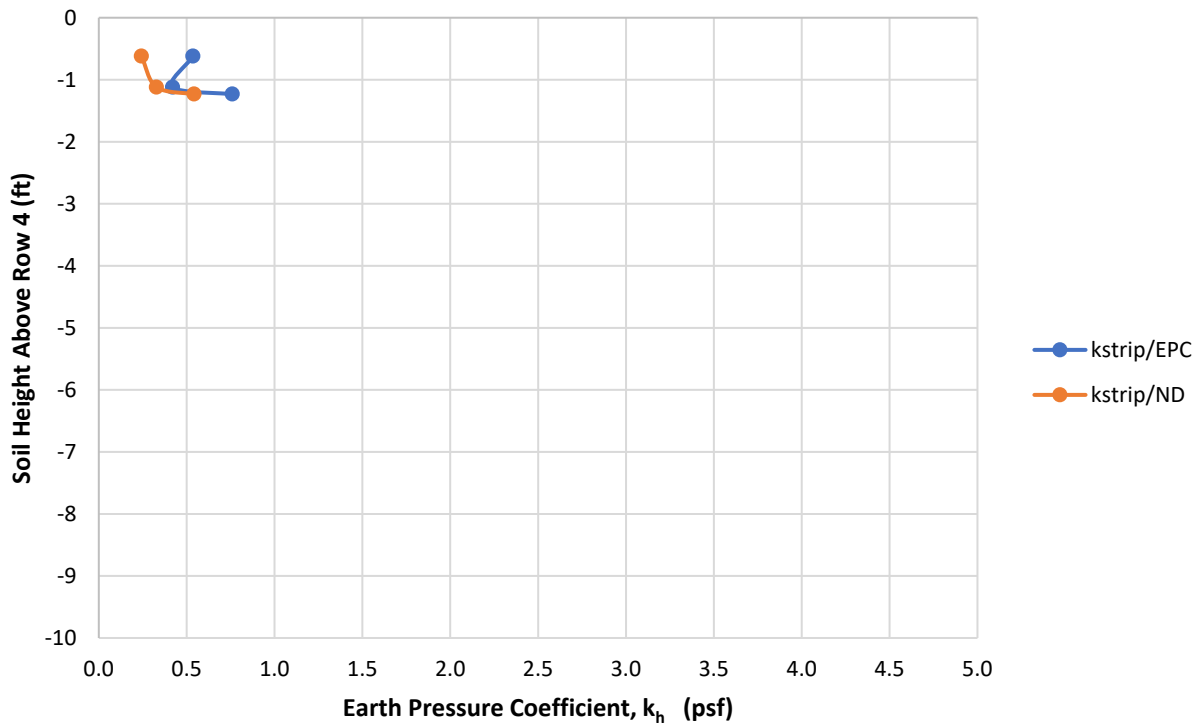


Figure 5-85. Row 4 – 95% compaction earth pressure coefficients from reinforcement strips.

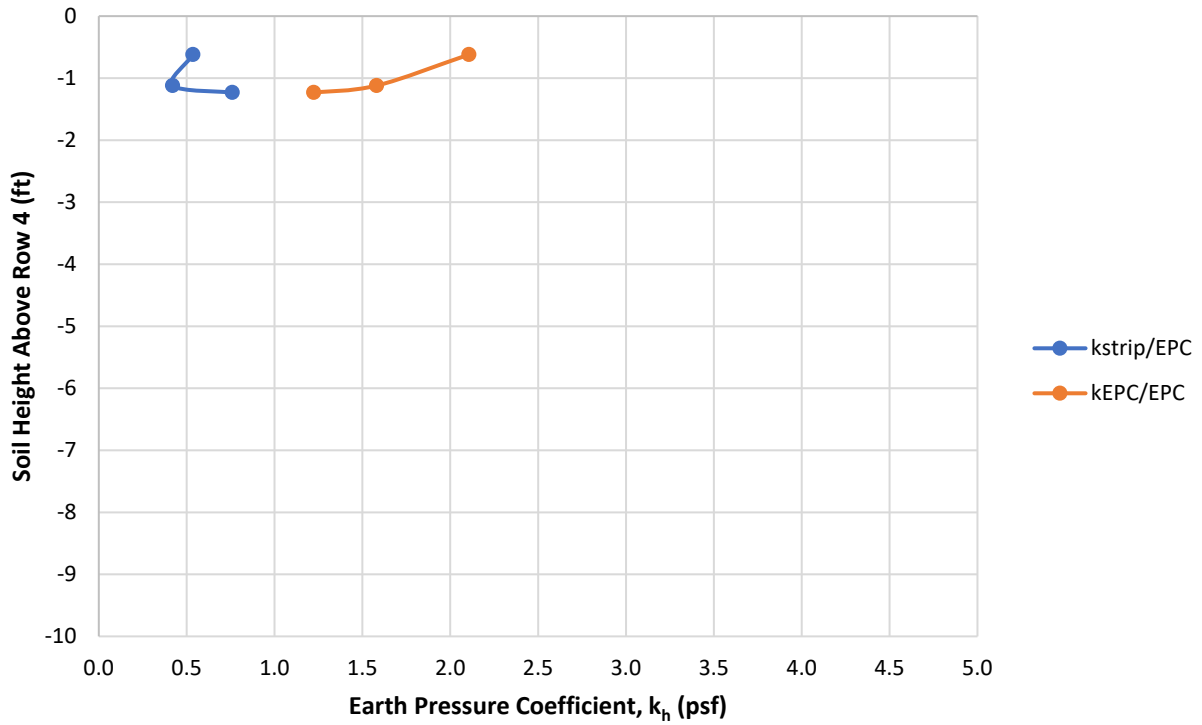


Figure 5-86. Comparing Row 4 – 95% compaction  $k_h$  using vertical stress from EPCs.

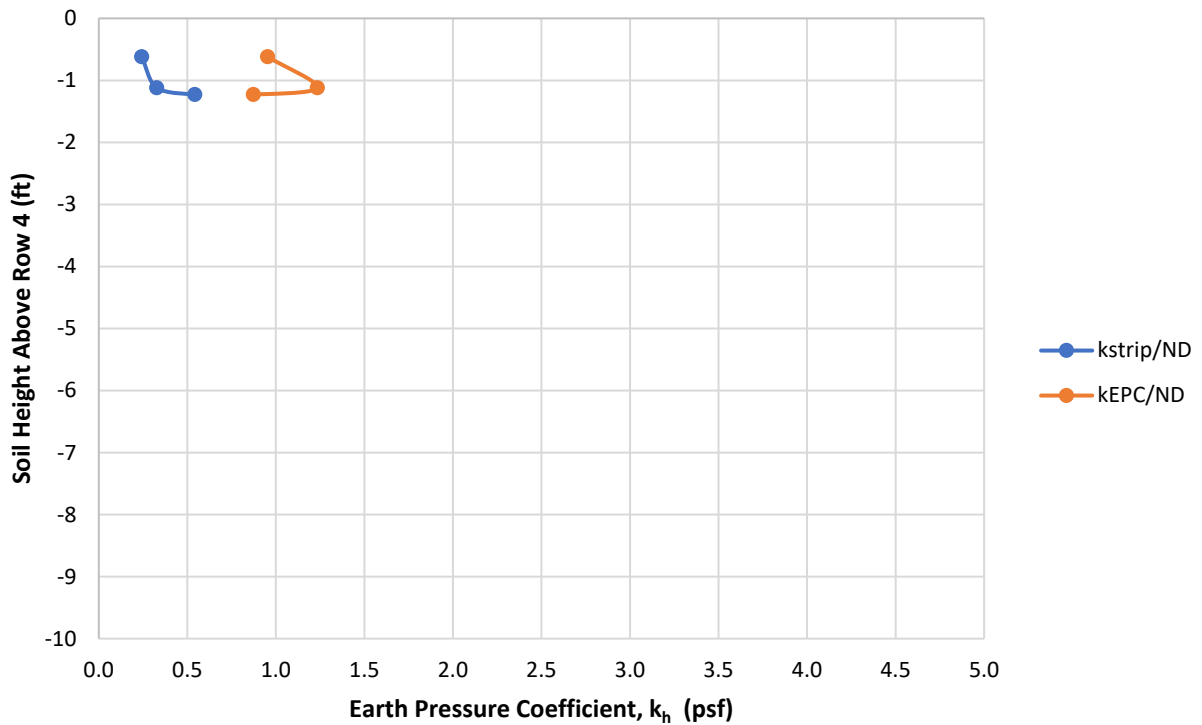


Figure 5-87. Comparing Row 4 – 95% compaction  $k_h$  using vertical stress from nuclear density.

5.6.6 Row 4 Construction Earth Pressure Coefficient Analysis – 103% of T-180

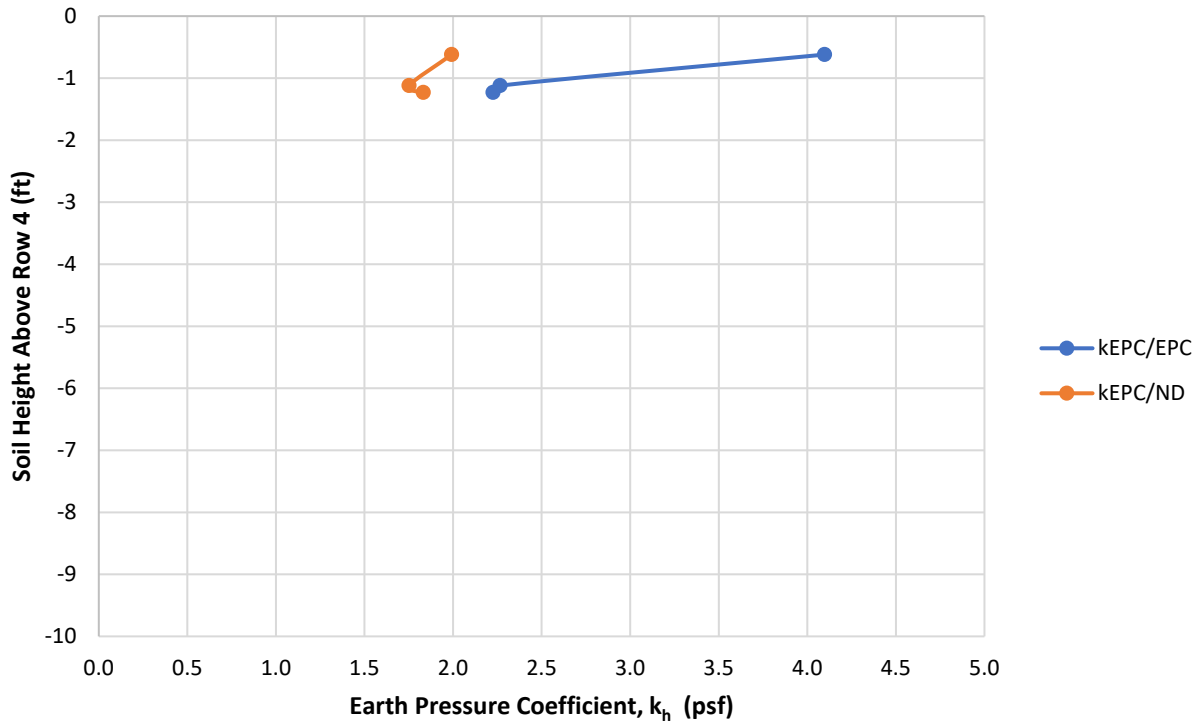


Figure 5-88. Row 4 – 103% compaction earth pressure coefficients from EPCs.

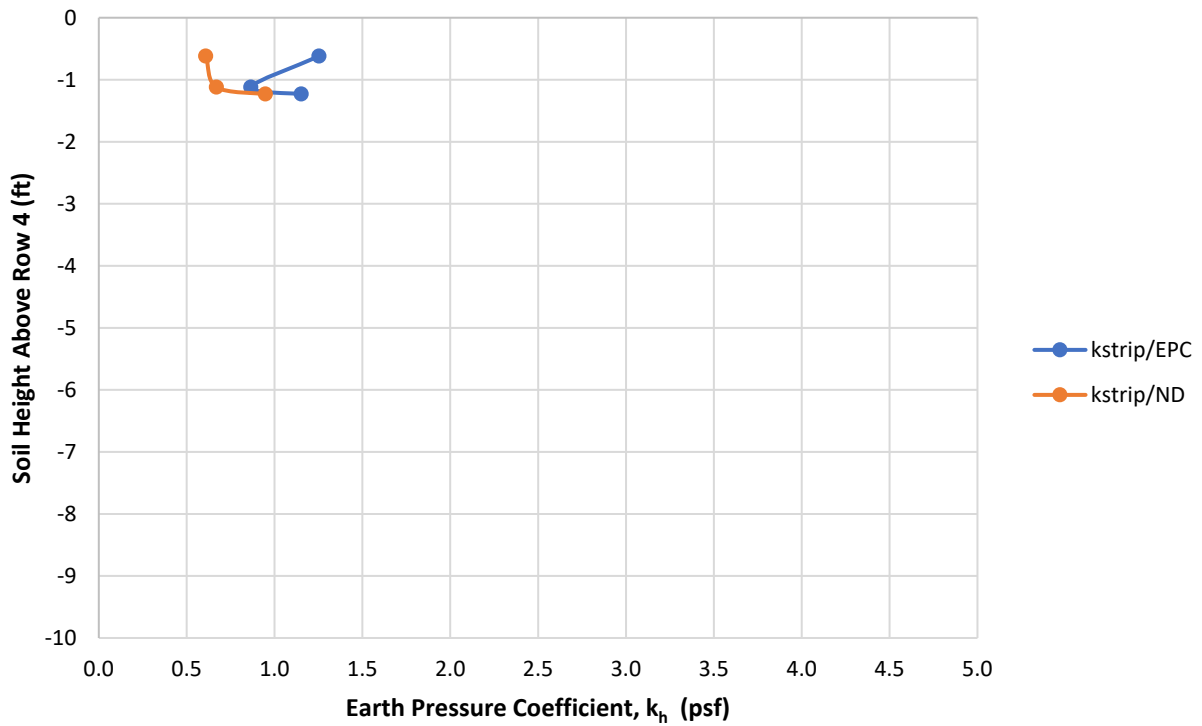


Figure 5-89. Row 4 – 103% compaction earth pressure coefficients from reinforcement strips.

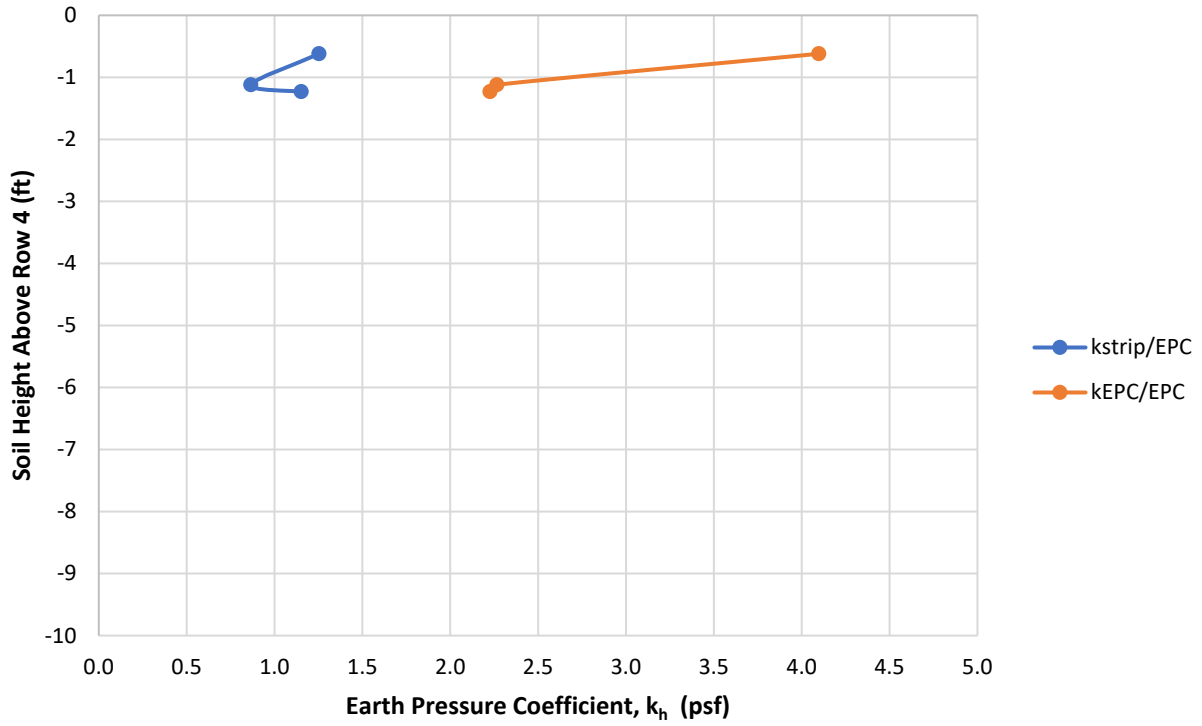


Figure 5-90. Comparing Row 4 – 103% compaction  $k_h$  using vertical stress from EPCs.

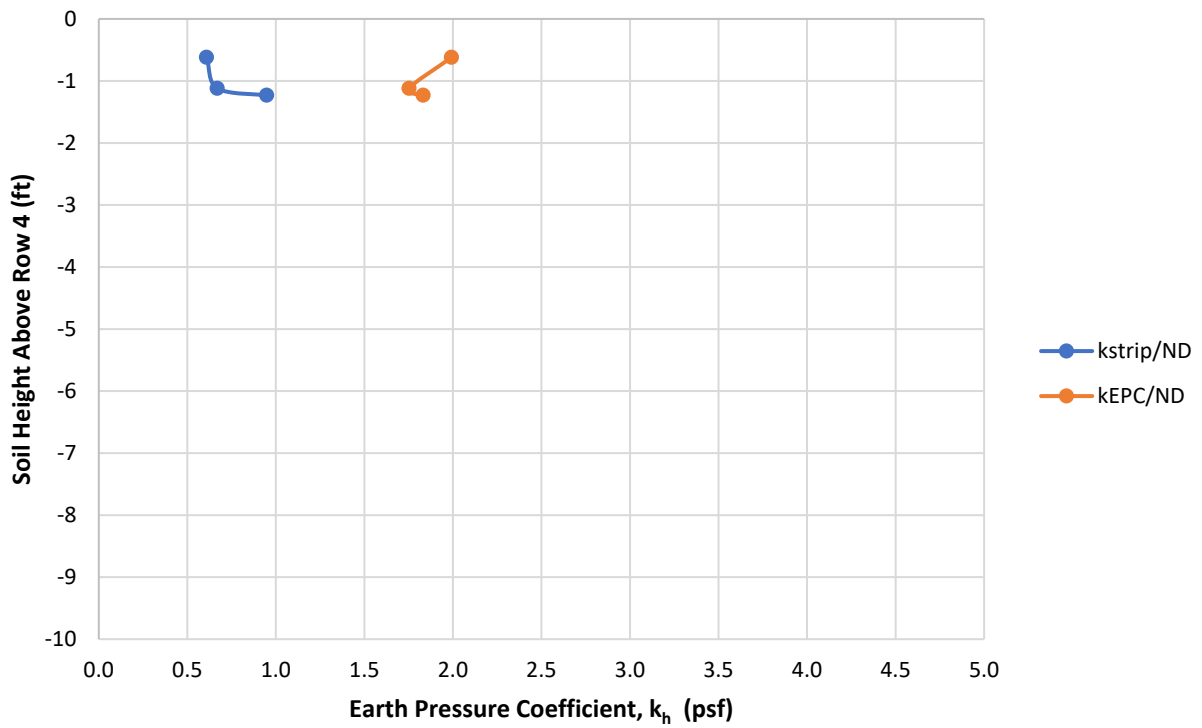


Figure 5-91. Comparing Row 4 – 103% compaction  $k_h$  using vertical stress from EPCs.

## 5.7 *Leveling Pad EPC Construction Analysis*

The earth pressures that developed in the EPCs underneath the leveling pads were found to produce a non-linear trend, Figures 5-92 to 5-94. However, the trends were influenced by the addition of wall panels and not just soil weight. Consequently, the leveling pad pressures are compared to the weight of the estimated soil column acting on the leveling pad and the weight of the walls (S+W) in each of the figures.

At the start of continuous recording, the depth of soil in the reinforced zone was 1.23 feet. At this point, the soil within the reinforced zone was prevented from interacting with the wall panels due to the construction specifications of not backfilling against the wall until after the first lift above the first row of reinforcements. The next lift of soil above this level was then allowed to be compacted to the wall panels. This was also the time where earth pressures and strip tensions were first recorded within the reinforced zone. Therefore, the leveling pad EPC depths are referenced to the soil height above Row 1.

Early in the construction process, the 103% side began to deviate from the 95% side and showed a larger increase in vertical earth pressure with respect to depth. This further suggested that down drag stresses (shear stress at the soil-wall interface) began developing on the wall in the 103% side due to the high compaction effort. At a depth of 3.23 feet, the earth pressure underneath the front wall on the 103% side exceeded the earth pressure within the reinforced zone based on the nuclear density results, further validating the hypothesis. Throughout the entire construction process, only the front wall on the 103% side showed higher vertical earth pressure than the reinforced zone. This suggests that the unyielding wall (back MSE wall) was less affected by down drag stresses due to its fixed position, whereas the front wall would be more prone due to potential rotational forces. Figures 5-95 and 5-96 present the wall displacement for the 95% side and 103% side, respectively. Observed in Figure 5-96, for the 103% side, the base of the wall initially moved away from the soil during construction but eventually began moving inward towards the soil, beyond its initial location, after the temporary braces were removed, further indicating rotational forces were acting on the wall. For both compaction efforts, the base of the wall did move inward towards the soil after the braces were removed, but the 95% side did not move beyond its original position as observed on the 103% side. This occurrence on the 103% was likely a result of the greater compaction effort that was able to be achieved above the Row 2 level of reinforcements as indicated by the nuclear density results. This is further supported by Figure 5-14 where strain gauge C4-R1-B1, the closest strain gauge location to the wall panels where displacement was measured, moved from tension to compression after the wall panel temporary bracing was removed. Additionally, the average strip tensions on the 103% side were higher than the 95% side during construction.

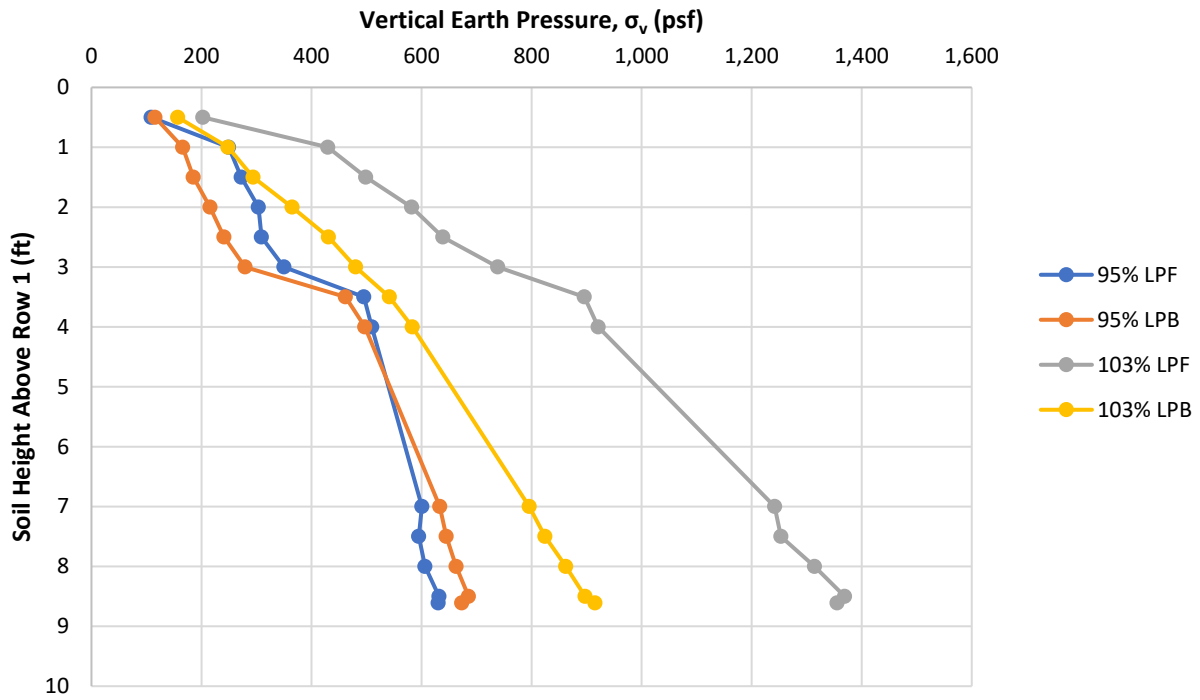


Figure 5-92. EPC vertical earth pressures under the leveling pads vs. depth.

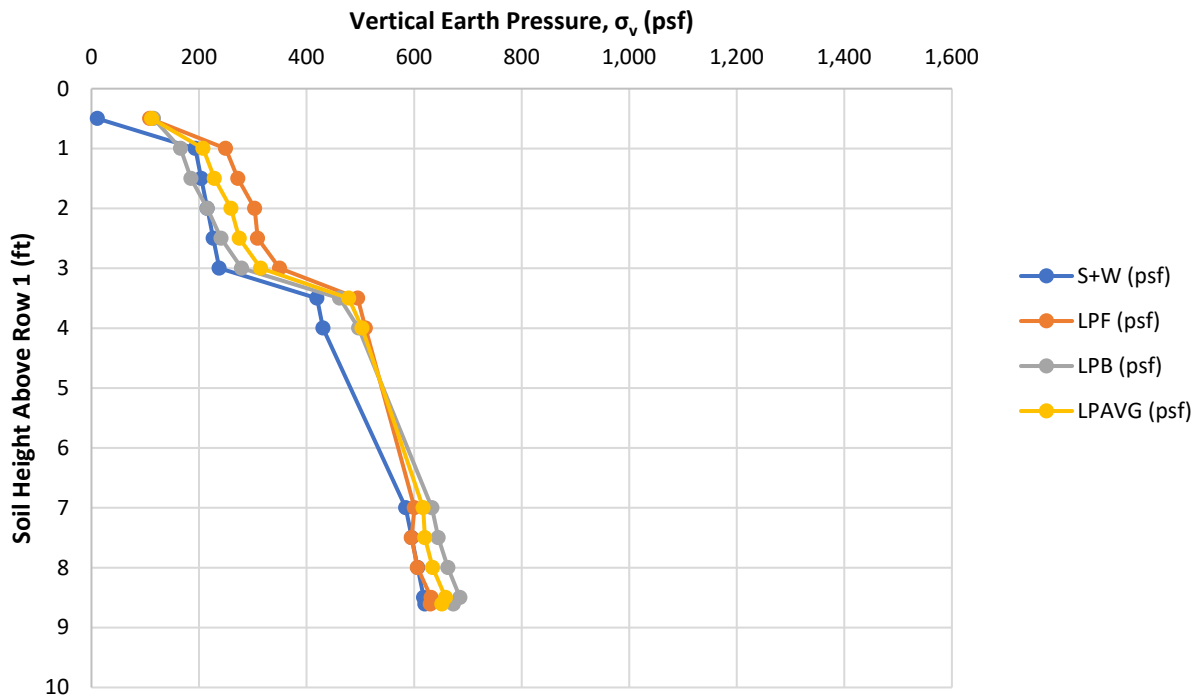


Figure 5-93. 95% compaction leveling pad pressures compared to the soil and wall weight.

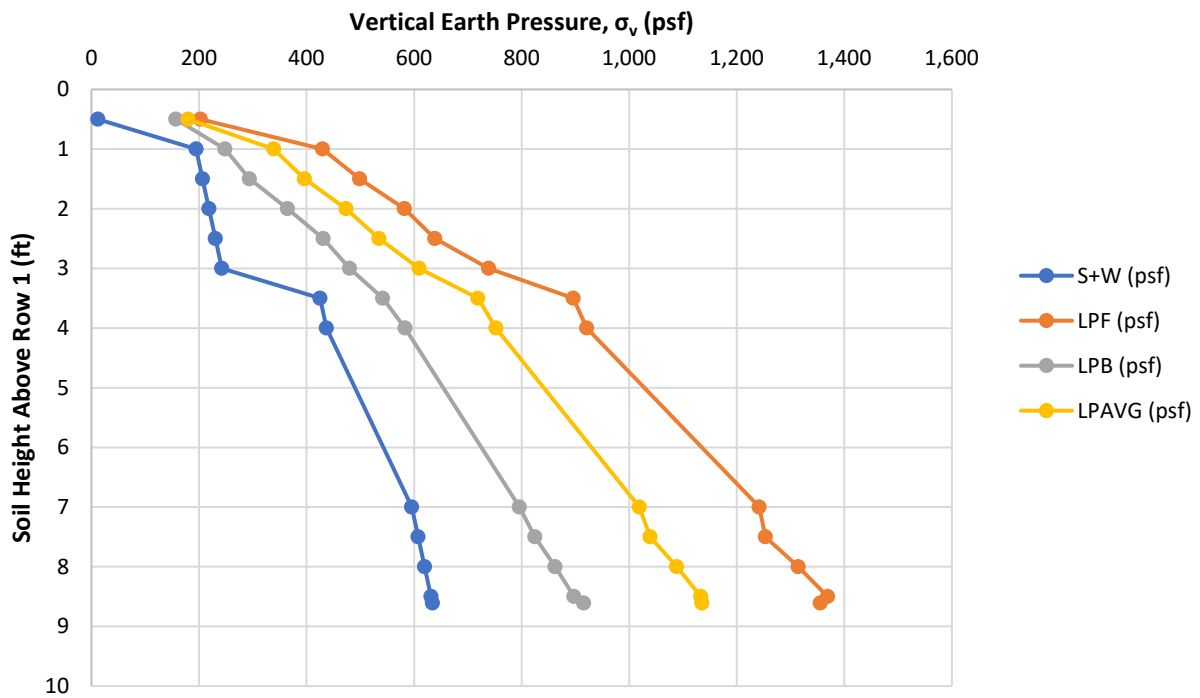


Figure 5-94. 103% compaction leveling pad pressures compared to the soil and wall weight.

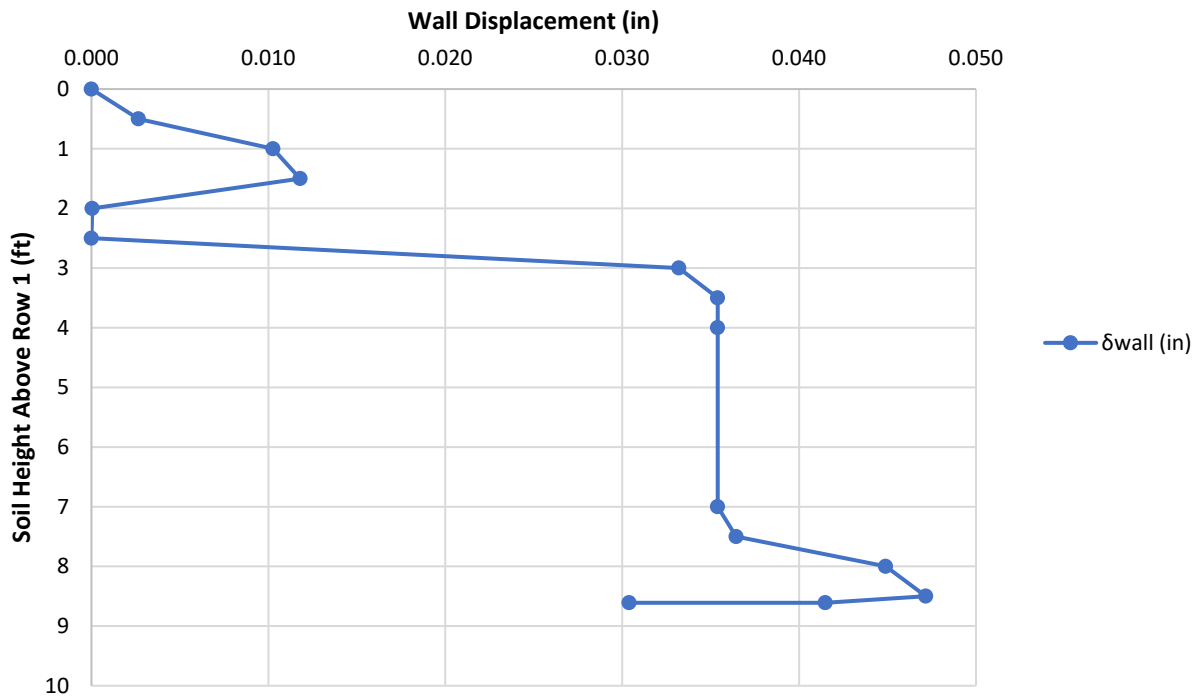


Figure 5-95. Wall displacement on the 95% of T-180 side.



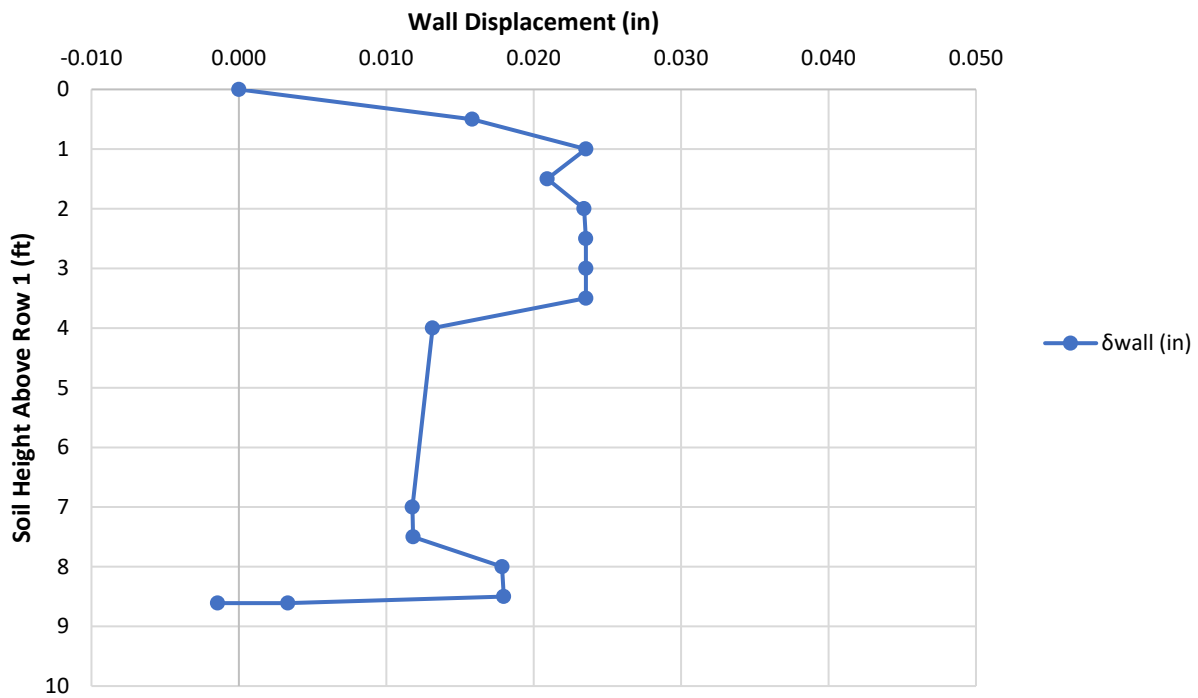


Figure 5-96. Wall displacement on the 103% of T-180 side.

### 5.8 Earth Pressure Coefficient Construction Analysis

Earth pressure coefficient construction analysis began by deriving an earth pressure coefficient for each depth recorded in each row. This was completed using the EPC lateral earth pressures and strip tributary area lateral earth pressures divided by the soil embedded EPC vertical earth pressures. Nuclear density was not considered for this part of the analysis because the results would not be applicable to the surcharge loading results in which nuclear density testing did not take place. Figure 5-97 provides the 95% side results and Figure 5-98 provides the 103% side results. As previously identified, there is more separation in the 95% side EPC and strip coefficients due to the loosened state of the reinforcement strips from under compacting the reinforced zone. Figure 5-99 combines all derived coefficients with an averaged equation curve presented. The “AVG EQN” curve was derived by averaging the earth pressure coefficients for each foot of depth as indicated in Figure 5-100.

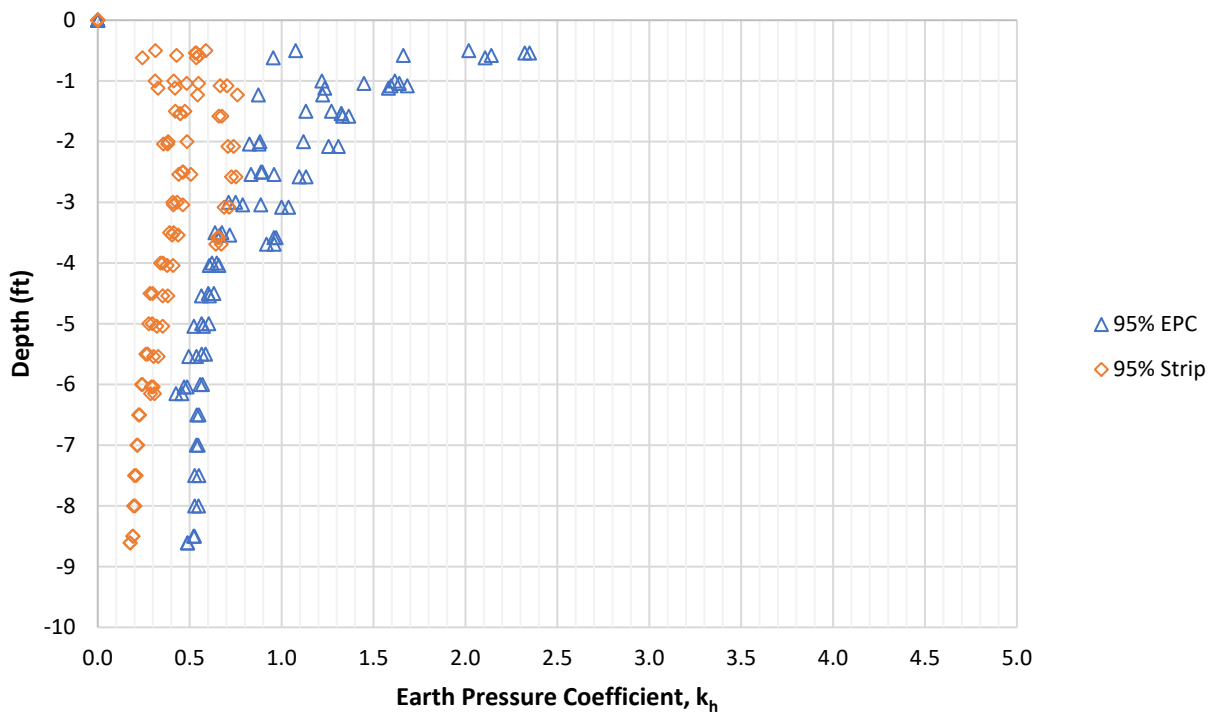


Figure 5-97. Comparing 95% of T-180 earth pressure coefficients from EPCs and strips vs. depth.

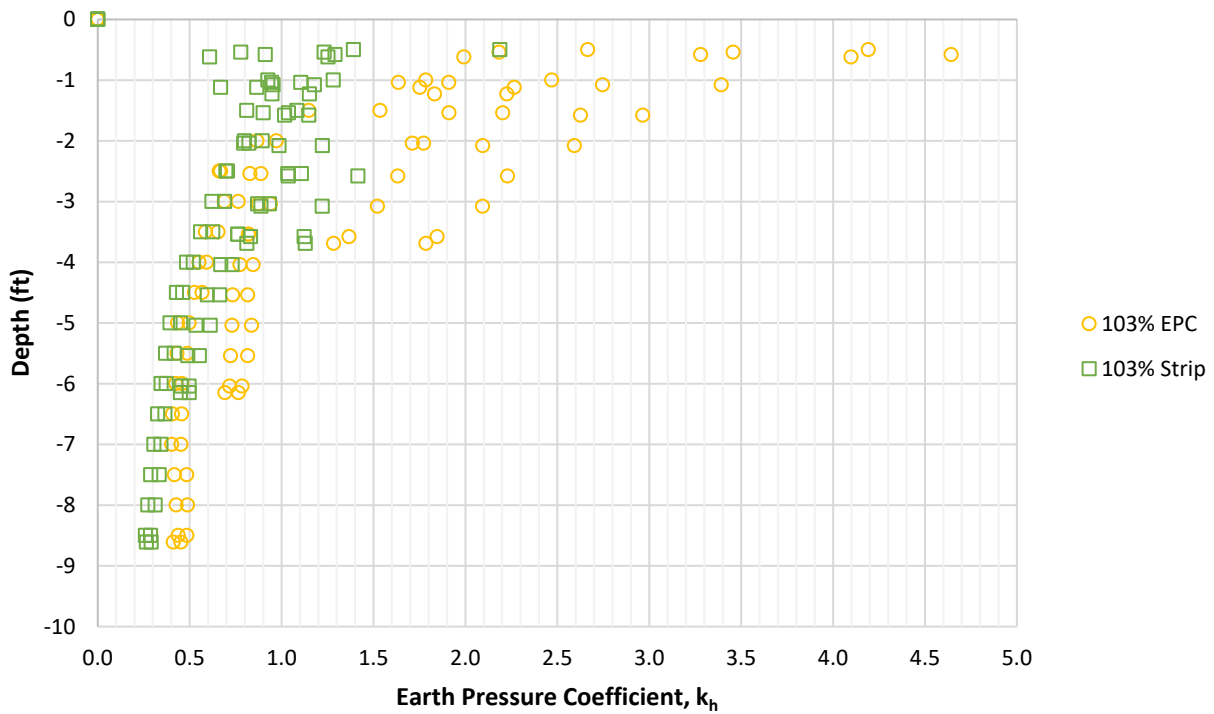


Figure 5-98. Comparing 103% of T-180 earth pressure coefficients from EPCs and strips vs. depth.

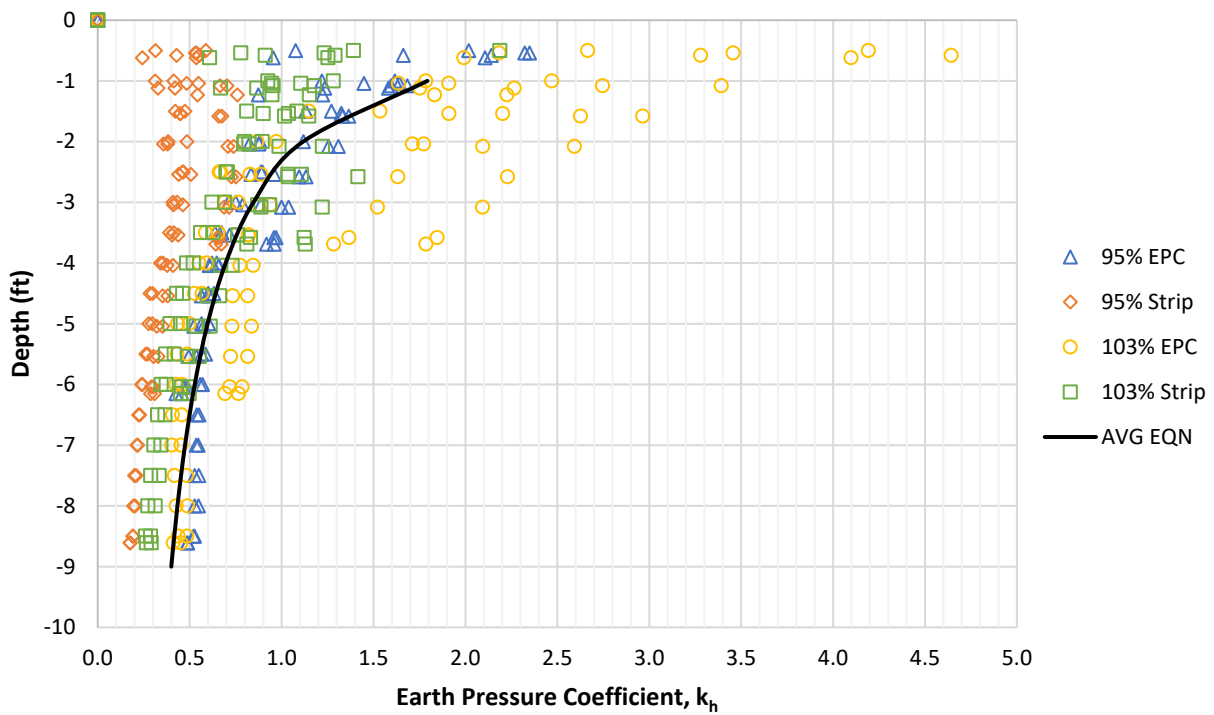


Figure 5-99. All earth pressure coefficients from EPCs and strips vs. depth.

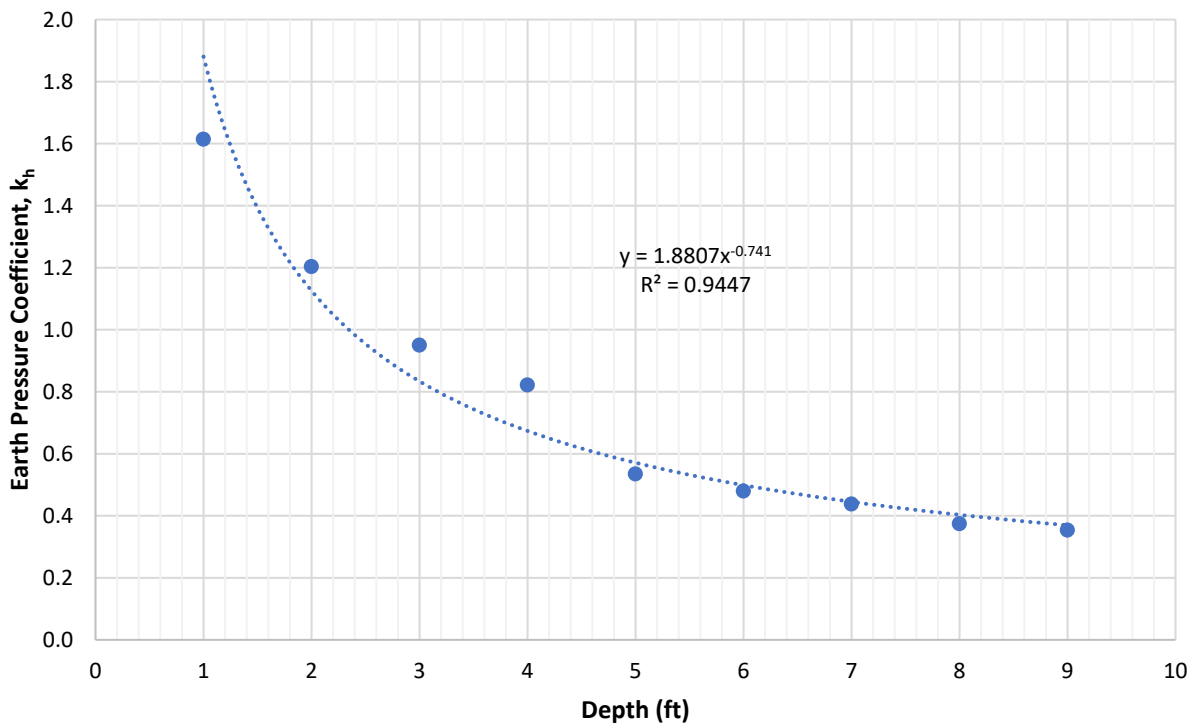


Figure 5-100. Average earth pressure coefficients as a function of depth including EPCs and strips.

Because the reinforcement strips may not be fully engaged during construction, and the EPCs are likely more accurate in measuring the lateral earth pressure, further analysis was conducted using only the EPC data. This analysis is presented in Figures 5-101 through 5-106. Figure 5-101 provides the results from the 95% side with an average equation derived as previously discussed and presented in Figure 5-102. As seen in Figure 5-101, the 95% earth pressure coefficients generally followed the same trend, regardless of the reinforcement level. Conversely, the 103% side displayed large variability between the levels of reinforcement as seen in Figure 5-103 (Note: The average equation in Figure 5-103 is derived in Figure 5-104). This indicates that over compacting the soil likely results in larger stress concentrations and less predictable and higher lateral earth pressures during construction. However, this was not true for every row. When comparing Row 1 from the 95% side and the 103% side in Figure 5-105, a very similar trend emerged, and nearly identical earth pressure coefficients were found below a depth of 2.5 feet which was when the second level of strip reinforcements were added (Note: The average equation in Figure 5-105 is derived in Figure 5-106). This suggests that the specified construction method of not backfilling to the wall until after the first row of reinforcements resulted in a very similar development of lateral stress in Row 1, regardless of the compaction effort. This implies that if the same procedure were conducted for the rows above the first level of reinforcement, it may be possible to alleviate unwanted variability in the resulting lateral earth pressures. Consequently, the UF researchers suggest that this method of back filling and compaction could be used in future construction when two MSE walls are tied together. The first row would be constructed as currently specified and compaction would then take place up to one foot prior to the next level of reinforcement. Once the soil level is one foot below the next level of reinforcements, backfilling to the wall should be prevented until the next level is connected to the wall. This process could be repeated throughout construction in an attempt to alleviate the variability in lateral stress.

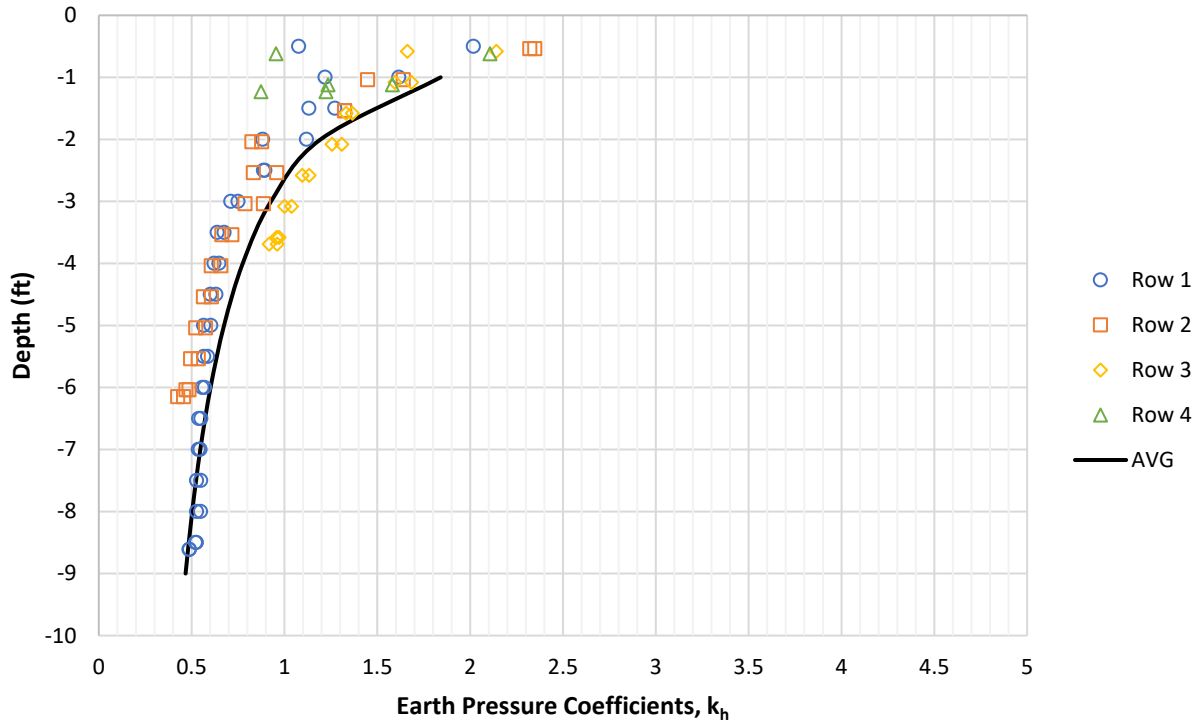


Figure 5-101. 95% compaction earth pressure coefficients from EPCs vs. depth.

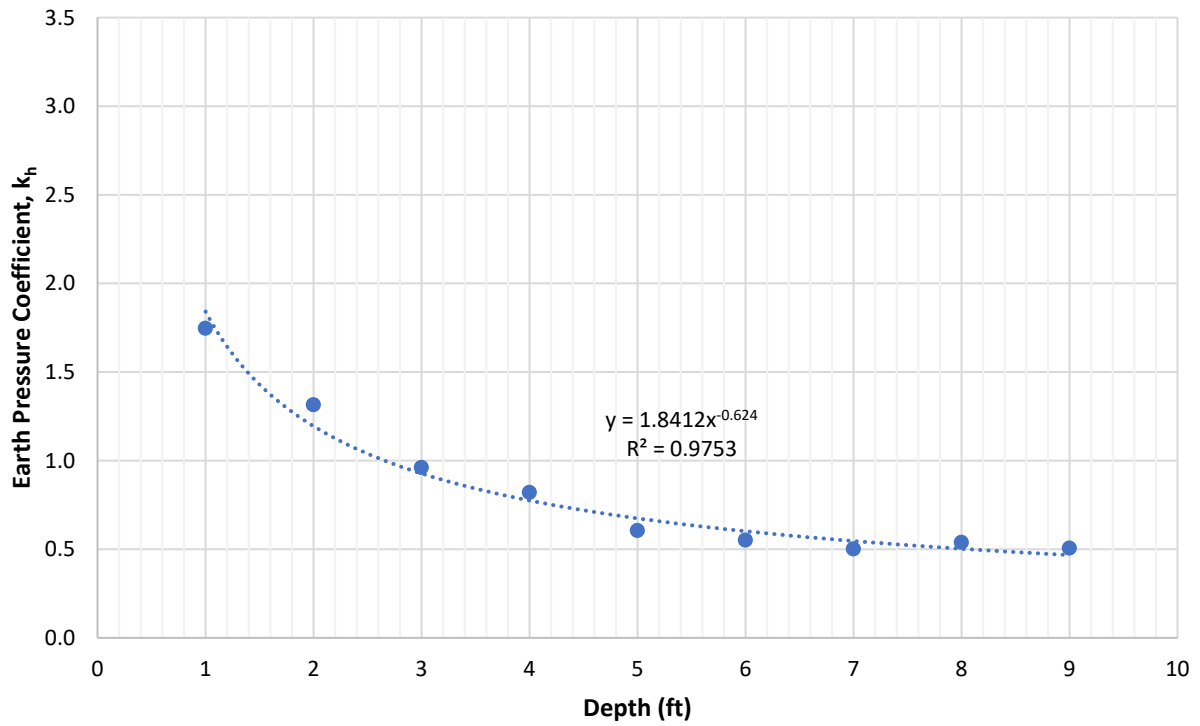


Figure 5-102. 95% of T-180 EPC average earth pressure coefficients as a function of depth.

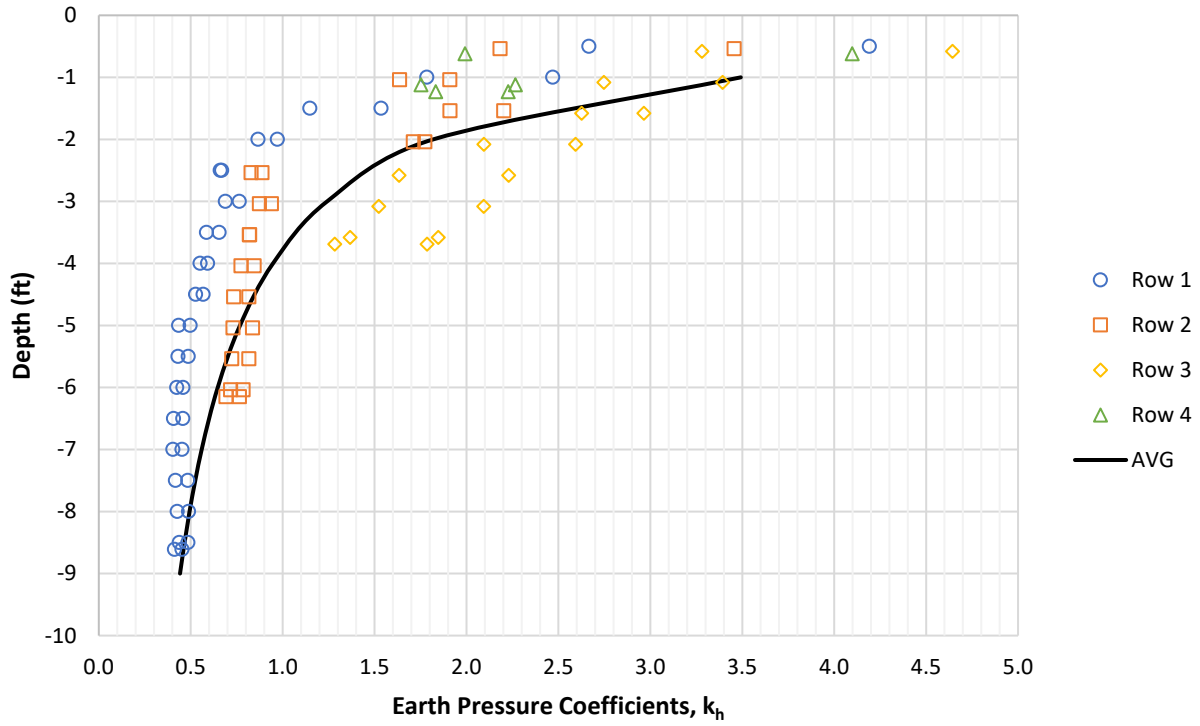


Figure 5-103. 103% compaction earth pressure coefficients from EPCs vs. depth.

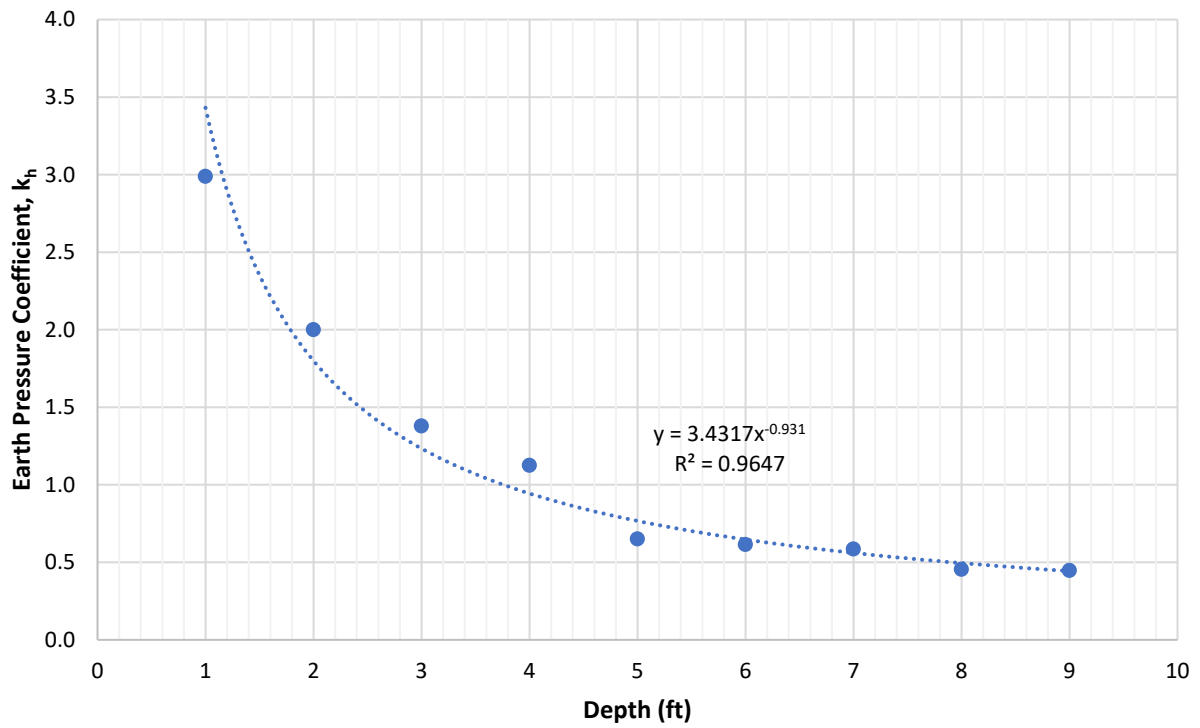


Figure 5-104. 103% of T-180 EPC average earth pressure coefficients as a function of depth.

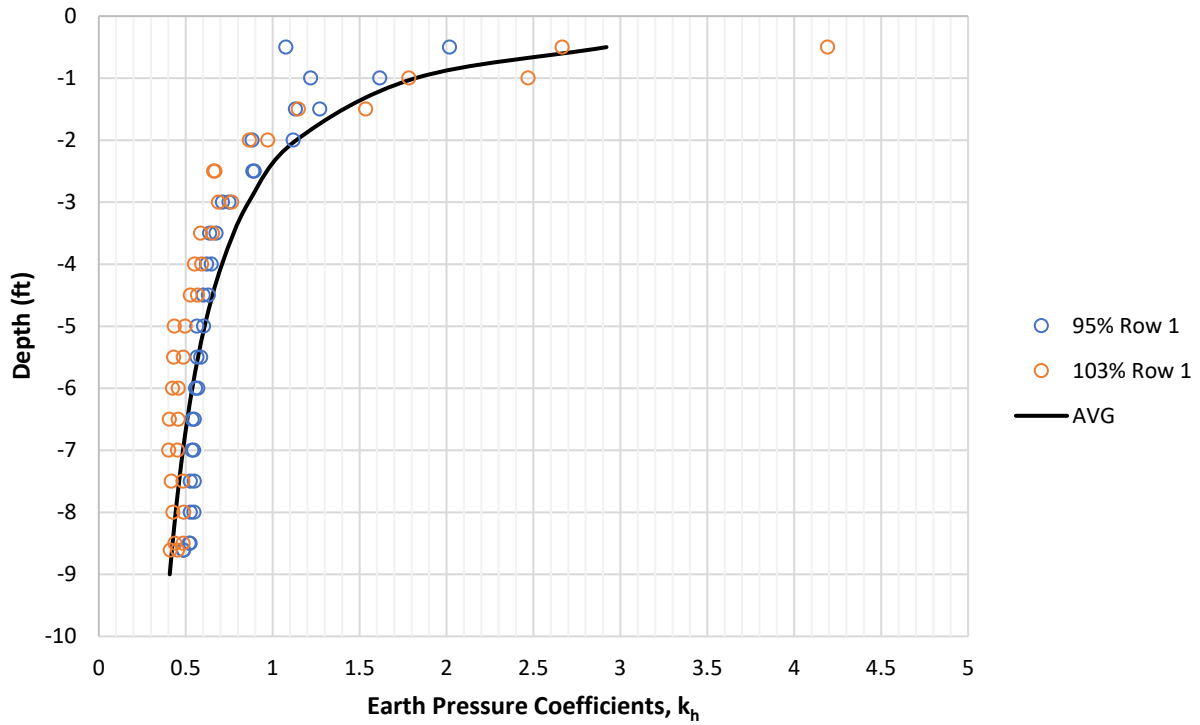


Figure 5-105. Comparing Row 1 earth pressure coefficients vs. depth.

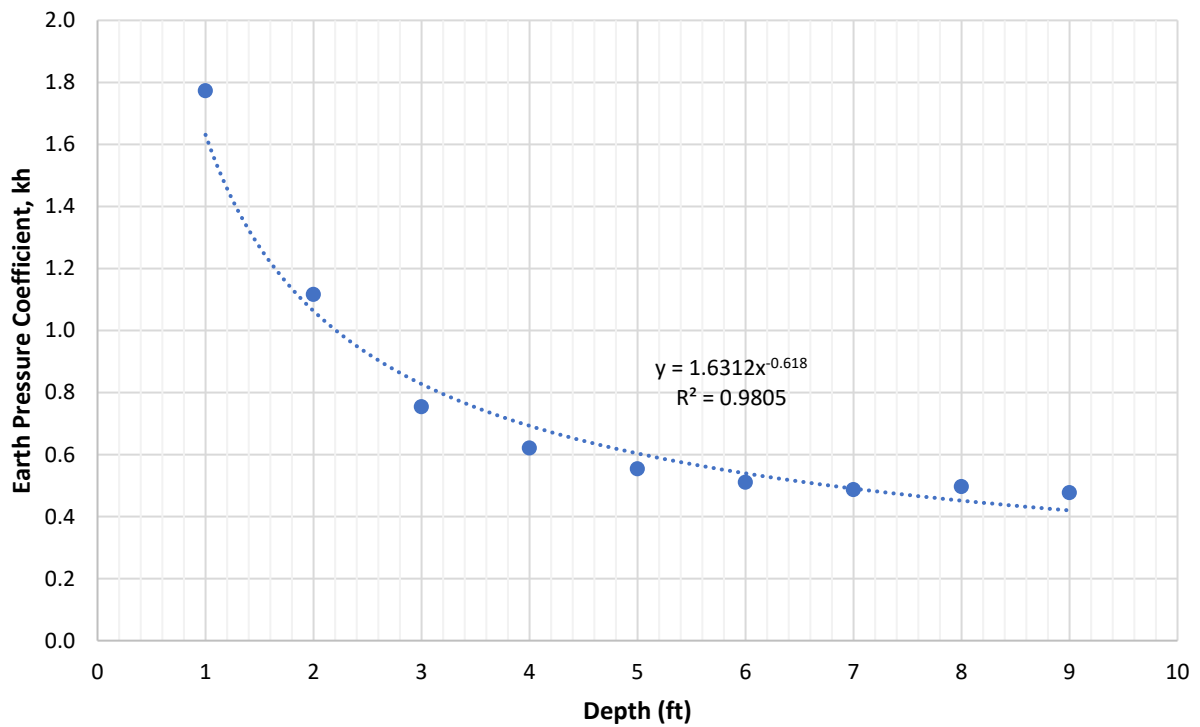


Figure 5-106.. Row 1 average earth pressure coefficients as a function of depth.

## 6 Simulated Earth Surcharge and Deriving Earth Pressure Coefficients

### 6.1 Simulated Earth Surcharge

In order to achieve the desired base (reinforced soil length) to wall height (B/H) ratio of 0.3, a simulated surcharge was required using the reaction frame-matjack system described in Chapters 3 and 4. The matjack system allowed the research team to implement controlled incremental surcharge loading that was sustained until the measured earth pressures and strip tensions at each reinforcement level stabilized. The matjack pressures were controlled by a manifold with six bays, depicted in Figure 6-1. During the first two load phases, it was observed that one of the bays located on the 103% compaction side was decreasing in pressure. The reaction frame was then removed from the 103% side and one of the small bags, indicated in Figure 6-2 by a red “X”, was determined to be leaking air. This bag was replaced and the 103% side reaction frame was reconstructed. The UF research team consulted with the FDOT project managers, and it was decided to move on to the third load phase, rather than repeat load Phases 1 and 2 again, because the soil was likely disturbed. During the third surcharge loading phase, it was observed that a different manifold bay was losing pressure on the 103% side. This manifold bay only controlled one larger airbag and the leaking bag was quickly identified. The reaction frame on the 103% side was removed again and the larger bag with a red “X” depicted in Figure 6-2 was replaced. Again, the UF research team and FDOT project managers agreed the load should be moved to Phase 4 as the soil was likely disturbed during Phase 3. Once the larger bag was replaced, no additional bag failures occurred and load Phases 4 through 8 were completed without issues.



Figure 6-1. Matjack system manifold with six bays.





Figure 6-2. Matjack failures on the 103% side during simulated surcharge Phases 1, 2, and 3.

The incremental surcharge pressures for each compaction effort were estimated based on the average loads measured from the reaction frame instrumented threaded rods divided by the surface area of the steel plates bearing on the soil. The simulated soil heights were estimated by dividing each incremental surcharge pressure by the average dry unit weight measured from nuclear density testing during construction. Tables 6-1 and 6-2 provide the results for each surcharge load phase for the 95% and 103% compaction efforts, respectively.

Table 6-1. Simulated surcharge loading results for 95% of T-180.

Load Phase	95% of T-180 - $\gamma_d = 101.26$ pcf	
	Surcharge (psf)	Simulated Soil Height (ft)
1	314	3.10
2	569	5.62
3	745	7.36
4	1,119	11.05
5	1,317	13.00
6	1,544	15.24
7	1,948	19.24
8	2,291	22.62

Table 6-2. Simulated surcharge loading results for 103% of T-180.

Load Phase	103% of T-180 - $\gamma_d = 108.53$ pcf	
	Surcharge (psf)	Simulated Soil Height (ft)
1	378	3.48
2	628	5.79
3	932	8.59
4	1,456	13.42
5	1,529	14.09
6	1,739	16.03
7	2,060	18.98
8	2,459	22.66

During load Phase 8, a surcharge pressure of 2,291 psf and 2,459 psf was applied to the 95% side and 103% side, respectively. The surcharge pressures were then divided by each respective soil density (i.e.,  $\gamma_{d95\%} = 101.26$  pcf and  $\gamma_{d103\%} = 108.53$  pcf) which equates to an equivalent surcharge height of 22.62 feet for the 95% side and 22.66 feet for the 103% side. When combined with the constructed wall height of 9.84 feet, this produced a total soil height of 31.23 feet for the 95% side and 31.27 feet for the 103% side. The reinforced soil zone was 9.75 feet in length which produced a B/H ratio of 0.30 for both compaction efforts and satisfied the criteria for when two walls would be tied together in practice, creating an unyielding condition.

Figures 6-3 and 6-4 provide depth profiles of the vertical earth pressure that developed during construction and was applied during surcharge loading (ND/DD – nuclear density / dywidag measurements), and the EPC measured vertical earth pressures at Row 1 (R1 EPC) for the 95% and 103% compactions efforts, respectively. Row 1 was used as the reference depth because this was the first time strip tension and the vertical and lateral stress within the reinforced soil mass were measured at the same time as wall displacement and leveling pad pressure. The simultaneous measurements were necessary to ensure force equilibrium was achieved (discussed later). In Figures 6-3 and 6-4, the first three surcharge load phases are identified by orange squares rather than orange circles. Observed in both figures, the matjack failures created more variability in the EPC measured vertical earth pressures but showed the same general trend compared to the construction phase and surcharge Phases 4 through 8 data points. Therefore, the data were considered acceptable during the analysis (Note: Phases 1 and 2 were more affected by the bag failures than Phase 3).

Observed in Figure 6-3, the applied and measured vertical stress were in good agreement at nearly every soil height above Row 1. This indicated there was minimal loss of vertical stress at Row 1 due to soil arching and likely minimal shear transfer to the wall panels on the 95% side. Conversely, Figure 6-4 indicates the measured vertical stress at Row 1 was less than the applied pressure at every soil height above Row 1 beyond a height of 2.5 feet, which is when the second row of reinforcements strips were added. This indicated that the higher compaction effort resulted in a higher degree of soil arching and shear transfer (down drag stresses) to the wall panels on the 103% side. These observations will be discussed further, later in the chapter.

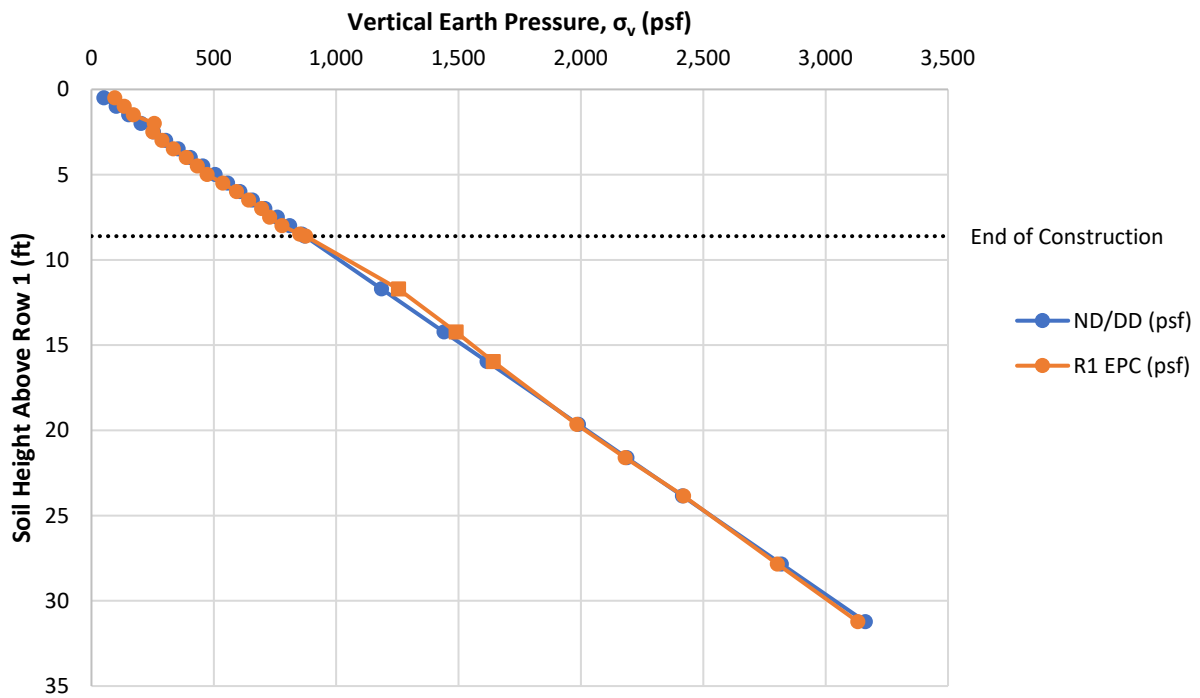


Figure 6-3. Depth profiles of applied and measured vertical earth pressure on the 95% side.

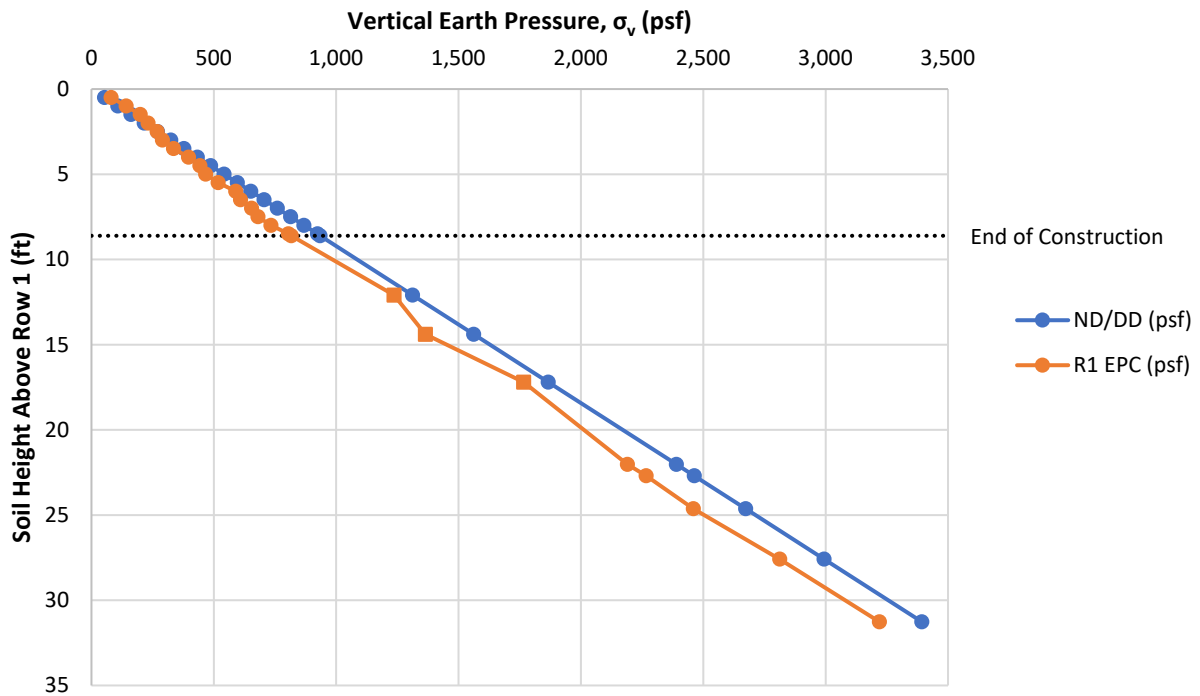


Figure 6-4. Depth profiles of applied and measured vertical earth pressure on the 103% side.

Once the surcharge load phases were complete, analyses were performed at each reinforcement level for both compaction efforts. The analyses included the average vertical earth pressure ( $\sigma_v$ ), average lateral earth pressure ( $\sigma_h$ ), average reinforcement strip tension (T), wall displacement ( $\delta_{wall}$ ), and the earth pressure coefficients ( $k_h$ ) derived for each compacted soil lift and surcharge height above the respective row of reinforcement strips.

## 6.2 Simulated Earth Surcharge Observations – 95% of T-180

The following section provides the analyzed data recorded for Row 1 on the 95% compaction side.

### 6.2.1 Row 1 Analysis

Observed in Figures 6-5 through 6-7, the ratio of lateral to vertical stress ( $k_h$ ) decreased during construction, moving from a passive condition during early compaction to an at-rest condition at the end of construction. During surcharge loading the  $k_h$  decreased until a soil height of approximately 20 feet above Row 1. Figure 6-7 shows that beyond this soil height, the stress ratio stabilized in an active condition. This indicates that the MSE wall should have continuously moved away from the reinforced soil mass during surcharge loading which is confirmed in Figure 6-6. Figure 6-5 indicates that the average strip tension was 2,892 lbf.

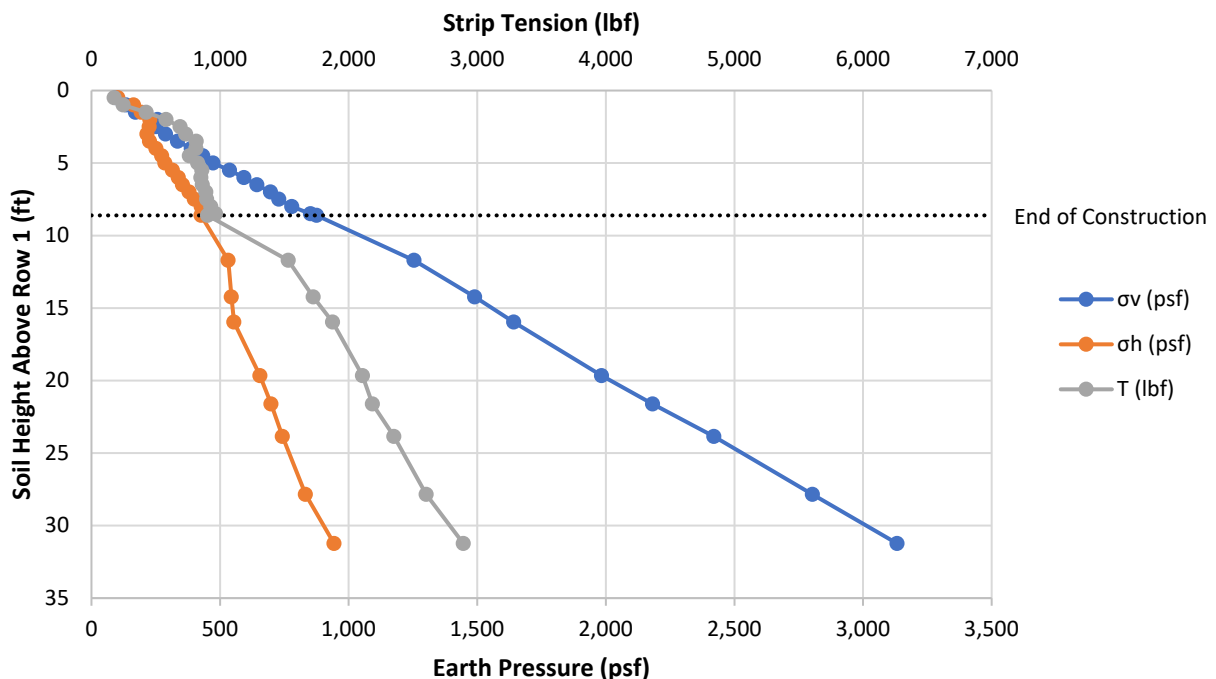


Figure 6-5. Depth profiles of earth pressure and strip tension at Row 1 on the 95% side.

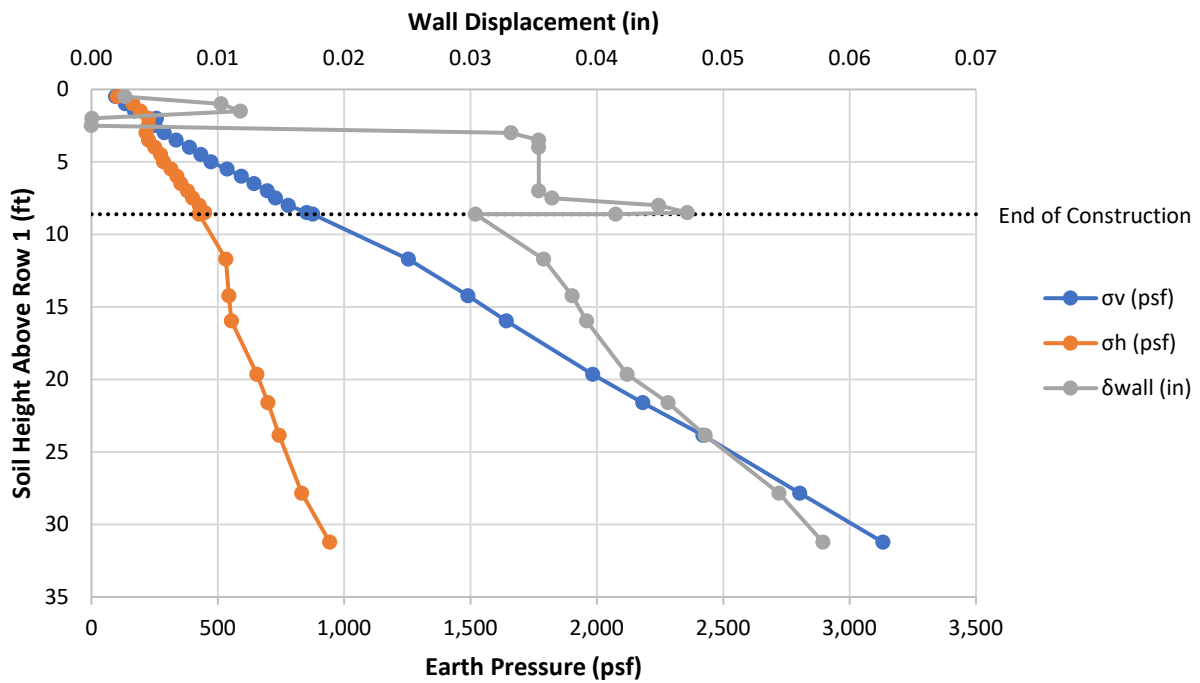


Figure 6-6. Depth profiles of earth pressure and wall displacement at Row 1 on the 95% side.

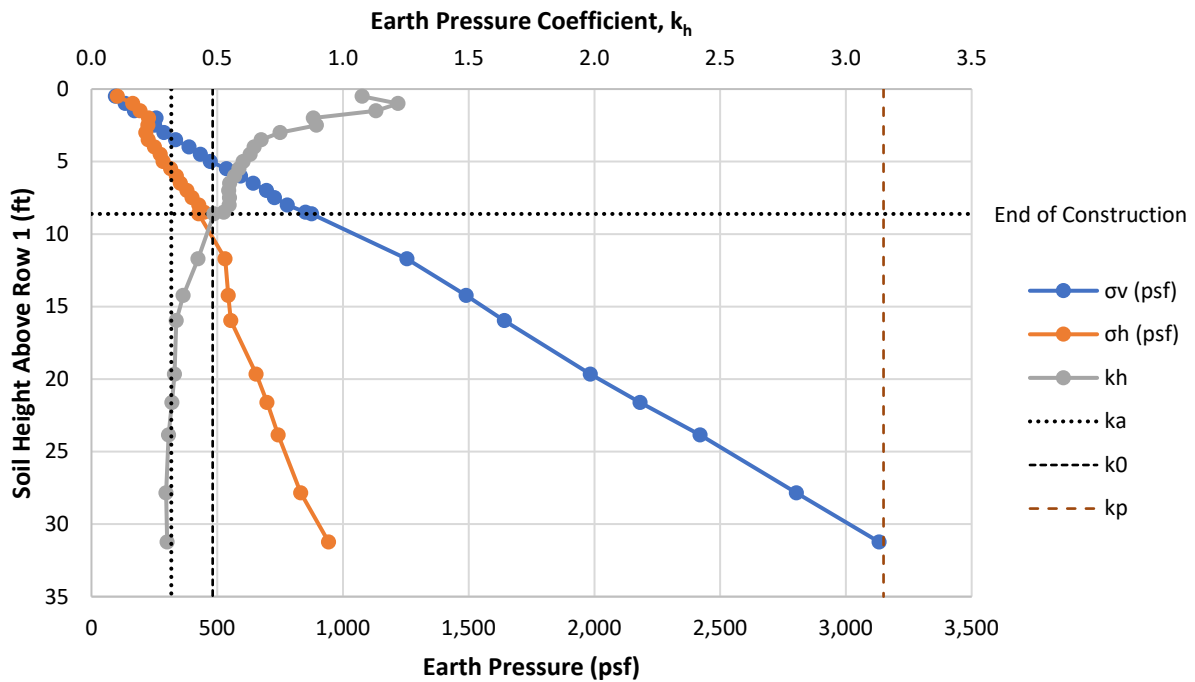


Figure 6-7. Depth profiles of earth pressure and pressure coefficients at Row 1 on the 95% side.

### 6.2.2 Row 2 Analysis

Similar to Row 1, Figures 6-8 through 6-10 show the  $k_h$  for Row 2 also decreased until a soil height of approximately 19.2 feet above Row 2 was achieved. Figure 6-10 shows that beyond this soil height, the stress ratio began to stabilize in an active condition. This further indicates the MSE wall should have continuously moved away from the soil mass during surcharge loading which is confirmed in Figure 6-9. Figure 6-8 indicates that the average strip tension was 3,560 lbf, which is an increase in tension of 668 lbf compared to Row 1.

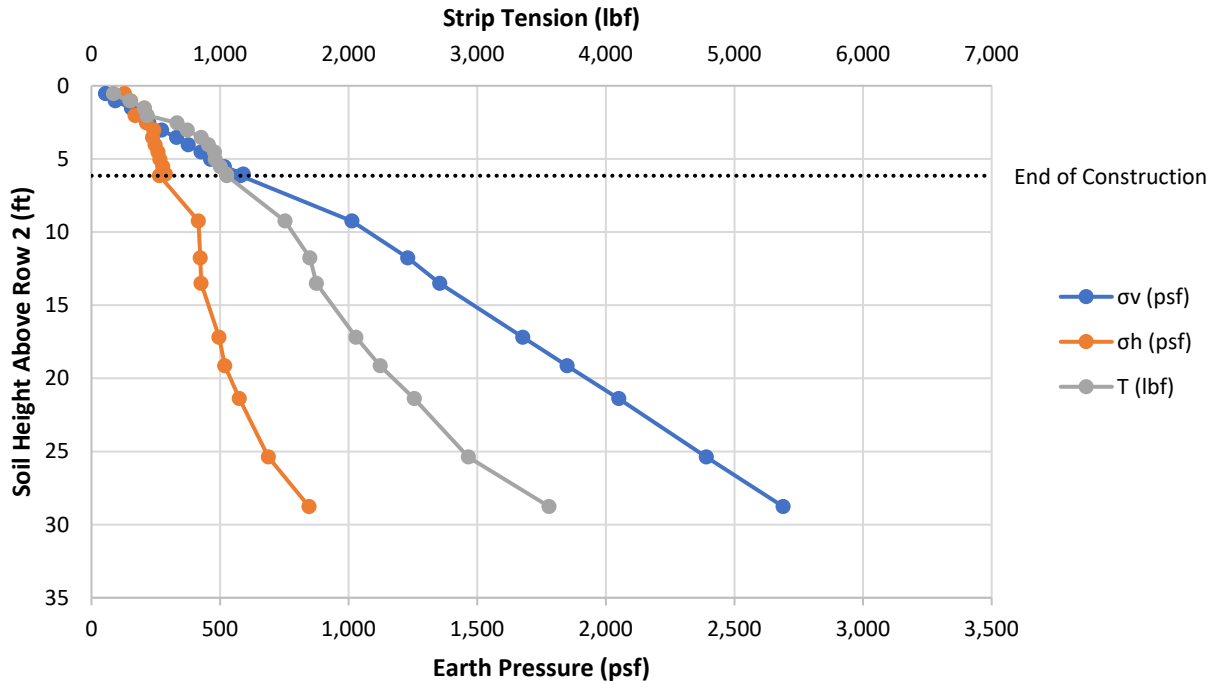


Figure 6-8. Depth profiles of earth pressure and strip tension at Row 2 on the 95% side.

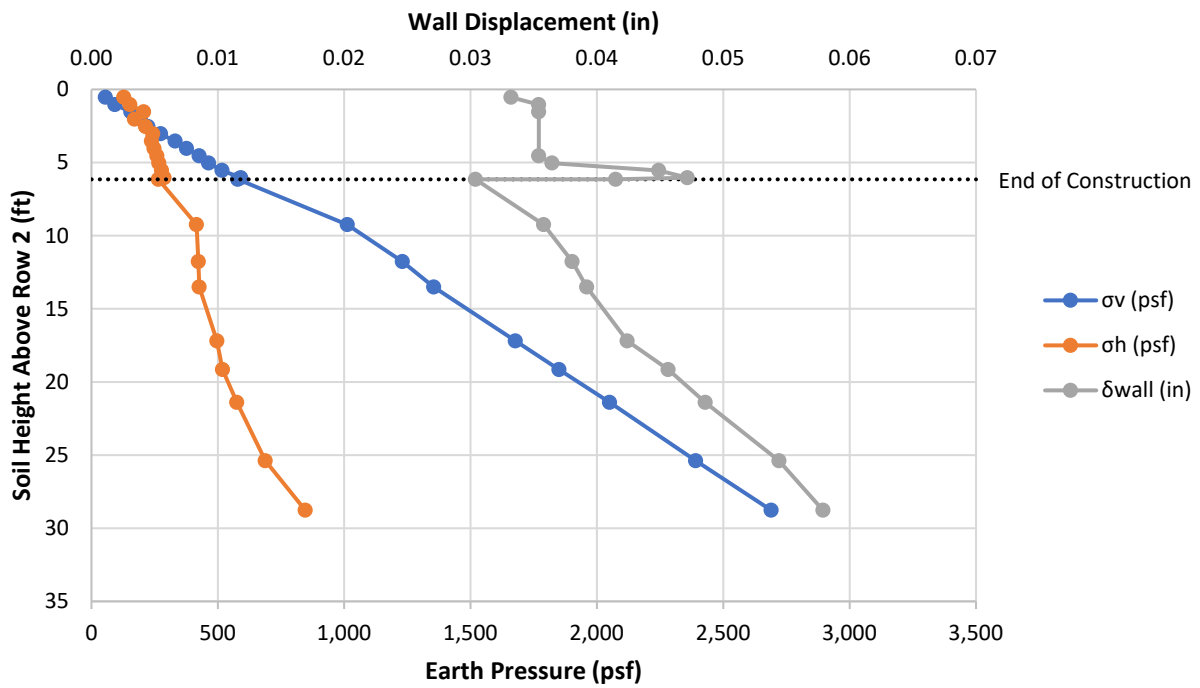


Figure 6-9. Depth profiles of earth pressure and wall displacement at Row 2 on the 95% side.

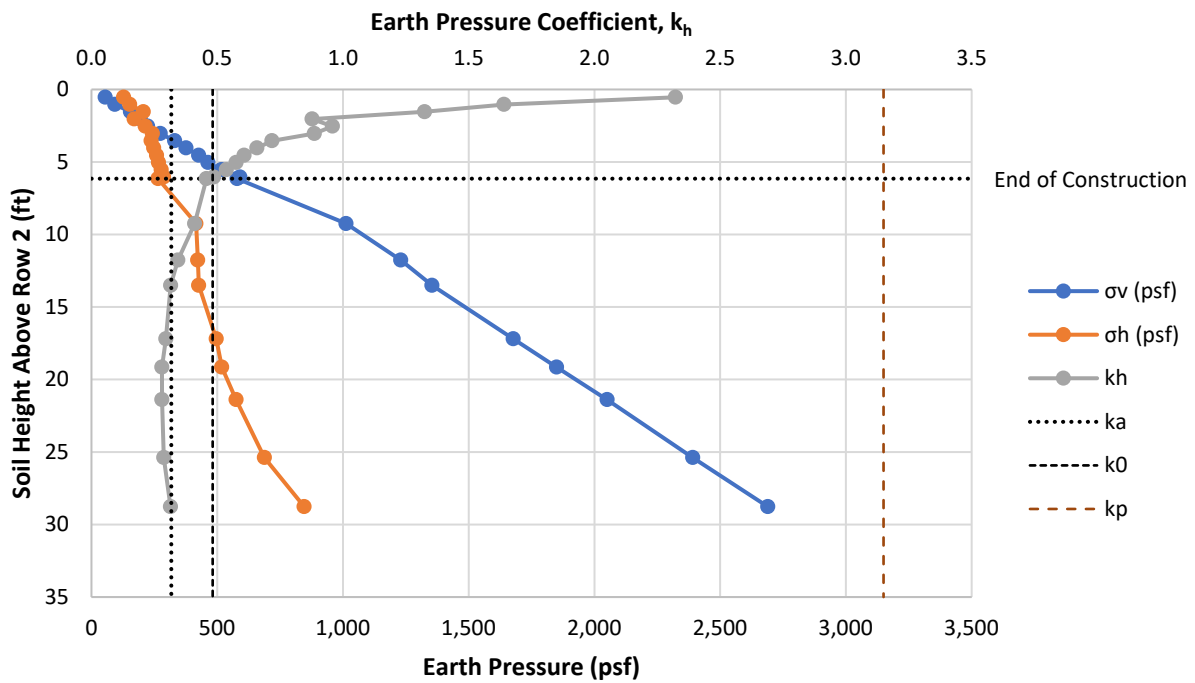


Figure 6-10. Depth profiles of earth pressure and pressure coefficients at Row 2 on the 95% side.

### 6.2.3 Row 3 Analysis

Reinforcement Rows 1 and 2 were both located in the bottom half of the MSE wall and behaved similarly. However, Row 3, located in the upper half of the MSE wall, displayed a behavior change. Figures 6-11 through 6-13 show the  $k_h$  for Row 3 decreased until a soil height of approximately 11.1 feet above Row 3 was achieved. Figure 6-13 shows that beyond this soil height, the stress ratio began to stabilize in an at-rest condition until a soil height of 18.9 feet above Row 3 was achieved. Beyond this soil height,  $k_h$  slightly decreased below the at-rest condition. This indicated the upper half of the MSE wall was at-rest during a portion of the surcharge loading, suggesting the higher compaction efforts in the upper half likely pushed the panels to fully engaging the reinforcement strips during construction, which prevented wall movement at the reinforcement level until the lower half panels fully engaged their reinforcement strips. This was confirmed when strip tension comparisons were made between the upper half of the wall and the lower half. Figure 6-11 indicates that the average strip tension at the end of surcharge loading was 5,312 lbf in Row 3, which is a significant increase in tension of 2,420 lbf compared to Row 1. When comparing the construction strip tensions, Row 3 exceeded the tension in Rows 1 and 2 by approximately 400 lbf, even though the soil height was only 3.69 above Row 3 whereas the soil heights were 8.61 ft and 6.15 ft above Rows 1 and 2, respectively. Therefore, the compaction effort in the upper half of the wall locked in higher stresses and strip tensions in Row 3 during construction.

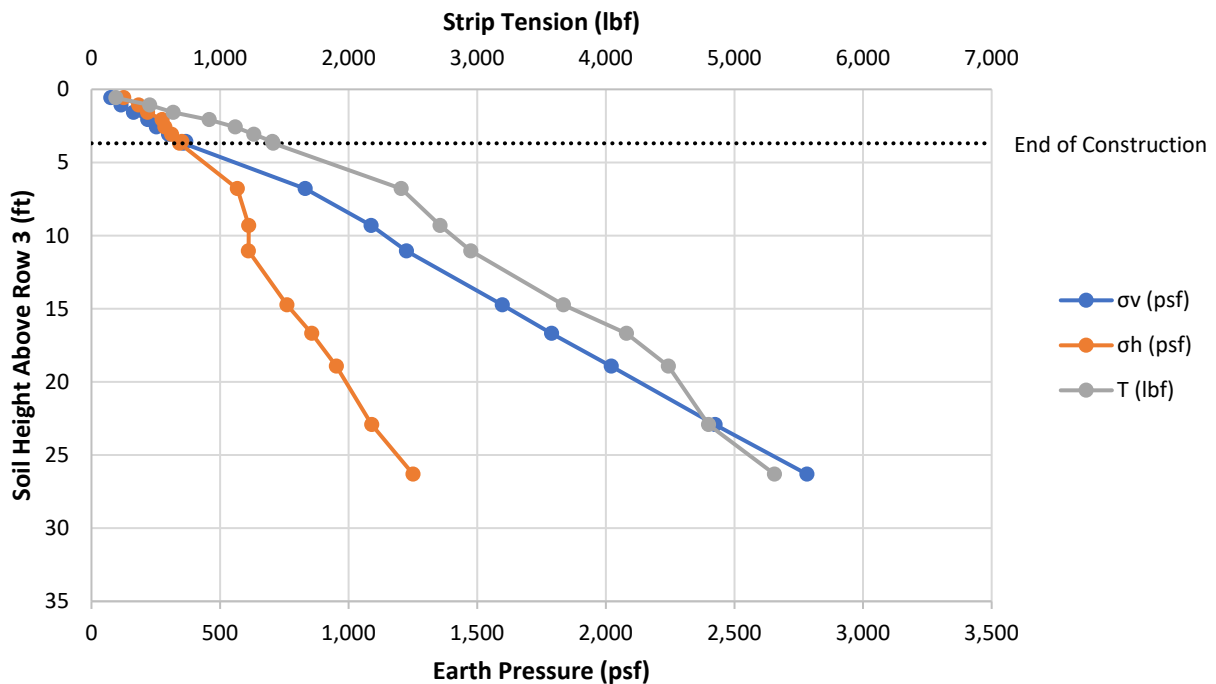


Figure 6-11. Depth profiles of earth pressure and strip tension at Row 3 on the 95% side.



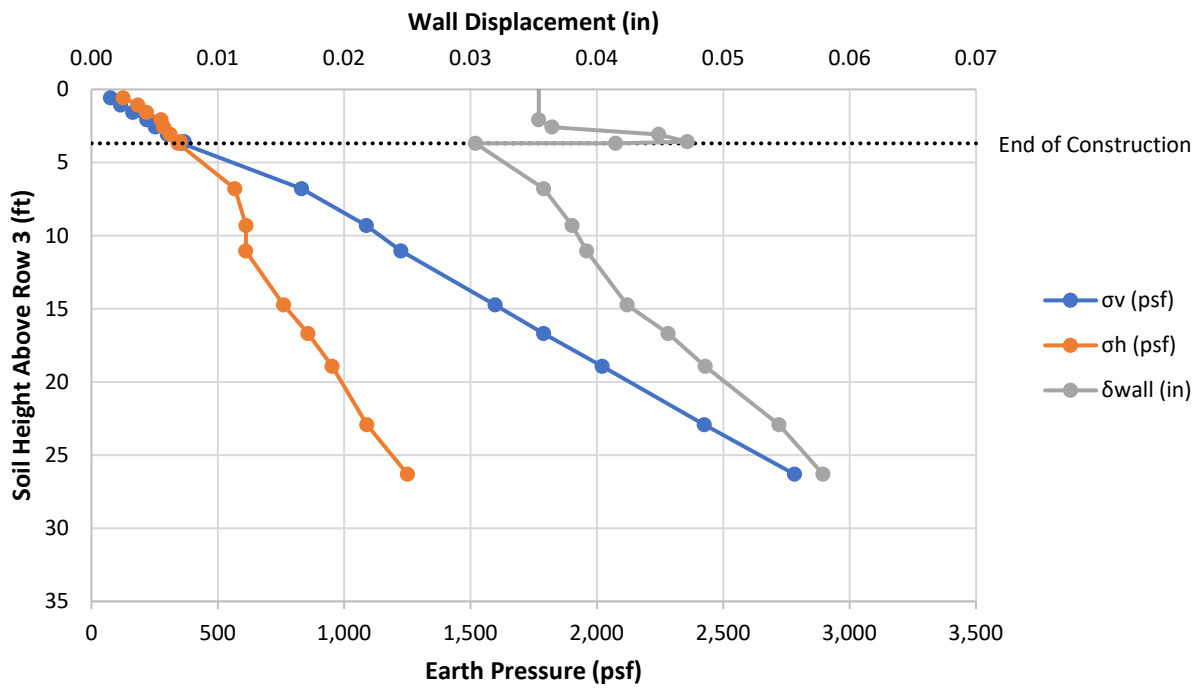


Figure 6-12. Depth profiles of earth pressure and wall displacement at Row 3 on the 95% side.

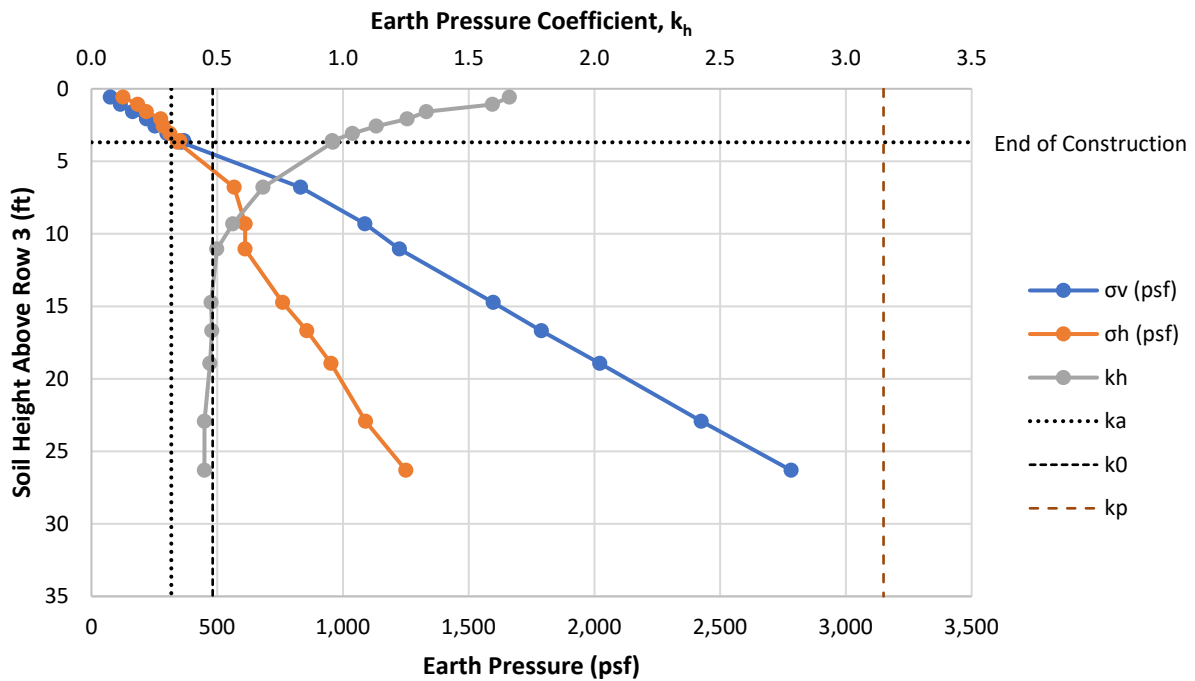


Figure 6-13. Depth profiles of earth pressure and pressure coefficients at Row 3 on the 95% side.

### 6.2.4 Row 4 Analysis

Figures 6-14 through 6-16 provide the Row 4 analyses for the 95% side. At Row 4, the strip tension of 5,582 was similar to Row 3 but again was significantly increased compared to Rows 1 and 2, further suggesting the upper half of the wall behaved differently compared to the lower half. However, the decreasing  $k_h$  with increasing soil height above Row 4 stabilized during the third load phase at a soil height of 8.59 feet. The  $k_h$  remained at a value of 0.94 for next two load phases and then began to increase during the final three load phases. The final load phase produced a  $k_h = 1.05$  which indicated the row was now heading towards a passive condition. The UF research team believes this was a result of the experimental setup, particularly the divider between the two compaction efforts. The top of the divider, near Row 4, was the weakest structural point of the experimental component. This portion of the divider had the least amount of soil on each side to counteract the large surcharge load induced. Due to the 103% side being loaded to a higher pressure (i.e.,  $q_{s103} = 2,459$  psf vs.  $q_{s95} = 2,291$  psf), required to achieve the necessary surcharge height, UF researchers believe the soil in the 103% side at Row 4 began moving towards the 95% and caused an increase in lateral stress. Inspection of the divider during the surcharge loading confirmed that the top of the divider was beginning to bow towards the 95% side. The results from Row 4 on the 103% side (discussed later) also support this hypothesis, as Row 4 on the 103% side indicated an active condition, whereas Row 3 on the 103% side was similar to the 95% side and indicated the earth pressure was moving from a passive to at-rest condition.

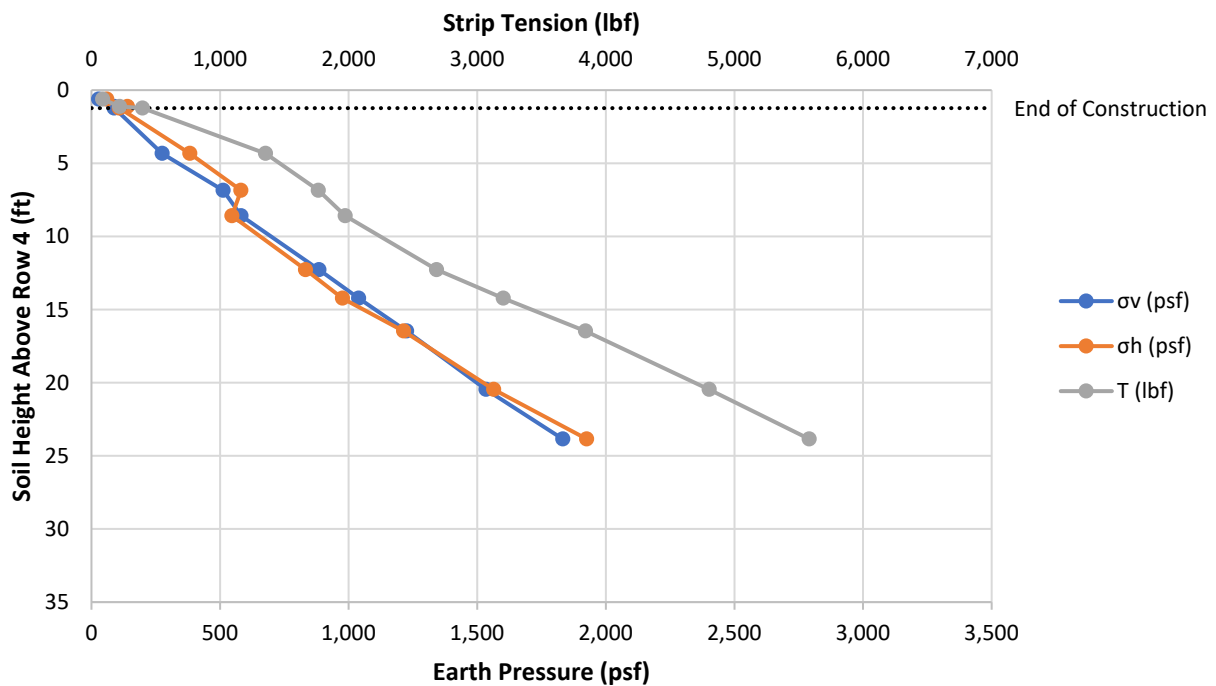


Figure 6-14. Depth profiles of earth pressure and strip tension at Row 4 on the 95% side.

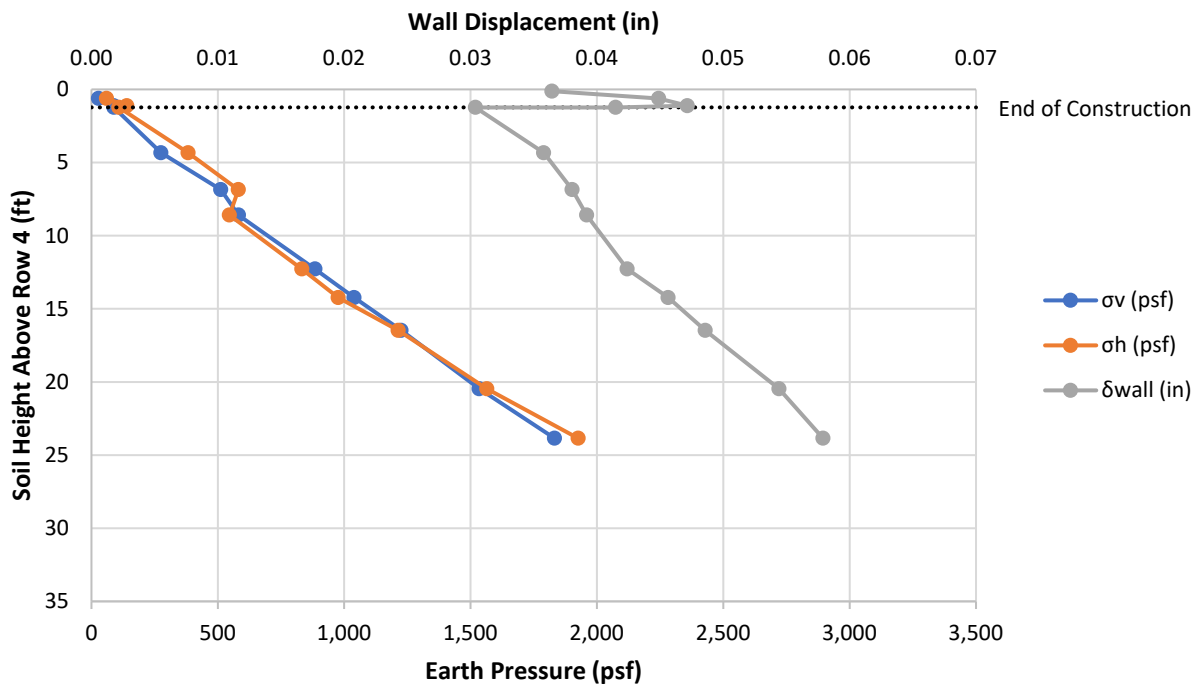


Figure 6-15. Depth profiles of earth pressure and wall displacement at Row 4 on the 95% side.

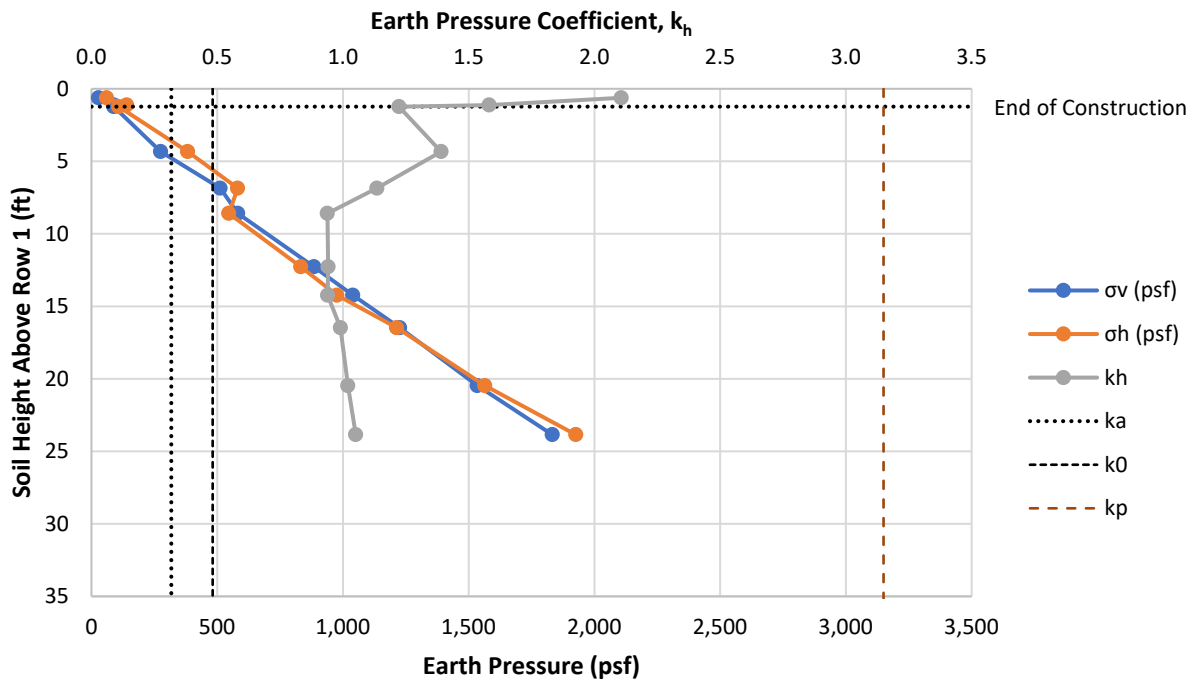


Figure 6-16. Depth profiles of earth pressure and pressure coefficients at Row 4 on the 95% side.

### **6.3 Simulated Earth Surcharge Observations – 103% of T-180**

The following section provides the analyzed data recorded for Row 1 on the 103% compaction side.

#### **6.3.1 Row 1 Analysis**

Observed in Figures 6-17 through 6-19, the Row 1 lateral to vertical stress ratio ( $k_h$ ) decreased until a soil height of approximately 6.5 feet above Row 1 was achieved. The  $k_h$  remained stable above an at-rest condition until a depth of 12.1 feet, where the  $k_h$  then began to decline for the remainder of loading and eventually moved below an active condition. Unlike the 95% side, Figure 6-18 shows that the MSE wall on the 103% side had limited displacement. In fact, once the temporary braces were removed after construction (soil height = 8.61 feet), the base of the wall moved inward towards the soil and beyond its original position. This suggests that the higher locked in compaction forces in the upper half of the wall, as suggested by the coherent gravity method, began to induce a slight rotational component that was introduced once the temporary braces were removed. However, the rotational component was minimal as close inspection of the wall panels confirmed they were still plumb and well within construction tolerance. The lack of total wall movement suggests the shear stress at the soil-wall interface was likely increased compared to 95% side. This is supported by Figure 6-4, where the measured vertical stress at Row 1 was noticeably reduced compared to the applied surcharge pressure and overburden. Consequently, the reduction of vertical stress within soil mass had to be redistributed to the wall panels. With limited wall movement, the increased stress at the wall must have been transformed into shear stress which increased the leveling pad pressure (discussed later). Figure 6-19 indicates that the average strip tension at Row 1 was 2,365 lbf which is 527 lbf less than the reinforcement strips at Row 1 on the 95% side. This further indicates that less wall movement occurred in the 103% side.

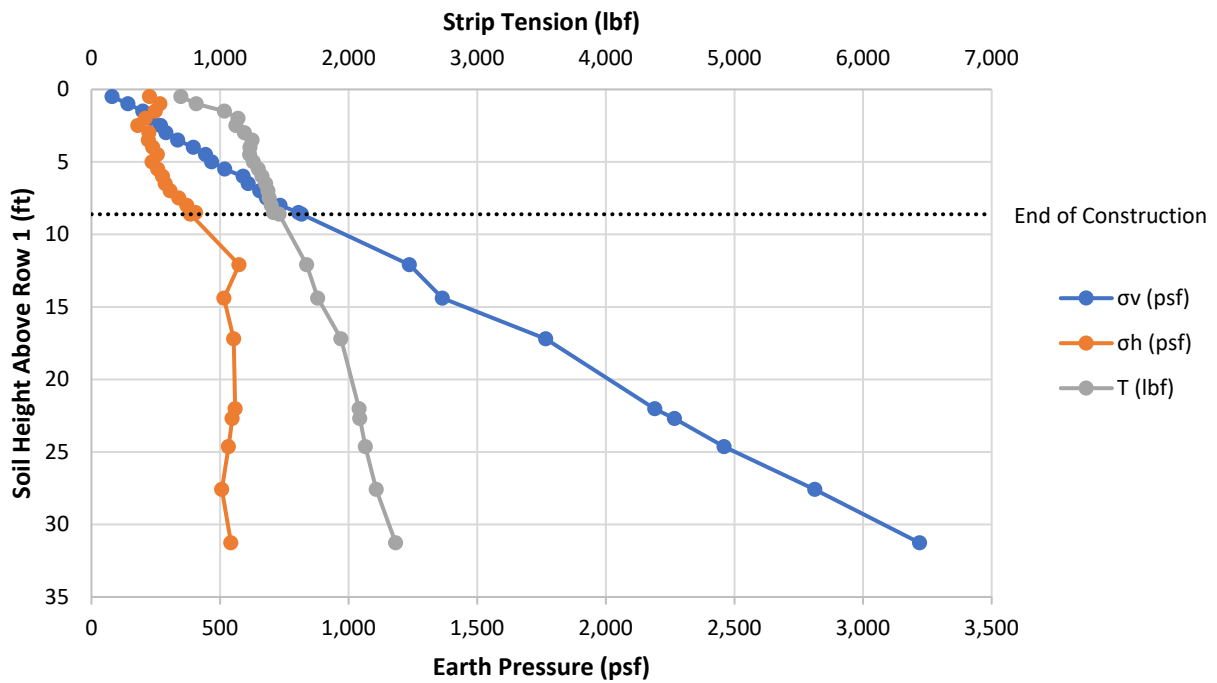


Figure 6-17. Depth profiles of earth pressure and strip tension at Row 1 on the 103% side.

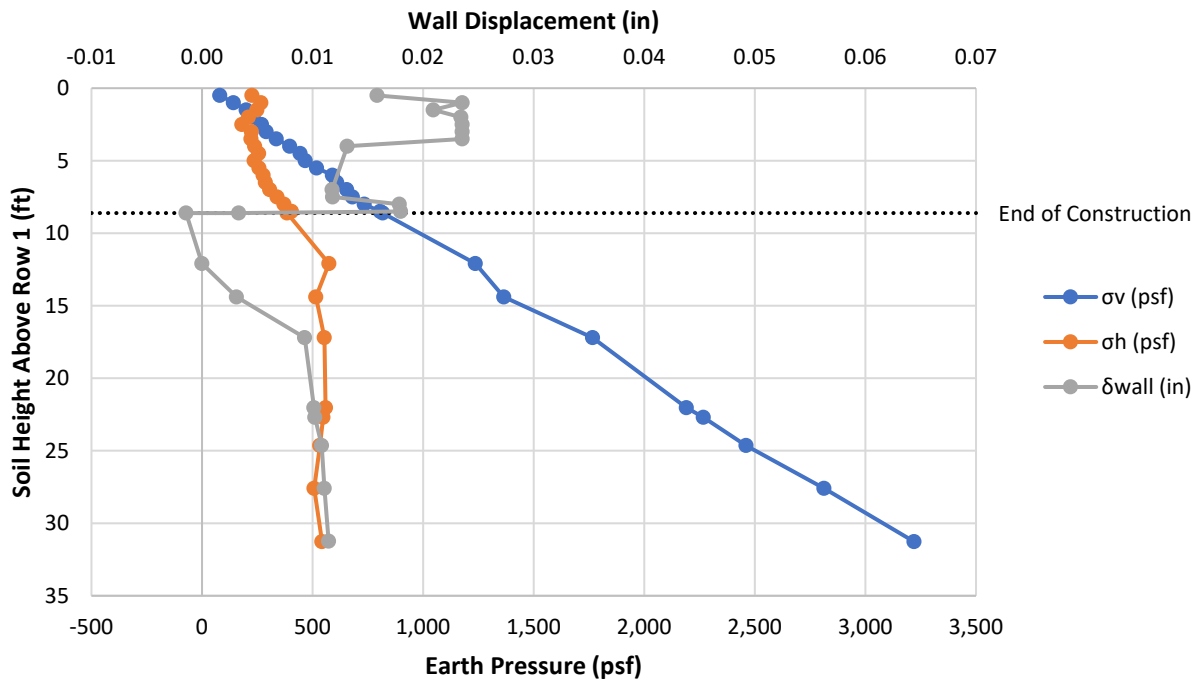


Figure 6-18. Depth profiles of earth pressure and wall displacement at Row 1 on the 103% side.

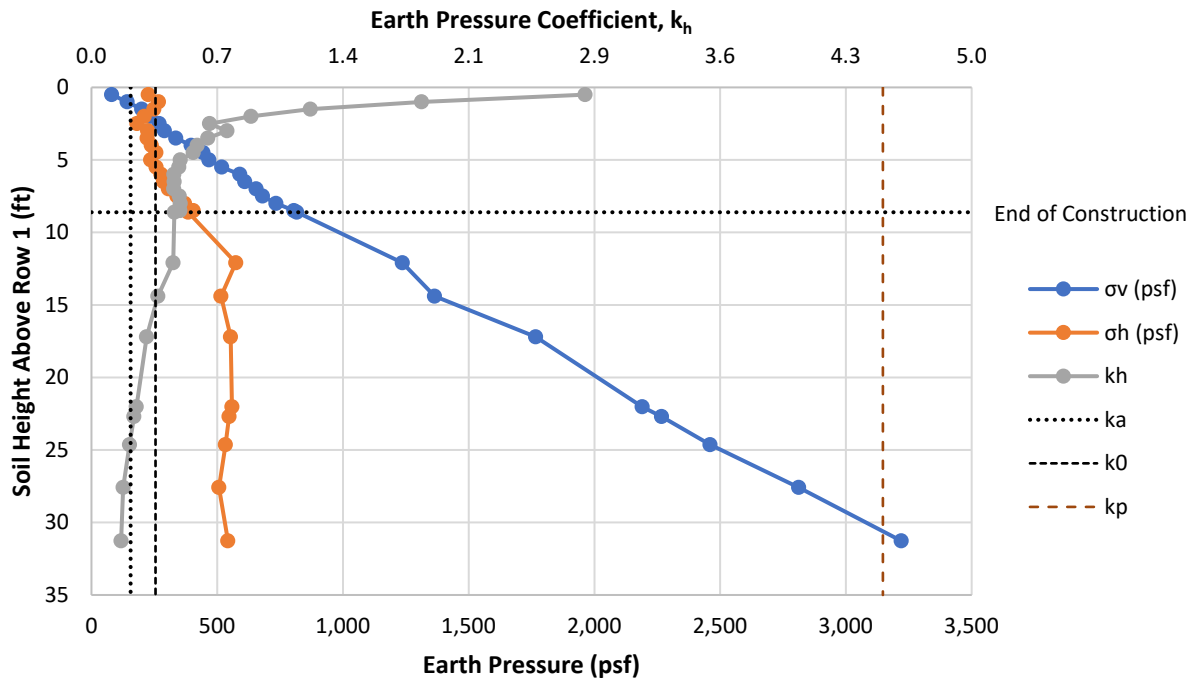


Figure 6-19. Depth profiles of earth pressure and pressure coefficients at Row 1 on the 103% side.

### 6.3.2 Row 2 Analysis

Similar to Row 1, Figures 6-20 through 6-22 show the  $k_h$  for Row 2 also decreased throughout construction and during the surcharge load phases and eventually moved below an active condition. Figure 6-21 indicates that the average strip tension was 2,686 lbf, which is an increase in tension of 321 lbf compared to Row 1 on the 103% side but an 874 lbf decrease compared to Row 2 on the 95% side, which further supports the observations made for Row 1 and the lower half of the MSE wall on the 103% side.

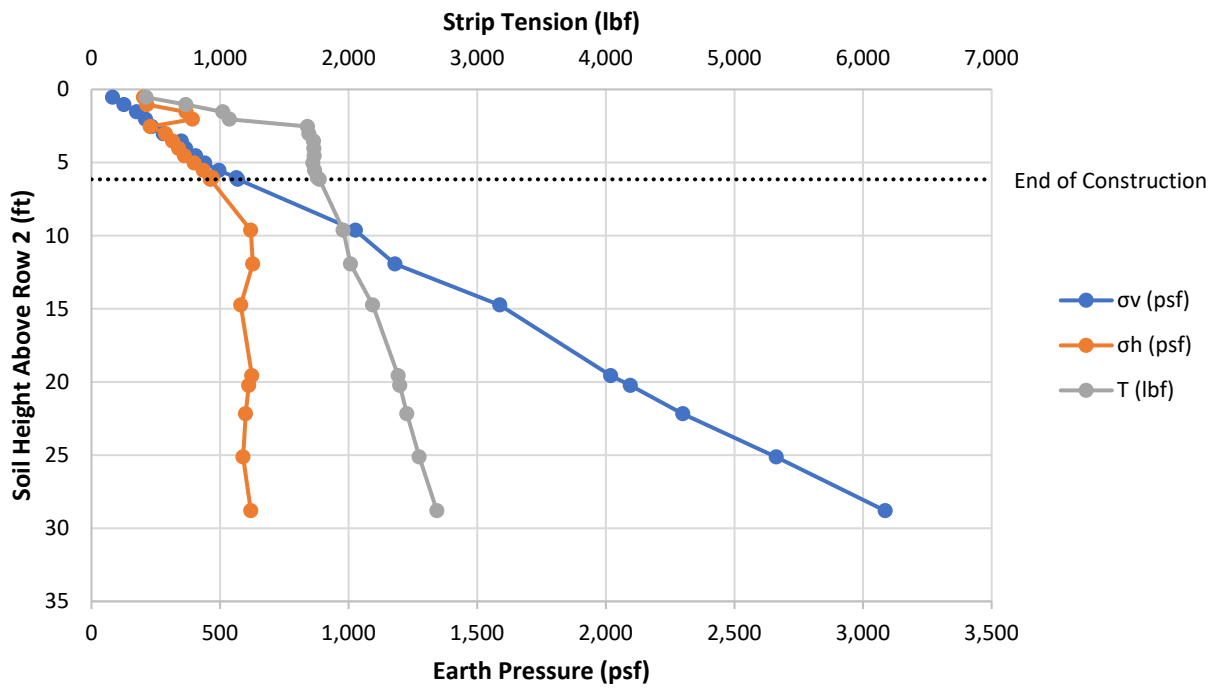


Figure 6-20. Depth profiles of earth pressure and strip tension at Row 2 on the 103% side.

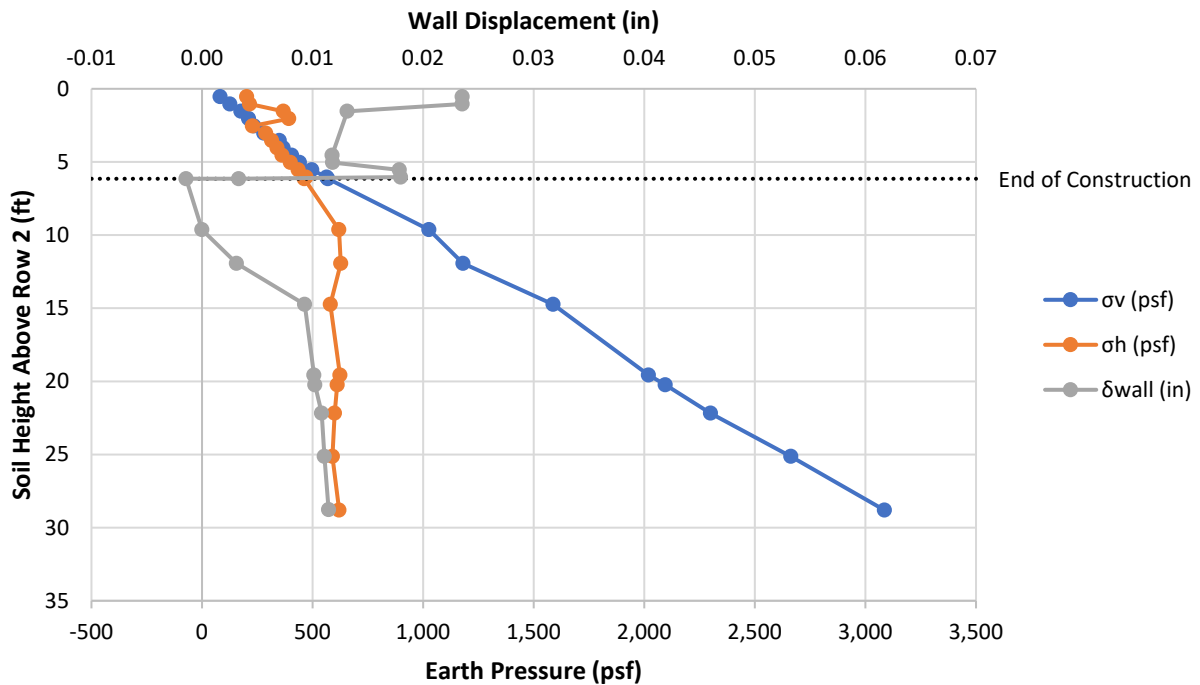


Figure 6-21. Depth profiles of earth pressure and wall displacement at Row 2 on the 103% side.

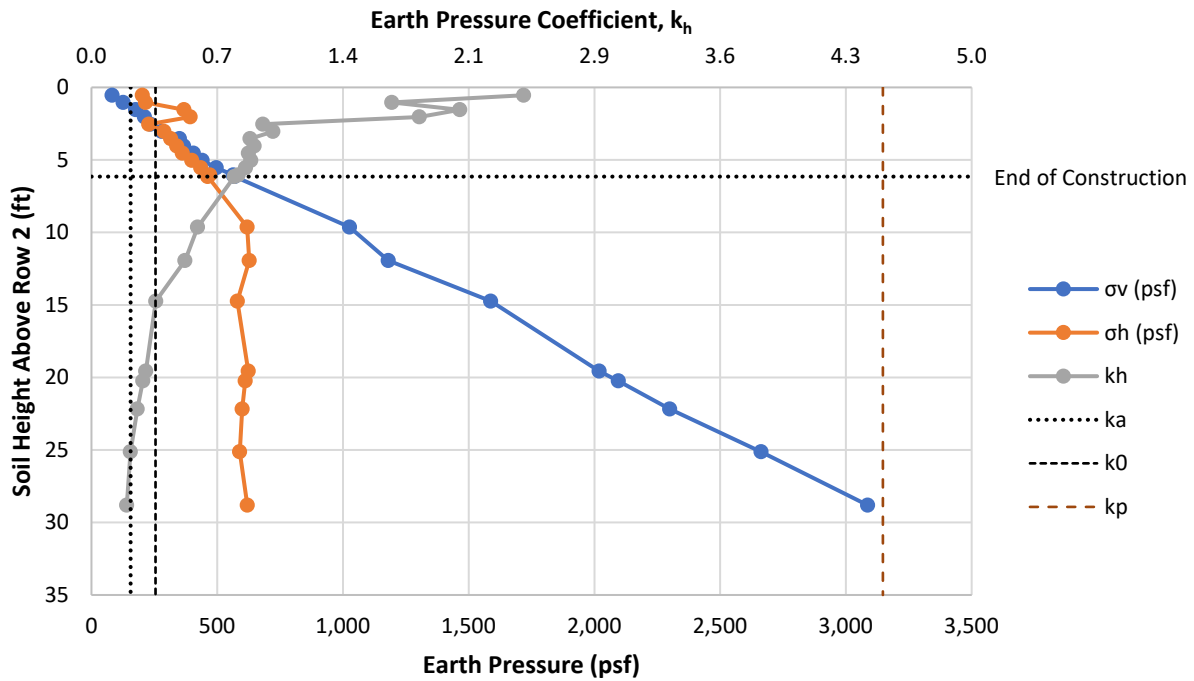


Figure 6-22. Depth profiles of earth pressure and pressure coefficients at Row 2 on the 103% side.

### 6.3.3 Row 3 Analysis

Similar to Row 3 on the 95% side, Row 3 on the 103% side indicated a soil behavior change in the upper half of the wall, likely due to locked in compaction forces as suggested by the coherent gravity method. Figures 6-23 through 6-25 show that during the first lift above the Row 3 reinforcement level, the soil was in a passive state. From that point on, the  $k_h$  declined throughout loading and was near an at-rest condition during the final load phase. The average strip tension at Row 3 was 3,885 lbf which was 1,199 lbf higher than Row 2 and 1,520 lbf higher than Row 1 on the 103% side. However, the strip tension was 1,427 lbf less than Row 3 on the 95% side, further indicating less wall displacement.



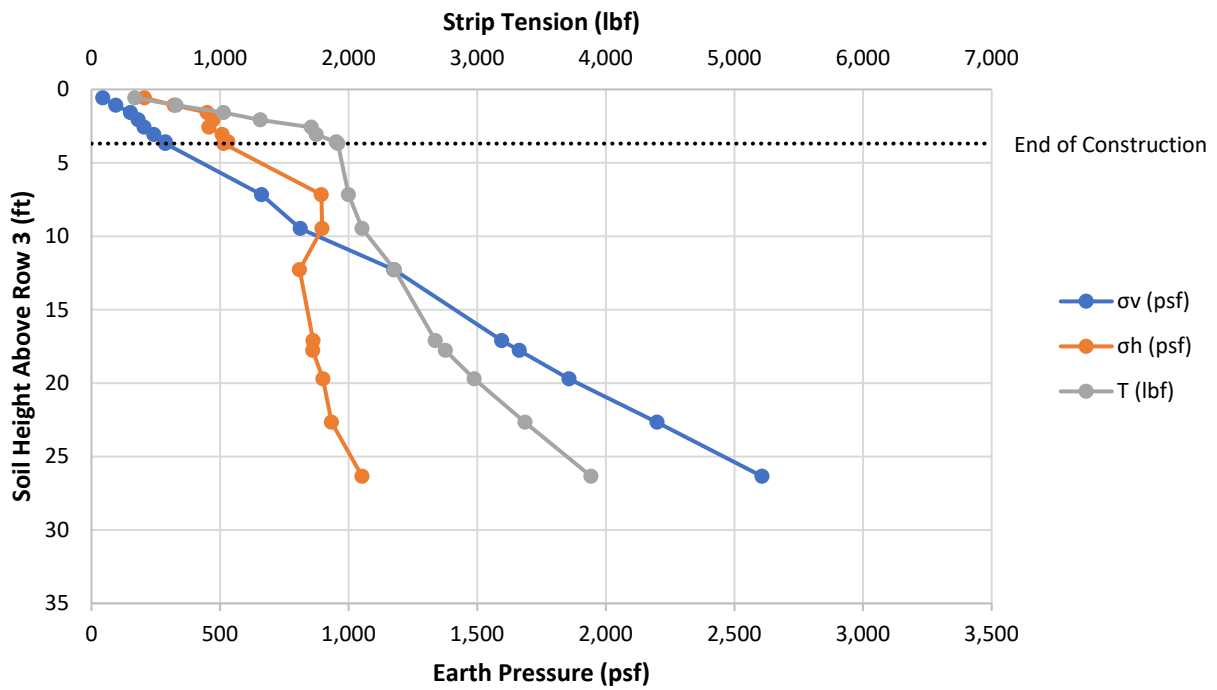


Figure 6-23. Depth profiles of earth pressure and strip tension at Row 3 on the 103% side.

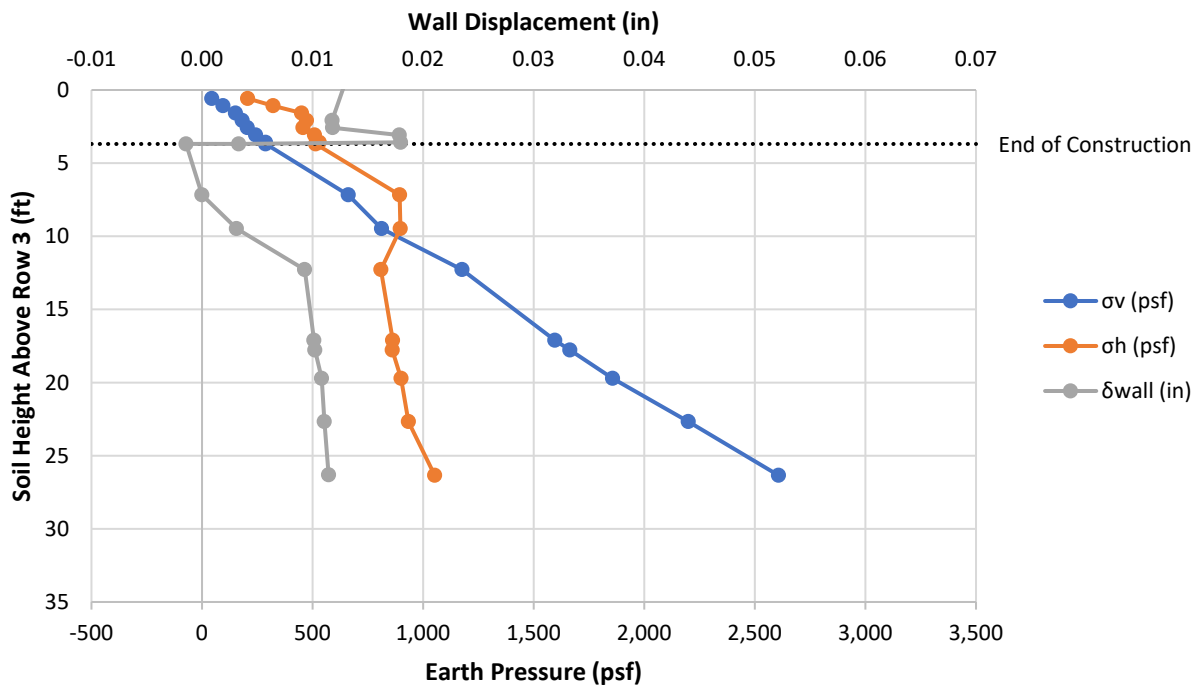


Figure 6-24. Depth profiles of earth pressure and wall displacement at Row 3 on the 103% side.

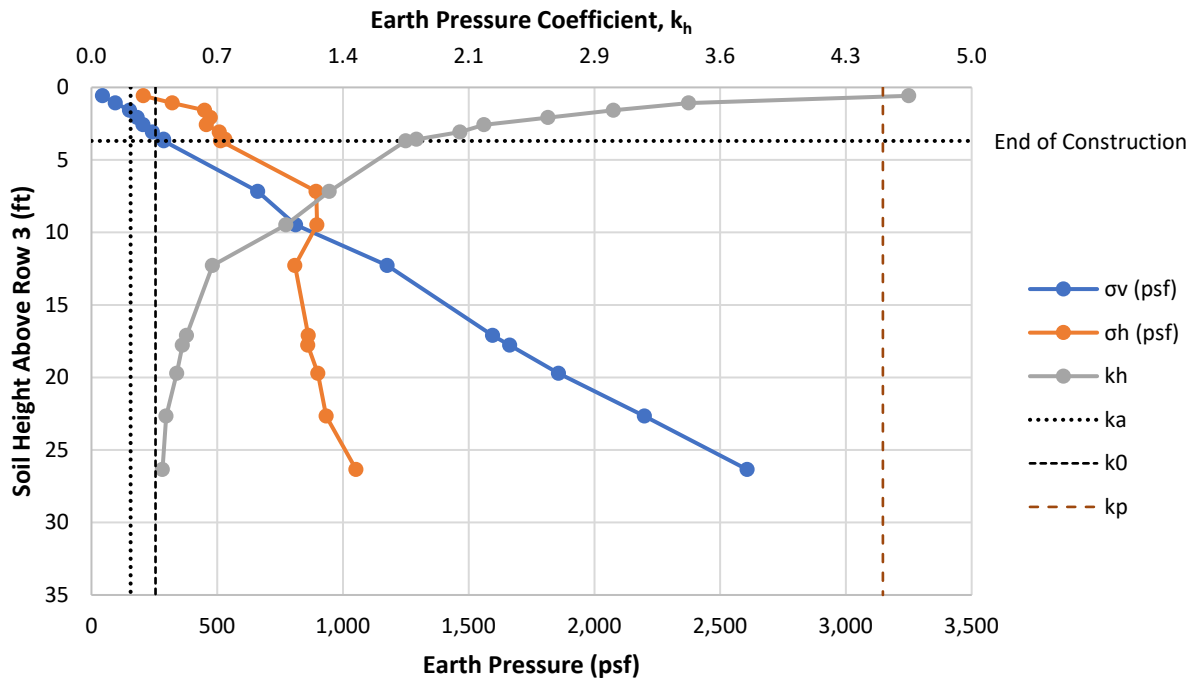


Figure 6-25. Depth profiles of earth pressure and pressure coefficients at Row 3 on the 103% side.

### 6.3.4 Row 4 Analysis

Figures 6-26 through 6-28 provide the Row 4 analyses for the 103% side. At Row 4, the strip tension was 4,141 lbf and the highest for the 103% side, but 1,441 lbf less than Row 4 on the 95% side. Interestingly, the difference in strip tensions between the two compaction efforts at Row 3 was a similar 1,427 lbf, indicating similar behavior in the upper halves of the two MSE walls. In both cases, a significant increase in strip tension was recorded in the upper half of the wall compared to the lower half. This further suggests the upper half of the wall is exposed to higher lock-in compaction forces, as suggested by the coherent gravity method. Also of interest, the strip tensions at each row were higher on the 103% side compared to the 95% side after construction but lower than the strip tensions on the 95% side after surcharge loading. This indicates that strip tension is largely influenced by wall movement because the 95% side was loaded at a lower surcharge pressure compared to the 103% side but did experience more than five times the wall displacement.

Although increased strip tension was observed for both compaction efforts at Row 4, the  $k_h$  was quite different. As previously discussed, the Row 4  $k_h$  on the 103% side was moving towards an active condition during loading. This is observed in Figure 6-28, where during the final three load phases the  $k_h$  was below an at-rest condition and nearly achieved an active condition during the final load phase. This further suggests the larger surcharge pressure on the 103% side was pushing the soil towards the 95% side at the top of the divider.

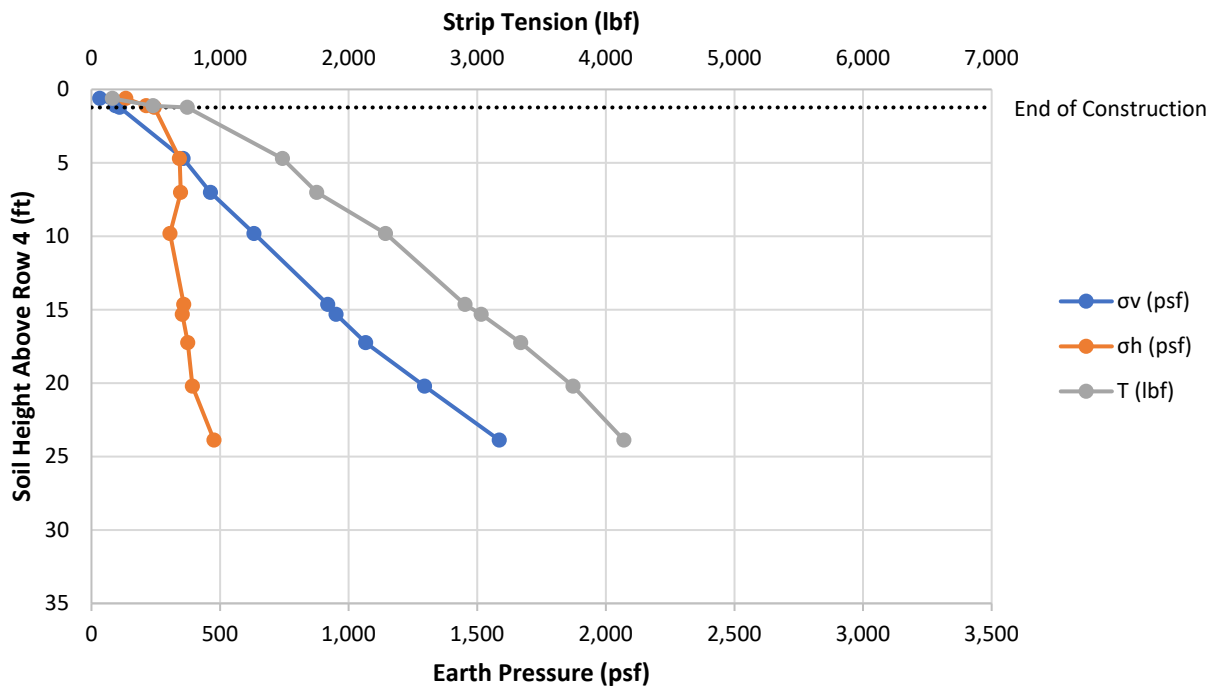


Figure 6-26. Depth profiles of earth pressure and strip tension at Row 4 on the 103% side.

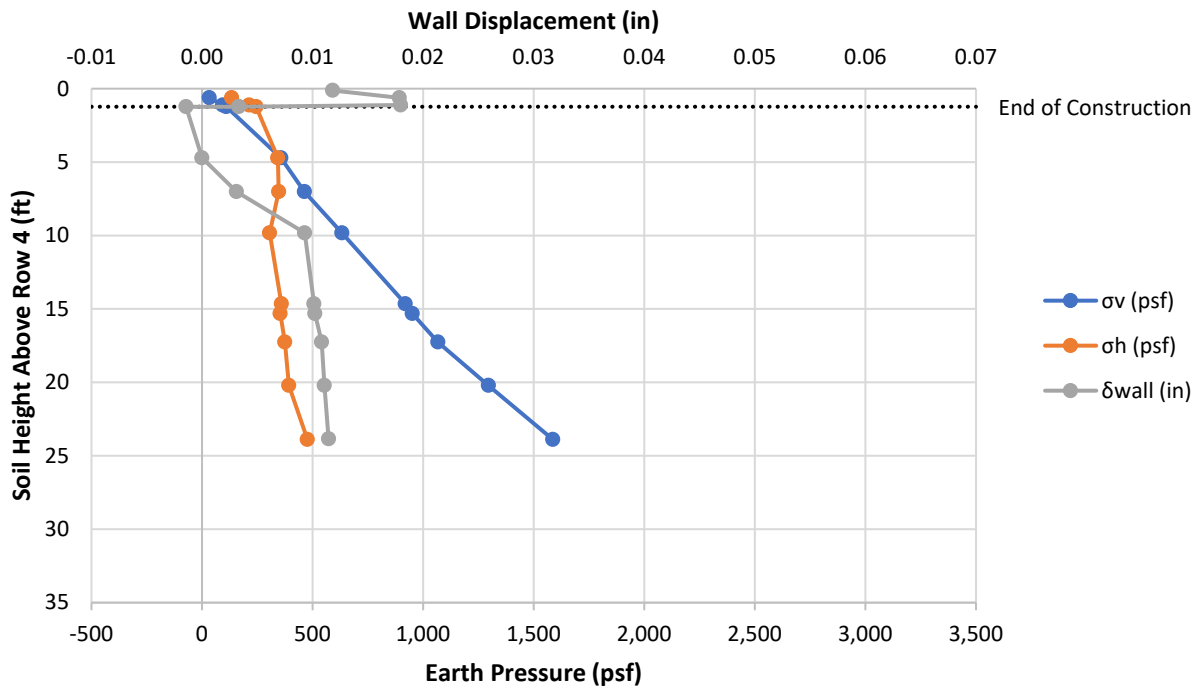


Figure 6-27. Depth profiles of earth pressure and wall displacement at Row 4 on the 103% side.

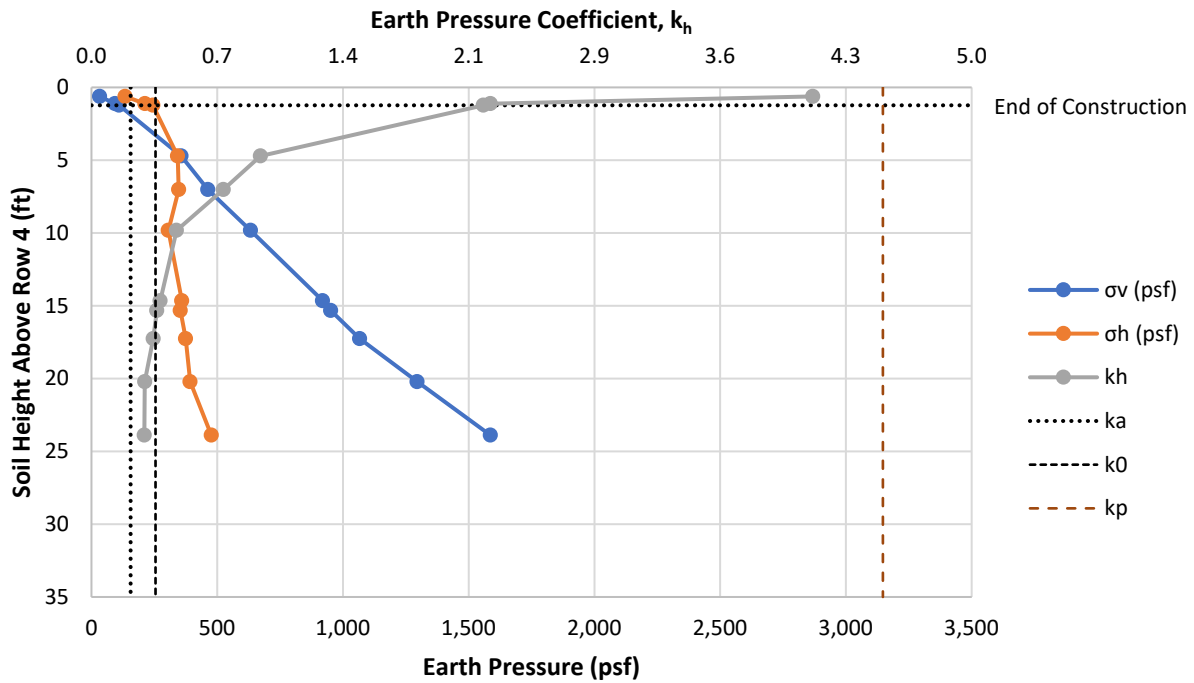


Figure 6-28. Depth profiles of earth pressure and pressure coefficients at Row 4 on the 103% side.

#### 6.4 Force Equilibrium Analysis

With the construction and surcharge loading data now analyzed, it was important to ensure force equilibrium was achieved to further validate the experimental results. Figure 6-29 provides a diagram of forces and pressures acting on the wall at Row 1. This includes the average vertical stress ( $\sigma_{vRow1}$ ), average lateral stress ( $\sigma_{hRow1}$ ), simulated surcharge ( $q_s$ ), shear stress at the wall ( $\tau_w$ ), weight of the wall panels ( $W_w$ ), weight of the soil column acting on the leveling pad ( $W_s$ ), and the force at the leveling pad (FLP). Although the prior analysis indicated the walls did move to some degree during construction and surcharge loading, stabilization did occur after each lift or surcharge load, which indicates static equilibrium. Therefore, the measured forces and stress should balance out.

When soil is placed behind a retaining wall, it settles due to its self-weight and the load applied by additional overburden (e.g., simulated surcharge). Simultaneously, the frictional resistance generated at the soil-wall interface resists the settlement of the soil, leading to an arching effect that reduces the overburden pressure within the retained soil and inherently the lateral stress at the wall. The reduction of overburden pressure is redistributed to shear stress at the soil-wall interface due to the frictional resistance. The added shear stress at the soil-wall interface is then transformed into additional leveling pad pressure/force beyond the weight of the wall and soil column acting on the leveling pad. Figures 6-30 and 6-31 provide depth profiles of the combined weight of the wall and soil column (S+W), leveling pad pressure under the front wall (LPF),

leveling pad pressure under the back wall (LPB), the average leveling pad pressure (LPAVG), and the wall displacement ( $\delta_{wall}$ ) for 95% side and 103% side, respectively.

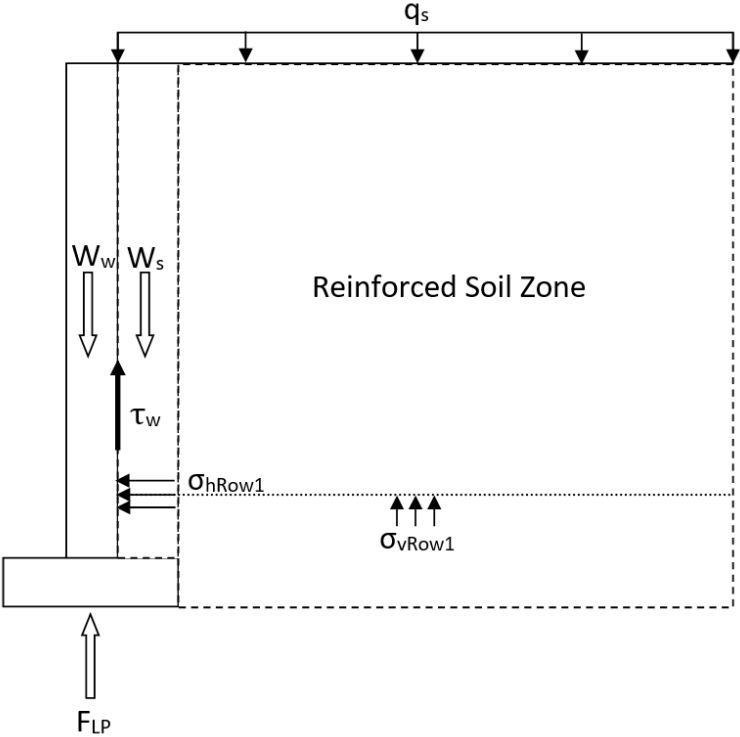


Figure 6-29. Force equilibrium diagram.

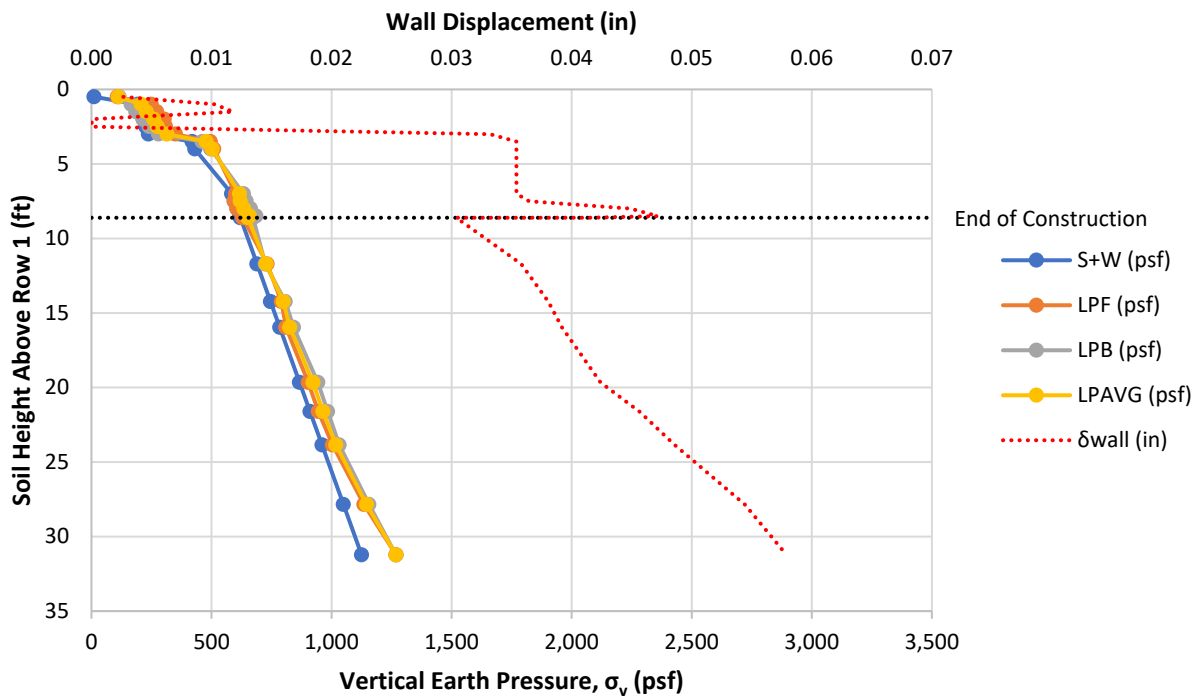


Figure 6-30. Depth profiles of leveling pad pressure and wall displacement on the 95% side.

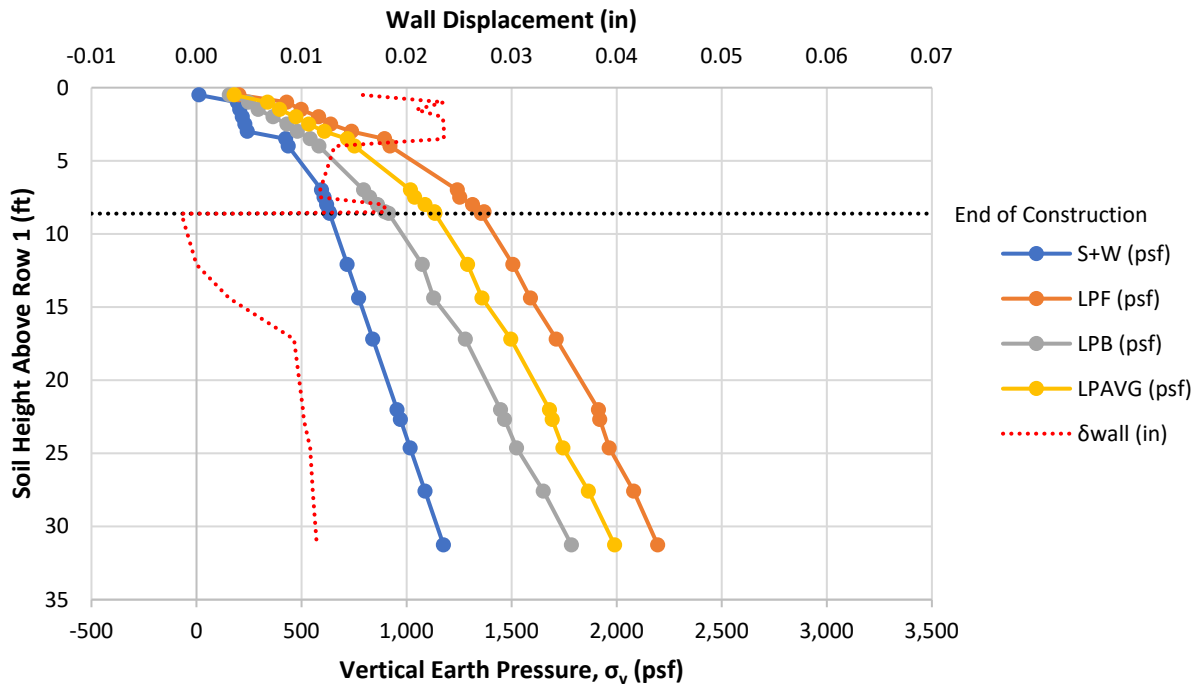


Figure 6-31. Depth profiles of leveling pad pressure and wall displacement on the 103% side.

From Figure 6-30, it is observed that the average leveling pad pressure on the 95% side generally followed the trends of the soil and wall weight during construction. However, during surcharge loading the average leveling pad pressure was slightly increased compared to the weight of the soil and walls and increased further during the final two load phases. This indicated that a small degree of soil arching likely occurred within the reinforced zone, and the loss of vertical stress indicated in Figure 6-3 should have been redistributed to the wall. This is verified when the vertical stress applied from the simulated surcharge and overburden soil is compared to the vertical stress measured at Row 1. From the final surcharge load, a vertical stress of 3,162.6 psf was applied at Row 1. The vertical stress measured at Row 1 during the final surcharge loading phase was 3,132.3 psf. This indicated an overburden reduction of 30.3 psf within the reinforced soil zone. The overburden reduction was then transformed into a vertical force by multiplying the stress by the reinforced zone area:

$$F_v = 30.3 \text{ psf} \times 9.58 \text{ ft} \times 9.75 \text{ ft} = 2,827 \text{ lbf}.$$

The vertical force was then divided by two in order to account for the front and back soil-wall interfaces, resulting in a vertical force of 1,413 lbf per wall. The vertical force was then divided by the area of the leveling pad (10 ft<sup>2</sup>), resulting in an equivalent average leveling pad pressure of 141.3 psf generated by the frictional forces at the soil-wall interface. Next, the measured additional average leveling pad pressure, beyond the weight of wall panels and soil column, of 143.4 psf was compared to the additional estimated pad pressure of 141.3 psf generated from soil arching. The two pad pressures were in excellent agreement with only a 1.5% difference between the values, indicating force equilibrium was achieved.

Next, the estimated shear stress available at the soil-wall interface was calculated using a common soil-wall friction angle ( $\delta$ ) of 30 degrees:

$$\tau_{wall} = \sigma_h \tan \delta = 943 \text{ psf} \times \tan 30 = 544 \text{ psf}.$$

The additional average leveling pad pressure of 143.4 psf was then transformed into an equivalent shear stress by first multiplying the value by the leveling pad area of 10 ft<sup>2</sup> which produced a vertical force of 1,434 lbf. The vertical force was then transformed into an equivalent shear stress by dividing the force by the area of wall face above Row 1:

$$\tau_{LP} = 1,434 \text{ lbf} \div (8.61 \text{ ft} \times 9.58 \text{ ft}) = 17.4 \text{ psf}.$$

This indicated the measured equivalent shear stress was significantly less than the available shear stress. Therefore, the available shear stress at the soil-wall interface was not exceeded and the limited wall height to surcharge height had no effect on the shear transfer from soil arching, further validating the results.

Observed in Figure 6-31, the average pressure on the 103% leveling pads exceeded the combined weight of the leveling pad soil column and wall panels by 814.3 psf. Therefore, the additional leveling pad pressure on the 103% side was more than five times the additional leveling pad pressure measured on the 95% side. This was due to the limited wall displacement on the 103% side which resulted in increased soil arching. From Figure 6-31, the wall was essentially

stationary when the soil height above Row 1 was 17.2 ft to 31.4 ft. Prior to these soil heights, the wall movement was also limited. As a result, the retained soil and leveling pad pressures were influenced by increased shear forces generated at the soil-wall interface. From Figure 6-4, it is observed that the vertical stress at Row 1 measured by the EPCs was reduced compared to the overburden soil and surcharge load applied, and Figure 6-19 shows that the lateral stress did not increase beyond a soil height of 12.1 feet, also indicating a reduction. Because there was limited to no horizontal wall displacement, the reduction in vertical and horizontal stress must have been redistributed to the leveling pads to provide static equilibrium. This is verified when the vertical stress applied from the simulated surcharge and overburden soil is compared to the vertical stress measured at Row 1. From the final surcharge load and overburden soil, a vertical stress of 3,393.5 psf was applied. The vertical stress measured at Row 1 during the final surcharge loading phase was 3,220.0 psf. This indicated an overburden reduction of 173.5 psf within the reinforced soil zone, which is more than five times the overburden reduction on the 95% side. The overburden reduction was then transformed into a vertical force by multiplying the stress by the reinforced zone area:

$$F_v = 173.5 \text{ psf} \times 9.58 \text{ ft} \times 9.75 \text{ ft} = 16,202 \text{ lbf}.$$

The vertical force was then divided by two in order to account for the front and back soil-wall interfaces, resulting in a vertical force of 8,101 lbf per wall. The vertical force was then divided by the area of the leveling pad (10 ft<sup>2</sup>), resulting in an equivalent average leveling pad pressure of 810.1 psf generated by the frictional forces at the soil-wall interface. Next, the measured additional leveling pad pressure of 814.3 psf was compared to the additional estimated pad pressure of 810.1 psf generated from soil arching. The two pad pressures were in excellent agreement with only 0.52% difference between the values, indicating force equilibrium was achieved.

Next, the estimated shear stress available at the soil-wall interface was calculated using the same common soil-wall friction angle ( $\delta$ ) of 30 degrees:

$$\tau_{wall} = \sigma_h \tan \delta = 542 \text{ psf} \times \tan 30 = 313.2 \text{ psf}.$$

The measured average leveling pad pressure of 814.3 psf was then transformed into an equivalent shear stress by first multiplying the value by the leveling pad area of 10 ft<sup>2</sup> which produced a vertical force of 8,143 lbf. The vertical force was then transformed into an equivalent shear stress by dividing the force by the area of wall face above Row 1:

$$\tau_{LP} = 8,143 \text{ lbf} \div (8.61 \text{ ft} \times 9.58 \text{ ft}) = 98.7 \text{ psf}.$$

This indicated the measured equivalent shear stress was approximately one-third of the available shear stress. Therefore, the shear stress at the soil-wall interface was increased on the 103% side but the available shear stress was not exceeded. Again, this confirmed the limited wall height to surcharge height had no effect on the shear transfer from soil arching, further validating the results.



These observations show that force equilibrium was achieved for both compaction efforts. Therefore, all stresses and forces were accounted for with minimal error. This indicated that the analyses and derived earth pressure coefficients were valid for use in making design recommendations, with the exception of the Row 4 data. Although the soil behavior at Row 4 did follow the observed behavior of the divider bowing inward towards the 95% side, the results are likely not representative of the true behavior that would have occurred if the divider was more structurally sound near Row 4. Consequently, Row 4 data from both compaction efforts were excluded during the design recommendations portion of this report.

## ***6.5 Derived Earth Pressure Coefficients and Design Recommendations***

### ***6.5.1 Derived Earth Pressure Coefficients***

For convenience, the derived earth pressure coefficients for each row of reinforcements, with the exception of Row 4, are presented in Figures 6-32 and 6-33 for the 95% side and 103% side, respectively. Also presented in the figures are the active earth pressure coefficient, at-rest earth pressure coefficient, and passive earth pressure coefficient for each compaction effort. The lower compaction effort resulted in a  $\phi = 31.2$  degrees and the higher compaction effort resulted in a  $\phi = 39.5$  degrees. Therefore, a large range of  $\phi$ , based on the compaction effort, was investigated for the select backfill.

Observed in Figures 6-32 and 6-33, the general trend of the data is that the earth pressure coefficients move from a passive condition to either an active or at-rest condition as the soil height above the row increases. The distinction of whether an active or at-rest condition will be reached at larger soil heights above the row can be made by where the reinforcement strip level is located. Rows 1 and 2 were both in the lower half of the wall and an active condition was reached for both compaction efforts (Note: Rows 1 and 2 in 103% side moved below an active condition due to the increased soil arching and reduction of lateral stress at the wall). However, Row 3 was in the upper half of the wall and an at-rest condition was reached for both compaction efforts. This further indicated that the lower half of the wall behaves differently than the upper half of the wall as suggested by the Coherent Gravity method.

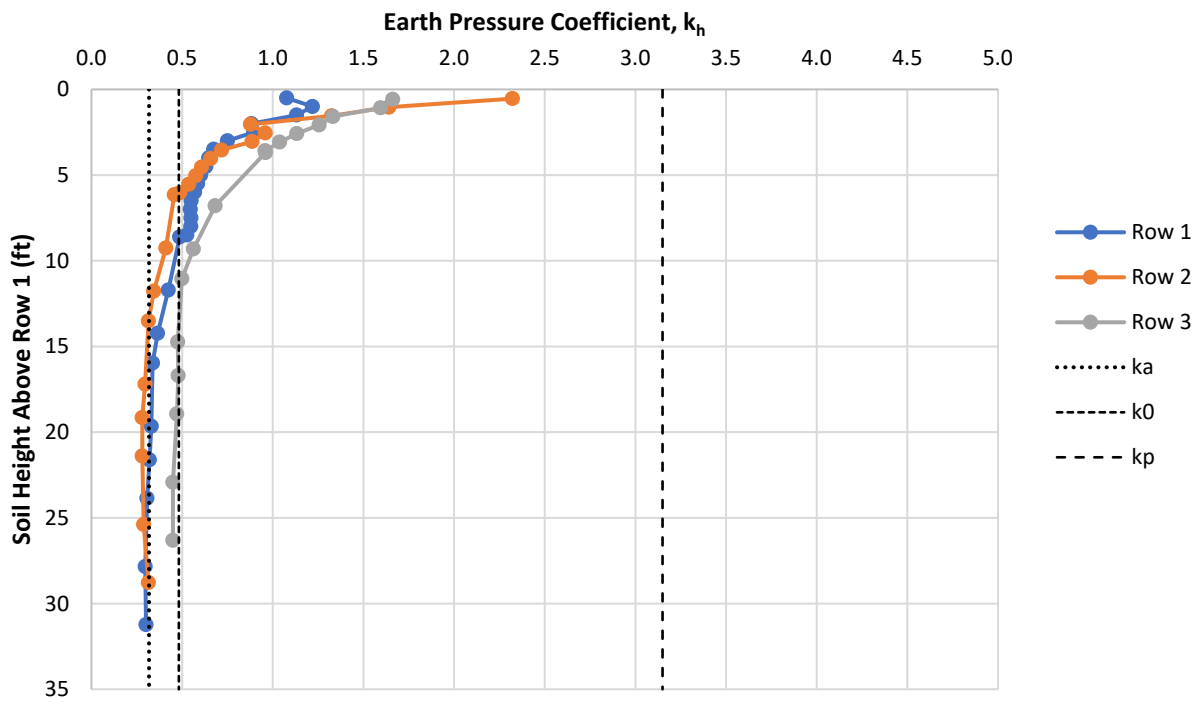


Figure 6-32. Depth profiles of earth pressure coefficients for 95% of T-180.

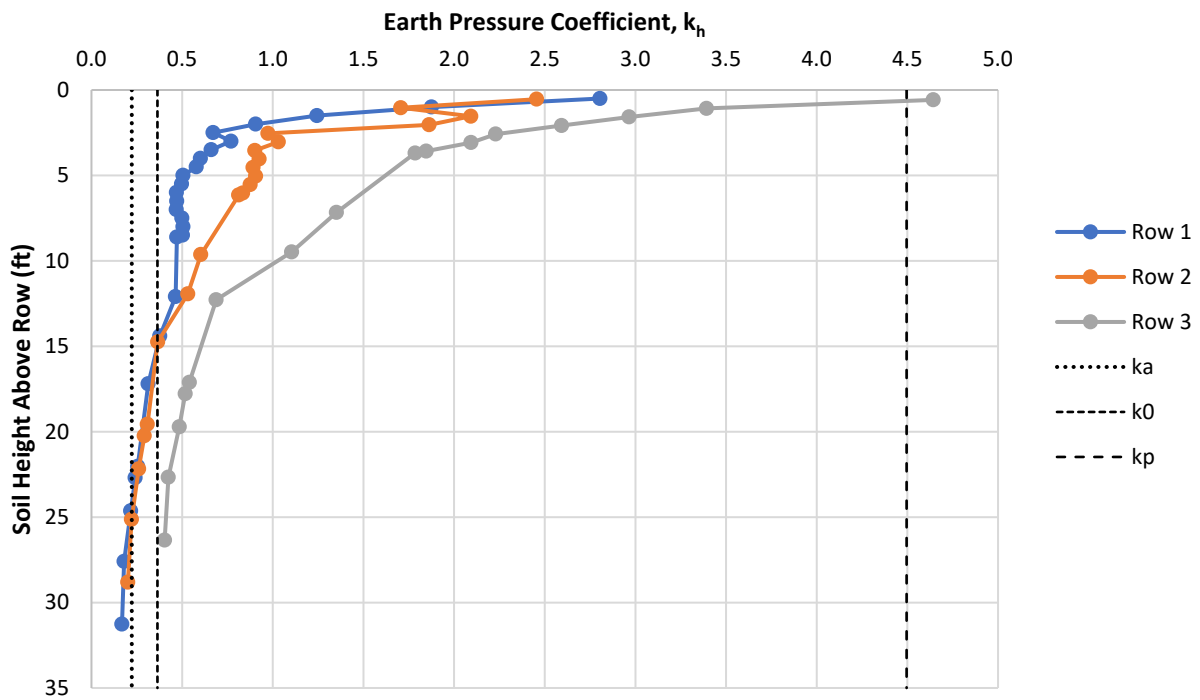


Figure 6-33. Depth profiles of earth pressure coefficients for 103% of T-180.

### 6.5.2 Design Recommendations for Soil Pressure Against Unyielding Surfaces

Figures 6-34 through 6-36 present the earth pressure coefficients derived from both compaction efforts during the research compared to the earth pressure coefficients estimated (red dashed line) from the Coherent Gravity method, AASHTO Simplified method, and Spangler & Handy (silo effect) method, respectively. Observed in each figure, the conventional methods are inadequate to quantify the additional lateral stress that develops from the compaction effort when two walls are tied together using inextensible reinforcement. Consequently, a new design method should be developed to more accurately quantify the increased lateral stress that develops from the compaction effort in an unyielding condition.

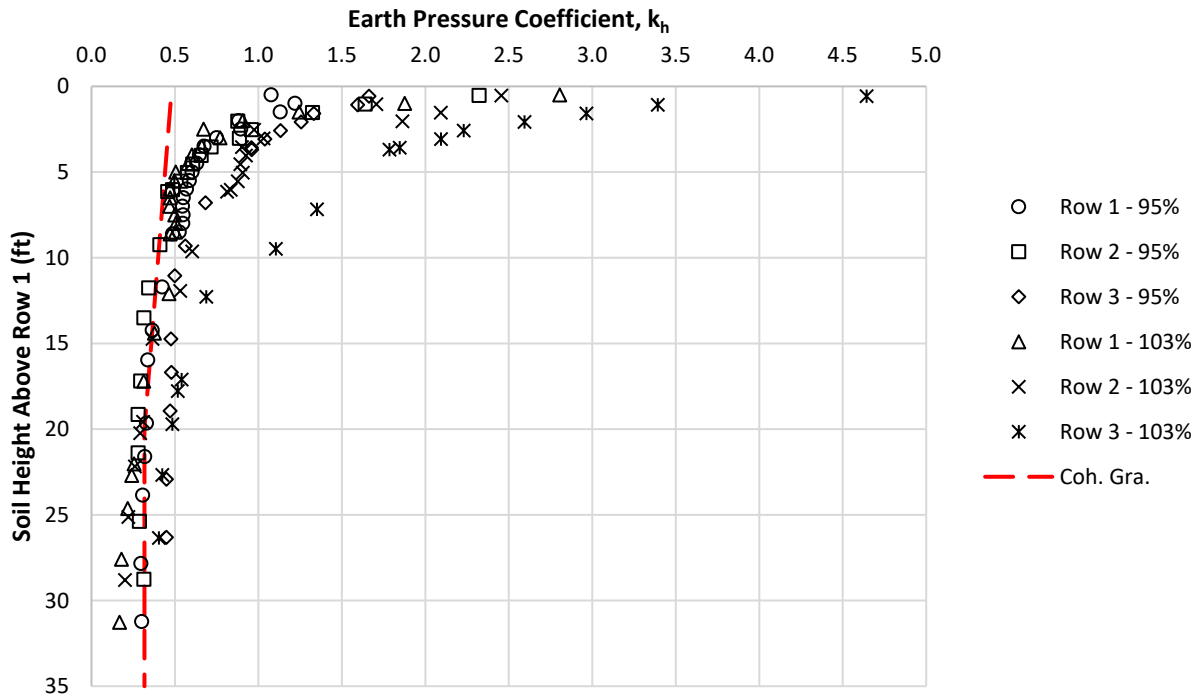


Figure 6-34. Depth profiles of earth pressure coefficients compared to the Coherent Gravity Method.

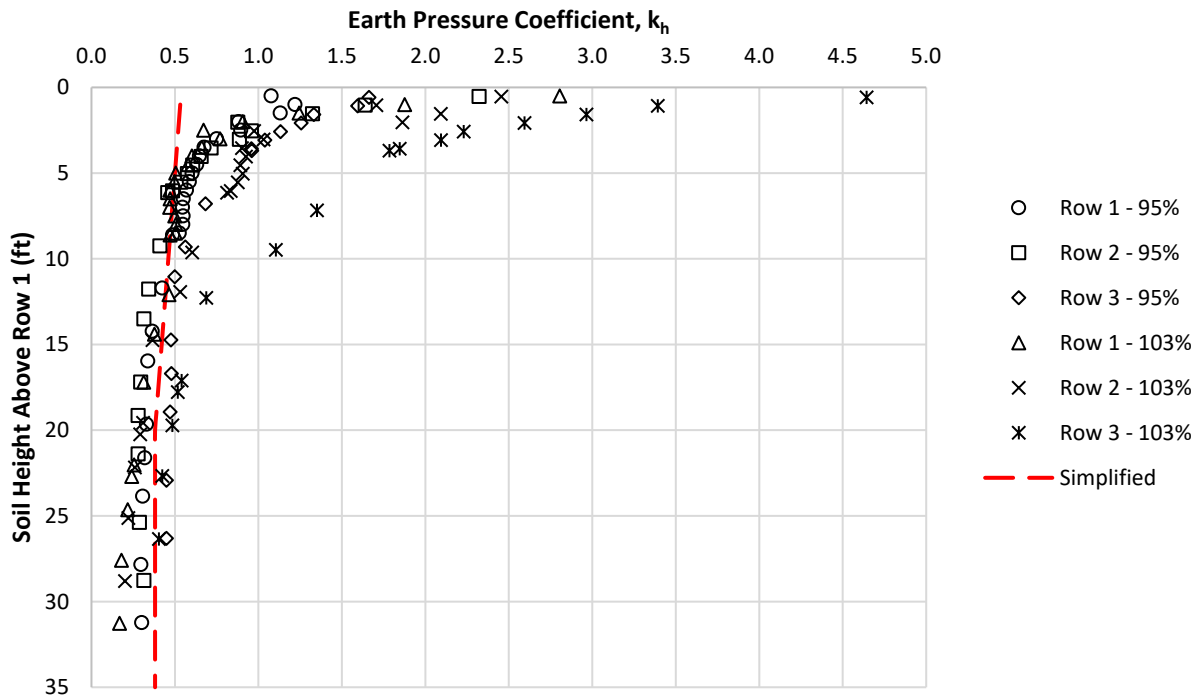


Figure 6-35. Depth profiles of earth pressure coefficients compared to the Simplified Method.

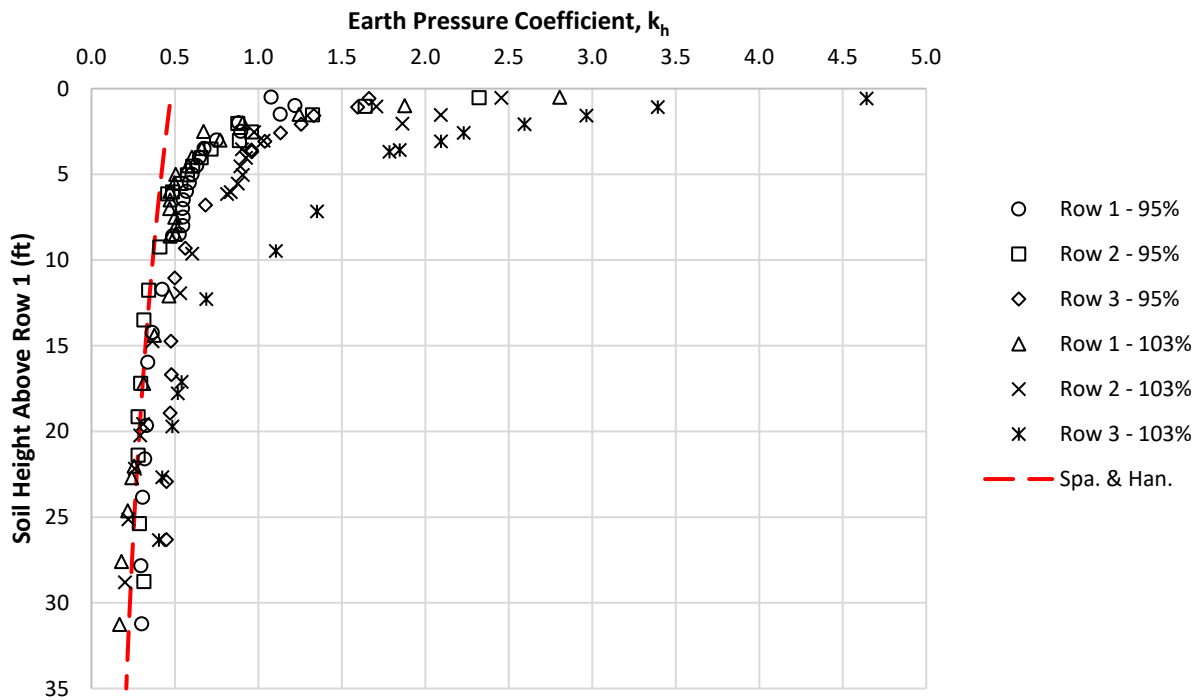


Figure 6-36. Depth profiles of earth pressure coefficients compared to Spangler & Handy's Method.

Due to the compaction effort and unyielding condition, the earth pressure coefficients tend to move from a passive condition to either an active condition or an at-rest condition as the soil height above the reinforcement level increases. Therefore, an ideal equation should consider a passive condition and either an active or at-rest condition. Additionally, because FDOT MSE wall requirements state that 95% of T-180 must be maintained within three feet of the wall face and 100% of T-180 must be maintained beyond three feet from the wall face, an ideal equation should also consider a variable range of  $\phi$  that may develop based on the compaction effort requirements. Due to the possible variability in construction and compaction efforts, it is quite reasonable to assume the soil beyond three feet from the wall face may experience over-compaction. Consequently, an over-compact state of soil density would be more ideal in equation development than 100% of T-180, because the increased compaction effort would increase the  $\phi$  and inherently the passive earth pressure coefficient. Considering each of these aspects of soil mechanics and FDOT design and construction requirements, a new equation form was developed (Eq. 6-1) to fit the needs of the unique MSE wall application.

$$k_h = k_{p@OC} \times z^b \quad (6-1)$$

Where,

- $k_h$  = Design earth pressure coefficient,
- $k_{p@OC}$  = Passive earth pressure coefficient for an over-compact state of soil density,
- $z$  = Depth below the top of the wall (ft),
- $b$  = Exponent parameter that quantifies a variable  $\phi$  based on the compaction effort and geostatic state of stress in the soil (i.e., active, at-rest, and passive).

In order to fully develop the equation, modified proctor must be performed in the laboratory at 95% of T-180 to satisfy the design requirements within three feet of the wall face and >100% of T-180 to quantify a possible over-compacted state of soil that may be achieved beyond three feet from the wall face. Direct shear testing is also required to determine the internal friction angle at each state of soil density. For demonstration, 103% of T-180, measured within the reinforced soil zone from nuclear density testing during the research, will be used during equation develop in this report. For the first trial, in Equation 6-2,  $k_h$  is set to an active condition for 95% of T-180 ( $k_{a@95}$ ) and  $z$  is set to 20 feet based on observed trends in the data and the Coherent Gravity design methodology:

$$k_{a@95} = k_{p@103} \times 20^b \quad (6-2)$$

Next, solve for  $b$  by first taking the log of each side of the equation as shown in Equation 6-3:

$$\log\left(\frac{k_{a@95}}{k_{p@103}}\right) = \log(20^b) \quad (6-3)$$

Following the rules of logarithms, b is removed from the exponent position on the right side of the equation as shown in Equation 6-4:

$$\log\left(\frac{k_{a@95}}{k_{p@103}}\right) = b \times \log(20) \quad (6-4)$$

Equation 3-4 is then rearranged to solve for b as shown in Equation 6-5:

$$b = \frac{\log\left(\frac{k_{a@95}}{k_{p@103}}\right)}{\log(20)} \quad (6-5)$$

Now that b is solved, Equation 6-1 can be used for design. Following the design methodology of the Coherent Gravity and AASHTO Simplified methods, beyond a depth of 20 feet (6 meters), a value of  $k_{a@95}$  is used rather than the  $k_h$  derived from Equation 6-1. Figure 6-37 provides the results of using this design method with the active earth pressure coefficient at 95% of T-180 ( $k_{a@95}$ ). Observed in Figure 6-37, the new design equation and methodology fit the data quite well for Rows 1 and 2 from both compaction efforts. As discussed, it was observed that both of these rows, located in the lower half of the wall, behaved similarly, and moved from a passive condition to an active condition, and the new equation and methodology quantified this behavior. However, using  $k_{a@95}$  underestimated the earth pressure coefficients for Row 3 from both compaction efforts (indicated in blue).

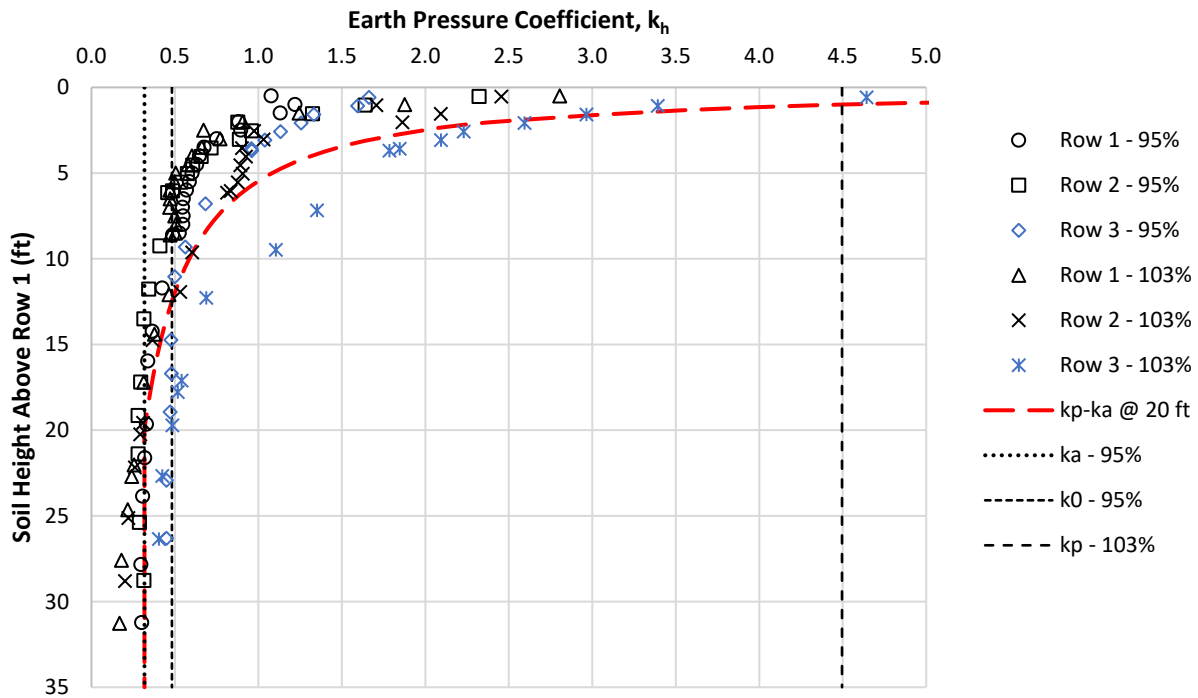


Figure 6-37. Depth profiles of earth pressure coefficients compared to the UF  $k_p$ - $k_a$  equation with a  $k_a$  cutoff applied.

As discussed, the upper half of the wall generally moved from a passive condition to an at-rest condition for both compaction efforts. Consequently, the at-rest earth pressure coefficient from 95% of T-180 is now used in equation development in attempt to quantify the Row 3 behavior from both compaction efforts. Equation 6-6 provides the  $b$  parameter that is now used in Equation 6-1, which considers the at-rest earth pressure coefficient from 95% of T-180 ( $k_{0@95}$ ).

$$b = \frac{\log\left(\frac{k_{0@95}}{k_{p@103}}\right)}{\log(20)} \quad (6-6)$$

Figure 6-38 provides the new equation compared to the derived earth pressure coefficients from the research effort. As shown in Figure 6-38, the updated equation now quantifies the behavior of Row 3, located in the upper half of the wall, from both compaction efforts quite well. The only two data points that are outliers are from the first two surcharge load phases when airbag failures occurred. Therefore, two equations were developed that consider a variable  $\phi$  based on the compaction effort that followed the trends of the data quite well for the lower half of the wall and the upper half of the wall constructed during the research. However, due to the limited wall height of 9.84 feet, the distinctions made for the lower and upper halves of the wall should be treated with caution. It is entirely possible the results of Row 3 from both compaction efforts, located in the upper half of the research MSE wall, could occur in the lower half of a much taller wall constructed in practice. UF researchers believe the difference in behavior between the lower

and upper halves of the walls may have been due to the unique construction procedure that occurs prior to reaching Row 1. During initial construction, soil is not placed or compacted against the wall facing until after the first row of reinforcements are connected. Once Row 1 is reached, soil is backfilled in the void space and then compacted, which suggests a loosened state at the soil-wall interface between the base layer and Row 1. It was observed during construction that it was more difficult to achieve the target compaction effort between Rows 1 and 2, where the average compaction effort was lowest compared to all other levels, which supports this hypothesis.

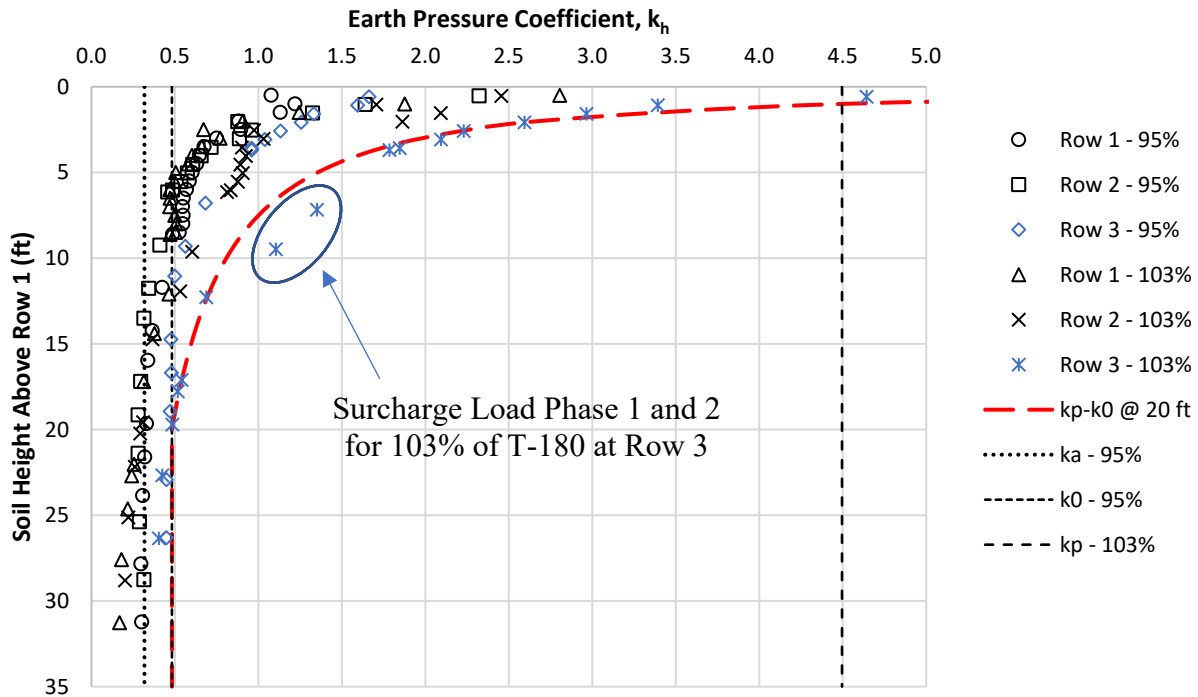


Figure 6-38. Depth profiles of earth pressure coefficients compared to the UF  $k_p$ - $k_0$  equation with a  $k_0$  cutoff applied.

It is also important to compare the newly developed equation to the earth pressure coefficients that were developed from the reinforcement strip tensions. In design, the lateral earth pressure is used to estimate the potential strip tension that may develop, which is used to determine the number of reinforcement strips required per tributary area. Figure 6-39 provides the new equation compared to the strip tension earth pressure coefficients, where the lateral stress is derived from the average strip tension in each respective row divided by the tributary wall area.



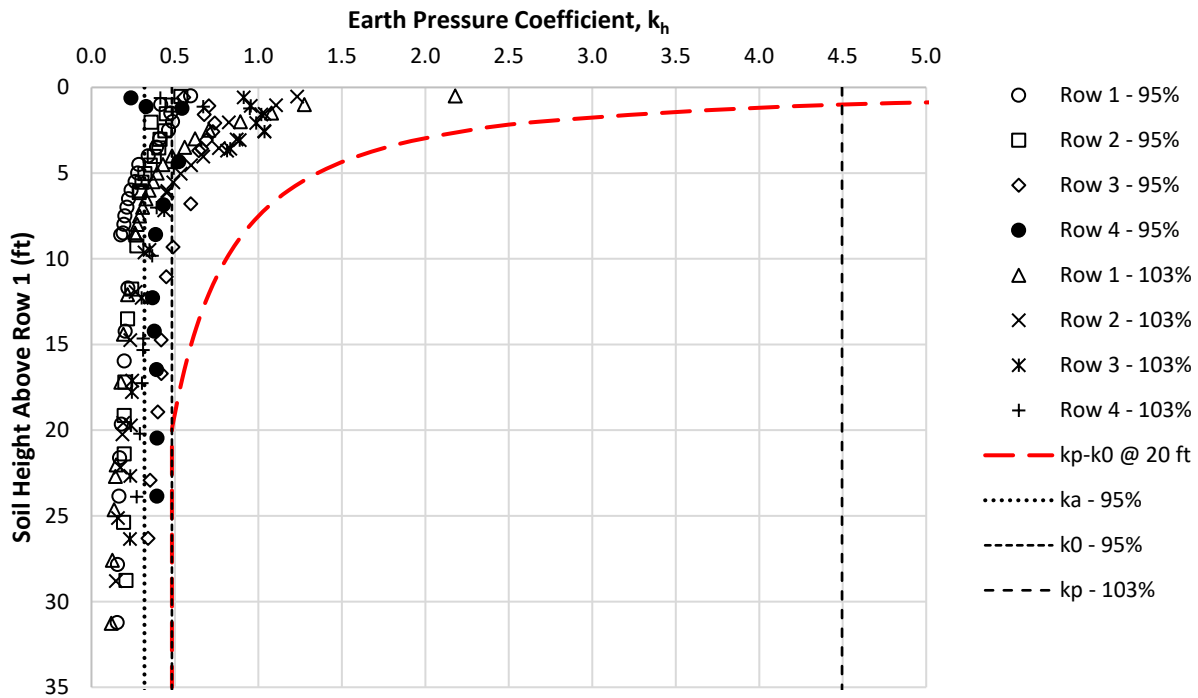


Figure 6-39.  $k_p - k_0$  equation with  $z = 20$  feet compared to strip tension derived earth pressure coefficients.

Observed in Figure 6-39, the equation appears overly conservative compared to the strip tension earth pressure coefficients that developed at shallower soil heights above each row. However, during the design phase, the Reinforced Earth Company (RECO) stated that strip tension mostly develops during the construction process (Section 3.1.6), and the research wall was only constructed to a height of 9.84 feet, with 23 feet of wall height simulated through surcharge loading. Consequently, full tension likely did not develop in the strips during construction of the research walls and higher strip tensions should be expected in the upper portion of a wall fully constructed to a height of 33 feet. For example, if the  $z$  value in Equation 6-1 was set to 9.84 feet (research constructed wall height) and then compared to the strip tension earth pressure coefficients, good agreement is found between the newly developed equation and the measured results as indicated by Figure 6-40. This suggests that the majority of strip tension develops from the compaction effort which generates wall movement throughout construction and inherently increases the tension in the strips. Furthermore, in most cases an MSE wall in an unyielding condition would likely be constructed to a height greater than 20 feet. Otherwise, the reinforcement would be six feet in length or less based on the necessary  $B/H = 0.3$  required to utilize the design approach, further justifying the new  $k_p - k_0$  equation with a 20 foot  $k_0@95\%$  cutoff applied. Therefore, it is the researchers' opinion that the lateral earth pressure produced from Equation 6-1, with  $z = 20$  feet, provides a good estimate of the potential strip tension that could develop within the reinforced zone of a full-scale MSE wall in an unyielding condition.

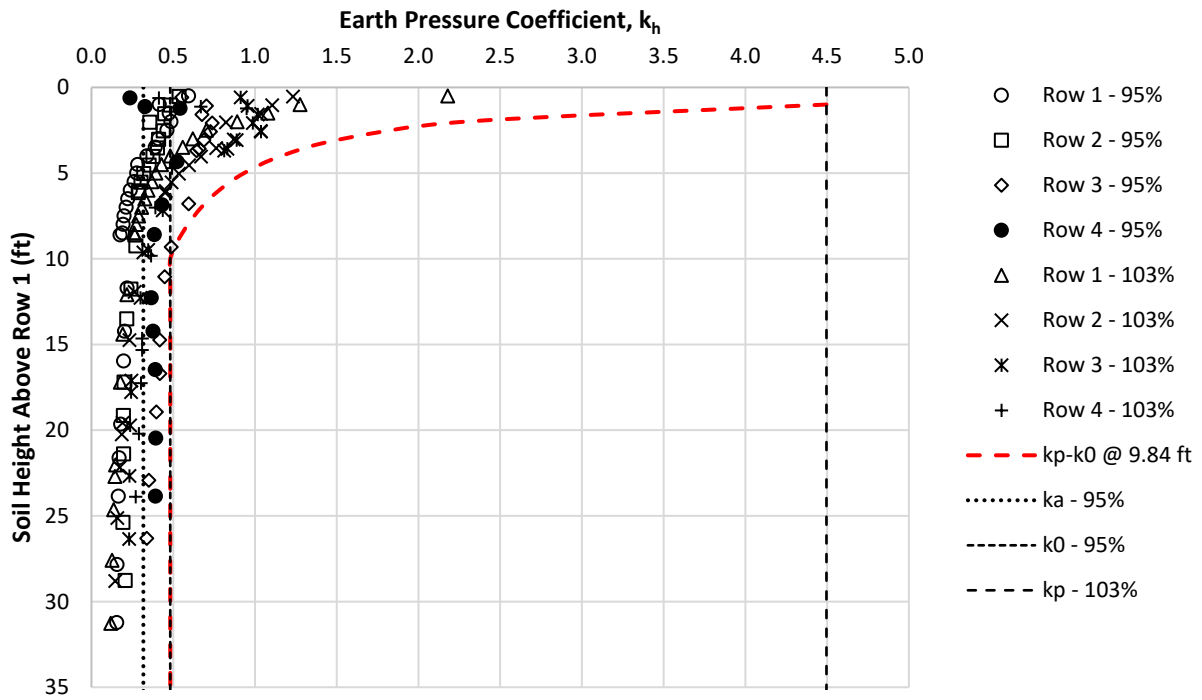


Figure 6-40.  $k_p - k_0$  equation with  $z = 9.84$  feet compared to strip tension derived earth pressure coefficients.

## 7 Conclusions

Based on the results of this study, the following conclusions can be drawn:

- The compaction equipment and techniques utilized throughout construction provided the necessary soil density to investigate an under compacted and over compacted state of soil density for an unyielding condition.
- Using the Matjack-airbag system, approximately 23 feet of overburden soil was simulated in a controlled manner. This in combination with the constructed wall height produced a B/H ratio of 0.3 for both compaction efforts. Achieving a B/H = 0.3 also validated the results of the study because this when two walls would be tied together in practice, creating an unyielding condition.
- Higher lateral earth pressures develop during construction in an unyielding condition compared to conventional MSE wall design. The additional stress occurs because the stress relief that occurs in conventional construction through minor deformation of the retaining structure is prevented by connecting the walls with inextensible reinforcement.
- A higher compaction effort leads to increased soil arching and shear transfer to the retaining wall in an unyielding condition. The increased shear transfer at the soil-wall interface generates increased pressure on the leveling pads the MSE wall rest on.
- Higher locked-in compaction forces were generated in the upper half of the constructed walls compared to the lower half as described by the Coherent Gravity and Simplified methods. This result was found when the soil was under compacted and over compacted. However, due to the limited wall height of 9.84 feet, the distinctions made for the lower and upper halves of the wall should be treated with caution.
- Increased shear transfer at the soil-wall interface leads to a reduction in lateral stress. Rows 1 and 2 on the 103% of T-180 side indicated the earth pressure coefficients were less than an active condition at the end of surcharge loading due to increased compaction and the unyielding condition, leading to increased soil arching, and reduced vertical and lateral stress as described by the Spangler and Handy (silo effect) method.
- The available shear stress at the wall was not exceeded for either compaction effort using a common soil-wall interface friction angle of  $\delta = 30$  degrees. Therefore, the limited wall height to surcharge height had no effect on shear transfer at the soil-wall interface, further validating the results for design recommendations.
- Force equilibrium was achieved for both compaction efforts, indicating all stresses and forces were accounted for with minimal error. Therefore, the analyses and derived earth pressure coefficients are valid for use in making design recommendations.
- When two MSE walls are tied together, earth pressure coefficients tend to move from a passive condition to either an active or at-rest condition as the soil height above the reinforcement level is increased. This is different than conventional MSE wall design where the earth pressure coefficients tend to move from an at-rest condition to an active condition as detailed by the Coherent Gravity and Simplified methods. However, the earth pressure coefficients developed in the unyielding condition generally stabilized in either an active or at-rest condition at an approximate depth of 20 feet as suggested by the Coherent Gravity and Simplified methods.
- A new equation was developed that incorporates a variable friction angle ( $\phi$ ) based on the compaction effort for an unyielding condition, and FDOT design and construction

requirements. When compared to the measured results, the new equation followed the trends of the data well.

## 8 Recommendations

The following recommendations are based on this study's findings:

- Using vibratory compaction equipment within three feet of the wall facing should be monitored closely during MSE wall construction. During the research it was found that a single pass with a plate compactor of appropriate weight resulted in a relative compaction closer to 100% than 95% for the select fill used. Therefore, the weight and vibratory action of the compactor may need to be adjusted based on the select fill used during construction to ensure 95% of T-180 is maintained throughout construction.
- When comparing Row 1 from the 95% side and the 103% side during construction, a very similar trend emerged, and nearly identical earth pressure coefficients were found below a depth of 2.5 feet which was when the second level of strip reinforcements were added. This suggests that the specified construction method of not backfilling to the wall until after the first row of reinforcements resulted in a very similar development of lateral stress in Row 1, regardless of the compaction effort. This implies that if the same procedure were conducted for the rows above the first level of reinforcement, it may be possible to alleviate unwanted variability in the resulting lateral earth pressures. Consequently, the UF researchers suggest that this method of back filling and compaction could be used in future construction when two MSE walls are tied together. The first row would be constructed as currently specified and compaction would then take place until the soil level is halfway to the next level of reinforcement. Once the soil level is halfway to the next level of reinforcements, backfilling to the wall should be prevented until the next level of reinforcement is connected to the wall. This would ensure compaction only occurs within the tributary area of each reinforcement level after the respective reinforcement strip is mechanically fastened to the wall panels. This process should be repeated throughout construction in an attempt to alleviate the variability in lateral stress observed during the research.
- During the design phase, modified proctor and direct shear testing should be completed for 95% of T-180, 100% of T-180, and >100% of T-180 to quantify a wide range of relative compaction densities and respective friction angles that may develop during construction. The results of tests should then be used with Equation 6-1 during internal stability design.
- Two earth pressure coefficient equations were developed during the research that consider a variable  $\phi$  based on the compaction effort that followed the trends of the data quite well for the lower and upper halves of the walls constructed. The different behavior observed in the upper half and lower half of the walls, likely due to higher locked-in compaction forces as described by the Coherent Gravity and Simplified methods, was observed for both compaction efforts. However, due to the limited wall height of 9.84 feet, the distinctions made for the lower and upper halves of the wall should be treated with caution. Consequently, UF researchers recommend using Equation 6-1 with the  $b$  parameter derived in Equation 6-6 (i.e., the  $k_p - k_0$  equation). This would provide a good conservative approach in design that would account for possible increases in lateral stress that may develop in a much taller wall.

## 9 References

- AASHTO. "LRFD Bridger Design Specifications, 4<sup>th</sup> Edition". American Association of State Highway and Transportation Officials. Washington, D.C. 2007.
- Allen T., Christopher B., Elias V., and DiMaggio J. "Development of the Simplified Method for Internal Stability Design of Mechanically Stabilized Earth Walls". Report No. WA-RD 513.1, Washington State Department of Transportation, Olympia, Washington, July, 2001.
- Anderson P.L., Gladstone R.A., and Withiam J.L. "Coherent Gravity: The Correct Design Method for Steel-Reinforced MSE Walls." *Earth Retention Conference 3*.GSP 208. 2010.
- Anderson P.L., Gladstone R.A., and Sankey J.E. "State of the practice of MSE wall design for highway structures." *Geotechnical Engineering State of the Art and Practice: Keynote Lectures from GeoCongress 2012*. GSP 226. 2012.
- Baquelin F. "Construction and Instrumentation of Reinforced Earth Walls in French Highway Administration." *Symposium on Earth Reinforcement*. ASCE. 1978.
- Bilgin O. and Kim H. "Effect of Soil Properties and Reinforcement Length of Mechanically Stabilized Earth Wall Deformations". *Earth Retention Conference 3*. GSP 208. 2010.
- Broms, B. "Lateral earth pressures due to compaction of cohesionless soils." *Proc., 4th Int. Conf. Soil Mechanics*. Budapest, Hungary. 1971.
- Chalermyanont, Tanit, and Craig H. Benson. "Reliability-Based Design for Internal Stability of Mechanically Stabilized Earth Walls." *Journal of Geotechnical and Geoenvironmental Engineering*. 130.2: 163-173, 2004.
- Chalermyanont, Tanit, and Craig H. Benson. "Reliability-Based Design for External Stability of Mechanically Stabilized Earth Walls." *Journal of Geotechnical and Geoenvironmental Engineering*. Volume 5, Issue 3, September 2005.
- Chen T. and Yung-Show F. "Earth Pressure due to Vibratory Compaction." *Journal of Geotechnical and Geoenvironmental Engineering*. Volume 134, Issue 4. 2008.
- D'Appolonia D.J., Whitman R.V., and D'Appolonia E. "Sand compaction with vibratory rollers." *Journal of Soil Mechanics & Foundations Division*. Volume 95, Issue 1Pages 263-284. 1969.
- D'Appolonia Engineering. "LRFD Calibration of Coherent Gravity Method for Metallically Reinforced MSE Walls". *Report for Association for Mechanically Stabilized Earth (AMSE)*. December 2007.
- Duncan, James M., and Raymond B. Seed. "Compaction-induced earth pressures under  $K_0$ -conditions." *Journal of Geotechnical Engineering*. 112.1: 1-22. 1986.

- Duncan, J. M., Williams G.W., Sehn A.L., Seed R.B. "Estimation earth pressures due to compaction." *ASCE Journal of geotechnical engineering*. Volume 117, Issue 12. 1991.
- FDOT. Standard Specifications for Road and Bridge Construction. Florida Department of Transportation. 2017.
- FHWA. Samtani N.C. and Nowatzki E.A. "Soils and Foundation Reference Manual – Volume I". *Publication No. FHWA-NHI-06-088*, Federal Highway Administration. Washington, DC, 2006.
- FHWA. Samtani N.C. and Nowatzki E.A. "Soils and Foundation Reference Manual – Volume II". *Publication No. FHWA-NHI-06-089*, Federal Highway Administration. Washington, DC, 2006.
- FHWA. Berg R.R., Christopher B.R., and Samtani N.C. "Design of Mechanically Stabilized Earth Walls and Reinforced Soil Slopes – Volume I". *Publication No. FHWA-NHI-10-024, FHWA GEC 011-Vol II*. Federal Highway Administration. Washington, DC, 2009.
- FHWA. Berg R.R., Christopher B.R., and Samtani N.C. "Design of Mechanically Stabilized Earth Walls and Reinforced Soil Slopes – Volume II". *Publication No. FHWA-NHI-10-025, FHWA GEC 011-Vol II*. Federal Highway Administration. Washington, DC, 2009.
- Handy, R. L. (1985). The arch in soil arching. *J. Geotech. Engng, ASCE* 111, No. 3, 302–318.
- Kim D. and Salgado R. "Load and Resistance Factors for Internal Checks of Mechanically Stabilized Earth Walls". *ASCE Journal of Geotechnical and Geoenvironmental Engineering*, Volume 138, Issue 8, August 2012.
- Kniss K.T., Wright S.G., Zornberg J., and Yang K. "Design Considerations for MSE Retaining Walls Constructed in Confined Spaces". *Report No. FHWA/TX-08/0-5506-1*, Texas Department of Transportation (TxDOT). Austin, Texas, 2007.
- Lawson C.R. and Yee T.W. "Reinforced Soil Retaining Walls with Constrained Reinforced Fill Zones". *Slopes and Retaining Structures Under Seismic and Static Conditions*, GSP 140, ASCE, Austin, Texas, 2005.
- Mitchell J.K. and Villet W.C.B. "Reinforcement of Earth Slopes and Embankments". *NCHRP Report No. 290*, National Cooperative Highway Research Program. Washington, D.C. June, 1987.
- McKittrick, David P. "Reinforced Earth: Application of Theory and Research to Practice". *Ground Engineering*. 1979.
- RECo. Documentation and Test Results for Clip Angle Connections used in Reinforced Earth Structures. 2003.

RECo. Design Manual for Reinforced Earth Walls. 2011.

Spangler, M. G. & Handy, R. L. (1984). Soil engineering, New York: Harper & Row.

WSDOT. "Geotechnical Design Manual". *M-46-03.01*, Washington State Department of Transportation (WSDOT). January 2010.